University of Strathclyde

HyperClass
Hyperspectral Classification of Space Objects

Massimiliano Vasile, Lewis Walker, Simao Marto
Aerospace Centre of Excellence, Department of Mechanical and Aerospace Engineering

Stephen Marshall, Paul Murray, Andrew Campbell
Hyperspectral Imaging Centre, Department of Electronic and Electrical Engineering

Vasili Savitski, Paul Mccartney
Fraunhofer Centre for Applied Photonics

HyperClass – Main Concept and Objectives

1- To extend the current high fidelity model and simulation to a wider range of materials and material properties, material distributions, geometries, attitude motions, optics.

2- To demonstrate, in simulation, the applicability of hyperspectral light-curve analysis to a wide range of objects with different surface composition, size, shape, attitude motion, orbit regimes, illumination conditions, in space and on ground sensors.

3- To demonstrate the use of deep learning for the classification of space objects from hyperspectral images and hyperspectral light curve analysis.

4- To demonstrate the use of deep learning for attitude motion reconstruction from hyperspectral light curve analysis.

5- To associate hyperspectral light curve analysis and attitude motion to identify patterns in space object behaviour

6- To design a prototype sensor that can be used in conjunction with a standard telescope on ground or in space on board a satellites

7- To test the concept in a lab environment with a mock-up of a small satellites. Possibly to be revised to: testing the concept with actual optical observations from ground.

8- To demonstrate the use of multispectral/hyperspectral imaging to identify the surface composition of resident objects in Low Earth Orbit, either using on ground or in orbit observations, and to improve their classification.

9- To demonstrate that the use of the time variation of the intensity at different wavelengths can be used to reconstruct the attitude motion better than by simply using light curve measurements.

WP1 - Hyperspectral light curve analysis and object classification

- Object simulation
- Sensor simulation
- Light decomposition
- Object classification

Object and Sensor Model

AEROSPACE CENTRE of EXCELLENCE

- Arbitrary shapes
- Coupled attitude orbit dynamics
- Various material elements on each surface
  - Self-shadowing
  - Elements contribute signal when both illuminated and visible
  - Fractional element illumination/visibility
  - Materials + reflectance spectra assigned to each element

- Low fidelity Lambertian Model. Integrate collected power in wavelength band $[\lambda_0, \lambda_0+d\lambda]$, summed over entire object:

$$P_{col}|_{\lambda_0}^{\lambda_0+d\lambda} = \sum_e \frac{\cos\theta_i^{(e)} \cos\theta_o^{(e)} d\Omega dA^{(e)}}{\pi} \int_{\lambda_0}^{\lambda_0+d\lambda} R(\lambda)^{(e)} \phi_{inc}(\lambda) d\lambda$$

- Hi-fidelity complete model of specular + diffuse reflection
  - Reflective surfaces – glass, solar panels, polished metals etc
  - More orientation sensitive – strong specular highlights

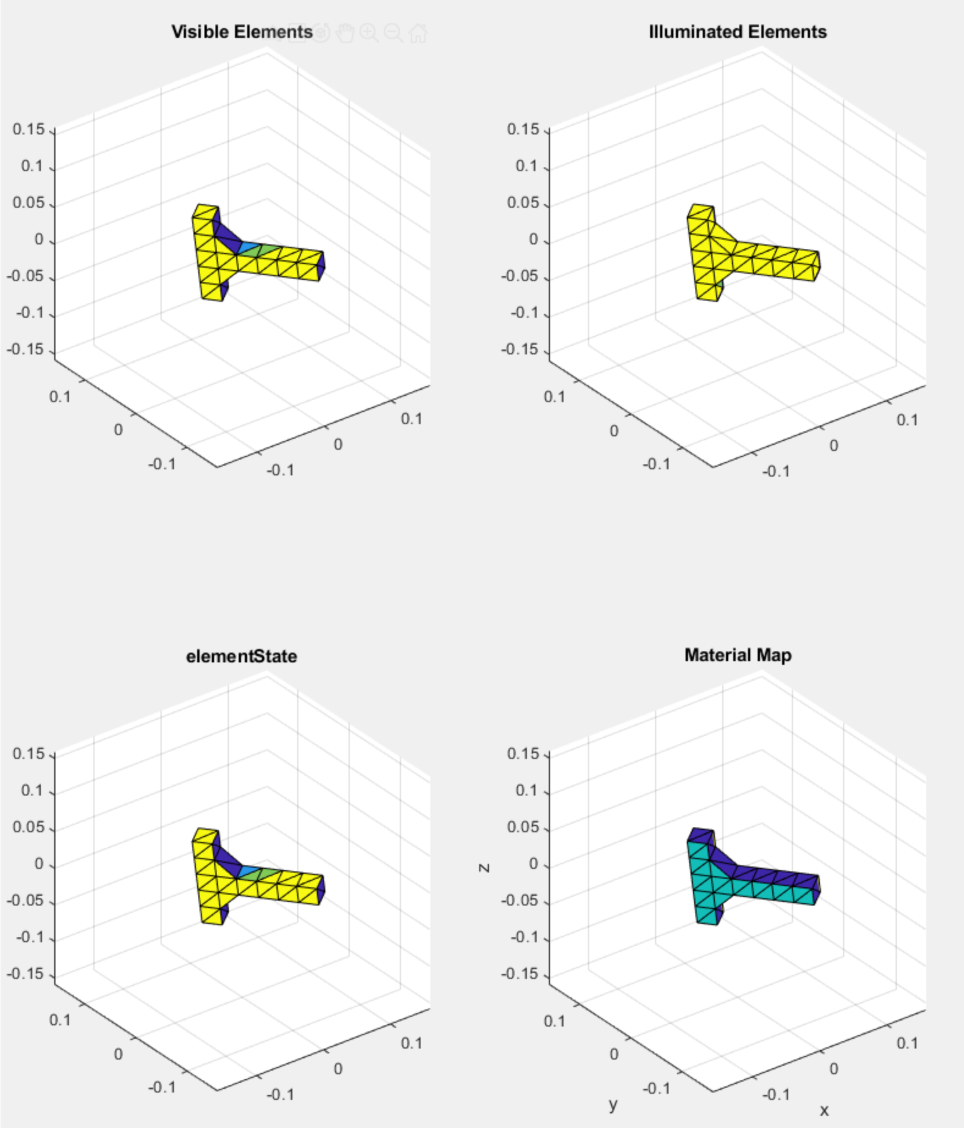

Example test object
Colours represent visibility state or materials

Object and Sensor Model

- Arbitrary shapes
- Coupled attitude orbit dynamics
- Various material elements on each surface
  - Self-shadowing
  - Elements contribute signal when both illuminated and visible
  - Fractional element illumination/visibility
  - Materials + reflectance spectra assigned to each element

- Low fidelity Lambertian Model. Integrate collected power in wavelength band [λ_0, λ_0+dλ], summed over entire object:

$$P_{col}|_{\lambda_0}^{\lambda_0+d\lambda} = \sum_e \frac{\cos\theta_i^{(e)} \cos\theta_o^{(e)} d\Omega dA^{(e)}}{\pi} \int_{\lambda_0}^{\lambda_0+d\lambda} R(\lambda)^{(e)} \phi_{inc}(\lambda) d\lambda$$

- Hi-fidelity complete model of specular + diffuse reflection
  - Reflective surfaces – glass, solar panels, polished metals etc
  - More orientation sensitive – strong specular highlights

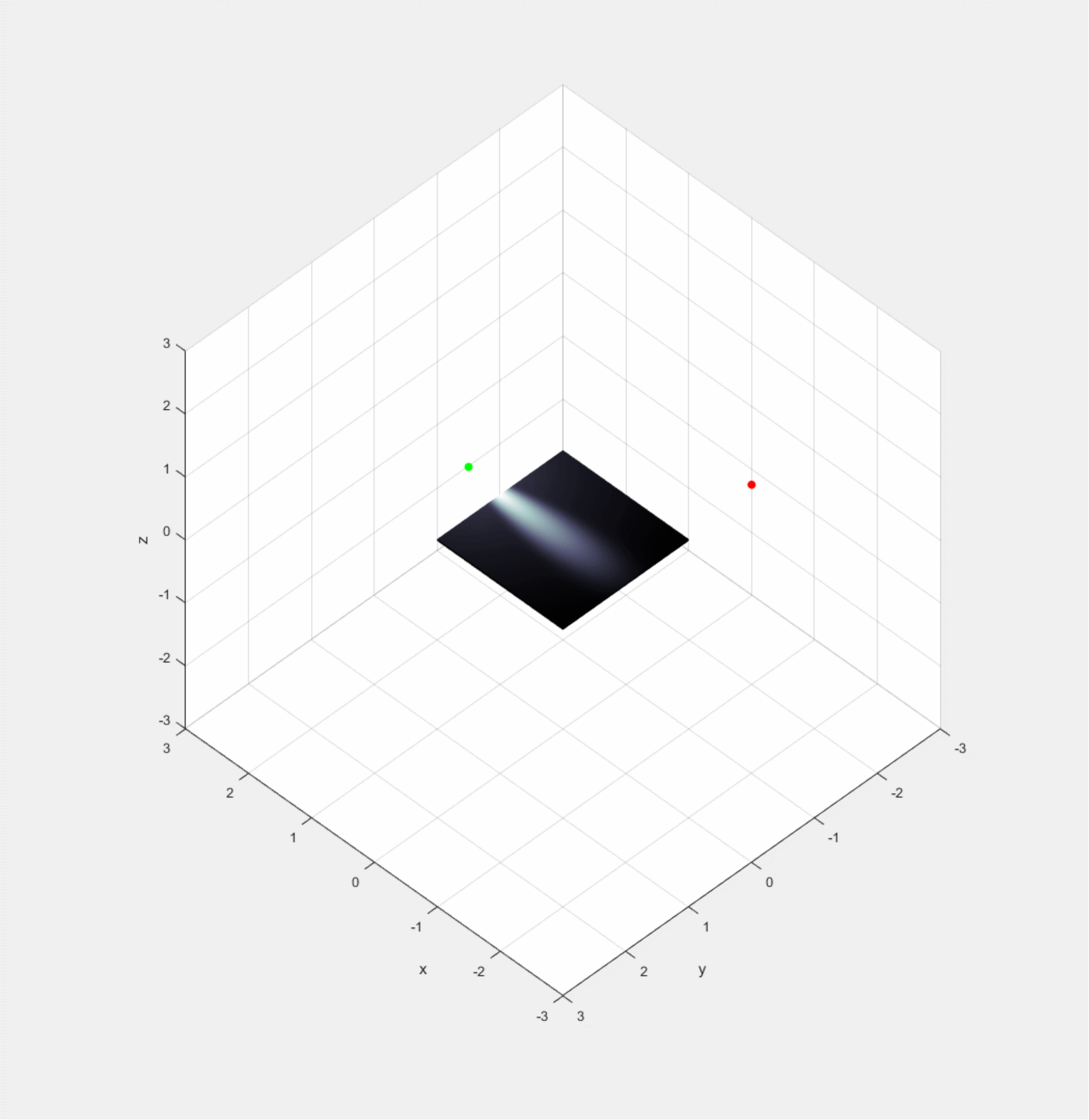

Example test object
Colours represent visibility state or materials

Object and Sensor Model

- Multiple shapes and material distributions.
- Exact spacecraft model is not required
- More important is the expected distribution of materials associated to different objects
- High fidelity reflection/diffusion/emission model tuned on representative surfaces

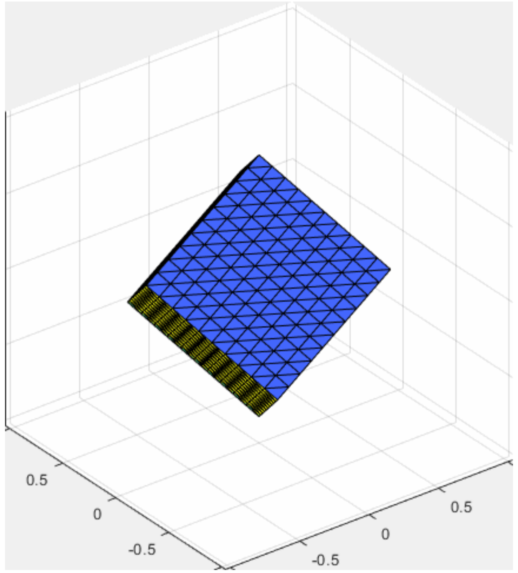

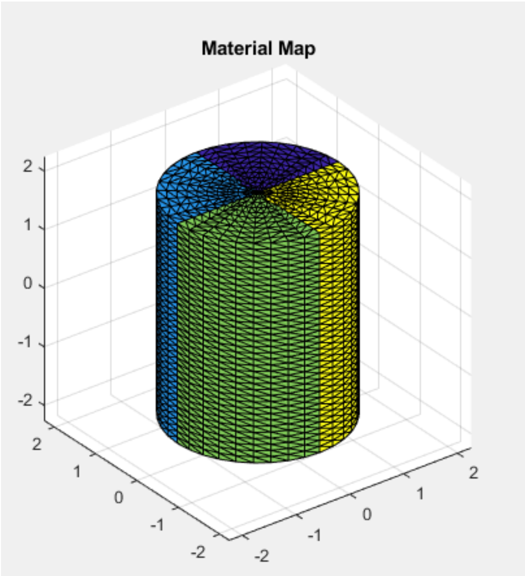

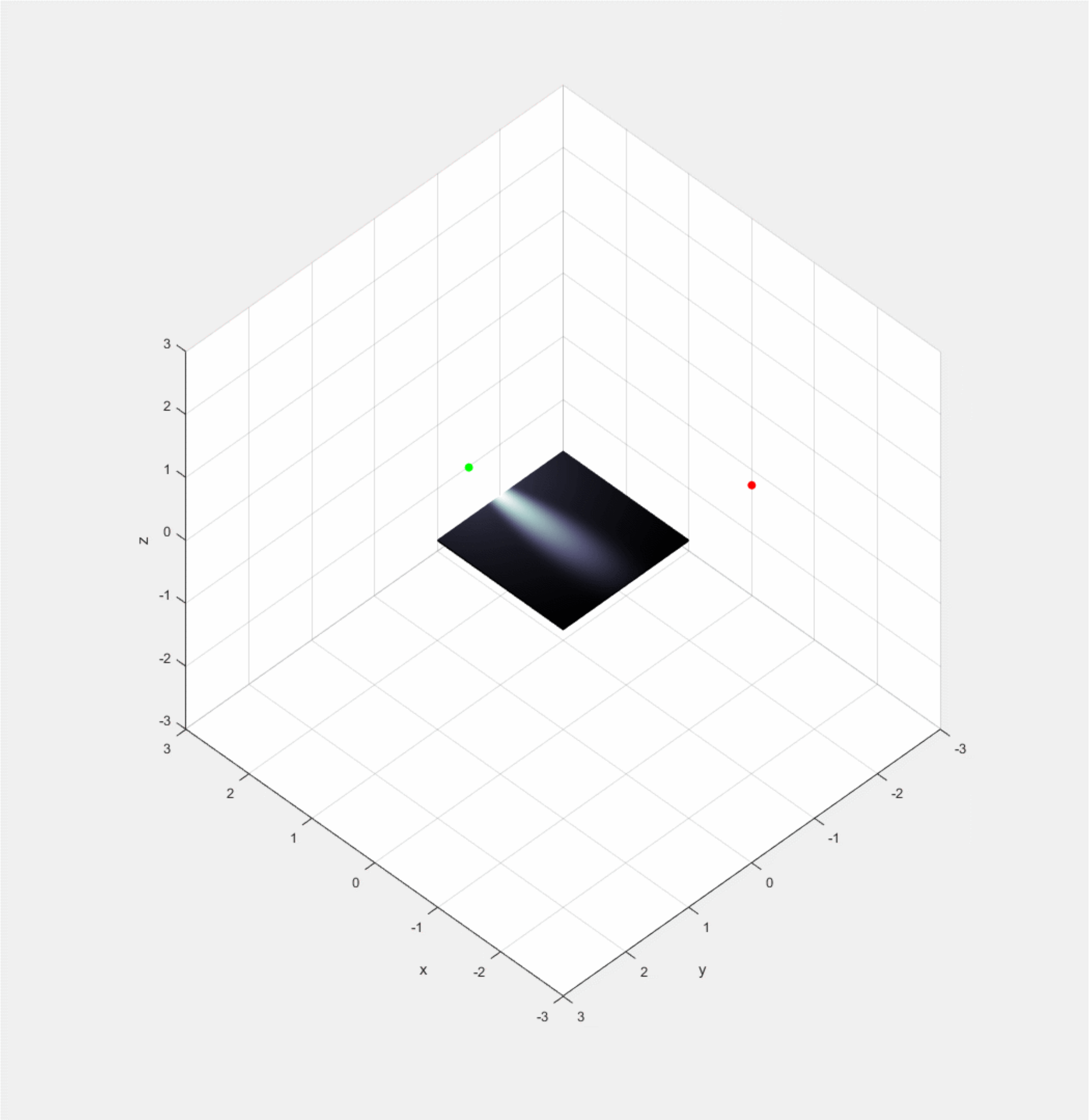

High-fidelity Model Calibration Against Lab Experiments

AEROSPACE CENTRE of EXCELLENCE

- Reflectance data for rotating cube
  - **Case 1 – Al only**
    - *One side Aluminum foil*
    - *Others black paint*
  - **Case 2 - 4 materials**
    - *Aluminum foil*
    - *Gold foil*
    - *Brass plate*
    - *Steel plate*

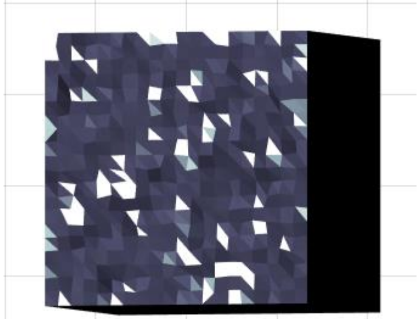

Crinkled foil (thermal blanket analogue) Modelled by refining cube mesh and adding noise offsets

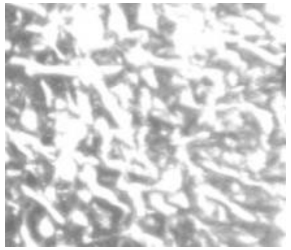

Real foil surface

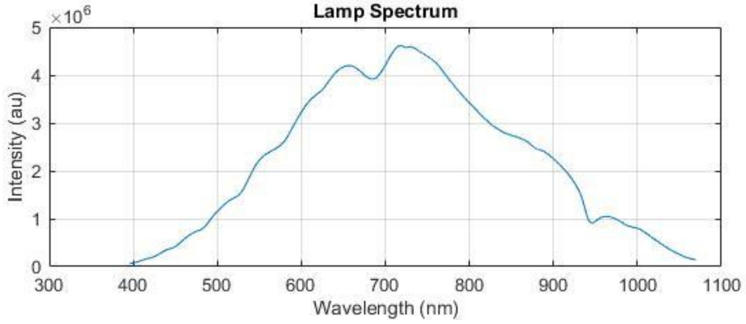

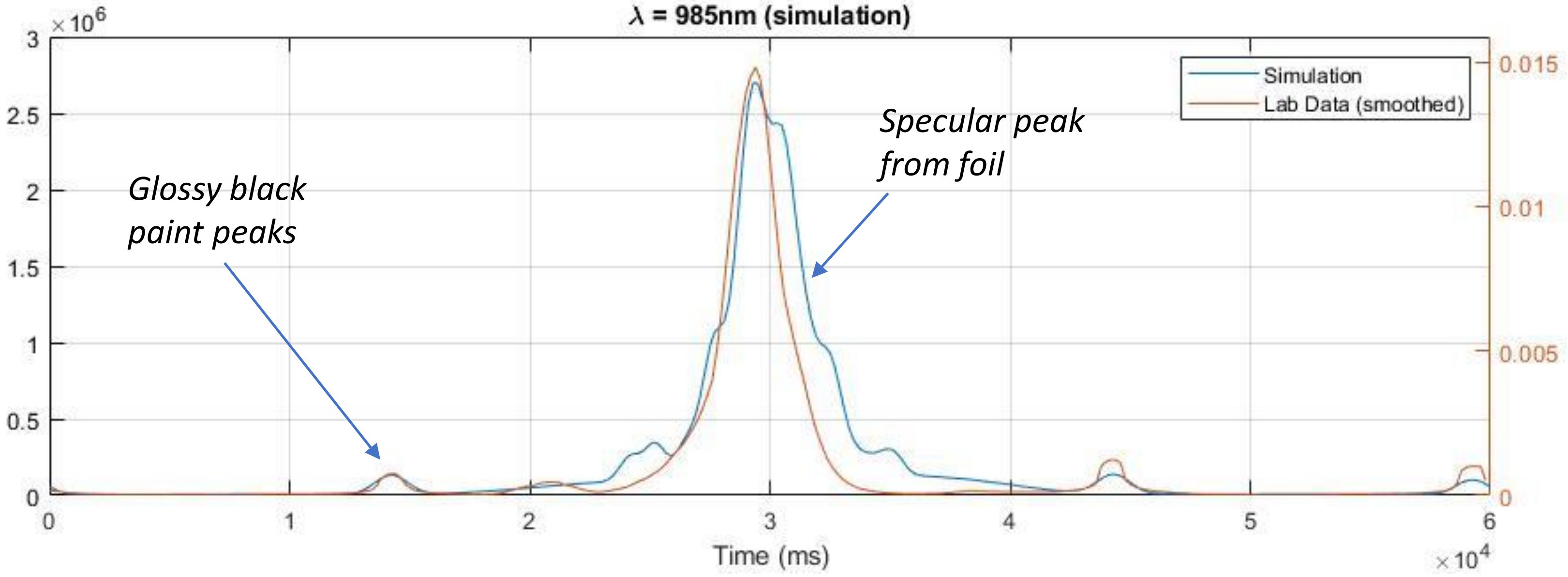

Comparison of simulated and lab data at 985nm (Case 1)

Object and Sensor Model

Space and ground-based sensors

- *Space sensor no attenuation*
- *Both reflected and re-emitted light*
- *Ground sensor - Atmospheric attenuation (spectrum + elevation)*

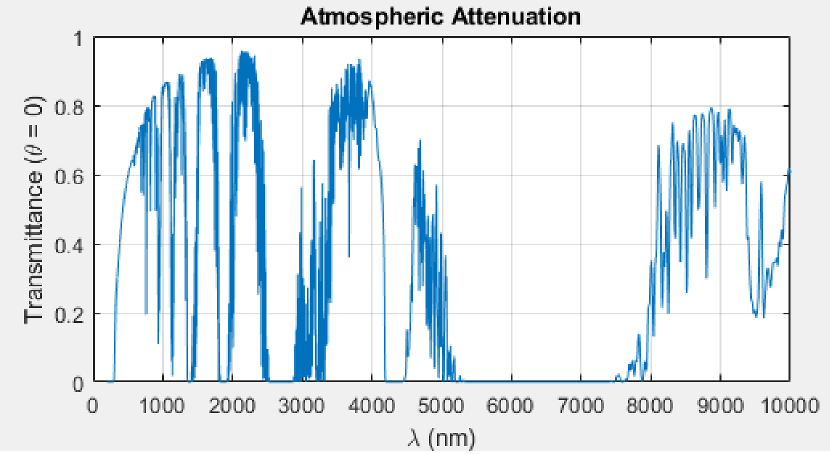

MODTRAN attenuation spectrum

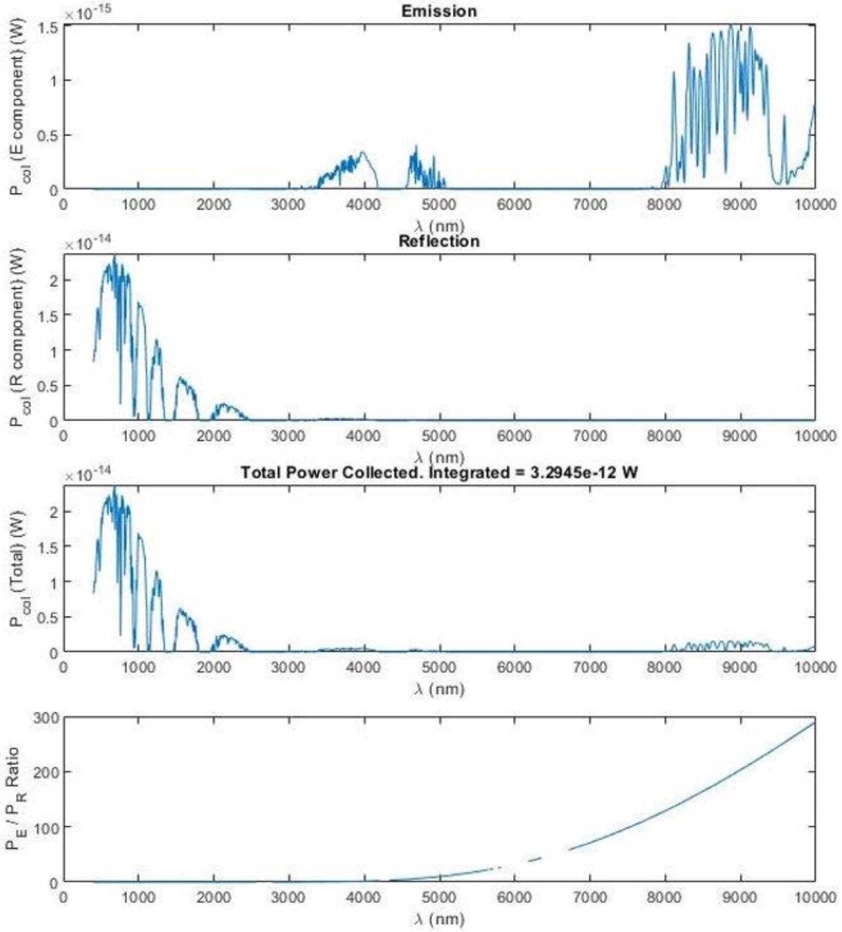

Simulated HSI output (single sample)
Space object, 11 inch optics
Atmospheric effects visible

WP1 - Hyperspectral light curve analysis and object classification

AEROSPACE CENTRE of EXCELLENCE

- Dynamics + Atmospheric effects
  - ***Lab case***
    - *Fixed-axis rotation*
    - *Fixed*
    - *Used for validation*
  - ***Space case***
    - *Free-space rotation/tumbling motion/precession*
    - *Orbit propagation*
    - *Tracks evolution of view + illumination directions*
    - *Ground-based and space-based observers*
    - *Atmospheric attenuation (spectrum + elevation)*

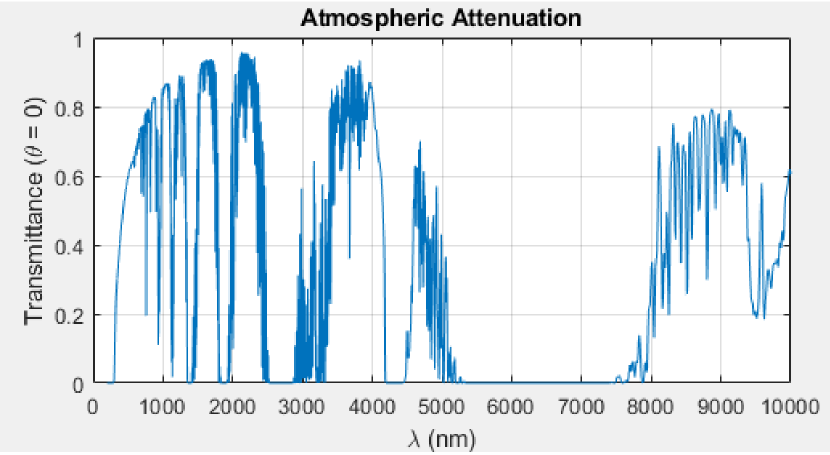

MODTRAN attenuation spectrum

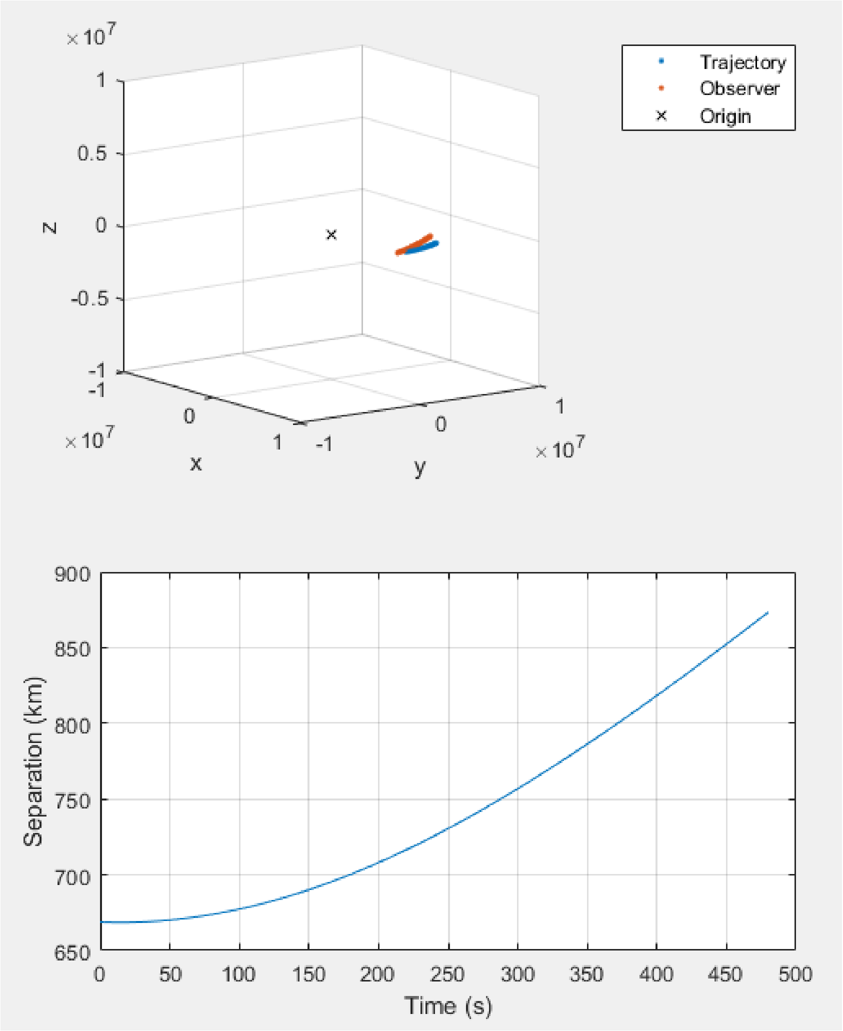

Propagated orbital tracks in space case

WP1 - Hyperspectral light curve analysis and object classification

AEROSPACE CENTRE of EXCELLENCE

Preliminary results

- Simulated sensor outputs for various objects and scenarios
  - *First iteration reflectance model*
  - *Ground- and space-based observers*
- Collected power estimate – informs telescope design
- Reflected and emitted components
  - *Night-time imaging*

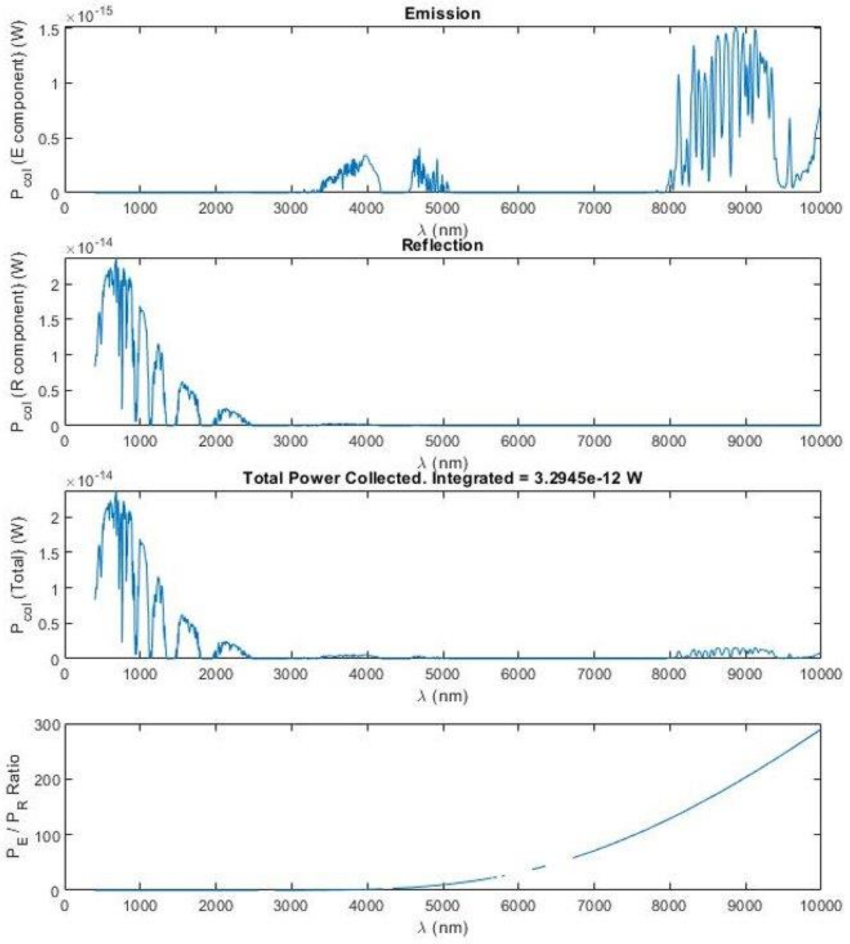

Simulated HSI output (single sample)
Space object, 11 inch optics
Atmospheric effects visible

WP1 - Hyperspectral light curve analysis and object classification

Preliminary results

More test cases – 2m cube, ground and space

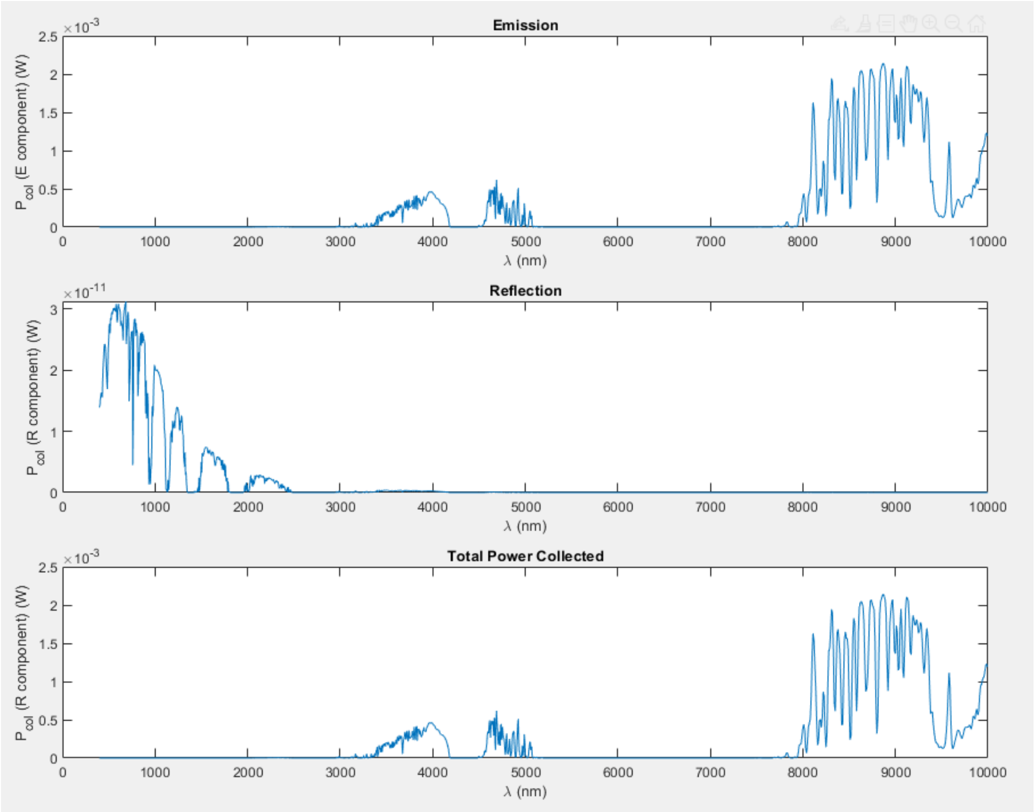

Ground based telescope (r = 5m)
~10^{-11} W Reflection
~10^{-3} W Emission (350K)

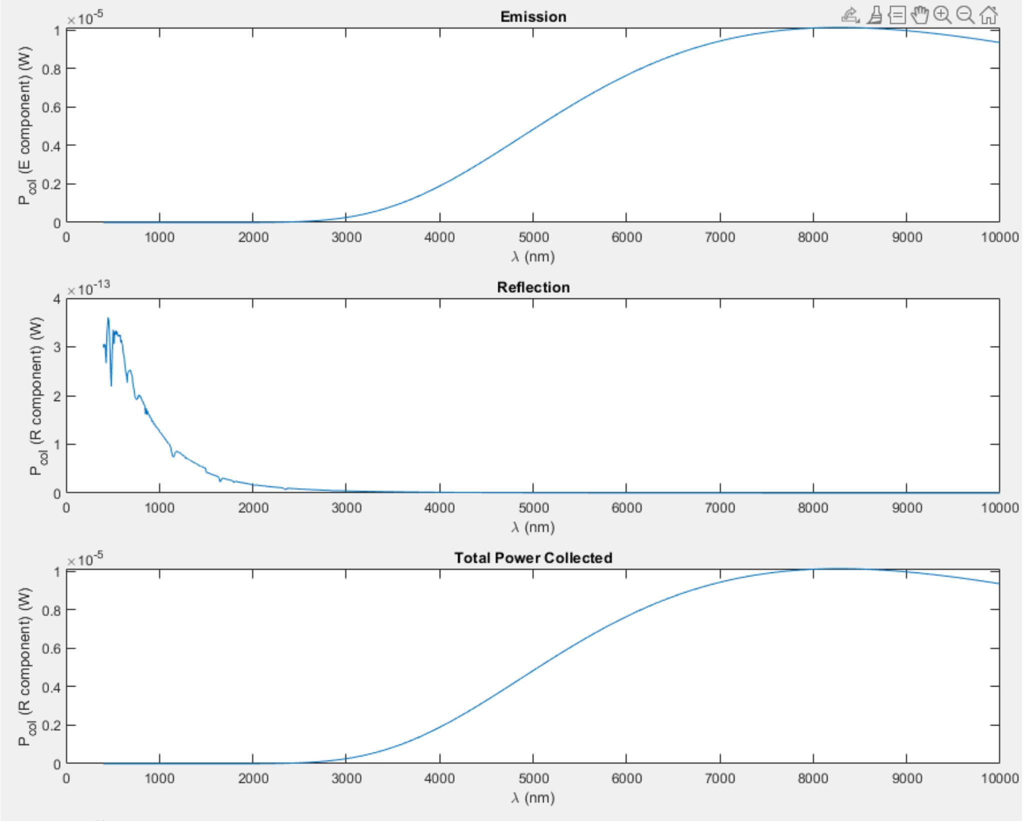

Space based telescope (r = 10cm)
~10^{-13} W Reflection
~10^{-5} W Emission (350K)

Parametric Analyses: elevation

- Same analysis with larger cylinder
- Soyuz upper stage analogue
- Dimensions – 1.33m radius, 6.7m length
- Same trend
- ~100x greater power returned

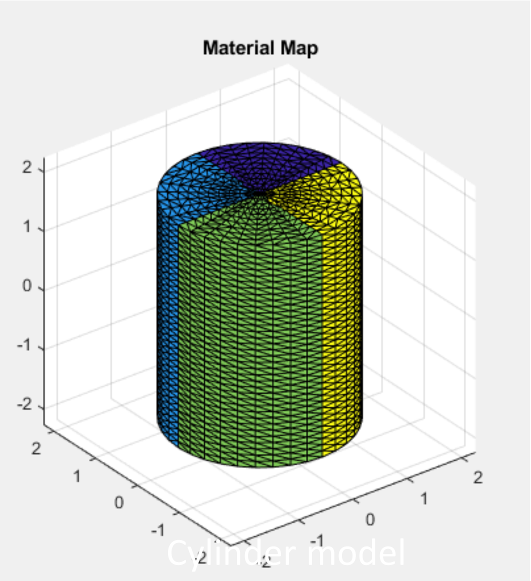

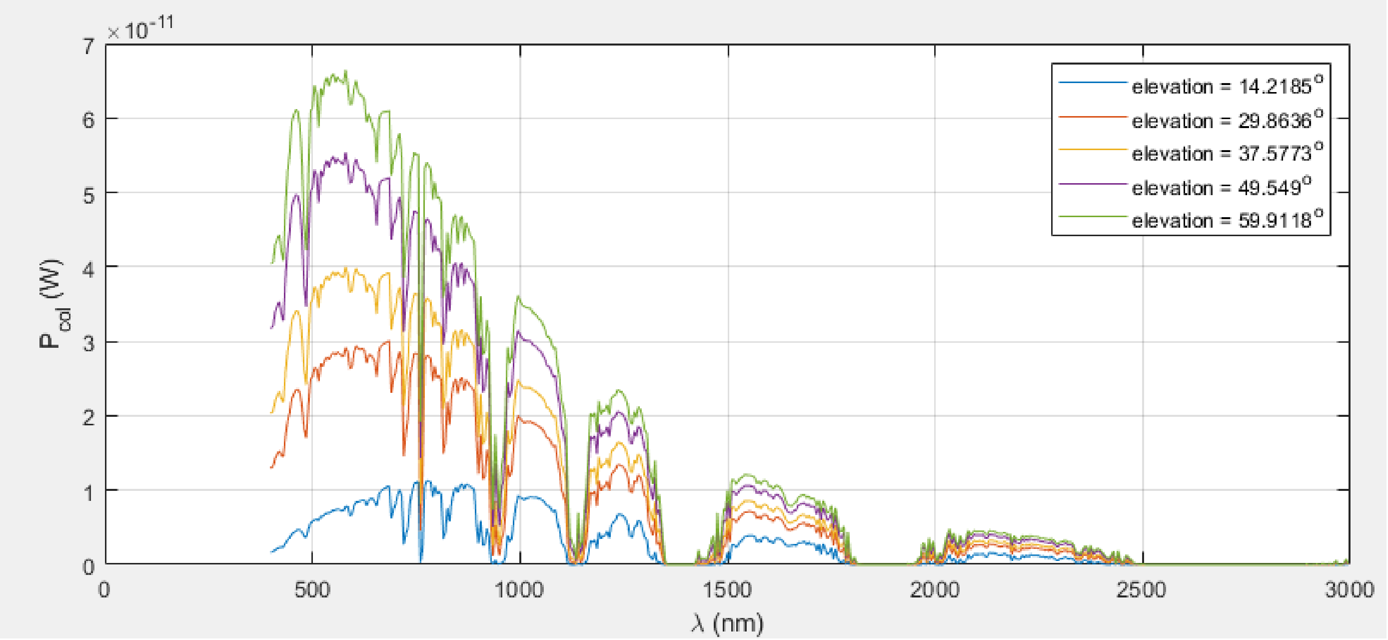

Endmember analysis

- Spectral unmixing
- Component spectra can be estimated using N-FINDR algorithm for endmember analysis
- Lambertian model
- Various material/shape configurations
- **Single pixel image**
- Multiple scenarios were simulated with an without atmotphere

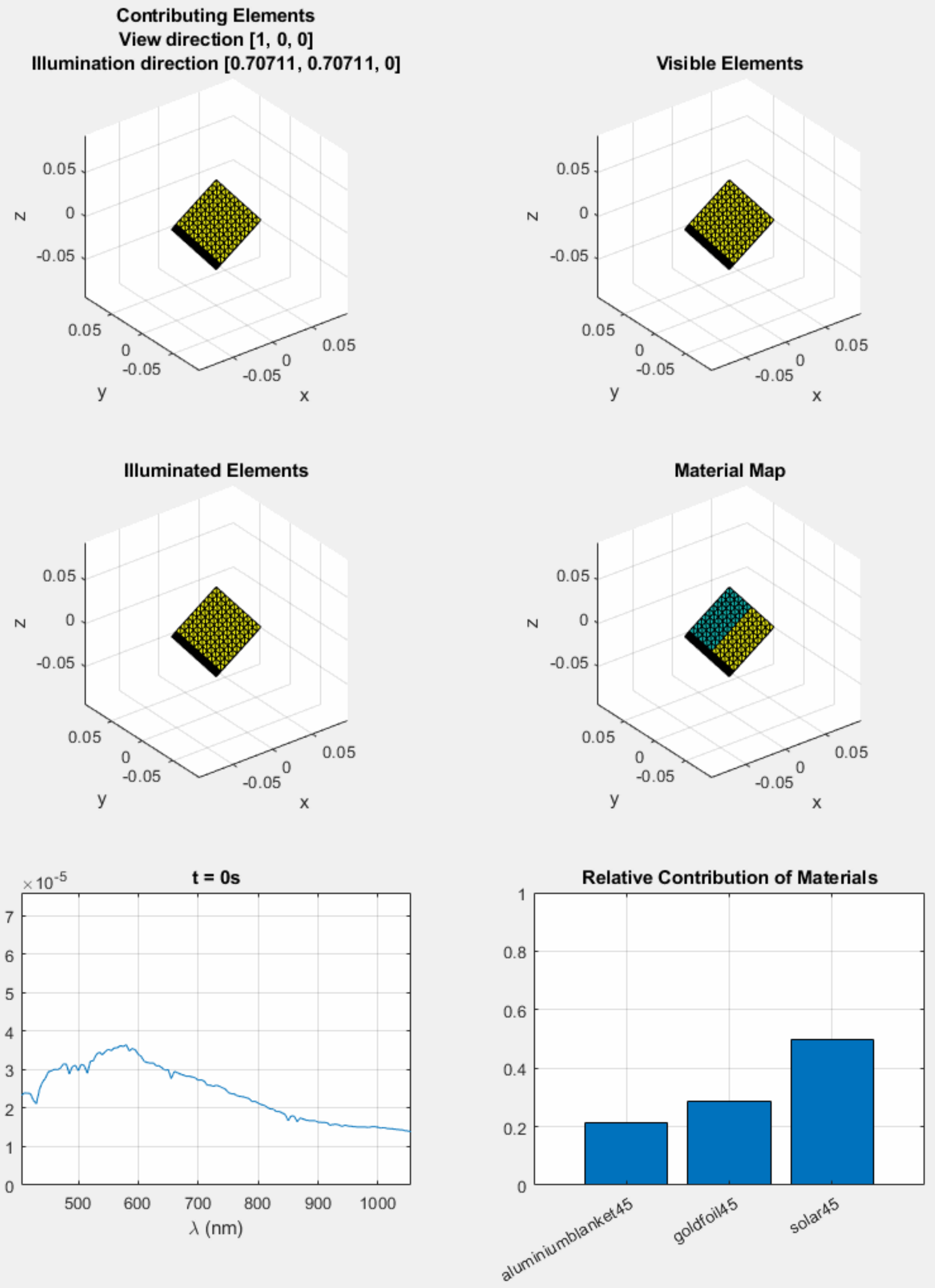

Mixed material rotating cube

Endmember analysis

Aerospace Centre of Excellence

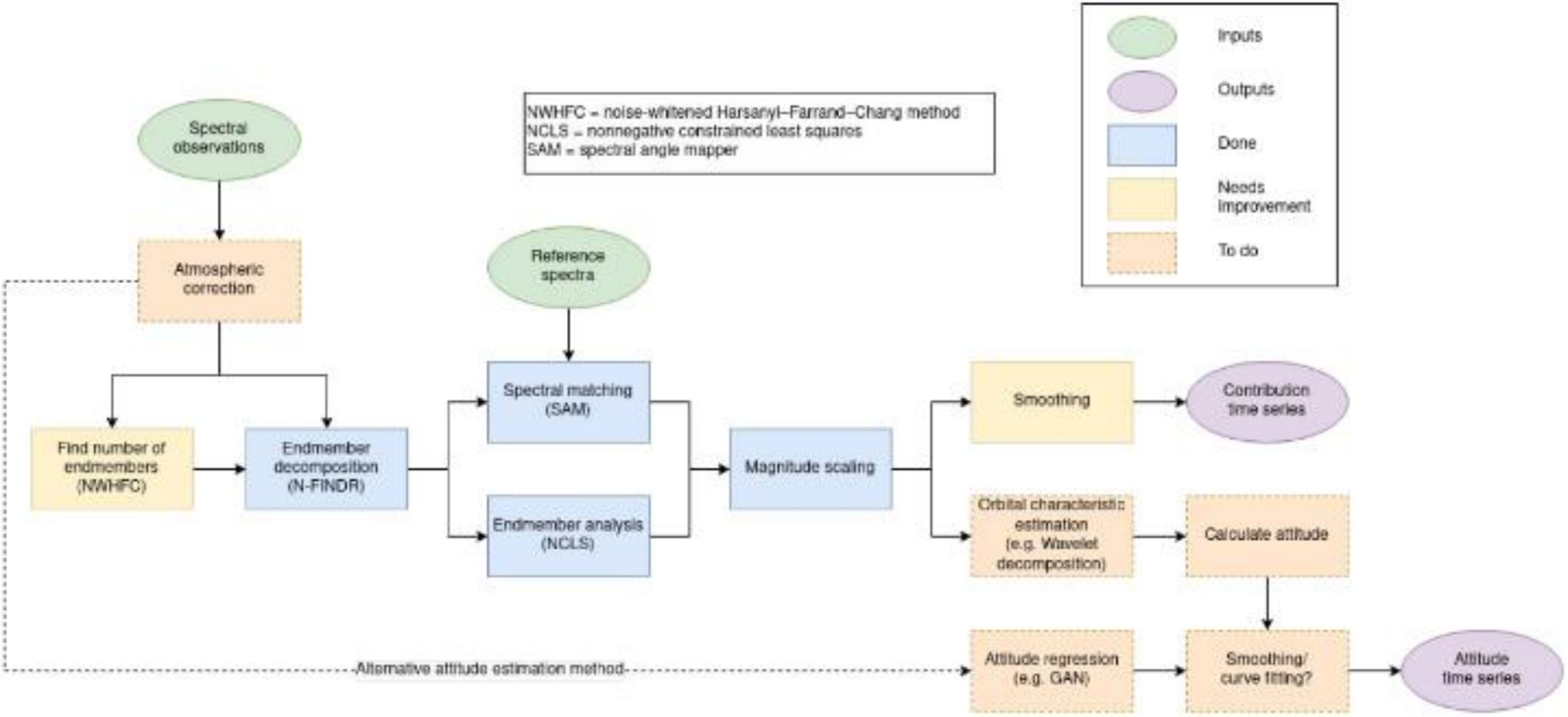

Endmember analysis

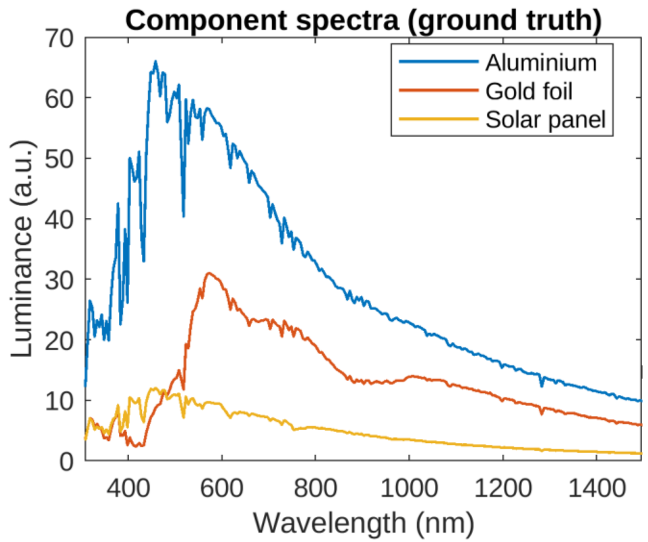

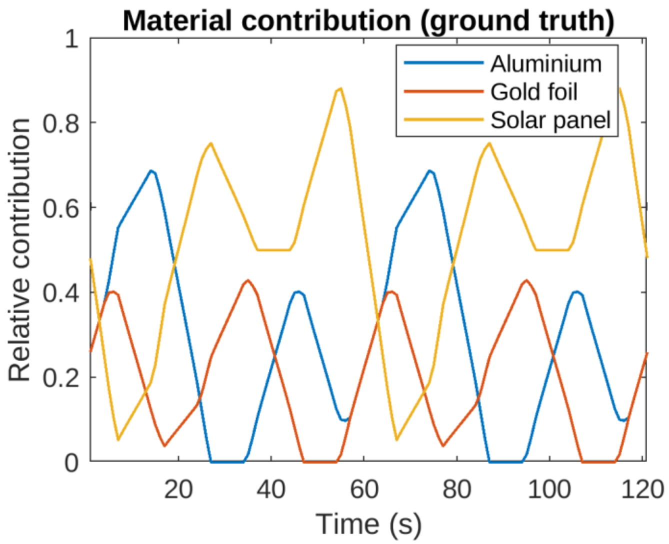

- Simulation using cube with mixed materials on each side
- Based on spectra for three materials captured in the lab in the range 300-1500 nm

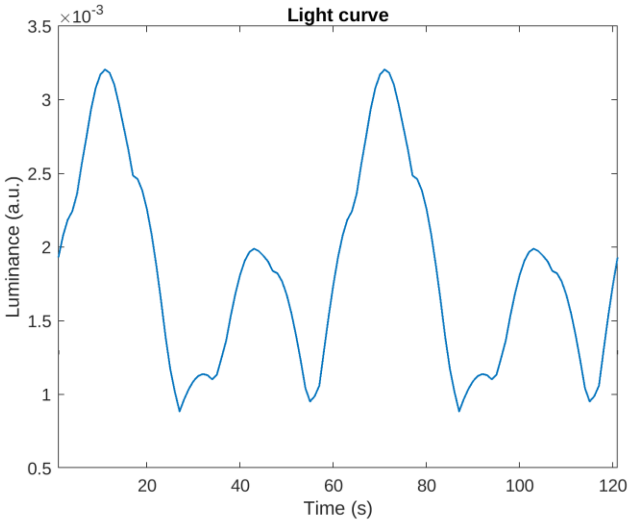

Endmember analysis

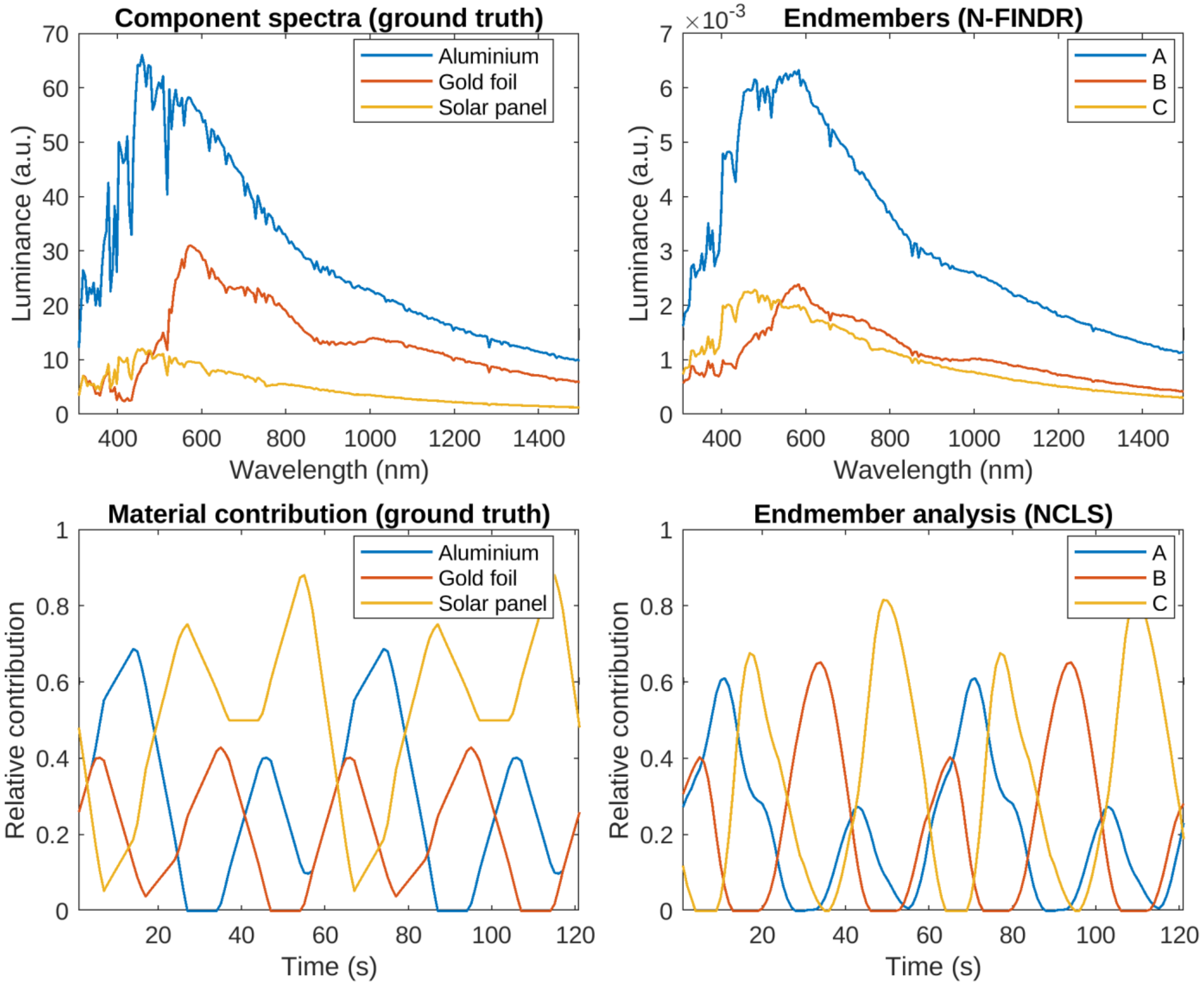

- Spectral angle mapper (SAM) for spectral matching

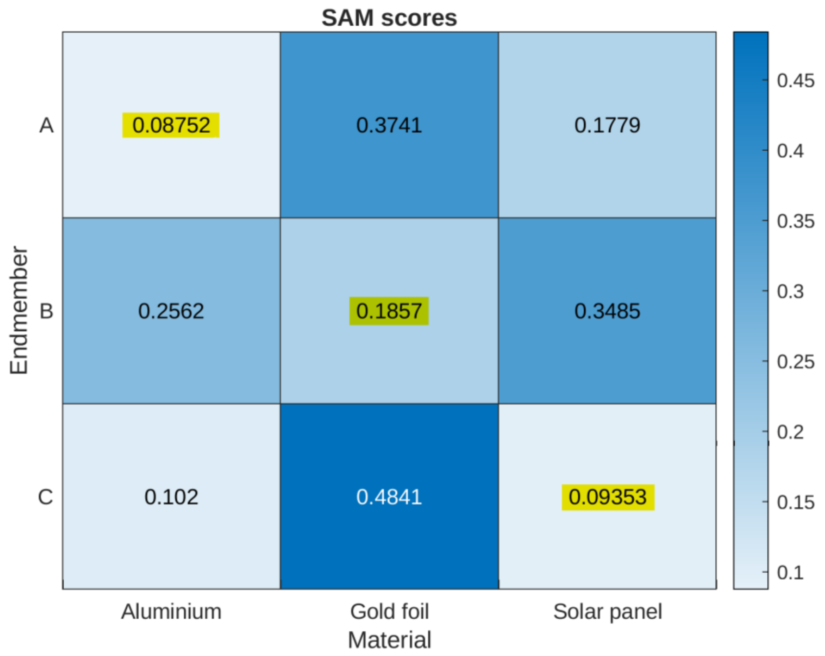

Endmember analysis

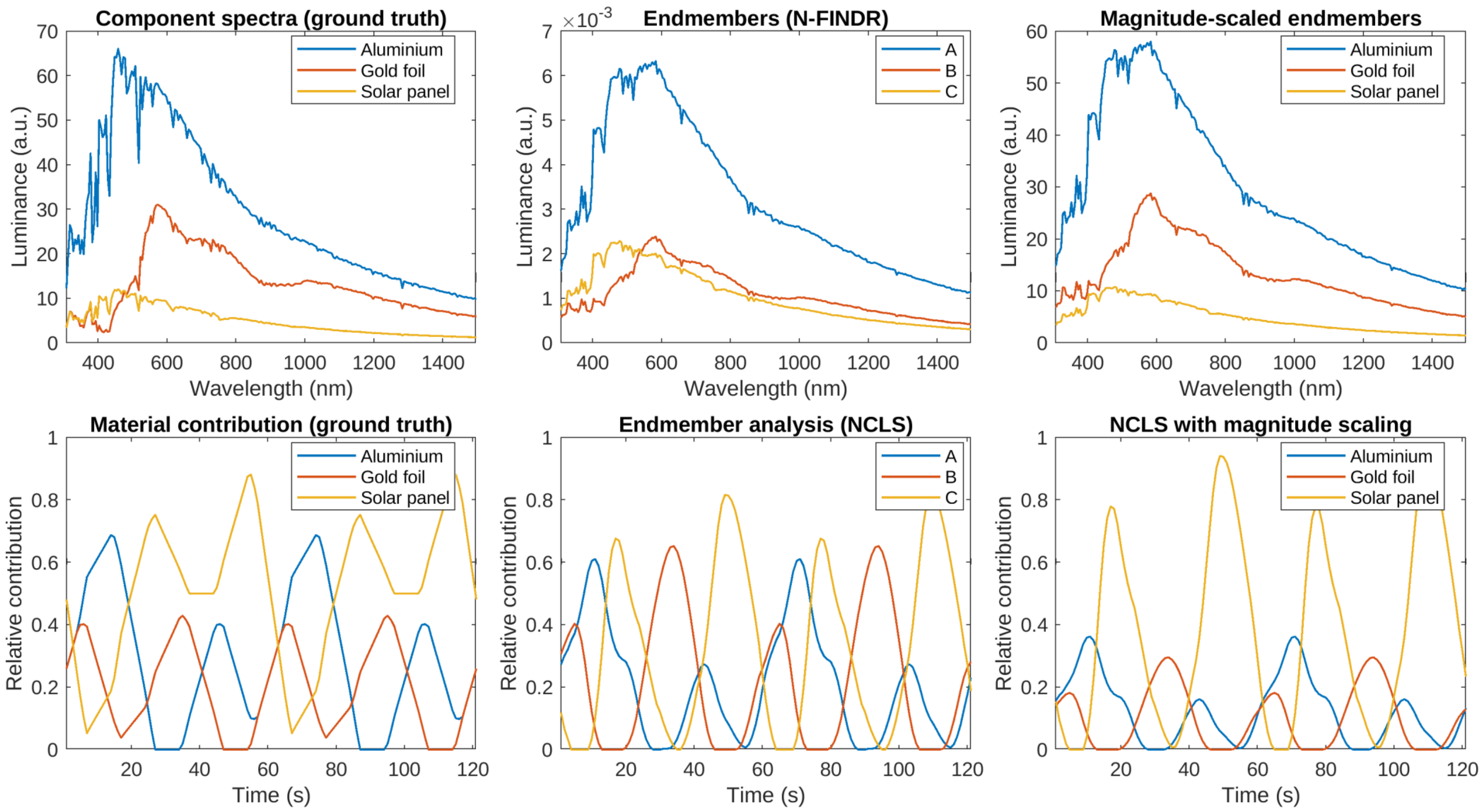

Endmember analysis

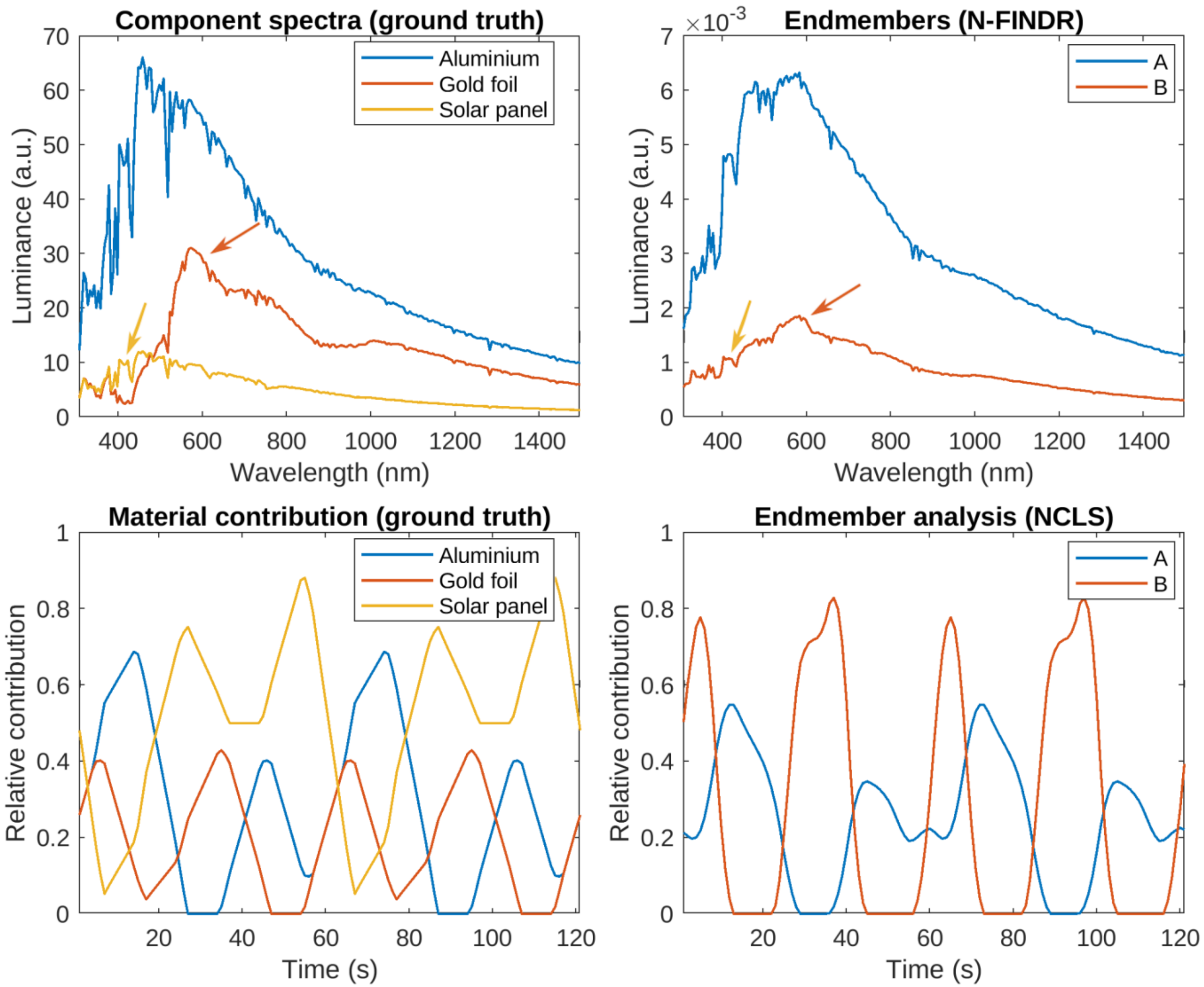

- With number of endmembers < number of ground truth materials
- Material B contains spectral properties of both gold and solar panel

Endmember analysis

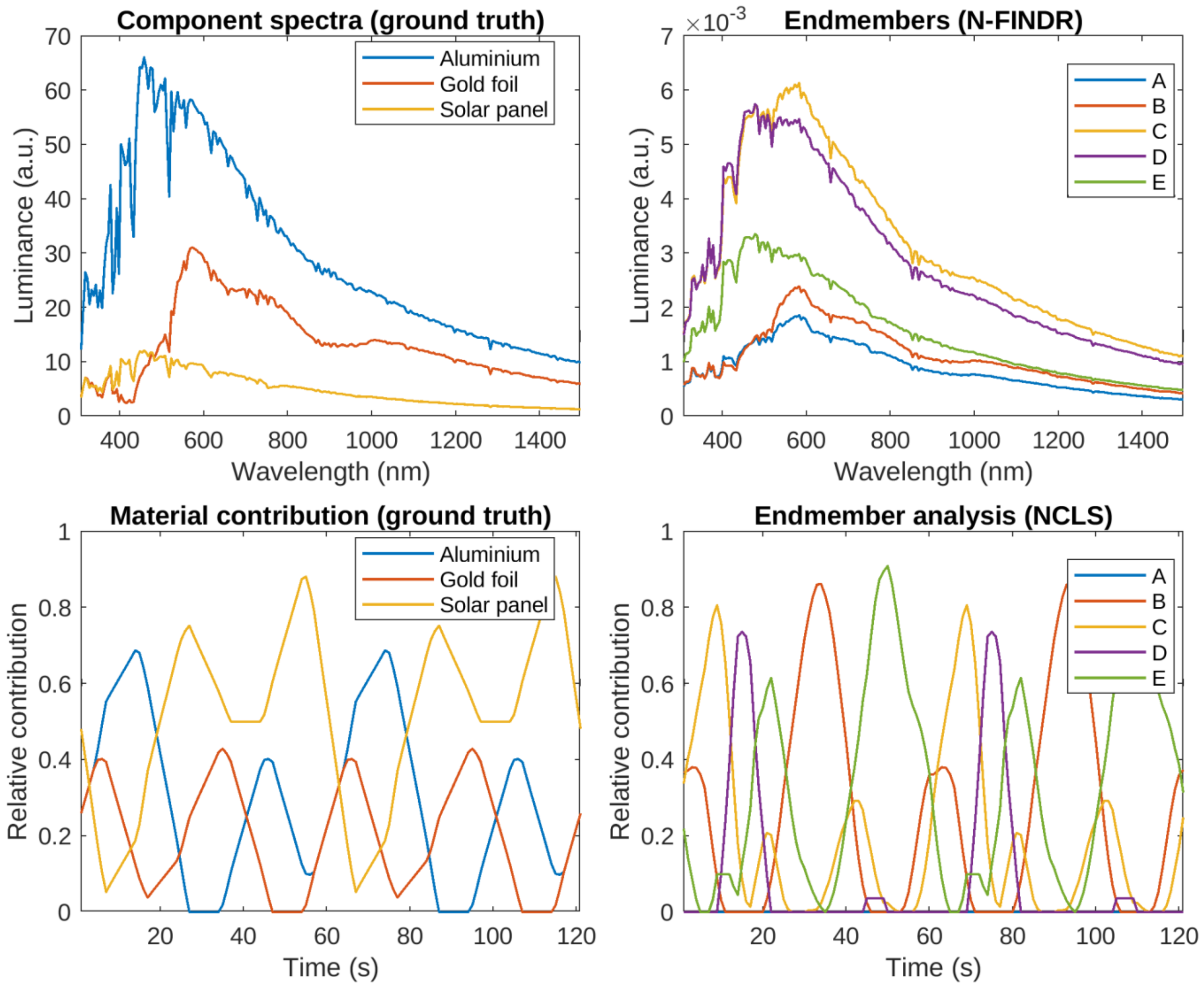

- With number of endmembers > number of ground truth materials
- Similar endmembers containing spectral properties of multiple materials
- Additional algorithms such as HFC can be used to establish correct number of endmembers

Simulation + Data Processing Pipeline

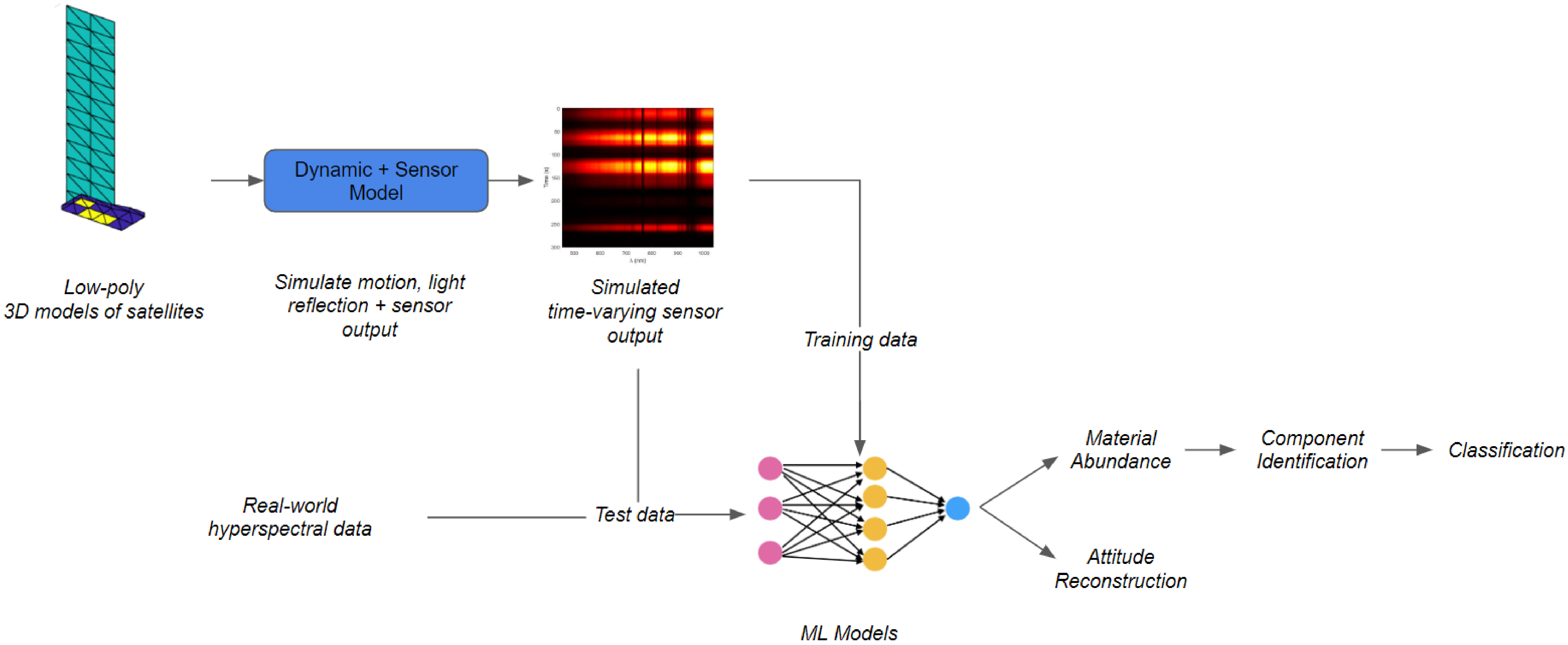

Material Abundance

- Previous work focuses on distinguishing e.g. two satellites
  - *No probing of materials*
  - *No other useful informaton gained*
  - *Does not generalise*
- Aim to classify based on key satellite components to build generalised pipeline
- Material abundance is key for detecting components
- Evolution of material abundance curves (MACs) over time (e.g. with rotation) contains information on distribution of materials
- Simulation model can output ground truth MAC
  - *Fraction of collected light due to each material at time t*
- Developed both traditional and ML-based methods to recover MACs

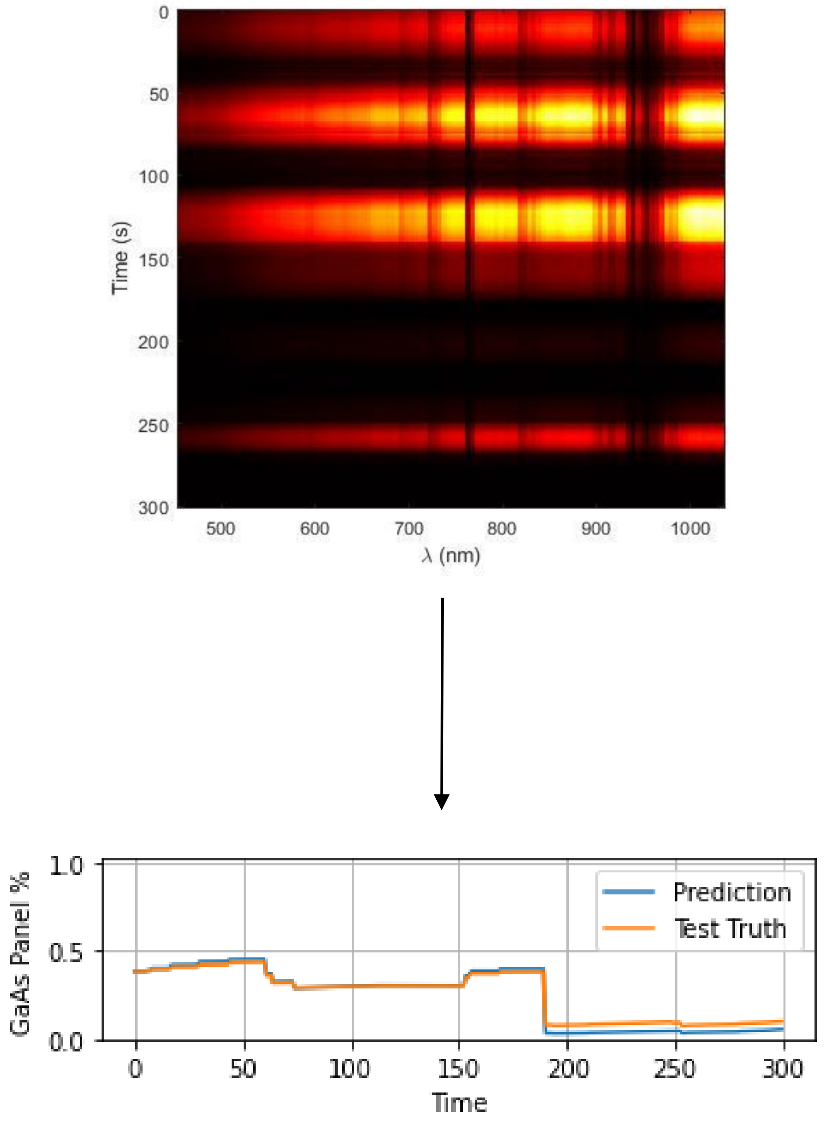

MAC with Machine Learning

- Artificial neural network trained on many linear combinations of N materials
  - *Basic feed-forward, fully-connected architecture*
  - *2 hidden layers (ReLU + tanh), 200/50 nodes*
  - *Softmax output activation: sum = 1 constraint*
  - *One output node per material*
- Color indexing transformation – removes absolute intensity variation, preserves shape
- Accurately extracts MACs for simulated data
  - *9 materials in current model*
- Model is inherently object-agnostic (generalised)

$$s(t,\lambda) \rightarrow -2.5\log_{10}\left(\frac{s(t,\lambda)}{s(t,\lambda_{ref})}\right)$$

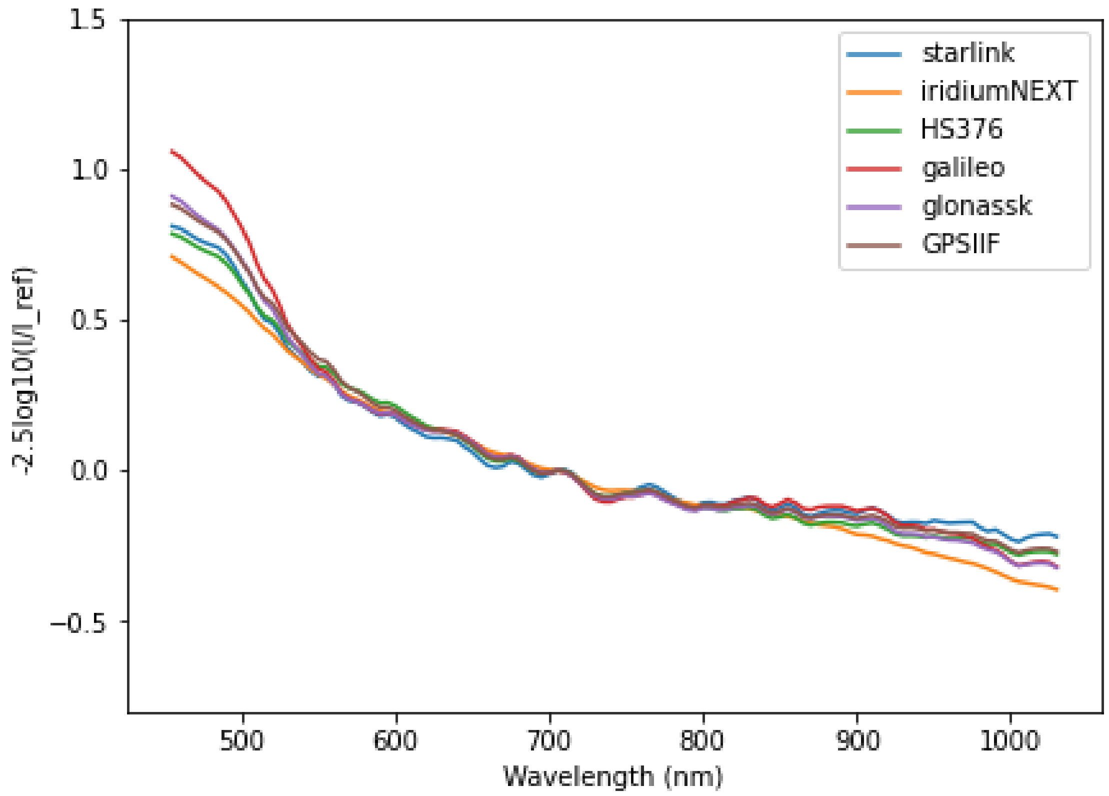

High-resolution colour indexing normalizes for signal strength

MAC with Machine Learning

- Artificial neural network trained on many linear combinations of N materials
  - *Basic feed-forward, fully-connected architecture*
  - *2 hidden layers (ReLU + tanh), 200/50 nodes*
  - *Softmax output activation: sum = 1 constraint*
  - *One output node per material*

- Color indexing transformation – removes absolute intensity variation, preserves shape

- Accurately extracts MACs for simulated data
  - *9 materials in current model*

- Model is inherently object-agnostic (generalised)

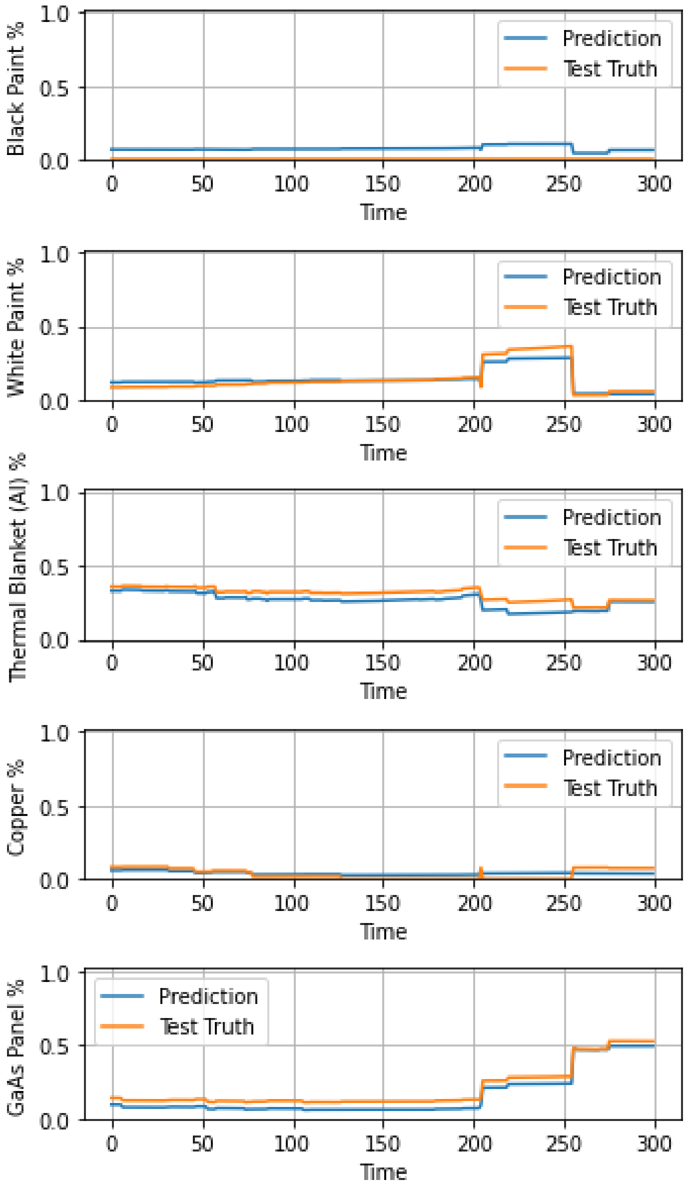

Non-ML Spectral Decomposition

- Also used non-ML methods (constrained least squares) to decompose spectra
- Similar performance is achieved from both methods
- Both methods considered semi-supervised
  - *Library must contain all dominant materials*

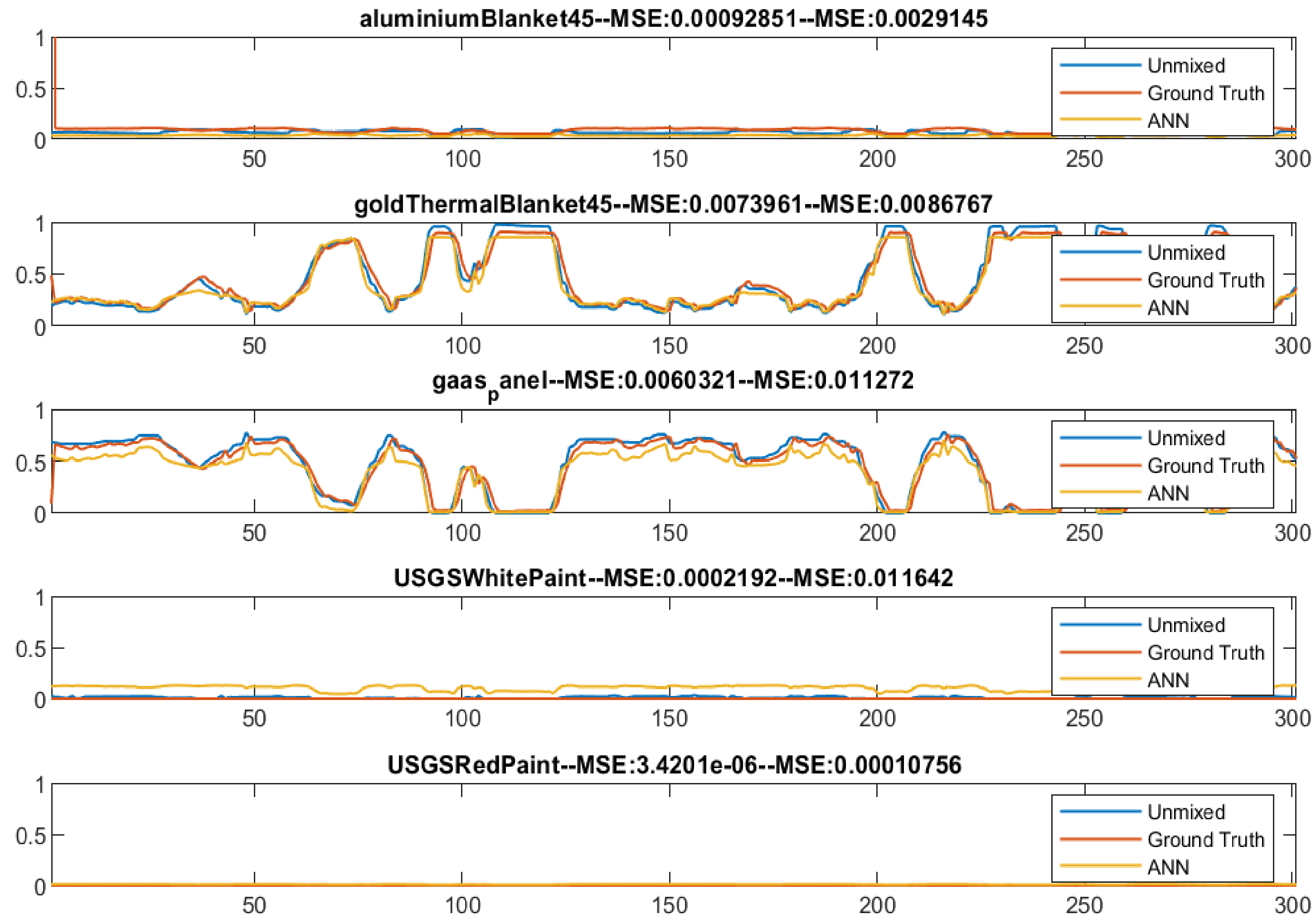

Component Detection Model

- Many satellites have large components made of distinctive materials
  - *Solar panels, Antennas, Rocket nozzle, Optics, TPCB*

- These should be detectable from MACs if:
  - *Components are composed of relatively unique materials*
  - *Components are large enough to cause detectable spectral changes*
  - *Object rotates sufficiently during integration period*

- Extract statistical features from set of 9 MACs
  - *Correlation coefficients, mean, std(), min(), max() etc...*

- Train ML models on MAC statistics
  - *Binary classifier for each component*
  - *Gradient boosted tree ensemble (XGBoost)*

Satellite	Solar arrays	Rocket Nozzle	Antenna	Baffle	TPCB[1]
Iridium-NEXT	1	0	1	0	1
Starlink	1	0	1	0	0
HS376	1	0[2]	1	0	0
GPS Block IIF	1	0	1	0	1
GLONASS-K	1	0	1	0	1
Galileo	1	0	1	0	1
DubaiSat-2	1	0	0	1	1
Landsat-8	1	0	0	1	1
CALIPSO	1	0	0	1	1
Proced'l Upper Stage	0	1	0	0	0
Proced'l Box-Wing	1	0	0	0	1
Proced'l CubeSat (panels)	1	0	0	0	0
Proced'l CubeSat (no panels)	0	0	0	0	0

Component Detection Model: Training Data

- Training data for component detection comes from a variety of 3D satellite models
  - *Assign material spectra to each polygon*
  - *Pure materials or combinations*
- Some based on real satellites, some generic templates with procedural generation e.g. Upper Stage
- 2000 simulations for each satellite, each with different orbital conditions and initial angular velocity vector
  - *Observer on ground*
- Dataset augmented by a set of cubes with similar material distribution
  - *e.g. cube with one face dominated by titanium (Rocket Nozzle)*
- Extremely high accuracy when tested on data from a 'seen' satellite:

Component	Panels	Engine	Antenna	Optics	TPCB
Error Rate	2.4%	5.8%	6.5%	2.4%	5.1%

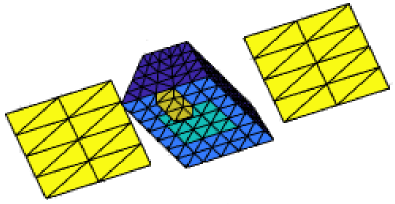

Iridium-NEXT

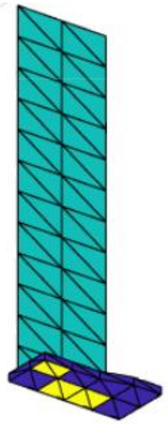

Starlink

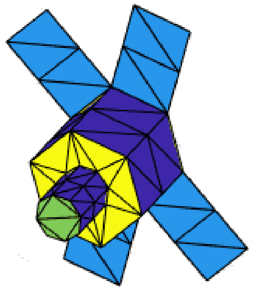

DubaiSat

3D models of various satellites used for training data generation

Final Classification

- Finally, classify satellites, based on detected components, into broad categories
  - *Comms, GNSS, EO, Rocket Bodies, CubeSats*
  - ***Not** aiming to determine the exact satellite*

- Final classification performed using k-Nearest Neighbours

Satellite	Classification	Solar arrays	Rocket Nozzle	Antenna	Baffle	TPCB[1]
Iridium-NEXT	Comms	1	0	1	0	1
Starlink	Comms	1	0	1	0	0
HS376	Comms	1	0[2]	1	0	0
GPS Block IIF	GNSS	1	0	1	0	1
GLONASS-K	GNSS	1	0	1	0	1
Galileo	GNSS	1	0	1	0	1
DubaiSat-2	Earth Obs.	1	0	0	1	1
Landsat-8	Earth Obs.	1	0	0	1	1
CALIPSO	Earth Obs.	1	0	0	1	1
Proced'l Upper Stage	Rocket Body	0	1	0	0	0
Proced'l CubeSat (panels)	CubeSat	1	0	0	0	0
Proced'l CubeSat (no panels)	CubeSat	0	0	0	0	0

Truth table for each satellite's present components, and the category it resides in

Generalisability of CDM and kNN

- Must test process on unseen satellites to ensure generalisability

- Procedure:
  - *Retrain CDM on MACs for all satellites* ***except*** *satellite X*
  - *Make predictions on MACs* ***from satellite X***
  - *Pass predictions through kNN to make final classification*
  - *Repeat for each satellite in the list*

- EO is the most challenging class
  - *Distinctive feature: optical baffle*
  - *Modelled by black paint – low, flat reflectance spectrum*
  - *Difficult to distinguish spectrally*

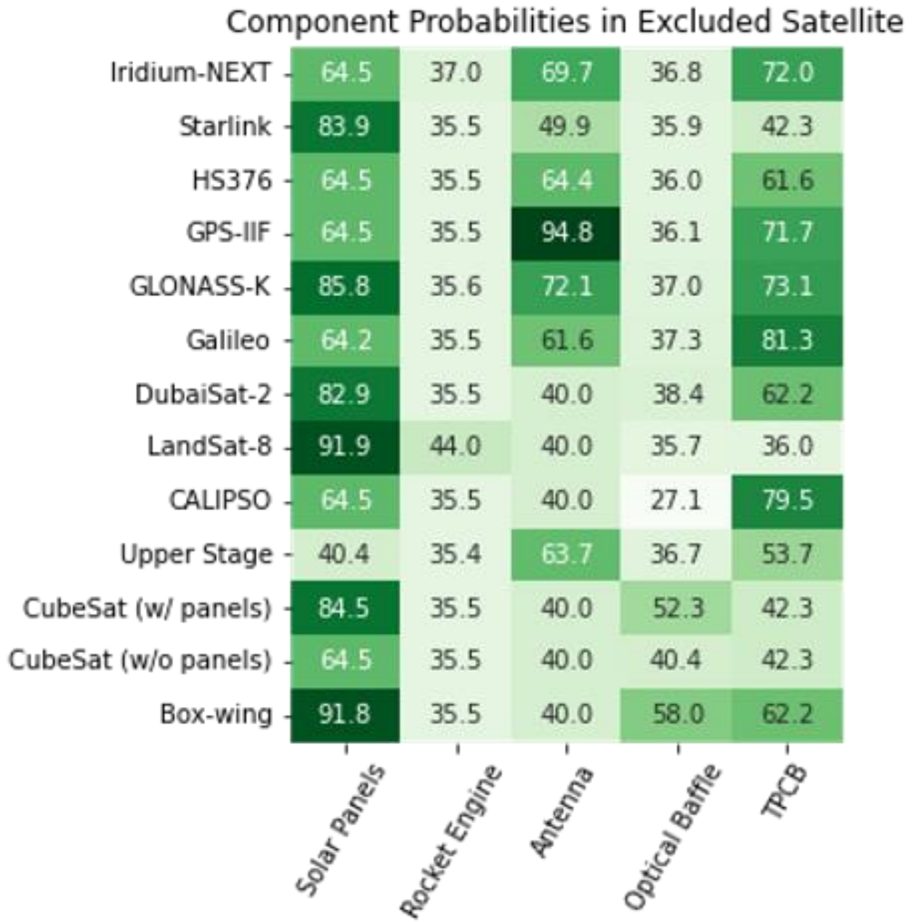

Average detection probability of each component for each unseen satellite.
(e.g. probability of CDM concluding that component Y is present)

Generalisability of CDM and kNN

AEROSPACE CENTRE of EXCELLENCE

- Must test process on unseen satellites to ensure generalisability

- Procedure:
  - *Retrain CDM on MACs for all satellites **except** satellite X*
  - *Make predictions on MACs **from satellite X***
  - *Pass predictions through kNN to make final classification*
  - *Repeat for each satellite in the list*

- EO is the most challenging class
  - *Distinctive feature: optical baffle*
  - *Modelled by black paint – low, flat reflectance spectrum*
  - *Difficult to distinguish spectrally*

True class		Comms	CubeSat	EO	GNSS	RocketBody
Comms	Iridium-NEXT	11.6	7.0	0.0	81.4	0.0
	Starlink	45.2	54.1	0.7	0.0	0.0
	HS376	99.5	0.4	0.0	0.1	0.0
GNSS	GPS-IIF	17.2	0.1	0.0	82.7	0.0
	GLONASS-K	0.6	0.9	0.0	98.6	0.0
	Galileo	0.0	0.2	0.0	99.8	0.0
EO	DubaiSat-2	0.0	0.1	0.0	99.9	0.0
	LandSat-8	0.0	100.0	0.0	0.0	0.0
	CALIPSO	0.0	2.1	14.5	83.4	0.0
RocketBody	Upper Stage	0.0	89.5	0.0	10.5	0.0
CubeSat	CubeSat (w/ panels)	0.0	99.7	0.3	0.0	0.0
	CubeSat (w/o panels)	0.0	99.9	0.1	0.0	0.0

Classification probability of each unseen satellite

Aged Materials

- Aim to investigate effect of inaccurate library spectra on ANN decomposition performance

- Literature: aging causes a 'reddening' of spectral response
  - No model exists -> use approximation

- Simulate aging by boosting red/NIR+ wavelengths
  - R(λ) -> red_boost_function(λ)*R(λ)
  - Ex
    - *R(500) -> 1*R(500)*
    - *R(1000) -> 1.1*R(1000)*

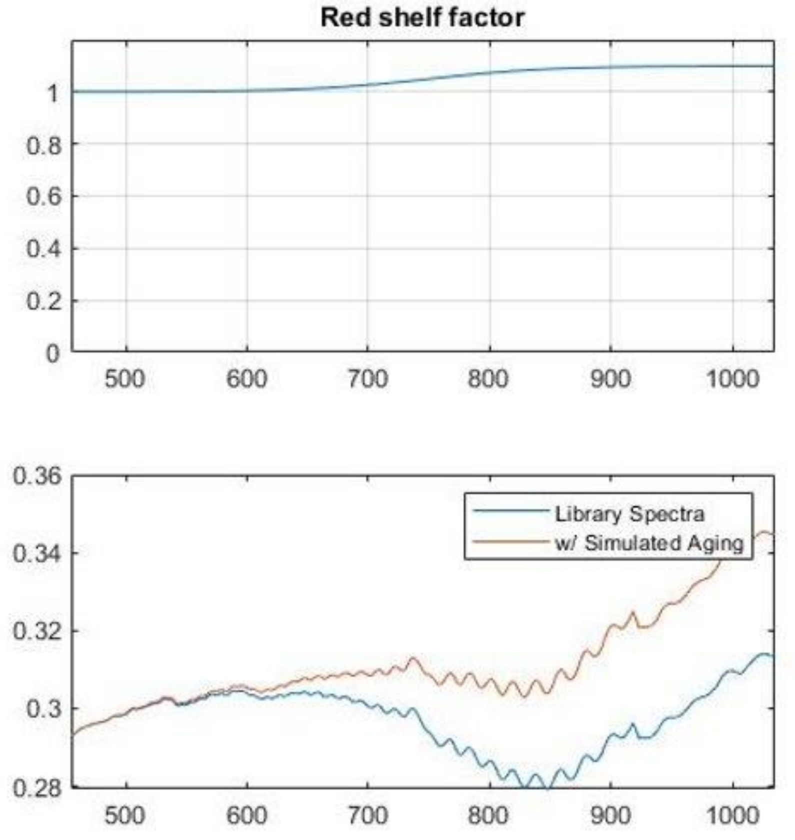

Simulated aging applied to Aluminium Spectrum

Aged Materials

- Retrained decomposition ANN with aged spectra
- Similar quality of predictions as with noon-aged materials

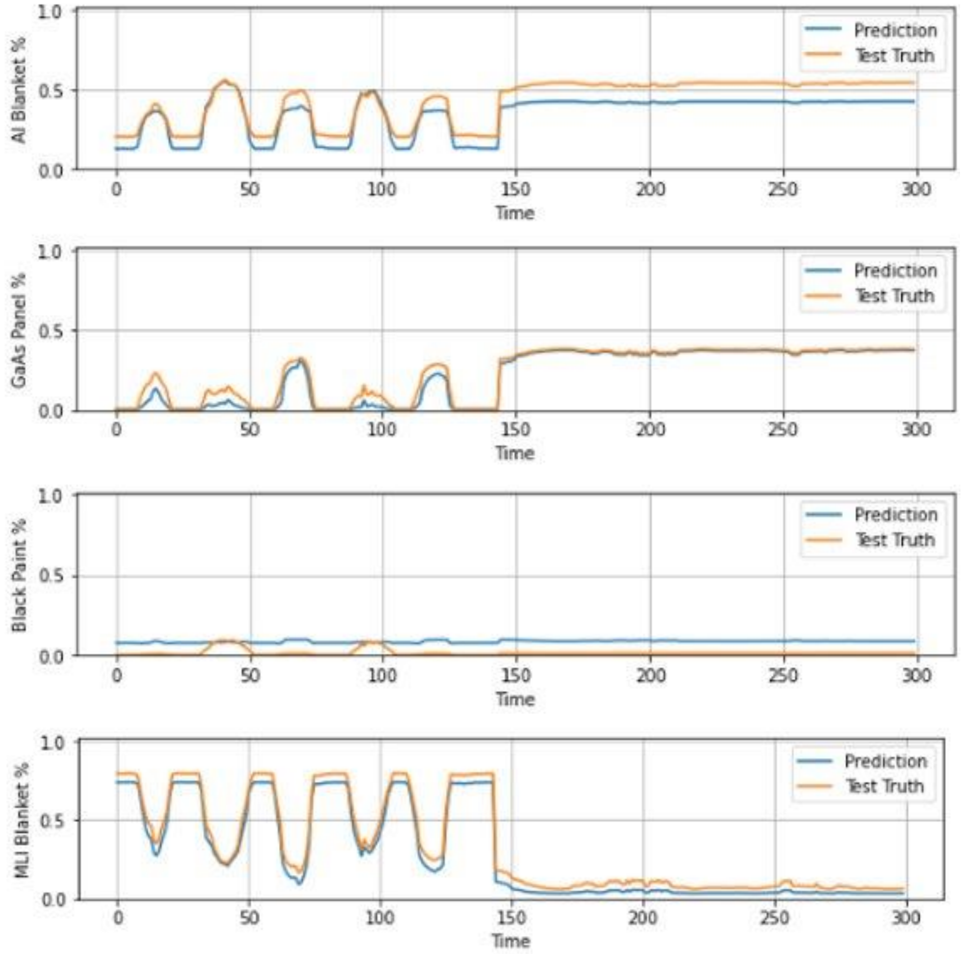

Aged Materials

- Generate data for satellites using aged spectra
- Make predictions with **old** ANN
  - *Trained on unaged ('incorrect') spectra*
- Significantly higher MSE with aging mismatch
- Overall curve shapes preserved but magnitudes incorrect
- Systematic overestimation of black paint
  - *Other materials 'squashed' to compensate*

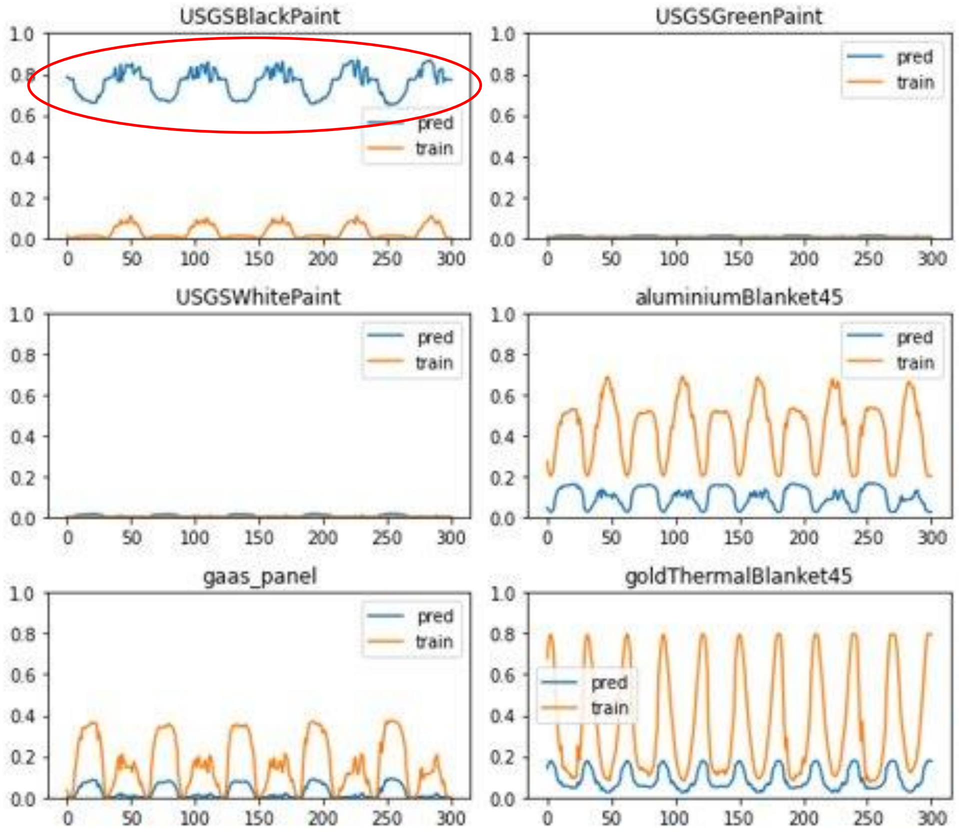

DubaiSat (aged)

Aged Materials

- Significantly higher MSE with aging mismatch
- Overall curve shapes preserved but magnitudes incorrect
- Systematic overestimation of black paint
  - *Other materials 'squashed' to compensate*

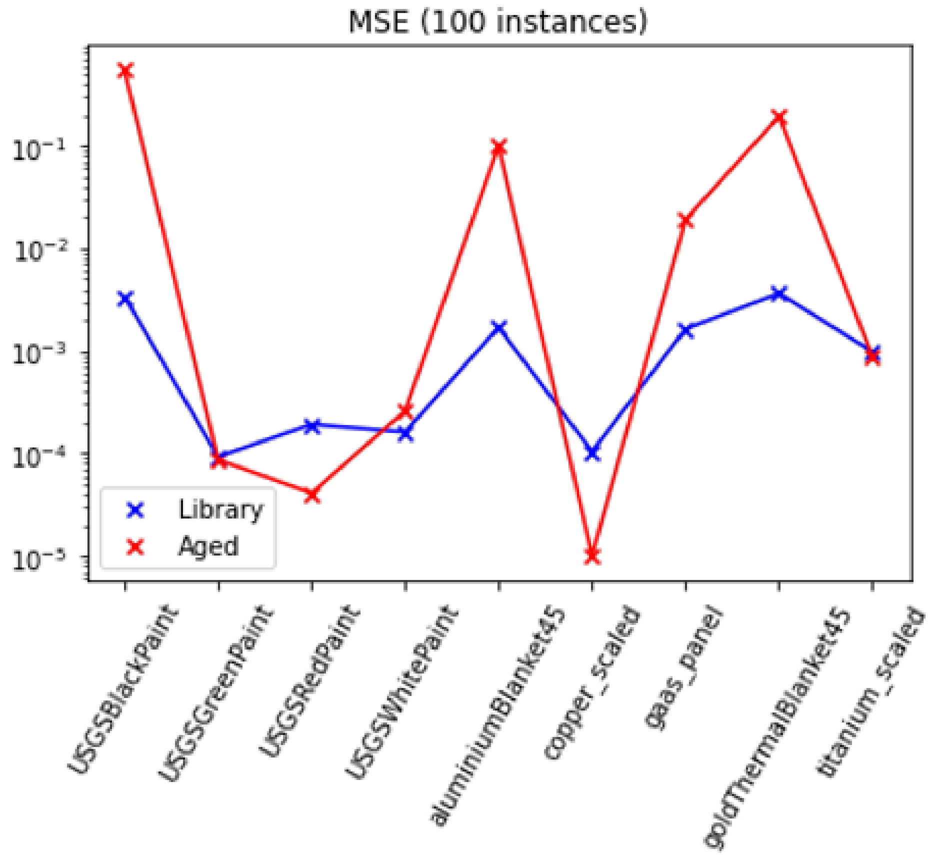

Material-wise MSE

Present materials -> higher MSE
Absent materials -> lower MSE
(squashed closer to zero)

Aged Materials

- Repeat with increasing red boost max values (ie increased aging)
  - 1.0
  - 1.025
  - 1.05
  - 1.075
  - 1.1

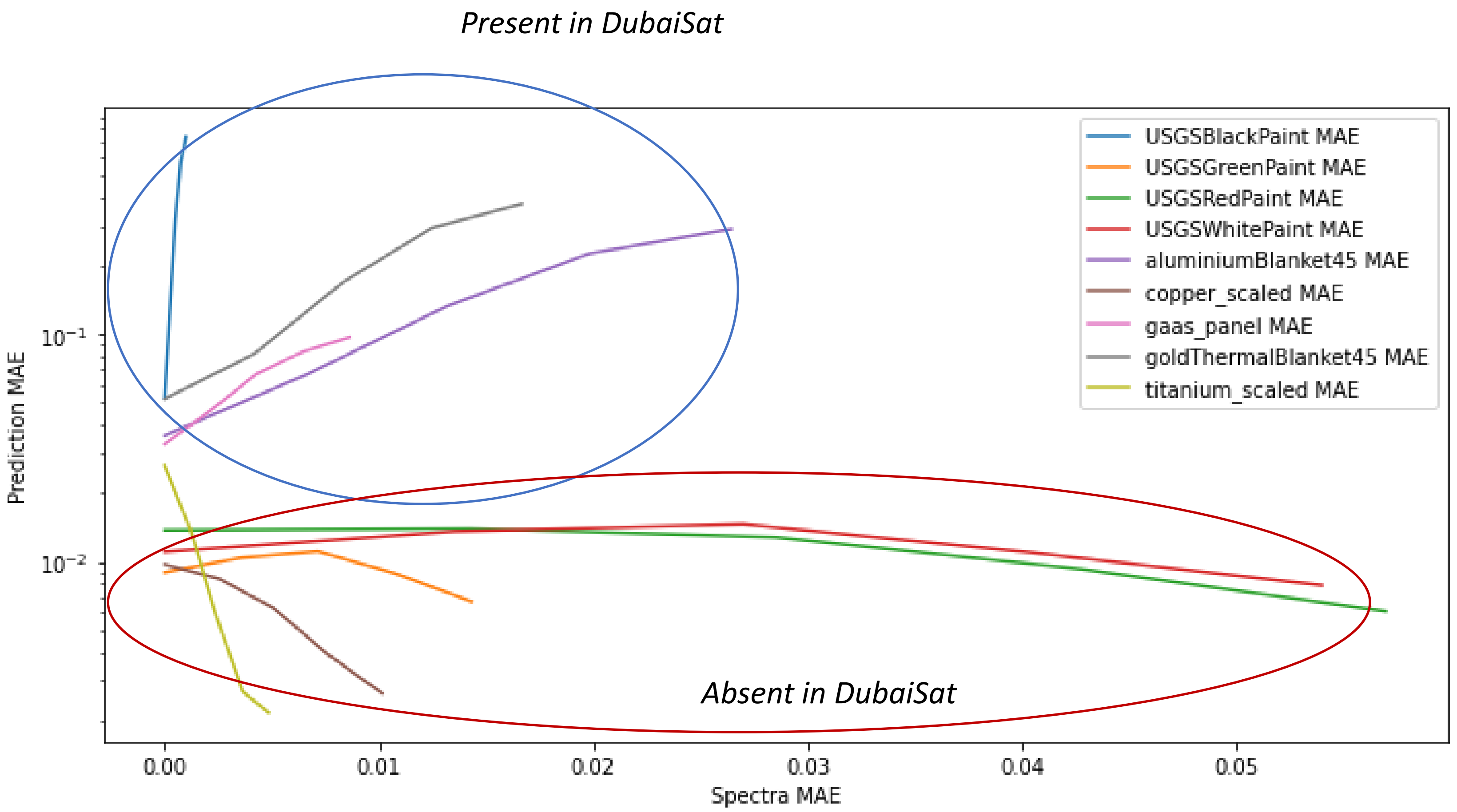

Aged Materials

- The non-machine learning library unmixing method has a few post processing steps
- This is applied to both library spectra and the received signal so will affect the difference between aged and non-aged materials
- It is not entirely clear if this has a net benefit and will depend on how aging really effects materials

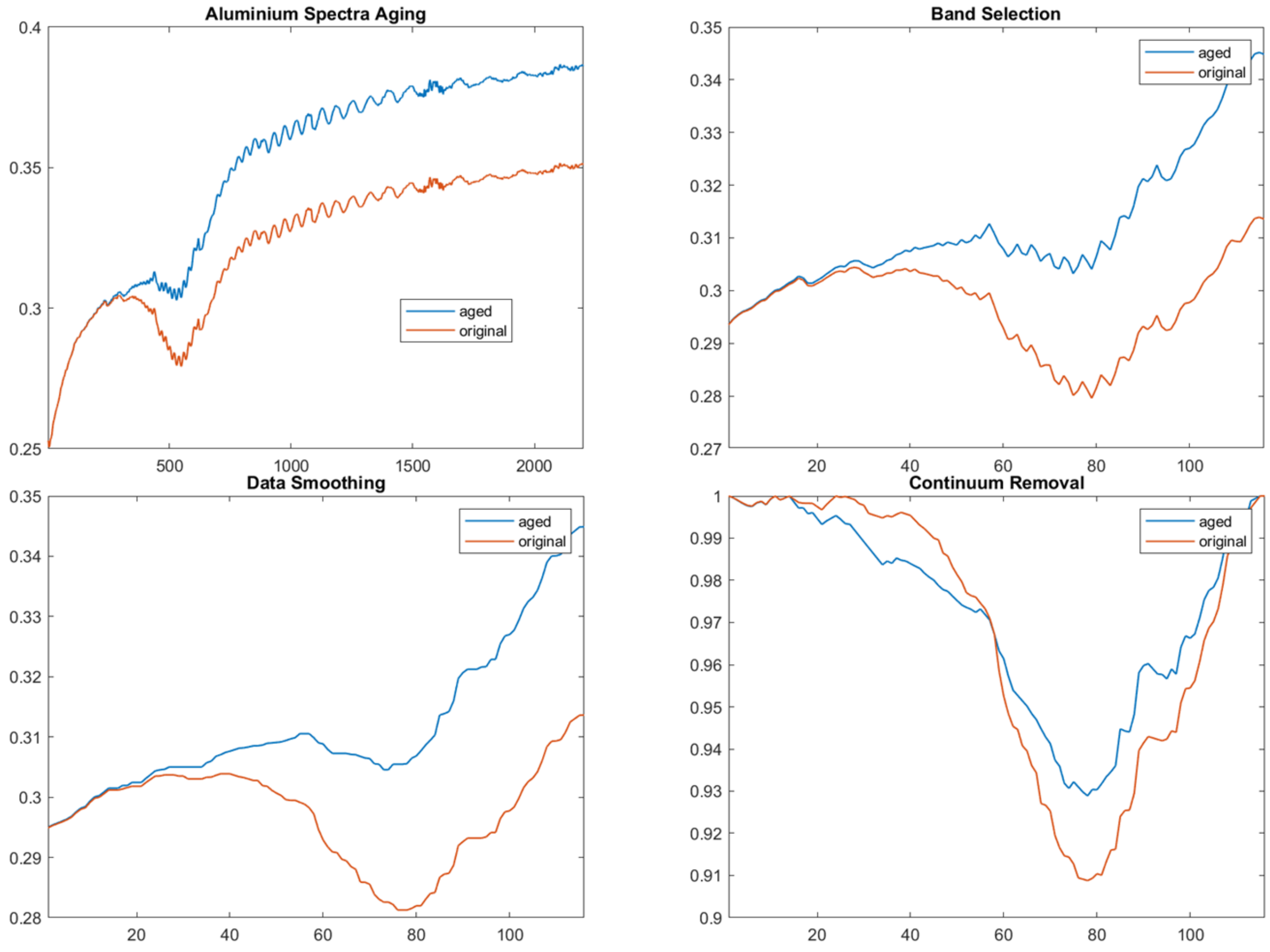

Non-machine learning processing of aged aluminium spectra

Aged Materials

- Aged spectra produce errors when performing library unmixing though these are different than experienced by the machine learning method
- Rather than a clear over or under estimation bias the general estimate is close but the trends in subtle changes to material abundance are missed

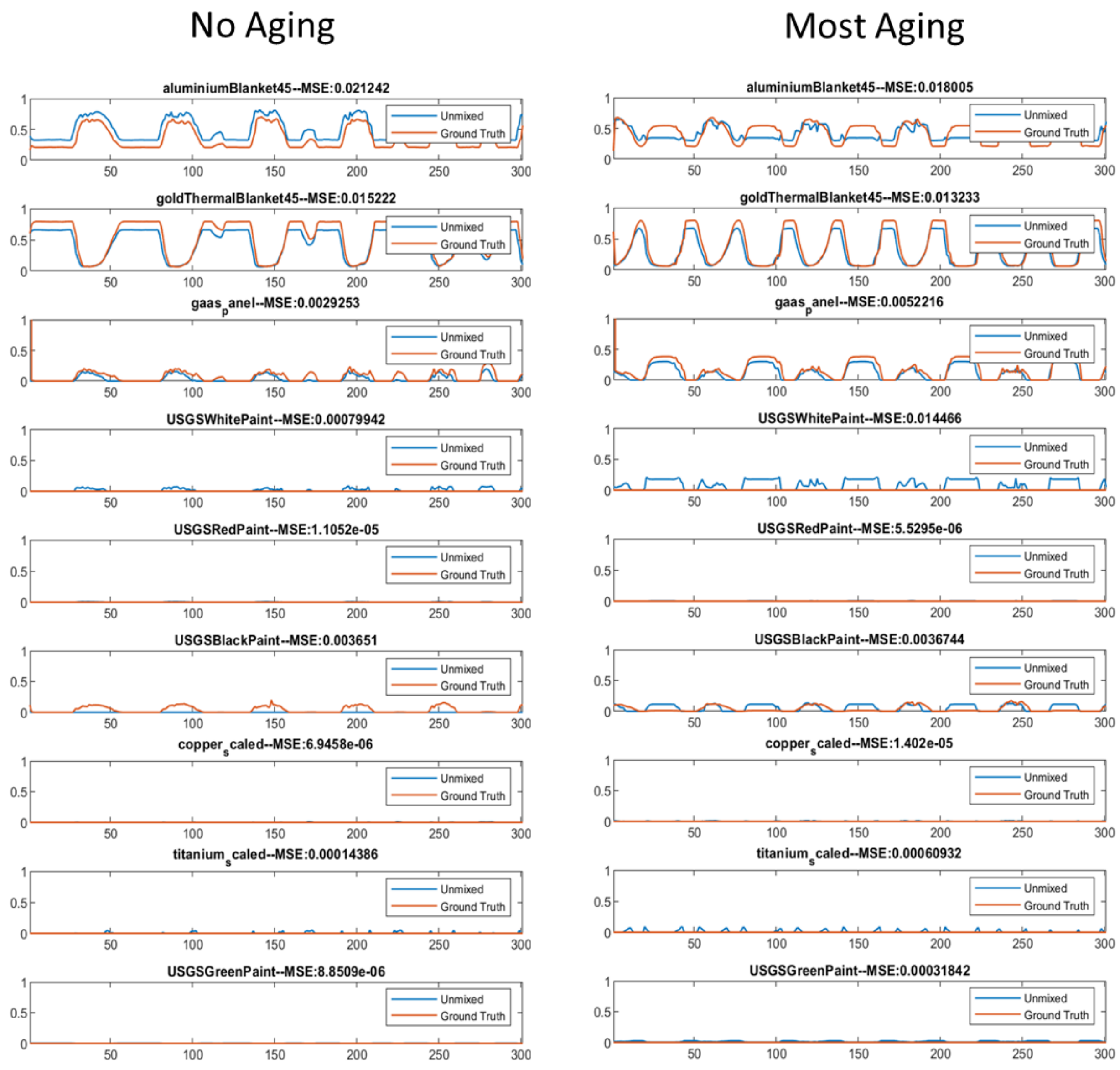

Library matching performance on aged spectra

Aged Materials

- As with machine learning methods updating the model, in this case by using a library containing aged spectra, improves results

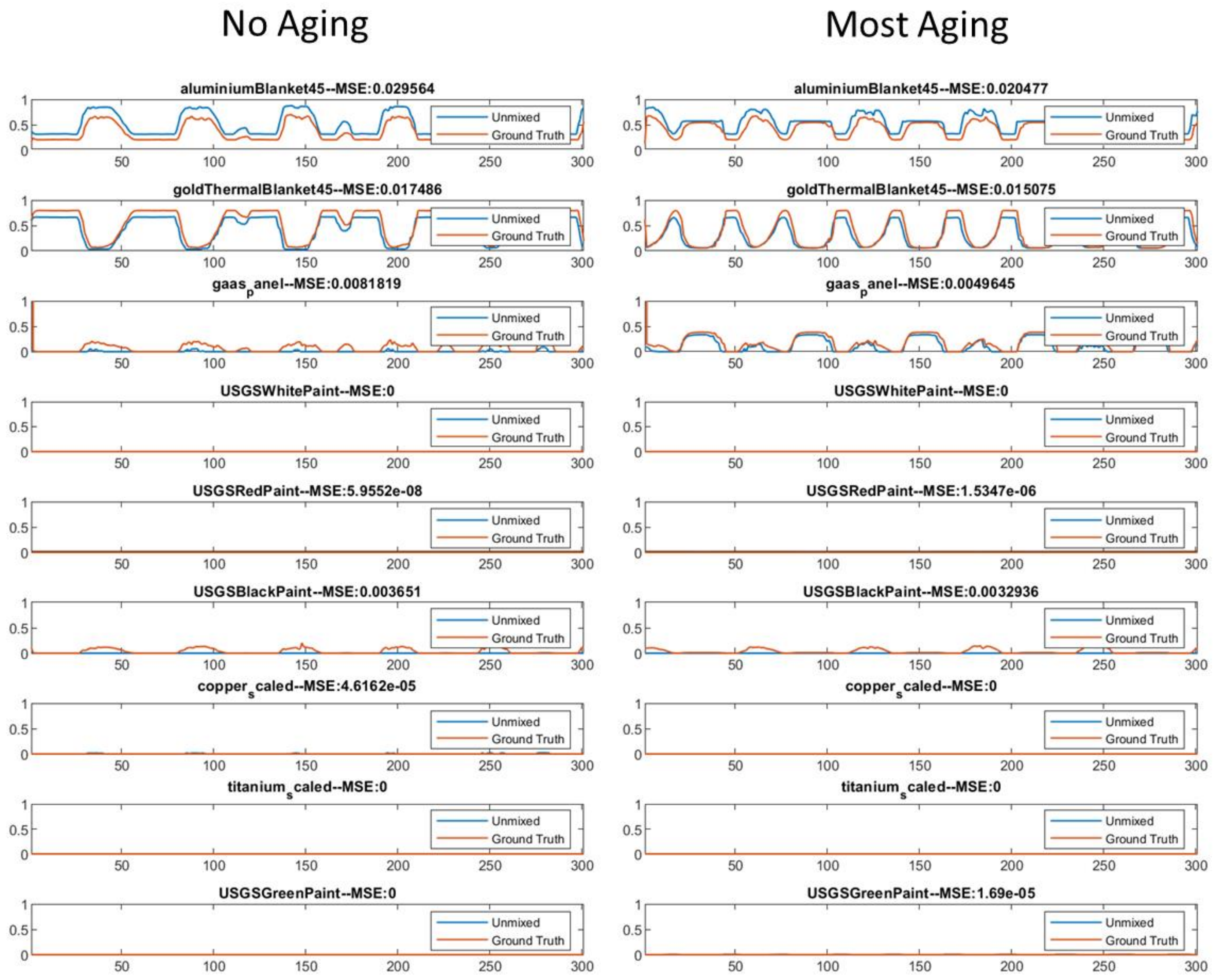

Updated library matching performance on aged spectra

Aged Materials

AEROSPACE CENTRE of EXCELLENCE

- Added l1 output regularization to address black paint boosting

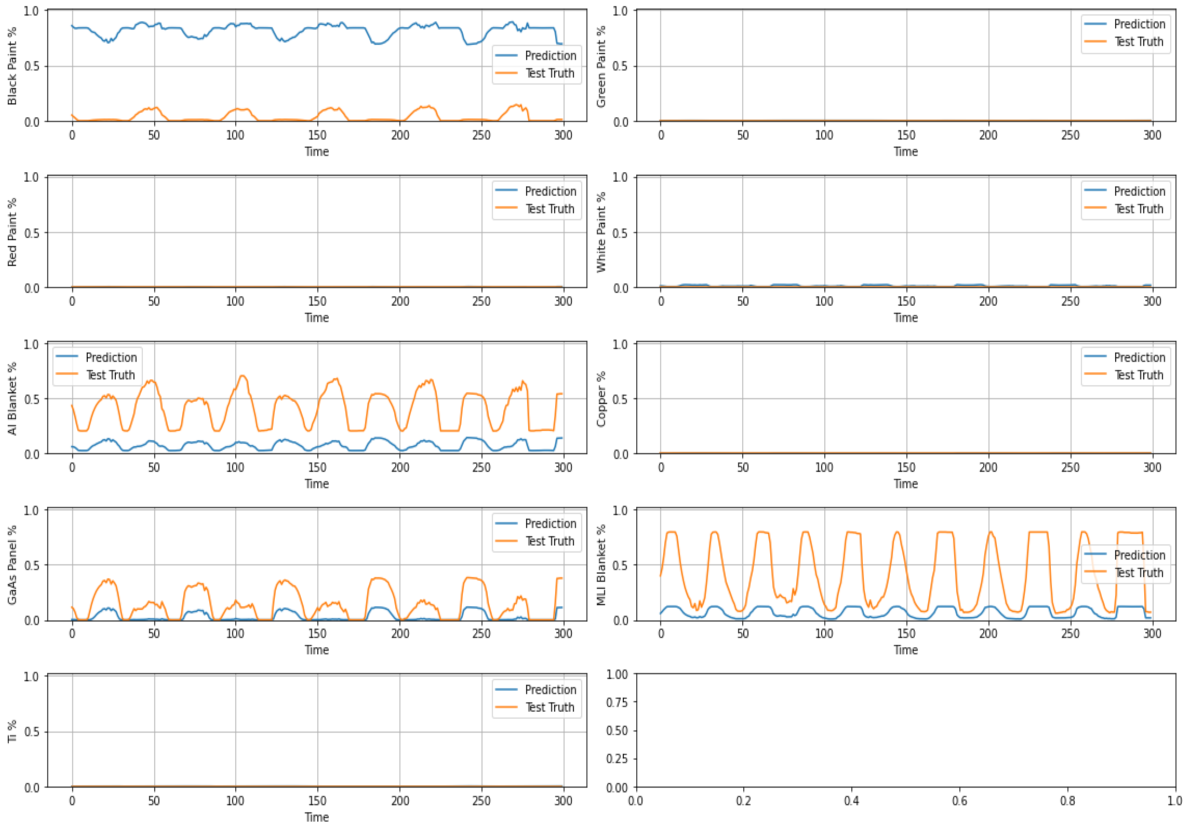

No Regularization
MSE = 0.11133

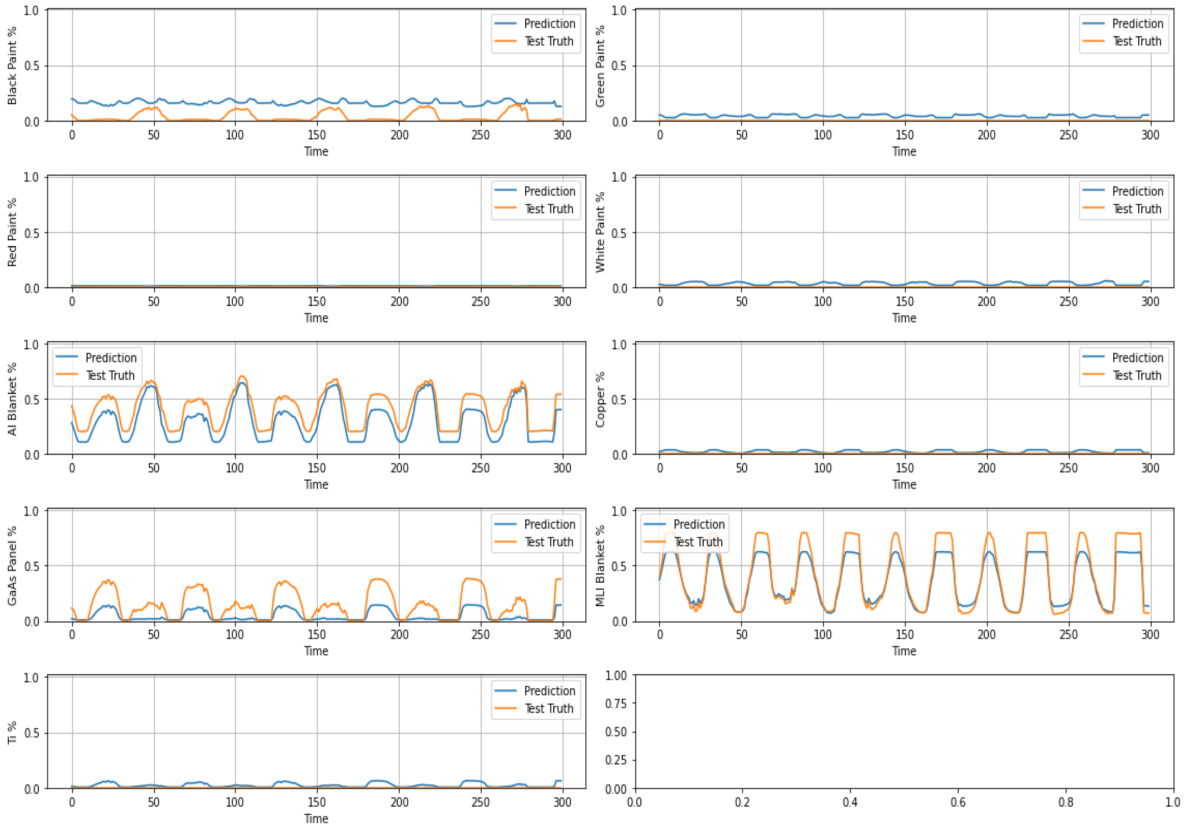

Aggressive regularization on black paint (lambda = 1)
MSE = 0.0071

Residuals with ML

- Retrain material curve ANN sans one material (GaAs Panel)
- Make predictions for a satellite (containing missing material) using new model

Black paint overestimation

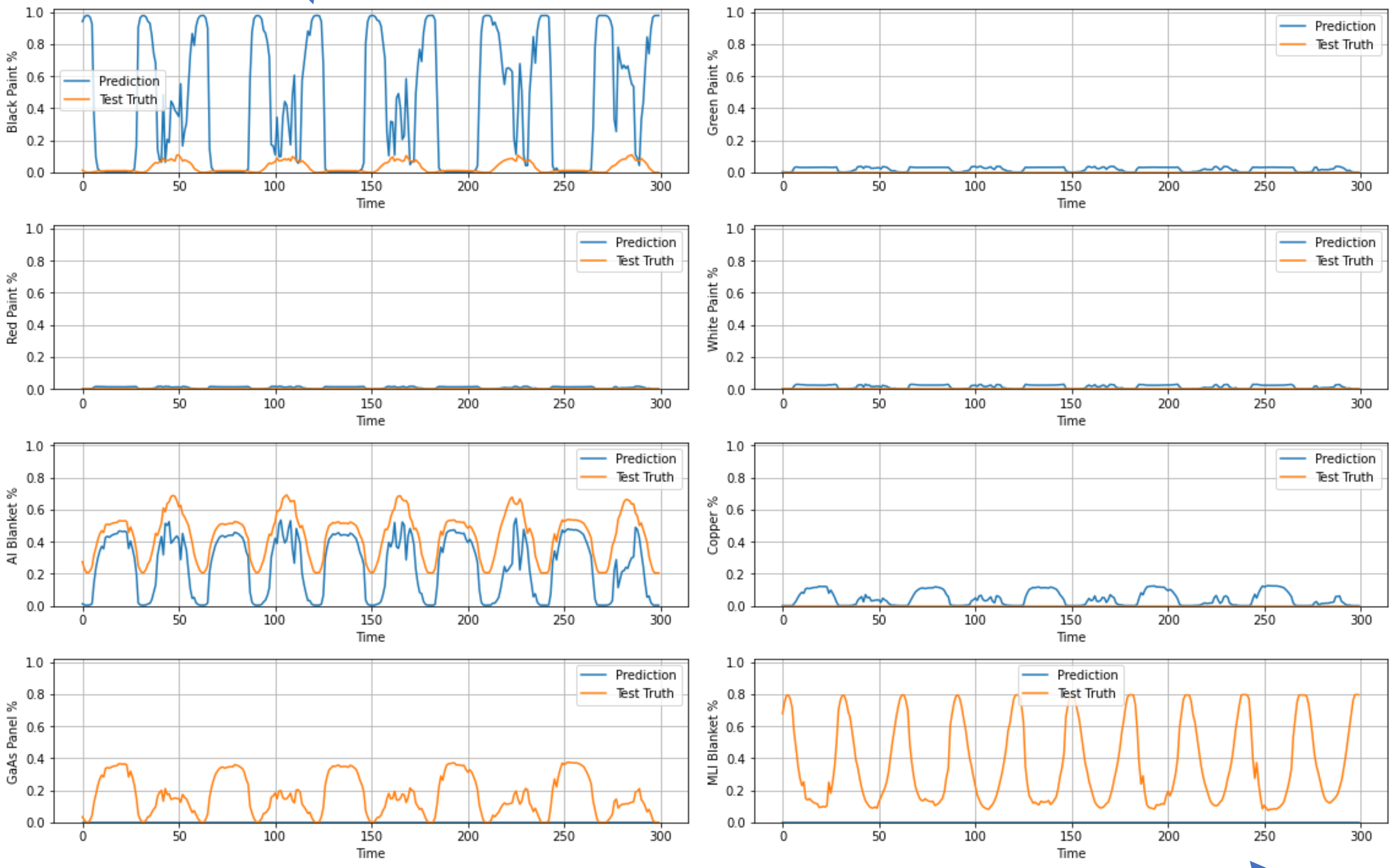

Material predictions for DubaiSat (model trained without GaAs)

Gold blanket underestimation

Residuals with ML

- Can recover missing material spectrum form residual

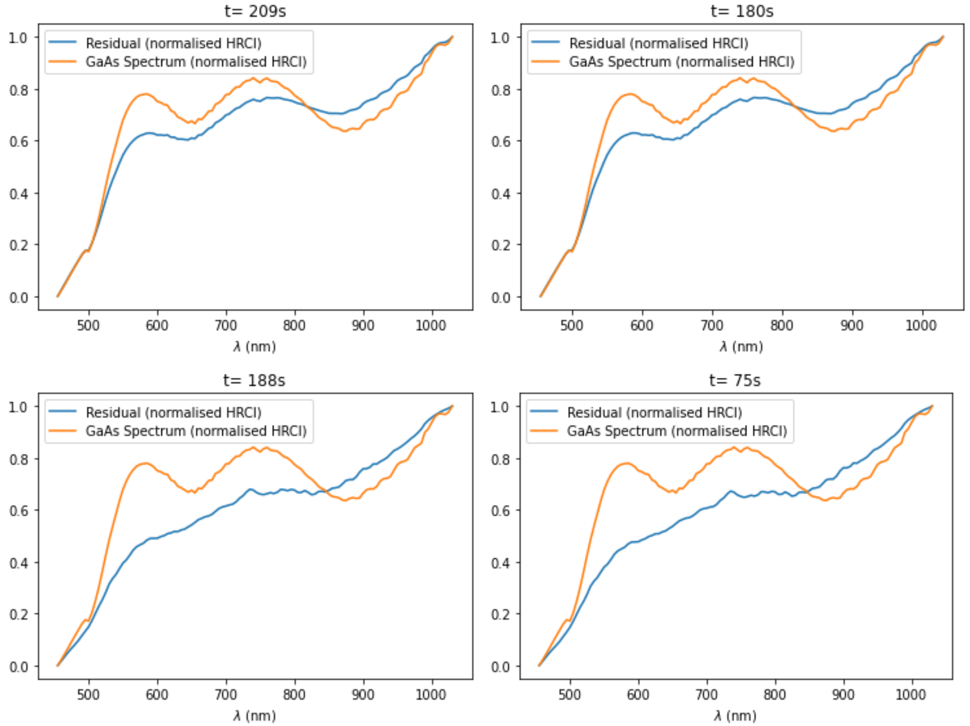

Residual at various times compared with GaAs spectrum

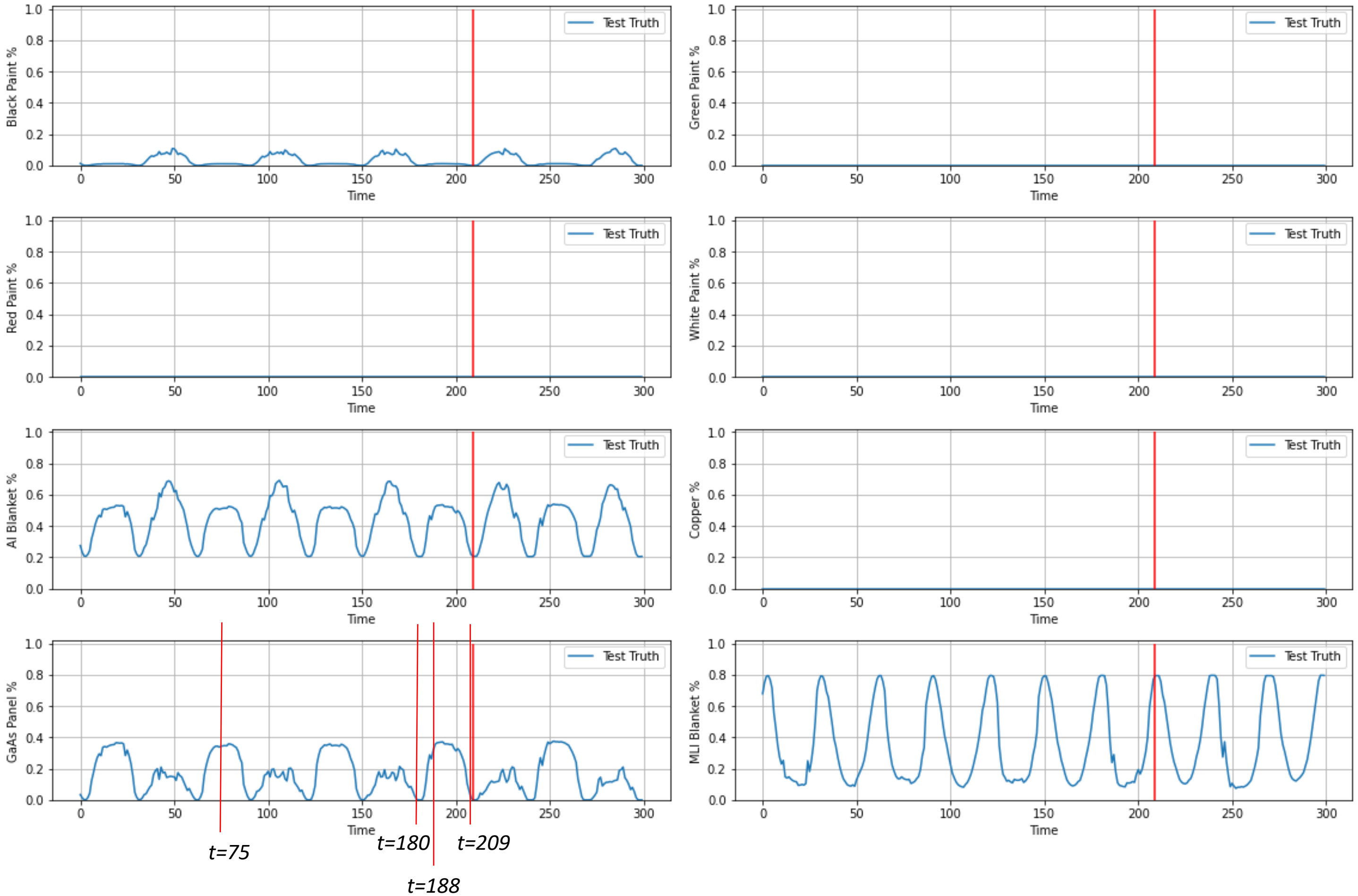

DubaiSat material contribution truth

Material Identification and Abundance

AEROSPACE CENTRE of EXCELLENCE

Unmixed Abundance

	GaAs	Aluminium	White Paint	Black Paint	Green Paint	Red Paint	Copper	Titanium	Gold
starlink	0.5658	0.2366	0.02134	0.05147	0.006672	0.01483	0.05622	0.03234	0.0147
iridiumNEXT	0.2466	0.2737	0.1045	0.05645	0.01379	0.01255	0.04354	0.0545	0.1944
HS376	0.6033	0.08568	0.09032	0.06008	0.005926	0.01683	0.0369	0.07778	0.02318
Upper Stage	0.01678	0.1393	0.5294	0.04499	0.01704	0.05019	0.03507	0.05607	0.1111
CubeSat(no panel)	0.0163	0.5035	0.0287	0.04195	0.3526	0.006248	0.005361	0.02163	0.02369
CubeSat(with panel)	0.2718	0.3352	0.02467	0.05638	0.2391	0.007772	0.008768	0.02418	0.03204
galileo	0.3994	0.03747	0.01884	0.04028	0.008942	0.007975	0.05012	0.01917	0.4177
calipso	0.616	0.0279	0.02317	0.09499	0.006622	0.006661	0.008309	0.01771	0.1985
glonassk	0.363	0.03343	0.1245	0.0638	0.01257	0.00939	0.02277	0.0327	0.3379
GPSIIF	0.4553	0.165	0.03626	0.0449	0.008395	0.01647	0.149	0.02781	0.09686
landsat8	0.3135	0.4182	0.1019	0.07372	0.006833	0.01408	0.01739	0.03617	0.01819
dubaiSat	0.09151	0.3643	0.02252	0.02977	0.01205	0.00552	0.01465	0.03397	0.4257
BoxWing	0.2951	0.0422	0.02603	0.04114	0.009918	0.004095	0.007879	0.02526	0.5484
dragon2	0.1853	0.04519	0.5874	0.0724	0.01521	0.01149	0.0248	0.04302	0.01513

Real Abundance

	GaAs	Aluminium	White Paint	Black Paint	Green Paint	Red Paint	Copper	Titanium	Gold
starlink	0.6185	0.2714	0	0	0	0	0.08563	0	0
iridiumNEXT	0.2513	0.297	0.1501	0	0	0	0.04649	0	0.2291
HS376	0.6357	0.07693	0.09237	0.1098	0	0.01297	0.02524	0.02744	0.01923
Upper Stage	0	0.1144	0.4382	0.2197	0	0.05659	0	0.04996	0.1205
CubeSat(no panel)	0	0.5508	0	0	0.4165	0	0.02491	0	0
CubeSat(with panel)	0.305	0.3711	0	0	0.2923	0	0.02231	0	0
galileo	0.4204	0.05817	0	0.006908	0	0	0.05339	0	0.4592
calipso	0.5382	0.04877	0	0.2169	0	0	0	0	0.1951
glonassk	0.3992	0.001392	0.1545	0.001392	0	0	0.02227	0	0.413
GPSIIF	0.476	0.1737	0.03425	0.01105	0	0	0.169	0	0.1326
landsat8	0.3543	0.4893	0.1446	0.01111	0	0	0	0	0
dubaiSat	0.1078	0.371	0	0.02841	0	0	0	0	0.4914
BoxWing	0.3124	0.07125	0	0.01504	0	0	0	0	0.5978
dragon2	0.2272	0.03075	0.6574	0.08403	0	0	0	0	0

Material Identification and Probability

Mean Probability of Detecting Materials

	GaAs	Aluminium	White Paint	Black Paint	Green Paint	Red Paint	Copper	Titanium	Gold
starlink	0.9413	0.7613	0.2573	0.5954	0.1491	0.2455	0.5519	0.3273	0.1835
iridiumNEXT	0.9696	1	0.9389	0.8706	0.2597	0.2608	0.7374	0.5536	0.9393
HS376	1	1	0.9999	0.9867	0.1356	0.3295	0.9927	0.9121	0.6339
Upper Stage	0.2649	0.8854	0.9993	0.9327	0.2275	0.823	0.5977	0.8982	0.8189
CubeSat(no panel)	0.2681	1	0.2776	0.4212	0.9677	0.1797	0.1121	0.3281	0.2283
CubeSat(with panel)	0.9829	0.9955	0.3024	0.8891	0.9767	0.2339	0.1896	0.3881	0.4928
galileo	0.994	0.9268	0.3894	0.7379	0.2092	0.2473	0.8974	0.3708	0.9997
calipso	1	0.5393	0.4129	0.9671	0.1265	0.1156	0.1025	0.3097	0.9993
glonassk	0.9923	0.7286	0.9869	0.9569	0.3496	0.2914	0.74	0.5781	0.9981
GPSIIF	0.9995	0.9879	0.8874	0.9224	0.2454	0.3617	0.9881	0.5161	0.987
landsat8	0.9967	0.9997	0.9923	0.9735	0.1771	0.211	0.2592	0.5393	0.2474
dubaiSat	0.9736	1	0.2783	0.4299	0.2265	0.1208	0.1858	0.4166	0.999
BoxWing	0.9958	0.6657	0.3893	0.5755	0.2173	0.1389	0.1223	0.3845	1
dragon2	0.9958	0.61	1	0.9206	0.2092	0.1274	0.3267	0.5225	0.1986

Real Abundance

	GaAs	Aluminium	White Paint	Black Paint	Green Paint	Red Paint	Copper	Titanium	Gold
starlink	0.6185	0.2714	0	0	0	0	0.08563	0	0
iridiumNEXT	0.2513	0.297	0.1501	0	0	0	0.04649	0	0.2291
HS376	0.6357	0.07693	0.09237	0.1098	0	0.01297	0.02524	0.02744	0.01923
Upper Stage	0	0.1144	0.4382	0.2197	0	0.05659	0	0.04996	0.1205
CubeSat(no panel)	0	0.5508	0	0	0.4165	0	0.02491	0	0
CubeSat(with panel)	0.305	0.3711	0	0	0.2923	0	0.02231	0	0
galileo	0.4204	0.05817	0	0.006908	0	0	0.05339	0	0.4592
calipso	0.5382	0.04877	0	0.2169	0	0	0	0	0.1951
glonassk	0.3992	0.001392	0.1545	0.001392	0	0	0.02227	0	0.413
GPSIIF	0.476	0.1737	0.03425	0.01105	0	0	0.169	0	0.1326
landsat8	0.3543	0.4893	0.1446	0.01111	0	0	0	0	0
dubaiSat	0.1078	0.371	0	0.02841	0	0	0	0	0.4914
BoxWing	0.3124	0.07125	0	0.01504	0	0	0	0	0.5978
dragon2	0.2272	0.03075	0.6574	0.08403	0	0	0	0	0

From Material Identification to Object Classification

AEROSPACE CENTRE of EXCELLENCE

- Classification on simulated satellites appeared to be causing over-fitting and would only perform well if satellite was already "seen"
- New approach is to learn based on expectations and simulated material combinations – similar to materials model
- Can now go from spectra, to materials probability, to satellite classification with models that have never seen a satellite before
- Performance good in most cases with 2 clear outliers. Starlink and Landsat8

Prediction Of Class

	Comms/ GNSS	EO	CubeSats	RocketBody	Capsule	UFO
starlink	0.3675	0	0.0405	0	0.4255	0.1665
iridiumNEXT	0.9265	0.0125	0.004	0.0575	0	0.001
HS376	0.999	0.0005	0.0005	0	0	0
galileo	0.9135	0.077	0.002	0	0	0.0075
glonassk	0.9135	0.0715	0.0055	0.011	0	0
GPSIIF	0.99	0.009	0	0	0	0.001
calipso	0.034	0.9295	0.0365	0	0	0
landsat8	0.027	0.0005	0.023	0.006	0.9435	0
dubaiSat	0.038	0.865	0.054	0	0	0.043
BoxWing	0.063	0.869	0.0625	0	0	0.0055
CubeSat(no panel)	0.0155	0	0.951	0	0.0005	0.033
CubeSat(with panel)	0.149	0	0.831	0	0.0185	0.0015
Upper Stage	0.0155	0.0005	0.041	0.983	0	0.001
dragon2	0.0555	0	0.0005	0.0105	0.934	0

WP2 - Hyperspectral light curve analysis and attitude motion reconstruction

- Attitude estimation from spectral light curves
- ML for attitude estimation from time variation of spectral curves

Attitude Estimation with Least Square

- Material-wise decomposition obtained from endmember analysis
- Measurement model for eCube (single band):

$$\mathbf{y}(\lambda) = \sum_{i=1}^{6} \max(0, -\mathbf{S}\cdot\boldsymbol{n_i}) \max(0, -\mathbf{V}\cdot\boldsymbol{n_i})\, \mathbf{F}_i \circ \mathbf{R}(\lambda)$$

$$\mathbf{F}_i = \begin{bmatrix} f_1^{(i)} \\ \vdots \\ f_m^{(i)} \end{bmatrix} \qquad \mathbf{R}(\lambda) = \begin{bmatrix} R_1(\lambda) \\ \vdots \\ R_m(\lambda) \end{bmatrix}$$

- $\mathbf{n}_i$ – normal to a given surface
- **S** – Sun direction
- **V** – observation direction
- **F** – fractions of each material on each face
- **R** – identified endmember spectra
- **y** – *mb* x 1 vector containing signal due to each material in each band
- Use measurement model to minimize cost function wrt rotation state **n**

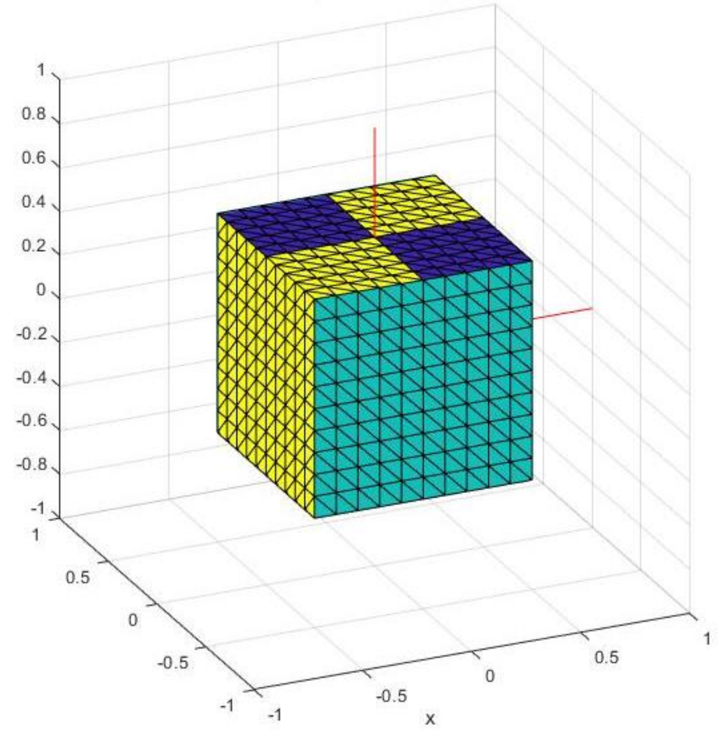

Example of ecube with mixed materials

$$J = \sum_j (T_j(\lambda_k) - \sum_i y_{ij}(\mathbf{n}))^2$$

Attitude Estimation with Least Square

- Material-wise decomposition obtained from endmember analysis
- Measurement model for eCube (single band):

$$\mathbf{y}(\lambda) = \sum_{i=1}^{6} \max(0, -\mathbf{S} \cdot \boldsymbol{n_i}) \max(0, -\mathbf{V} \cdot \boldsymbol{n_i}) \, \mathbf{F}_i \circ \mathbf{R}(\lambda)$$

$$\mathbf{F}_i = \begin{bmatrix} f_1^{(i)} \\ \vdots \\ f_m^{(i)} \end{bmatrix} \qquad \mathbf{R}(\lambda) = \begin{bmatrix} R_1(\lambda) \\ \vdots \\ R_m(\lambda) \end{bmatrix}$$

- $\mathbf{n}_i$ – normal to a given surface
- **S** – Sun direction
- **V** – observation direction
- **F** – fractions of each material on each face
- **R** – identified endmember spectra
- **y** – *mb* x 1 vector containing signal due to each material in each band
- Use measurement model to minimize cost function wrt rotation state **n**

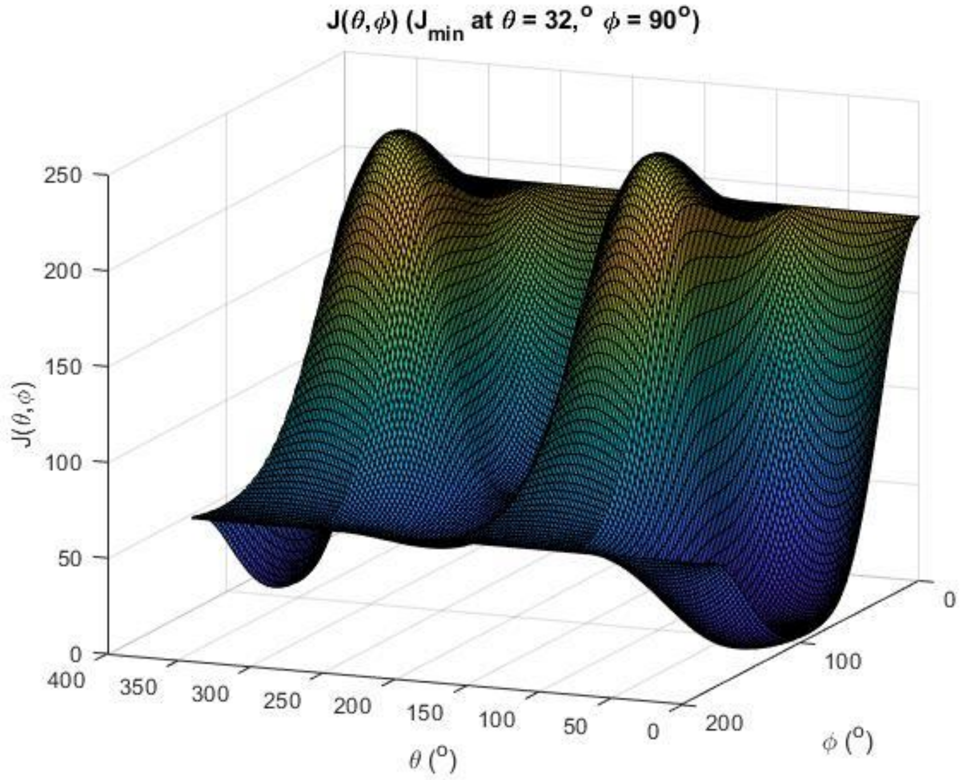

Example of ecube with mixed materials

$$J = \sum_j (T_j(\lambda_k) - \sum_i y_{ij}(\mathbf{n}))^2$$

Attitude Estimation with SVM

- Machine learning algorithms can be used to directly predict quaternion values based on the spectral data
- Over 20000 simulated time series of quaternions and related measured spectra.
- Cube with faces covered with mix of materials

Single spectral response (1 vector array input) → Machine Learning model → Quaternion value prediction (1 scalar output)

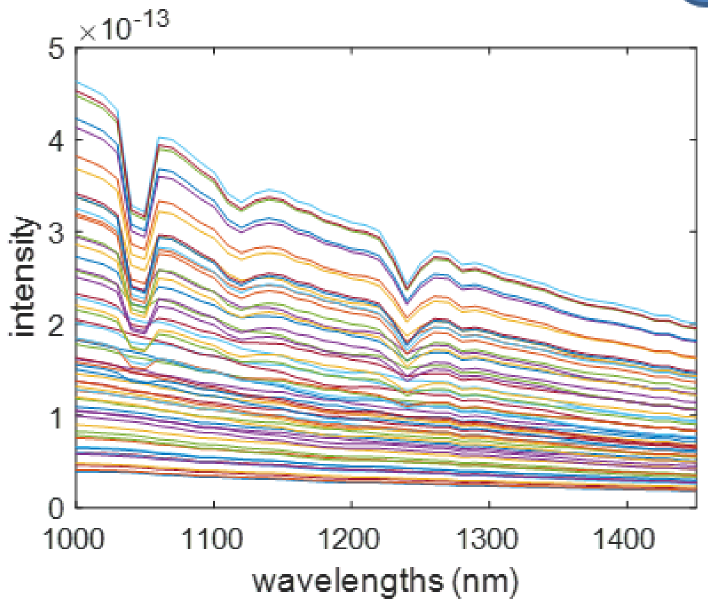

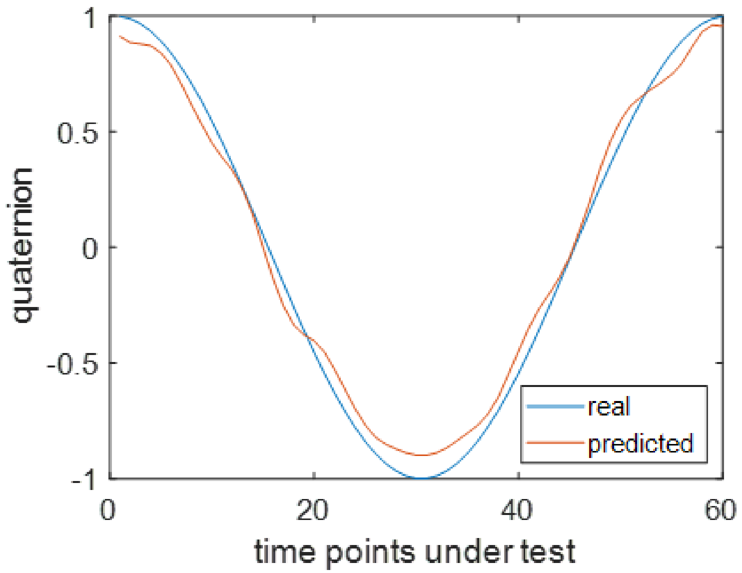

- Support Vector Machine (SVM) regression with prior Principal Component Analysis (PCA) can be implemented to achieve this

Attitude estimation

- These are prediction results for different cases: (a) and (b) show reasonable performance…
- …however, the addition of more data in (c) and (d) can affect the performance of the model – it is not able to generalise
- The reason is that the model expects similar spectral responses for similar quaternion values, however, responses are different due to observation changes over the time

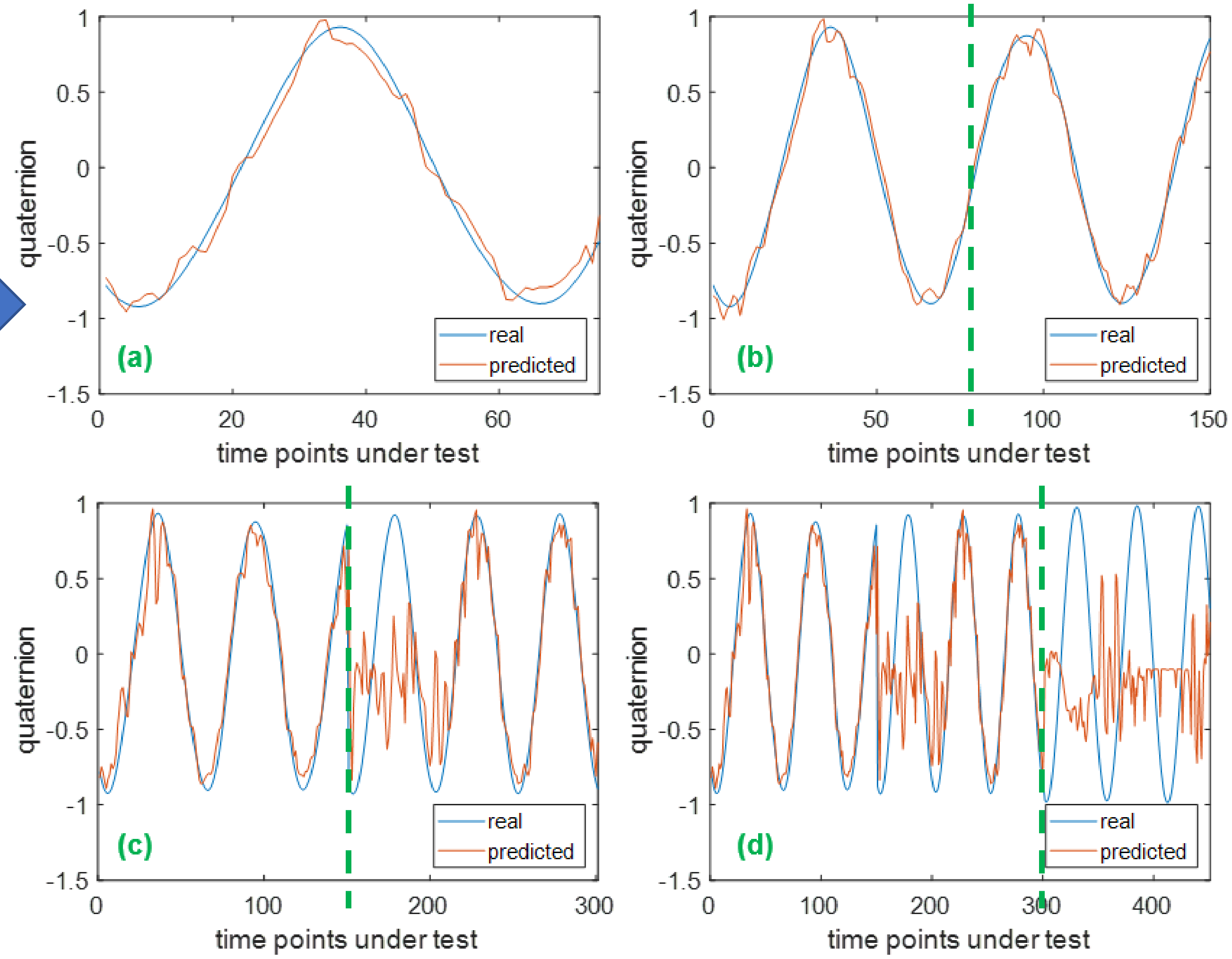

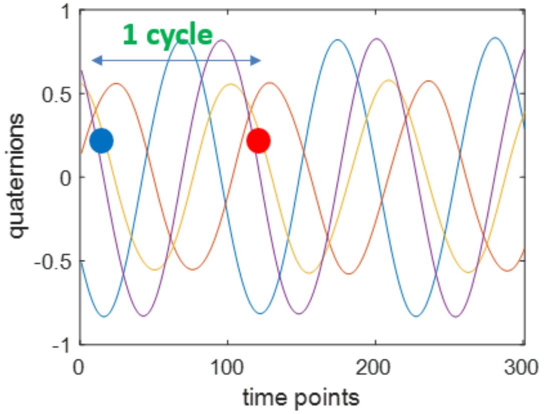

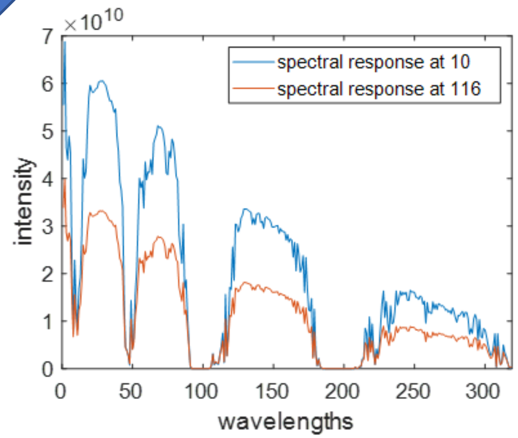

Attitude Estimation with SVM

- **Problem:** multiple observations of the same attitude but in different illumination conditions introduce a considerable noise in the training dataset

- **Solution:** changes over the time in spectral responses that correspond to similar/equivalent quaternions can be considered by introducing observation parameters as prior knowledge.

- We assume a known illumination and observation directions at a given epoch

Before

$R2=0.7473$

$RMSE=0.3271$

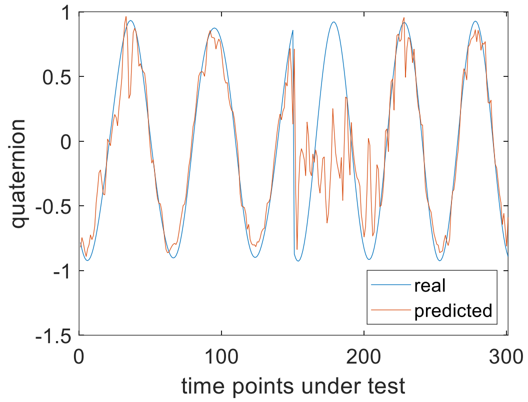

Single spectral response
(1 vector array input)
+
Three observation parameters

Machine Learning model

After

$R2=0.9797$

$RMSE=0.0999$

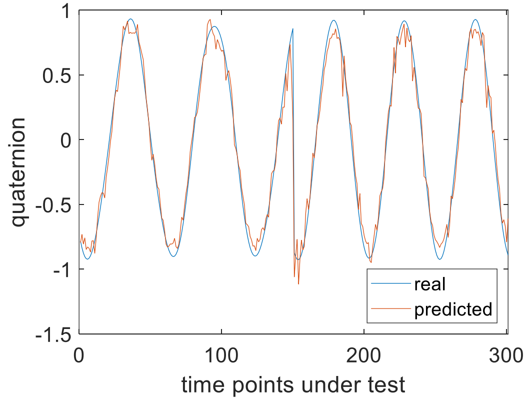

Attitude Estimation with ANN

- Additionally, SVM regression can be replaced by Artificial Neural Network (ANN) regression, with presumably a higher generalisation ability:

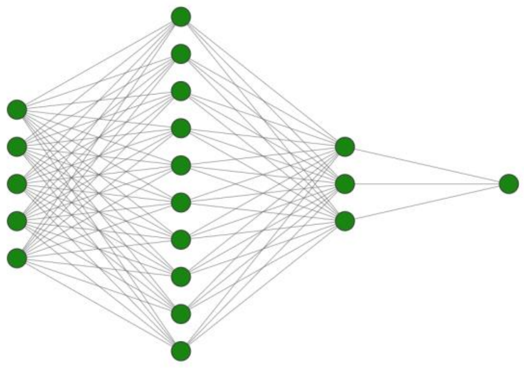

<u>SVM</u>

$R2=0.9308$

$RMSE=0.1752$

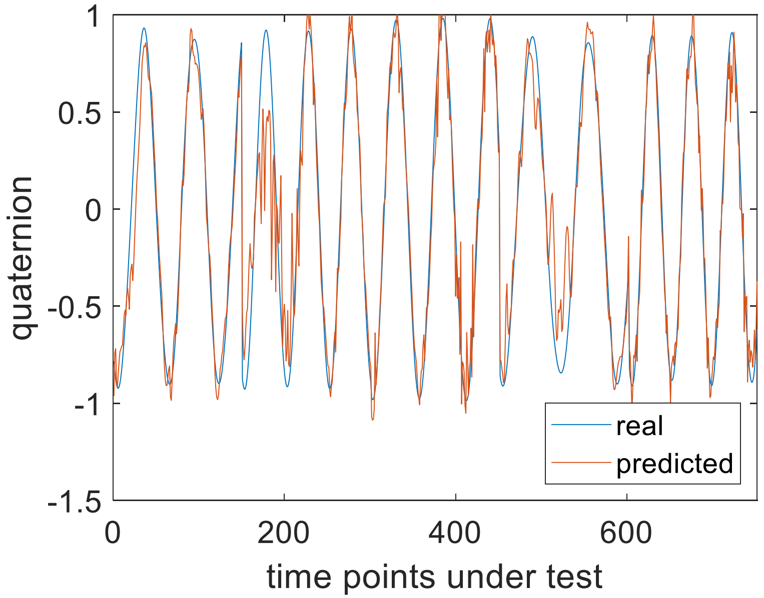

<u>ANN</u>

$R2=0.9829$

$RMSE=0.0861$

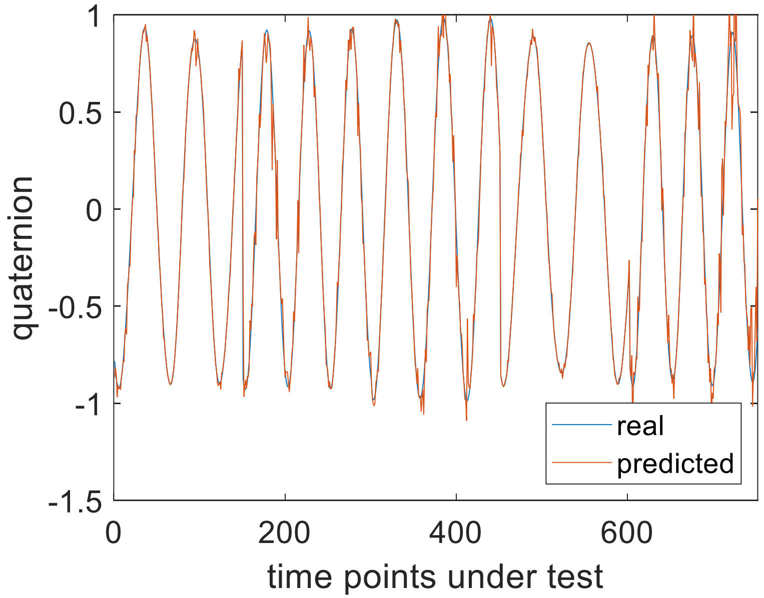

Attitude estimation

- Different approaches based on ANN can be investigated in the future. For example, using the entire time series (rather than single spectral responses) to estimate quaternions:
- Quaternions could be represented using sine waves (estimation), so that the models only need to predict 3 values for a time series

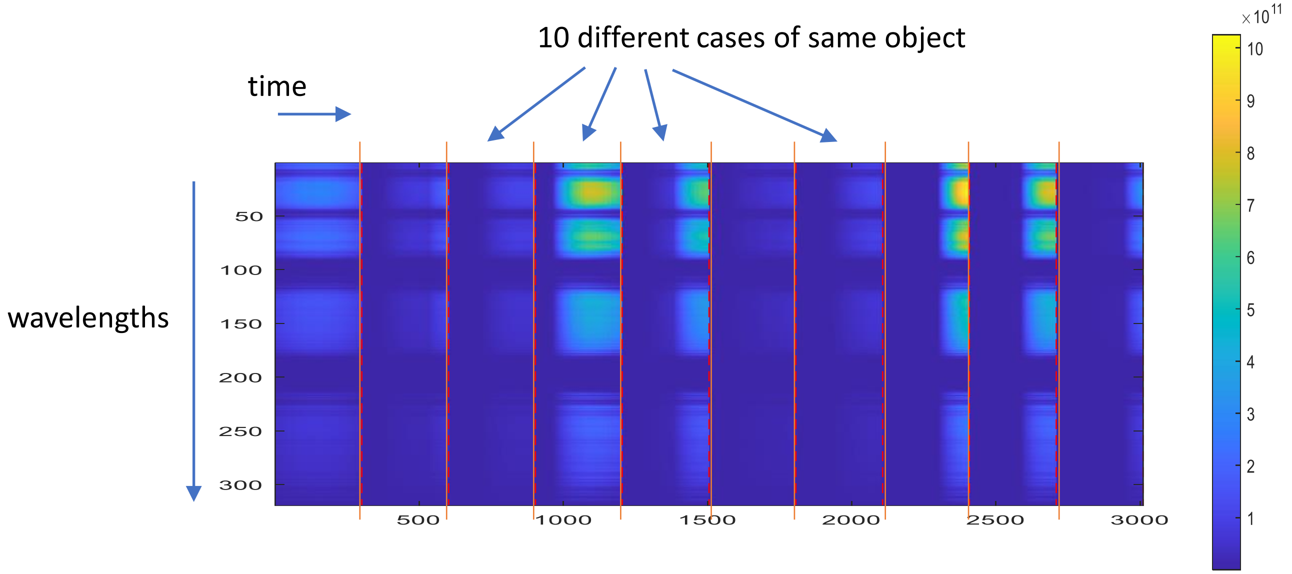

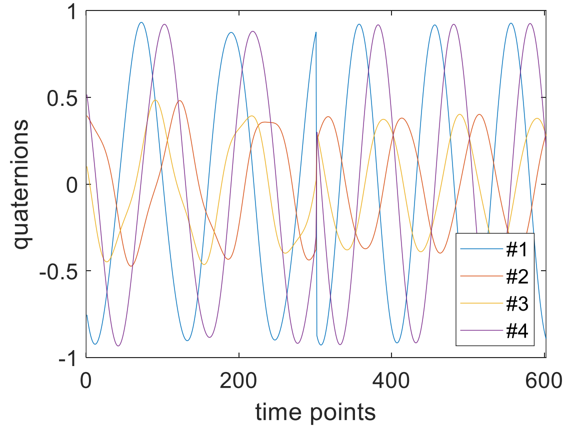

Spectral responses (time series - 2D image) → Machine Learning model (NN) →

Regression for:
- Sine amplitude
- Sine frequency
- Sine phase

Regularized batch loss

- $J_\omega = \int_0^T |\boldsymbol{\omega}|^2 dt \approx \frac{1}{\Delta t} \sum_{i=1}^{N-1} \theta_{i\to i+1}^2 \approx \frac{4}{\Delta t} \sum_{i=1}^{N-1} (1 - < q_i, q_{i+1} >^2)$
- $J_\alpha = \int_0^T |\boldsymbol{\alpha}|^2 dt \approx \frac{1}{\Delta t} \sum_{i=1}^{N-1} |\omega_{i+1} - \omega_i|^2 \approx \frac{1}{\Delta t^2} \sum_{i=1}^{N-2} \left| q_{i+2} q_{i+1}^c - q_{i+1} q_i^c \right|^2$
- J_ω - penalizes high angular velocities (large rotations between timesteps to be exact) - **Implemented**
- J_α - penalizes high angular accelerations (large differences between consecutive estimates of the angular velocity) – **Implemented**
- **Implemented Analytical Gradients for all loss functions**

Painted cube – measurement vs theory

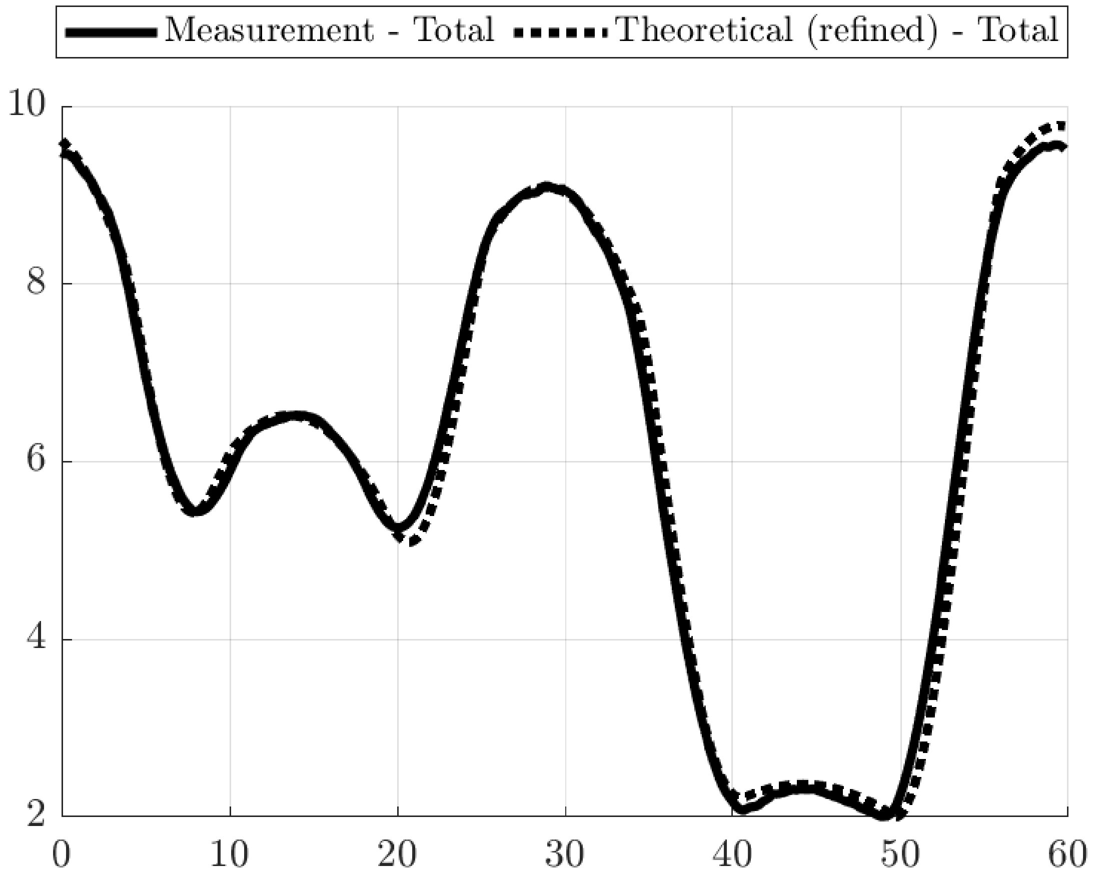

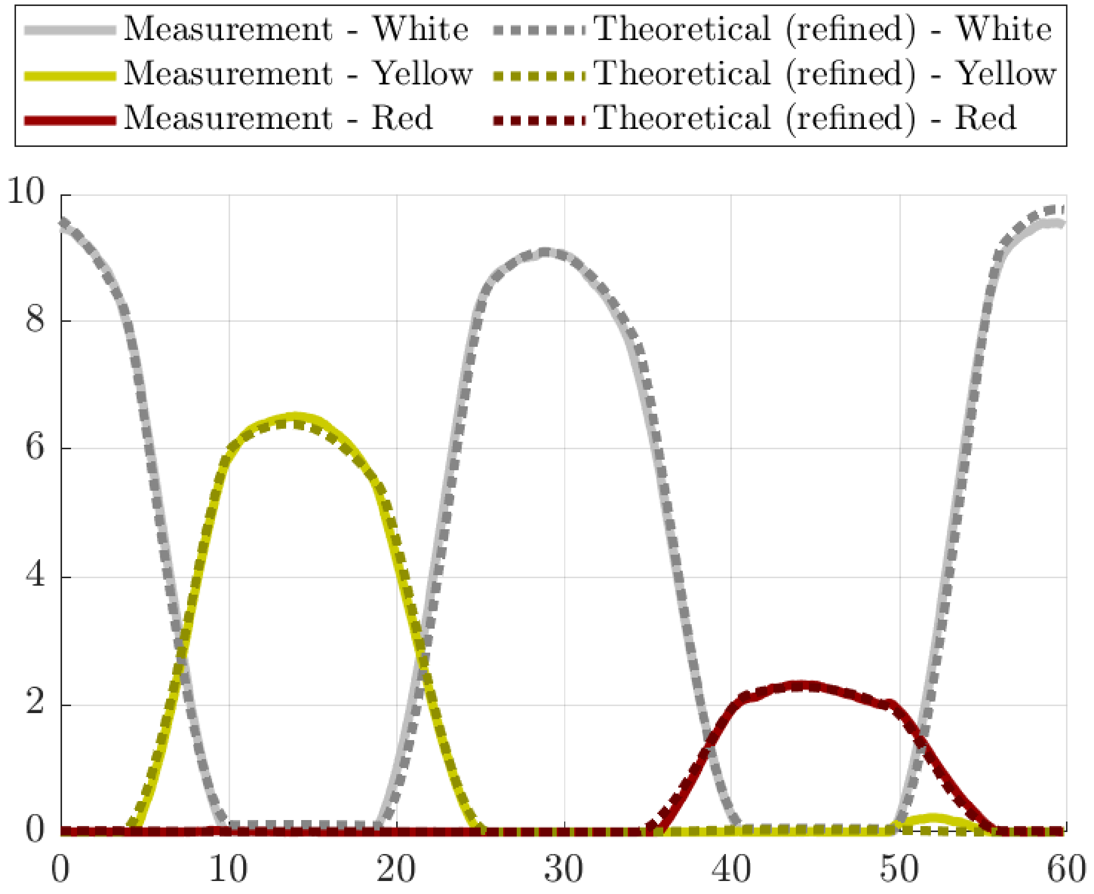

Regularized batch loss

- Optimizer tends to converge to local optima that are far from global optima.
- Currently, this is being solved by doing a grid search for the initial guess (using the tools in MACS to define uniform search directions on a sphere)

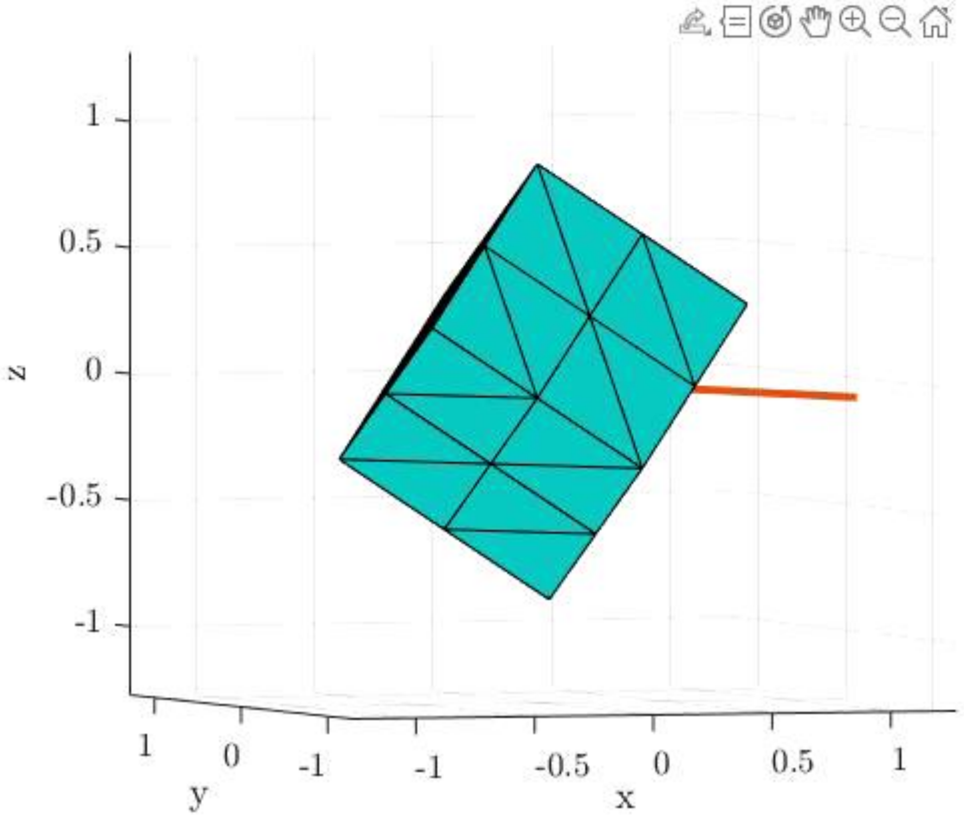

Regularized batch loss

- Sometimes, optimizer converges to a solution that results in the same observed spectral lightcurve, but is the opposite rotation to the ground truth

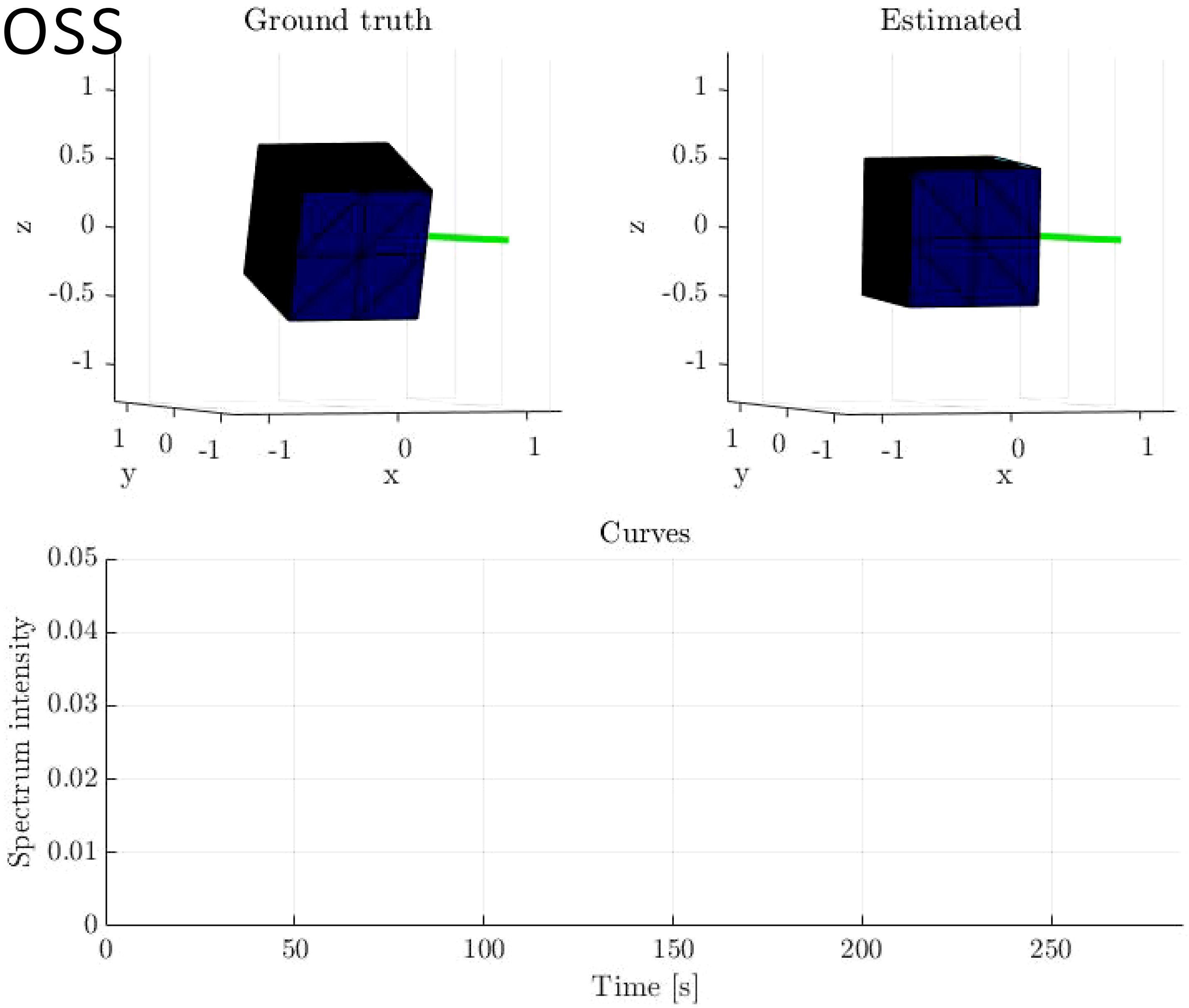

Possible solutions

- Grid search assuming fixed axis rotation on a subset of the trajectory
  - Estimate angular velocity from Fourier analysis
  - Sample directions uniformly
  - Use lowest cost as initial guess
- Dynamic programming with discretized states
  - Create a discrete state space by uniformly sampling attitudes
  - Use DP to solve problem, where control is angular acceleration
- GMM Filter
- 1st is simpler to implement, but fixed axis rotation might not generalize.
- 2nd besides being more complicated may also be slow
- 3rd would involve work that could probably go into SOBA

Next work

- Test with different objects DONE
- Tweaks on initial guess generation DONE
- Fix an issue on synthetic data generation for training data DONE
- Start training a NN on the attitude determination problem (fixed axis for now) [started, but need to look into the results more carefully]

Initial guess generation – rotation period

- Because the signal components are not sinusoidals, nor are they smooth FFT analysis can be misleading [Silha, Stellingwerf]
    - even without occlusions, when a surface stops being visible due to no longer facing the observer/light, a non-smooth point exists
    - Inserting Rodrigues formula into the light function suggests double frequency components could be dominant

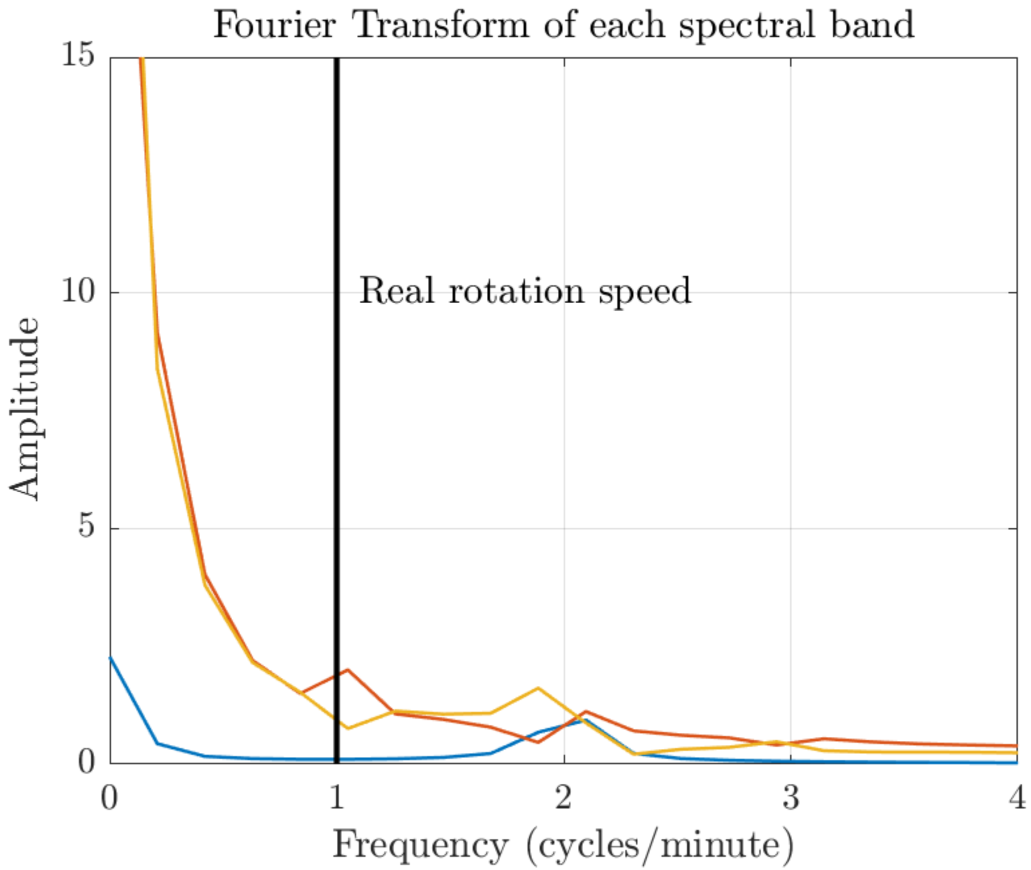

Initial guess generation – rotation period

- Phase dispersion minimization (PDM) has better results, but the presence of low frequency terms can make it give misleading results

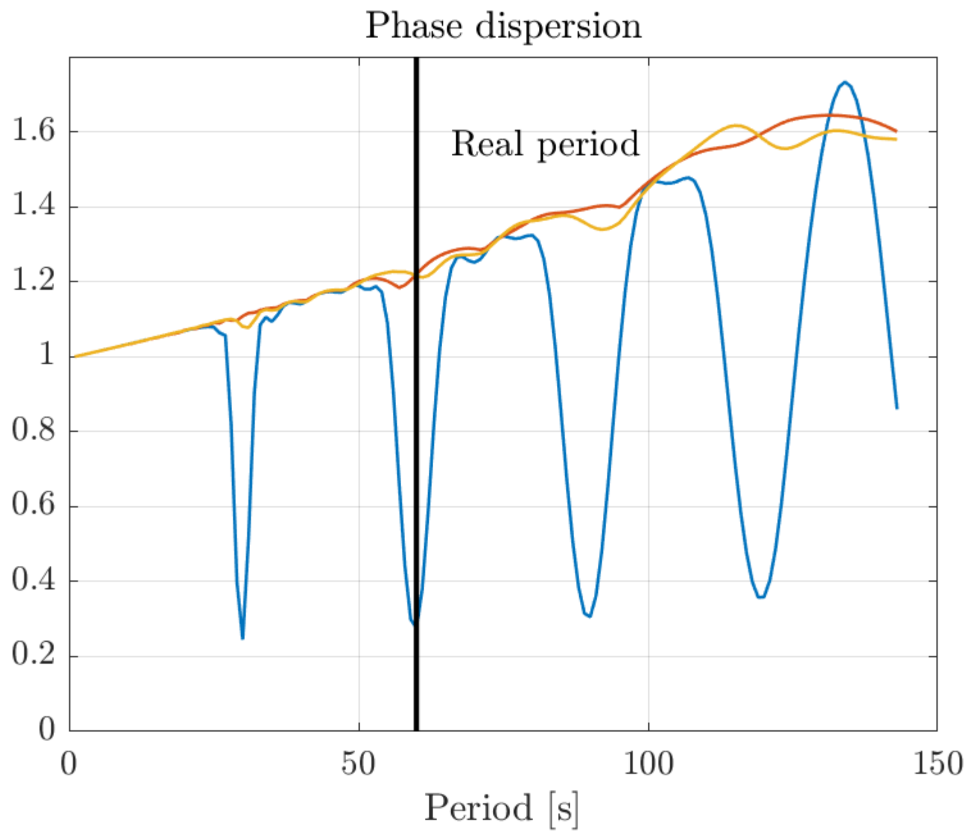

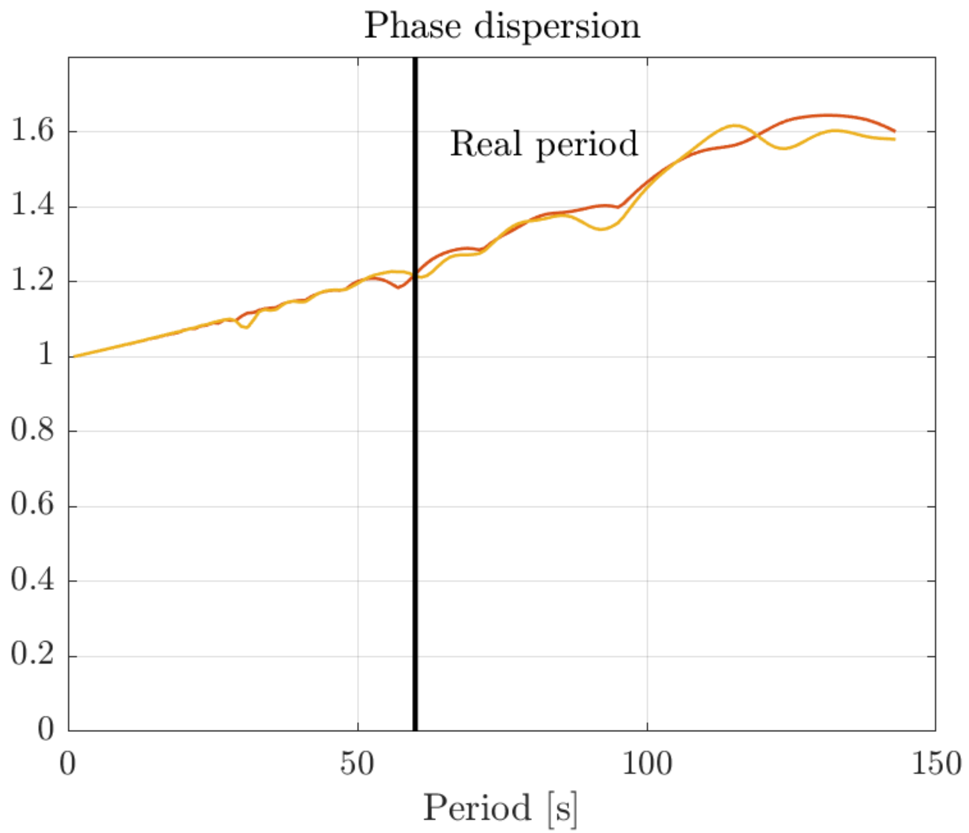

Initial guess generation – rotation period

- Phase dispersion minimization (PDM) has better results, but the presence of low frequency terms can make it give misleading results

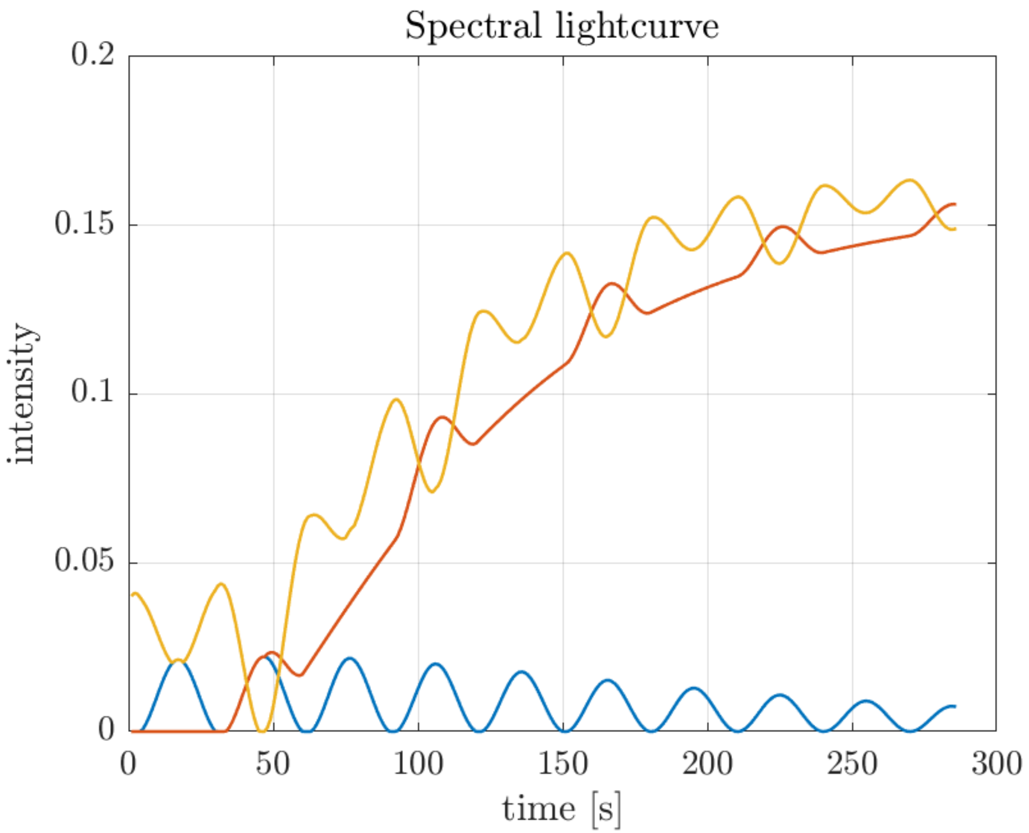

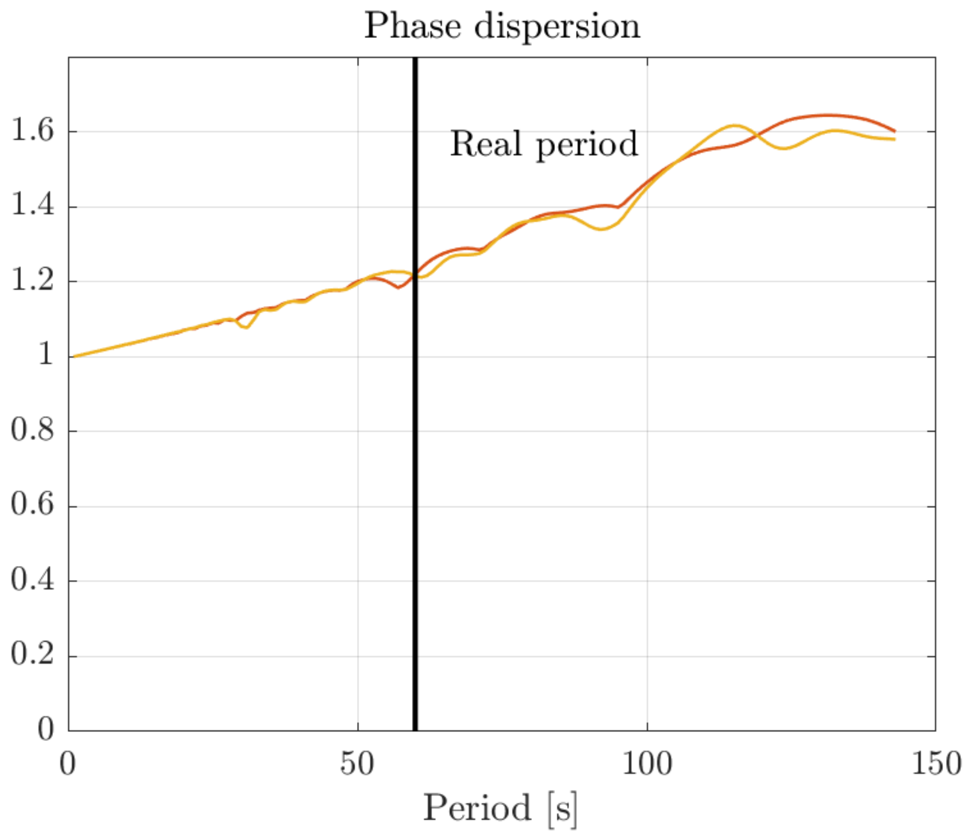

Initial guess generation – rotation period

- Those low frequency terms are due to phase variation, which tends to have a period of the order of the observation time

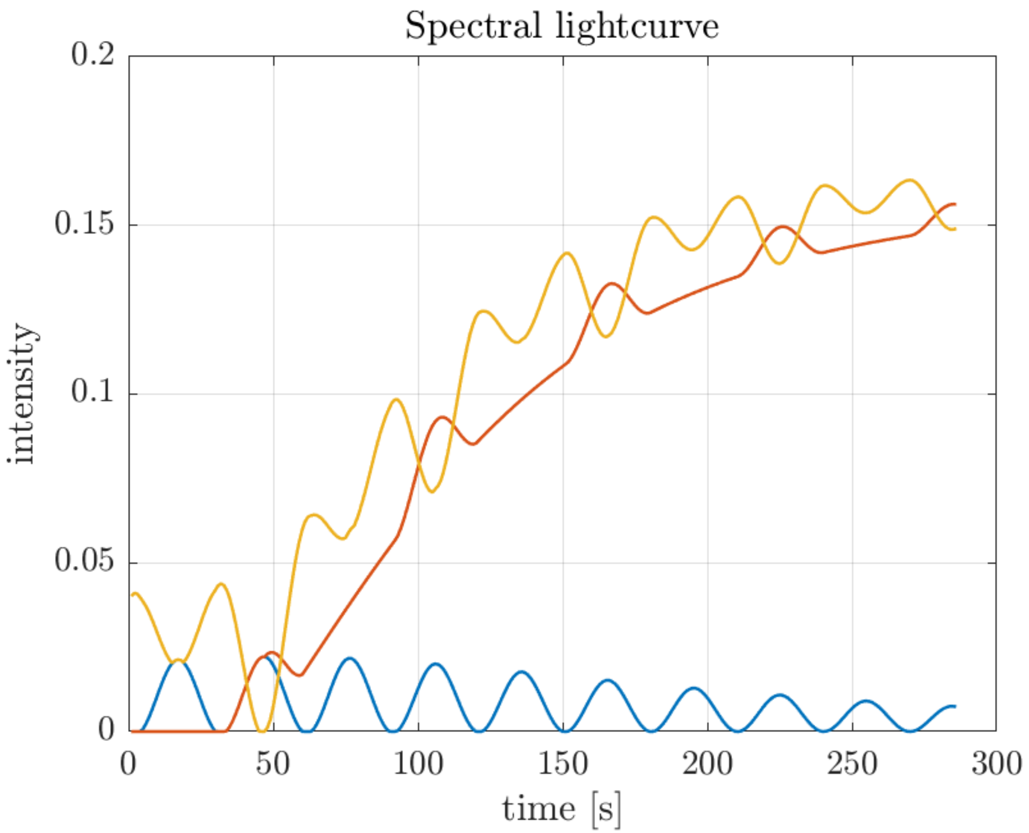

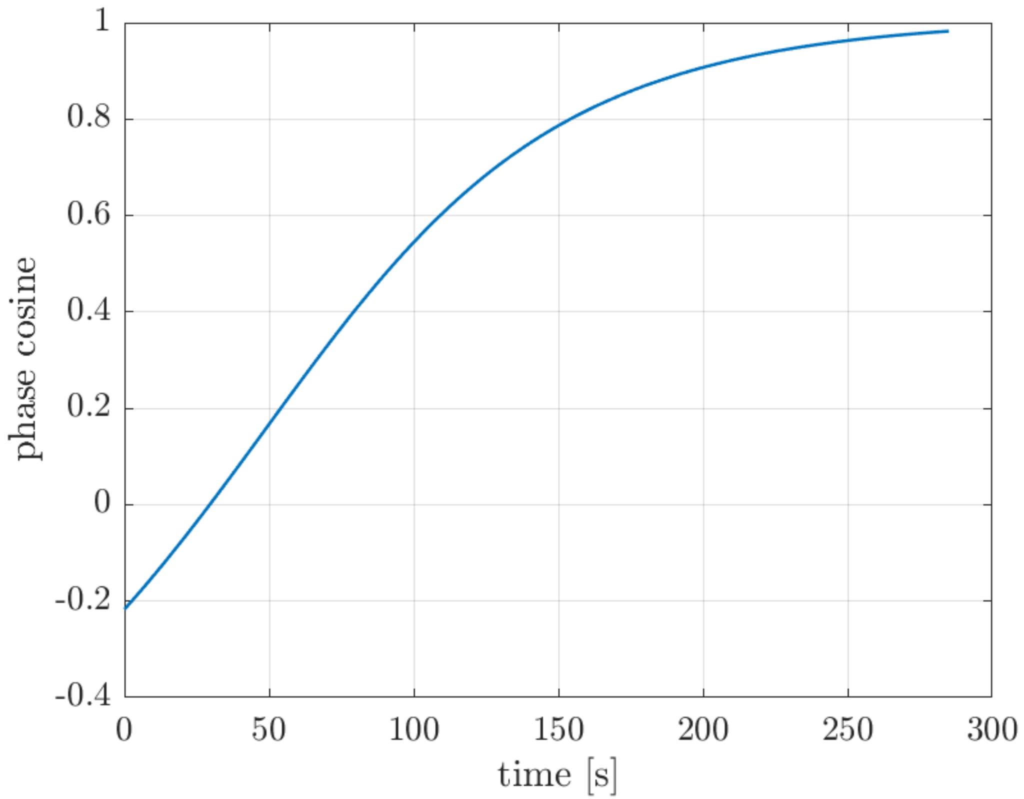

Initial guess generation – rotation period

- A high pass filter seems to solve this problem
  - Noise, absent in this test, may need to be removed with a low-pass filter

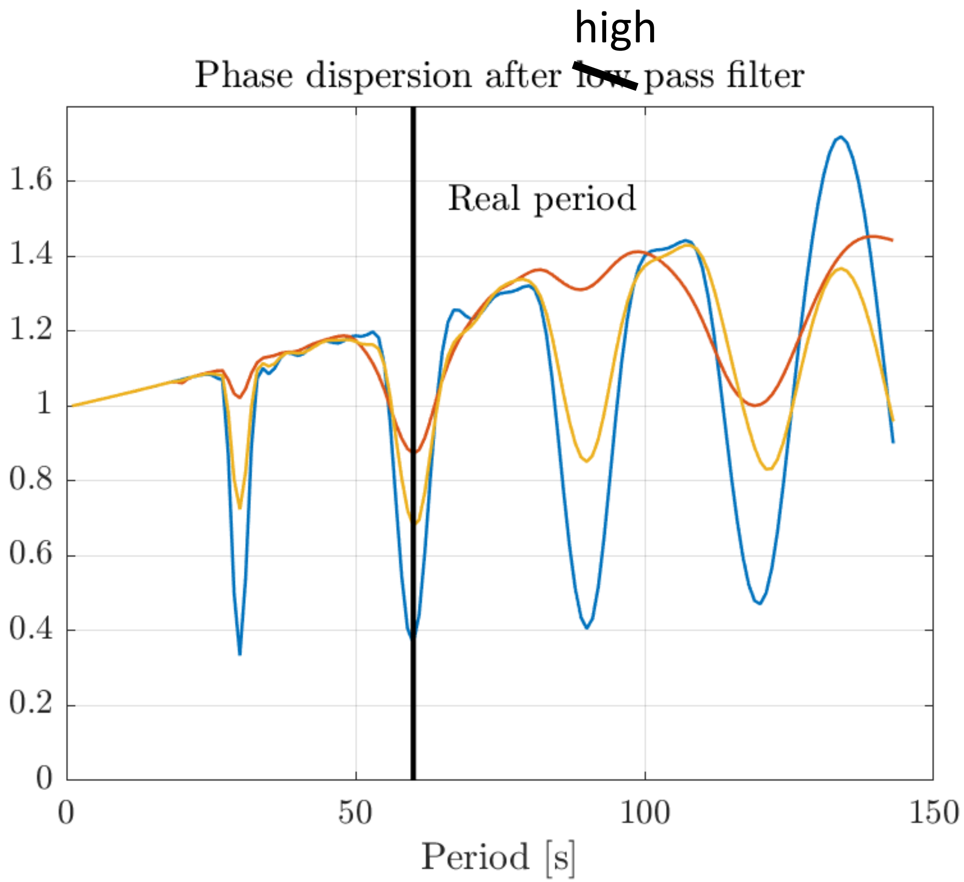

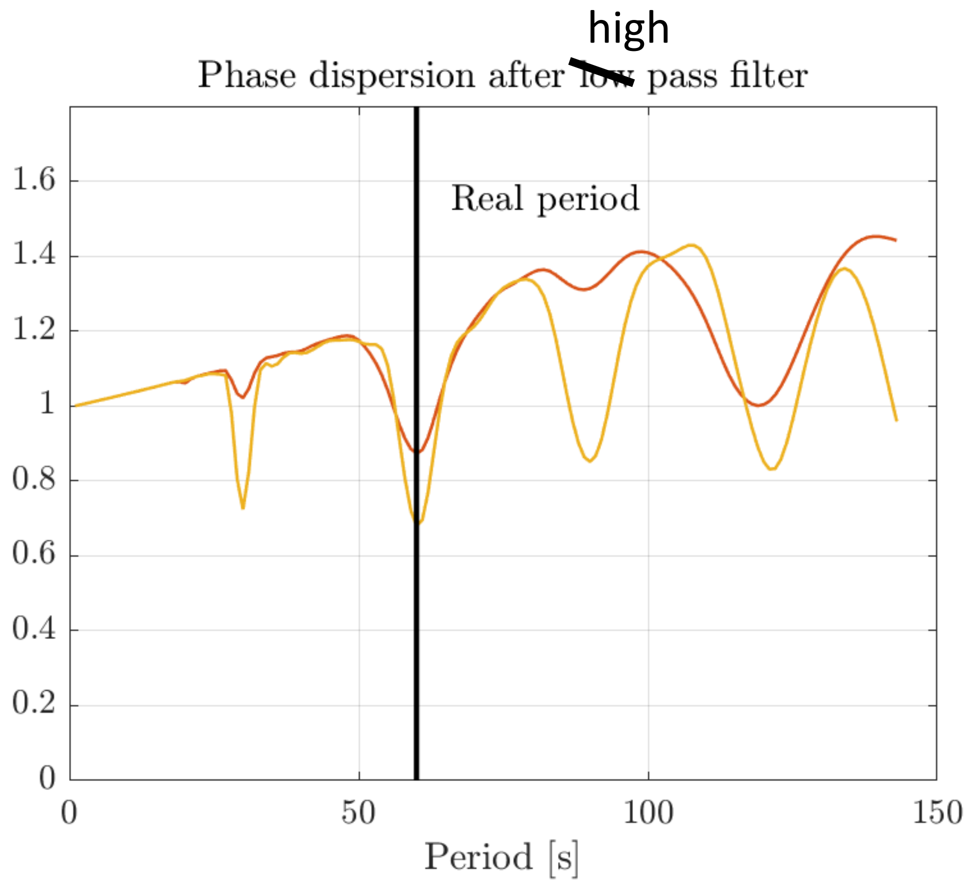

Initial guess generation – initial conditions

- Assuming fixed axis rotation, the initial orientation q_0 and the axis of rotation a are sampled.
  - The sampling is obtained using MACS's algorithm for generating a uniform distribution of directions. The resulting distribution is uniform for a, but technically the sample of q_0 does not represent a uniform distribution of SO(3) [Shuster (2003)]. I will not worry about this for the moment though.
- The lightcurve for a single period, found with PDM, is compared with the observations, and the closest match is used as an initial guess.
- This initial guess is refined with a local search over the same period still constrained to fixed axis rotation
  - Now that the test cases consist of objects rotating about a fixed axis, this initial guess estimation seems to do most of the heavy lifting. The overall search strategy may need to be improved once precession/tumbling is considered.
- Finally, the regularized batch optimization strategy mentioned before is used to get a result over the whole lightcurve observation.

Regularized batch loss – success cases

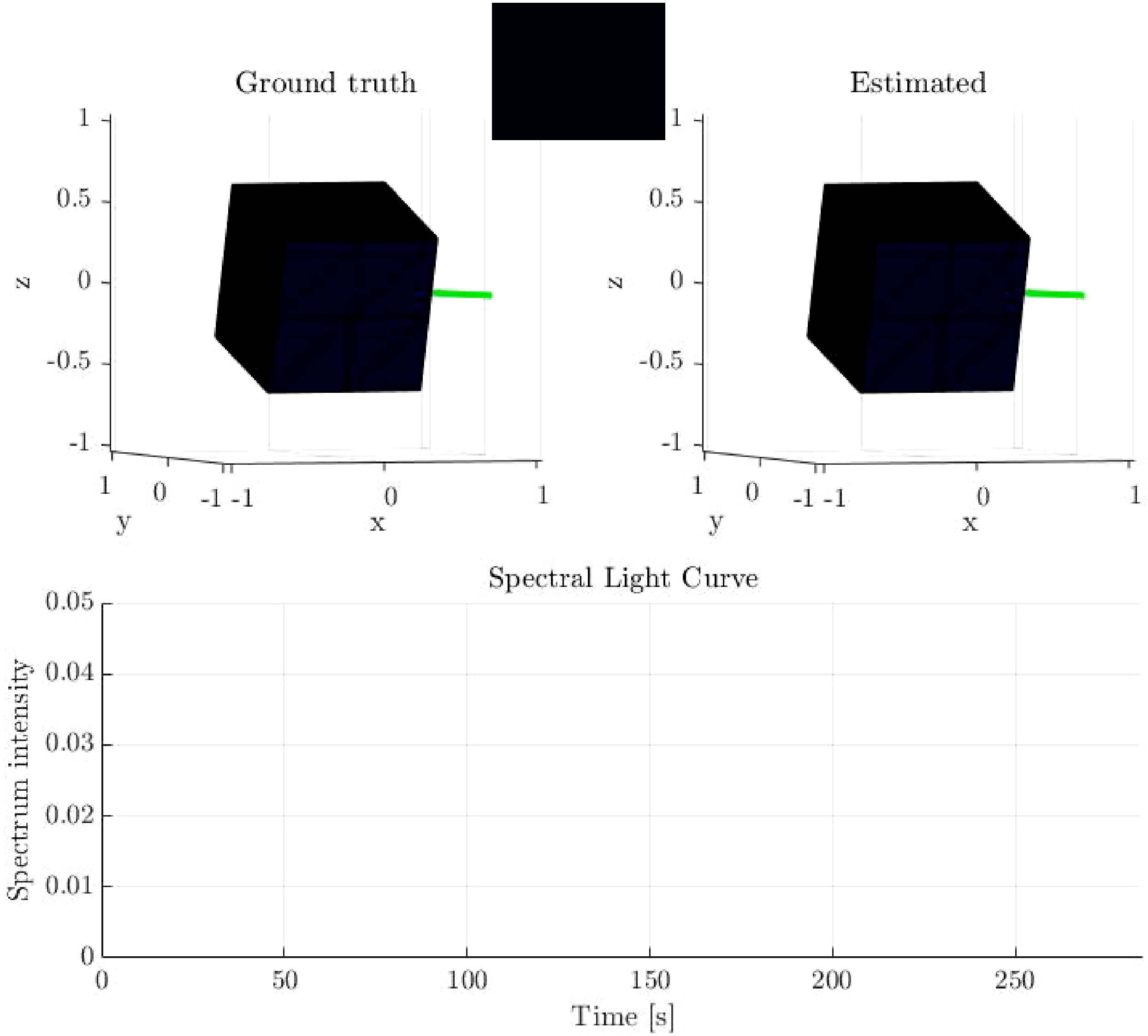

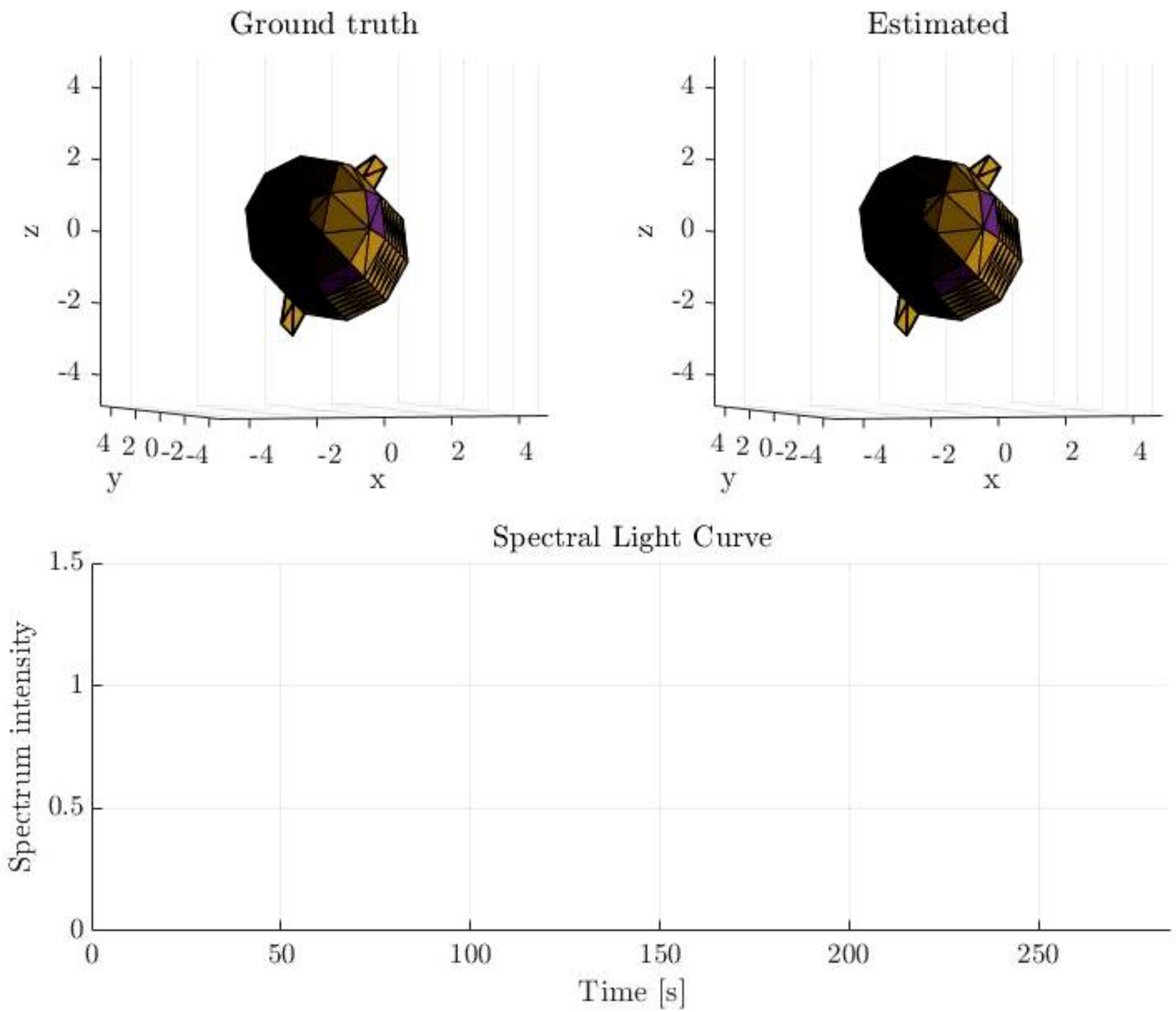

Regularized batch loss – failure case

- Still have issues – the segment of the LC used to fit an initial guess may be misleading
- (using the whole LC to evaluate an initial guess leads to failure if the estimated period is even slightly off)
- Here we converge to a non-global local optimum as a result of the bad initial guess
- Before trying to solve this it may be a good idea to look at non-fixed axis rotation, to avoid crafting a solution that only works on this case

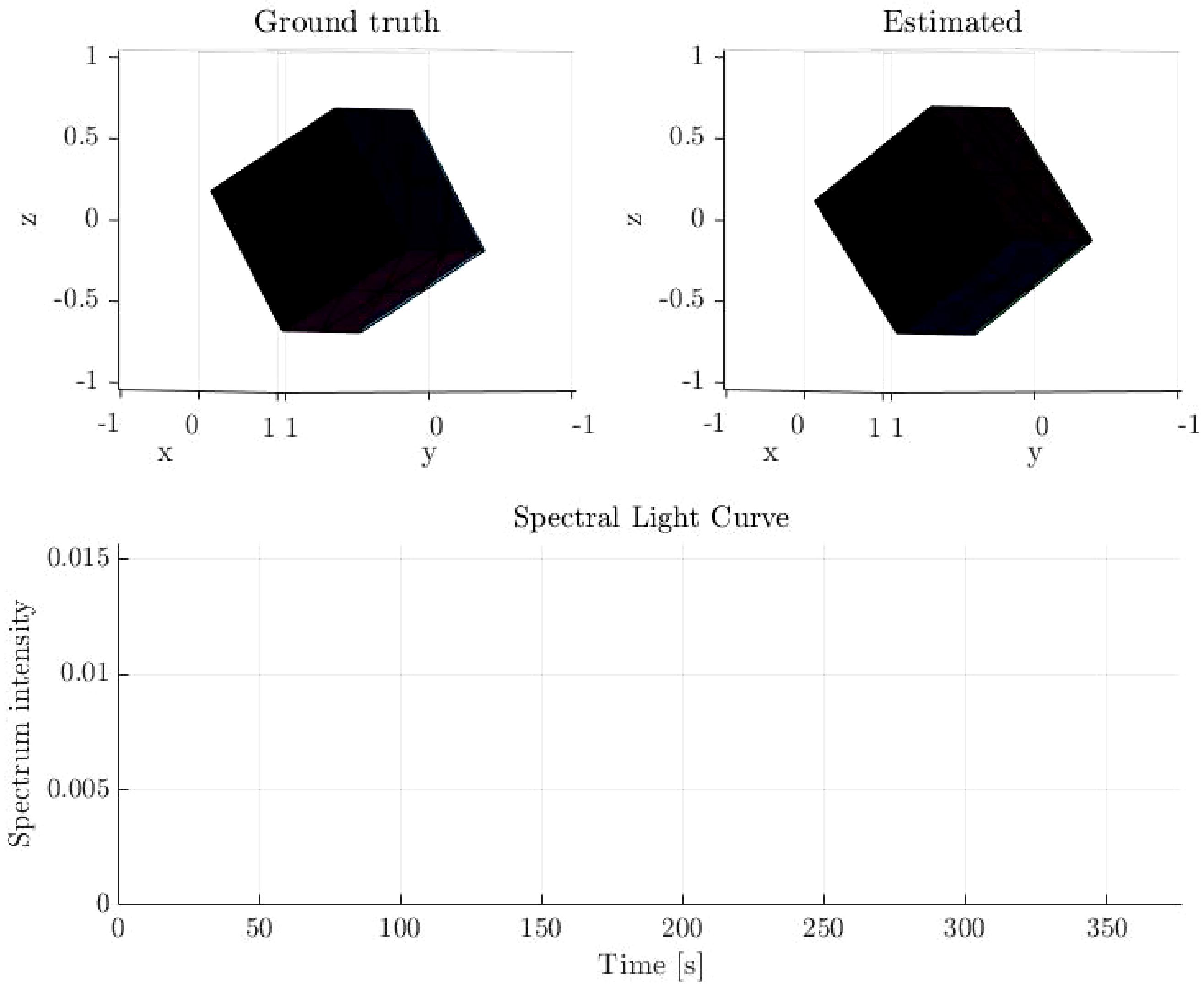

Regularised batch least squares - Summary

- Cost function:
  - $J = J_D + J_\alpha$
  - $J_D = \sum \left(\hat{S}_i - S\big(q(t_i), v_I(t_i), s_I(t_i)\big) \right)^2$
  - $J_\alpha = \int_0^T |\boldsymbol{\alpha}|^2 dt \approx \frac{1}{\Delta t} \sum_{i=1}^{N-1} |\omega_{i+1} - \omega_i|^2 \approx \frac{1}{\Delta t^2} \sum_{i=1}^{N-2} \left| q_{i+2} q_{i+1}^c - q_{i+1} q_i^c \right|^2$
  - Cost function penalises high angular accelerations
  - Initial guess q_0 obtained using PDM followed by grid search
- All attitude histories in $\mathcal{R}(q_0)$ are used as initial guesses for separate optimisations, as they all tend to be local optima

Symmetry in Lightcurve Inversion

- Spectrum function recap:
  - $S = S(v_B, s_B, O) = S(s_B, v_B, O)$
- Swapping view and illumination vectors results in same lightcurve
- Therefore there is always a symmetry of the form
  - $R_h(\pi)$, i.e. a 180 deg rotation about the bisector
  - I.e., attitude q and its transformation $R_h(\pi)q$ result in the same spectrum
- In addition, there are body symmetries

Symmetry in Lightcurve Inversion

- Let us now write the spectrum function as

$$S = S(R_{BH}, \alpha) = S(T_H R_{BH} T_B, \alpha)\ \forall T_H \in \mathcal{T}_H\ ,\ \forall T_B \in \mathcal{T}_B$$

  - $R_{b\to h}$ converts body frame coordinates to h frame, a frame with x axis along bisector, and xy plane coincident with the sv plane
- We can recover (v_B, s_B) from $(R_{b\to h}, \alpha)$ as
  - $s_b = R_{b\to h}^T \left[\cos\left(\frac{\alpha}{2}\right), \sin\left(\frac{\alpha}{2}\right), 0\right]$
  - $v_b = R_{b\to h}^T \left[\cos\left(\frac{\alpha}{2}\right), -\sin\left(\frac{\alpha}{2}\right), 0\right]$
- T_H are the reflections about the planes in Fig, and their composition $R_h(\pi)$
  - T_B are body symmetries

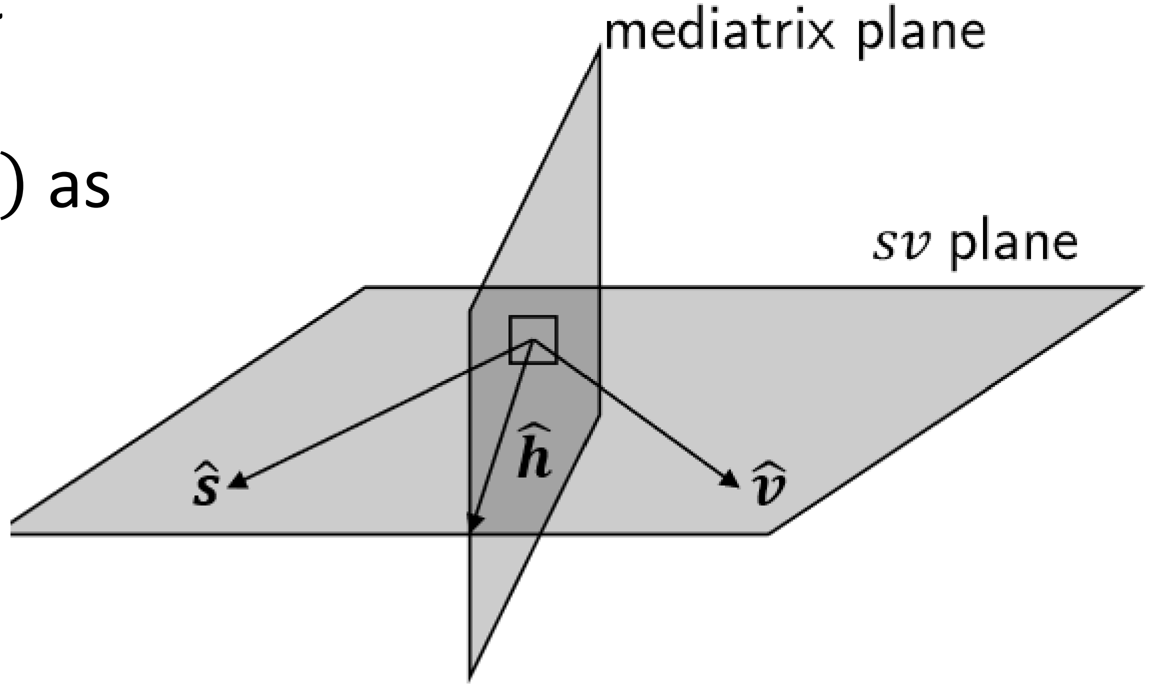

Figure 6: Diagram showing the symmetry planes

Symmetry in Lightcurve Inversion

- For an object attitude in the inertial reference frame R_{BI}, the attitudes in the following set will all produce the same spectrum:

$$\mathcal{R}(R_{BI}) = \left\{ \begin{array}{c} R_{BI}^S = R_{IH}^T T_H R_{IH} R_{BI} T_B : \det(R_{BI}^S) = 1, \\ \forall T_H \in \mathcal{T}_H \;,\; \forall T_B \in \mathcal{T}_B \end{array} \right\}$$

- The condition $\det\left(R_{BI}^S\right) = 1$ is to enforce R_{BI}^S to be a rotation, which is necessary for it to describe the attitude of the object. This means, if the object is asymmetric, above set only contains R_{BI} and $R_{IH}^T R_h(\pi) R_{IH} R_{BI}$
- If there is at least one reflection symmetry in $\mathcal{R}$, other elements T_H can be used in elements of $\mathcal{R}$

Symmetry in Lightcurve Inversion

- Example of attitudes in $\mathcal{R}$ for an object with a single reflection symmetry about the xz plane

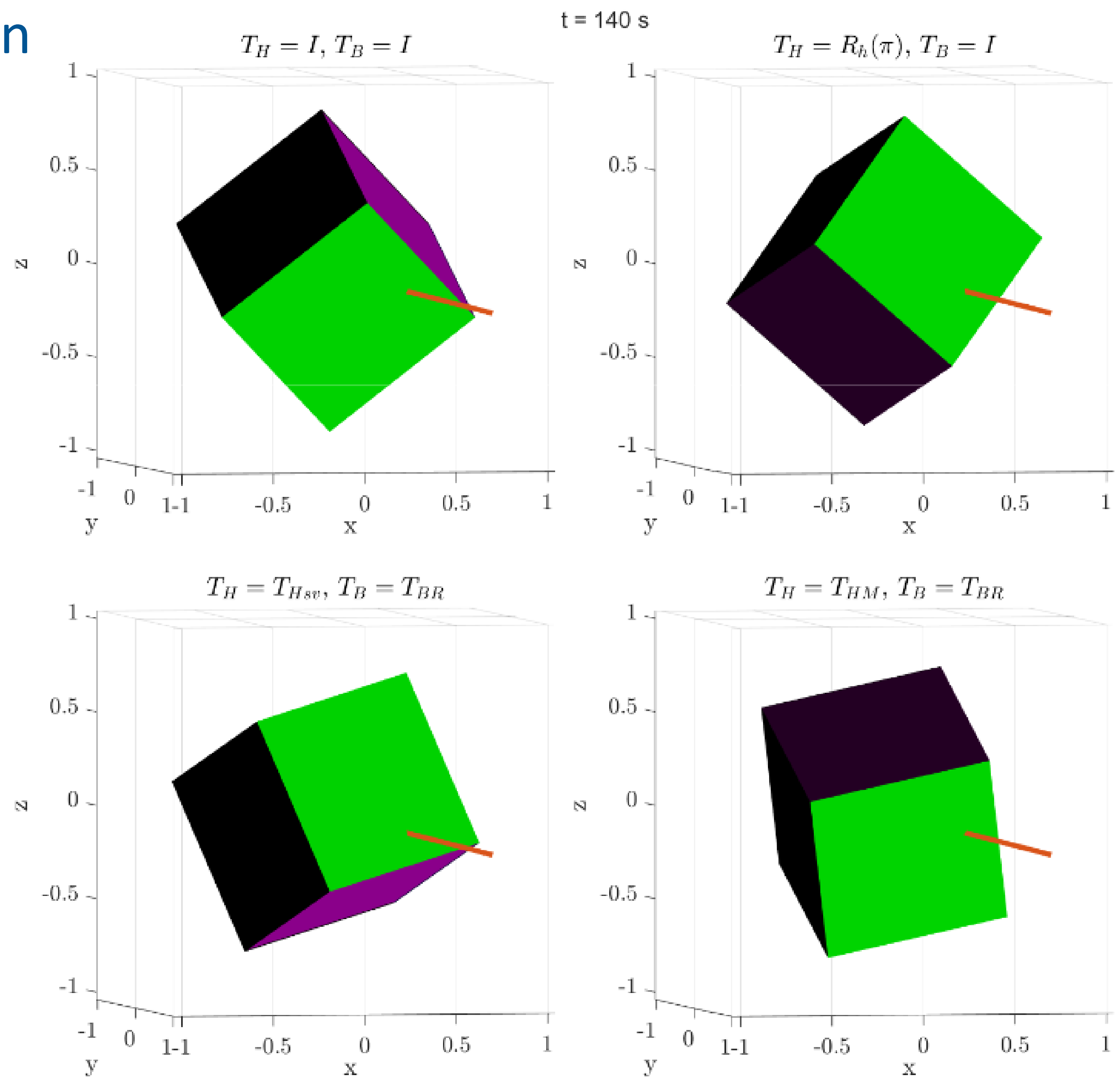

LS results – cube without symmetry

- The attitude histories obtained from noiseless data on this dataset produced a nearly identical spectral lightcurve to the observation. In all cases, perfect results were obtained.

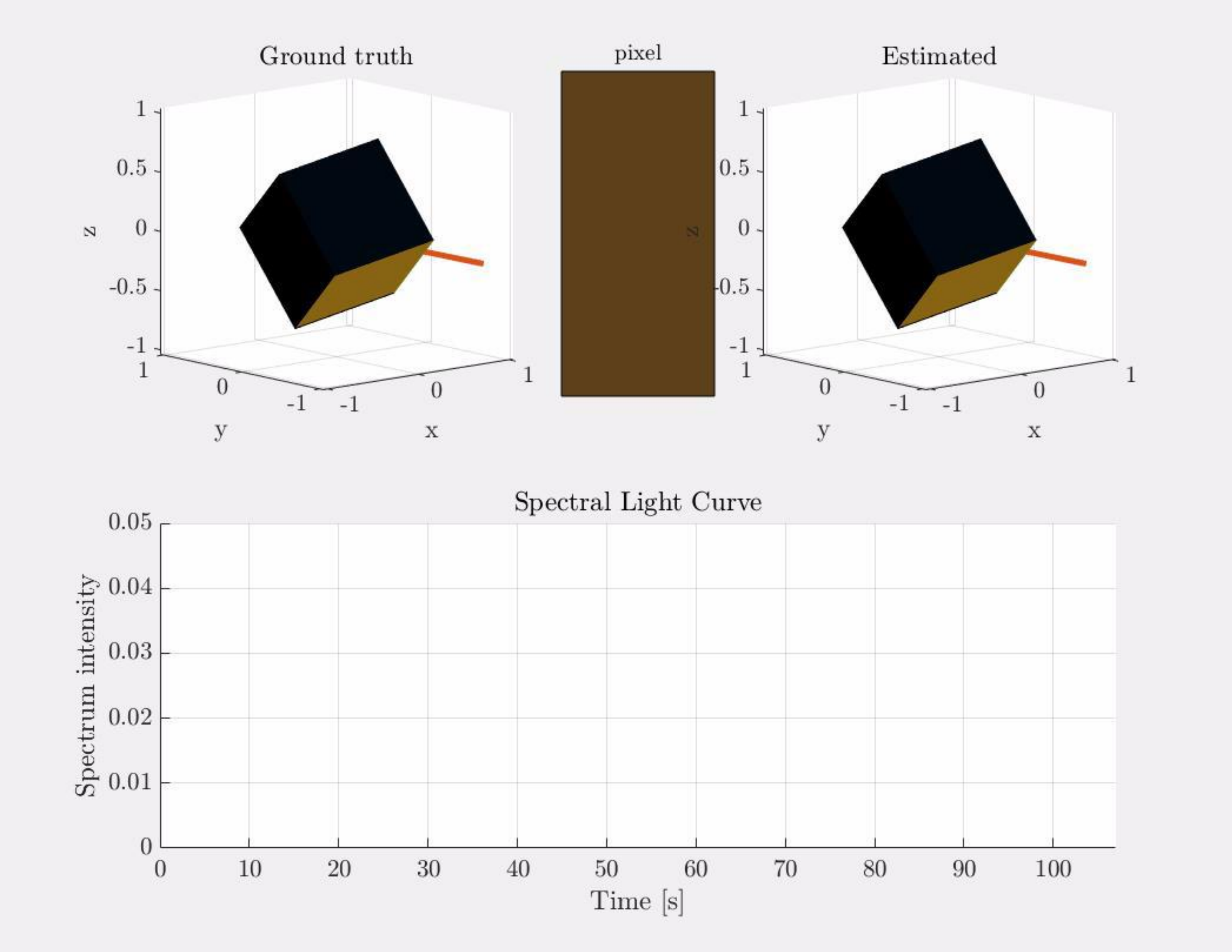

LS results – cube with symmetry

AEROSPACE CENTRE of EXCELLENCE

- The use of symmetry group improves the quality of the results. Starting only from the initial guess obtained with PDM+grid search (grey column) would lead to worse results:

Table 1: $log_{10}(L)$ when using elements of $\mathcal{R}(\mathbf{q}_0)$ as initial guess for test case 1

method	interior point		DDP	
T_h	I	$R_h(\pi)$	I	$R_h(\pi)$
$\hat{S}^{(1)}$	-3.59	$\mathbf{-11.89}$	-4.82	-8.53
$\hat{S}^{(2)}$	-1.81	$\mathbf{-11.82}$	-4.19	-8.28
$\hat{S}^{(3)}$	$\mathbf{-11.73}$	-2.39	-8.07	-4.13
$\hat{S}^{(4)}$	-1.05	$\mathbf{-11.94}$	-2.57	-8.55
$\hat{S}^{(5)}$	$\mathbf{-11.54}$	-1.55	-8.65	-1.52
$\hat{S}^{(6)}$	-4.33	$\mathbf{-13.48}$	-6.03	-9.29

- DDP usually produces worse results for the loss function, but in this case only slightly (these are log values), but it's faster:
  - interior-point: $\mu = 29s$
  - DDP: $\mu = 19s$
- A probable reason for DDP's inferior performance may be related to the current implementation's use of finite difference instead of analytical gradients used with interior point.

LS results – cube without symmetry

- The attitude histories obtained from noiseless data on this dataset produced a nearly identical spectral lightcurve to the observation. In all cases, perfect results were obtained.

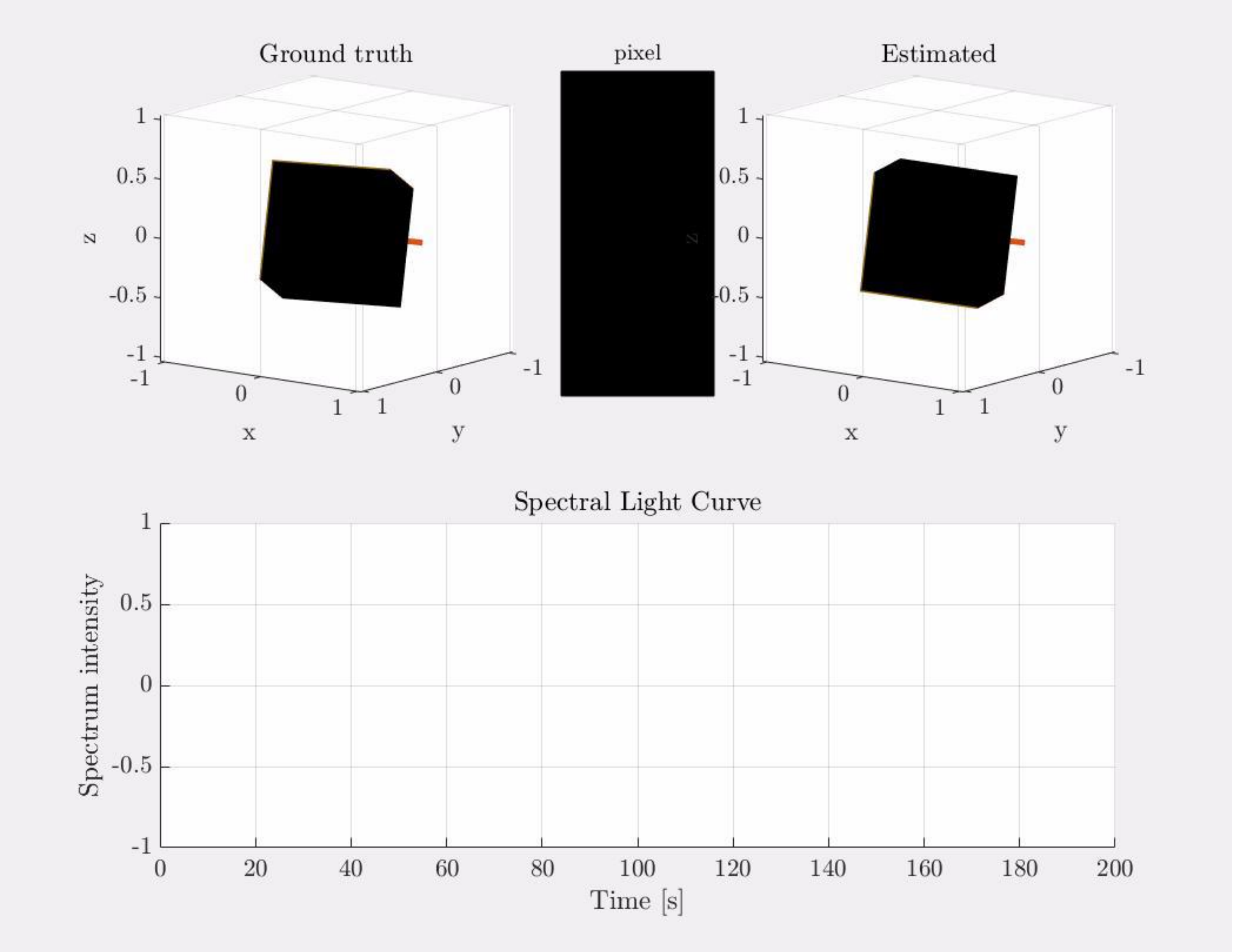

LS results – cube without symmetry

- The attitude histories obtained from noiseless data on this dataset produced a nearly identical spectral lightcurve to the observation. In all cases, perfect results were obtained.

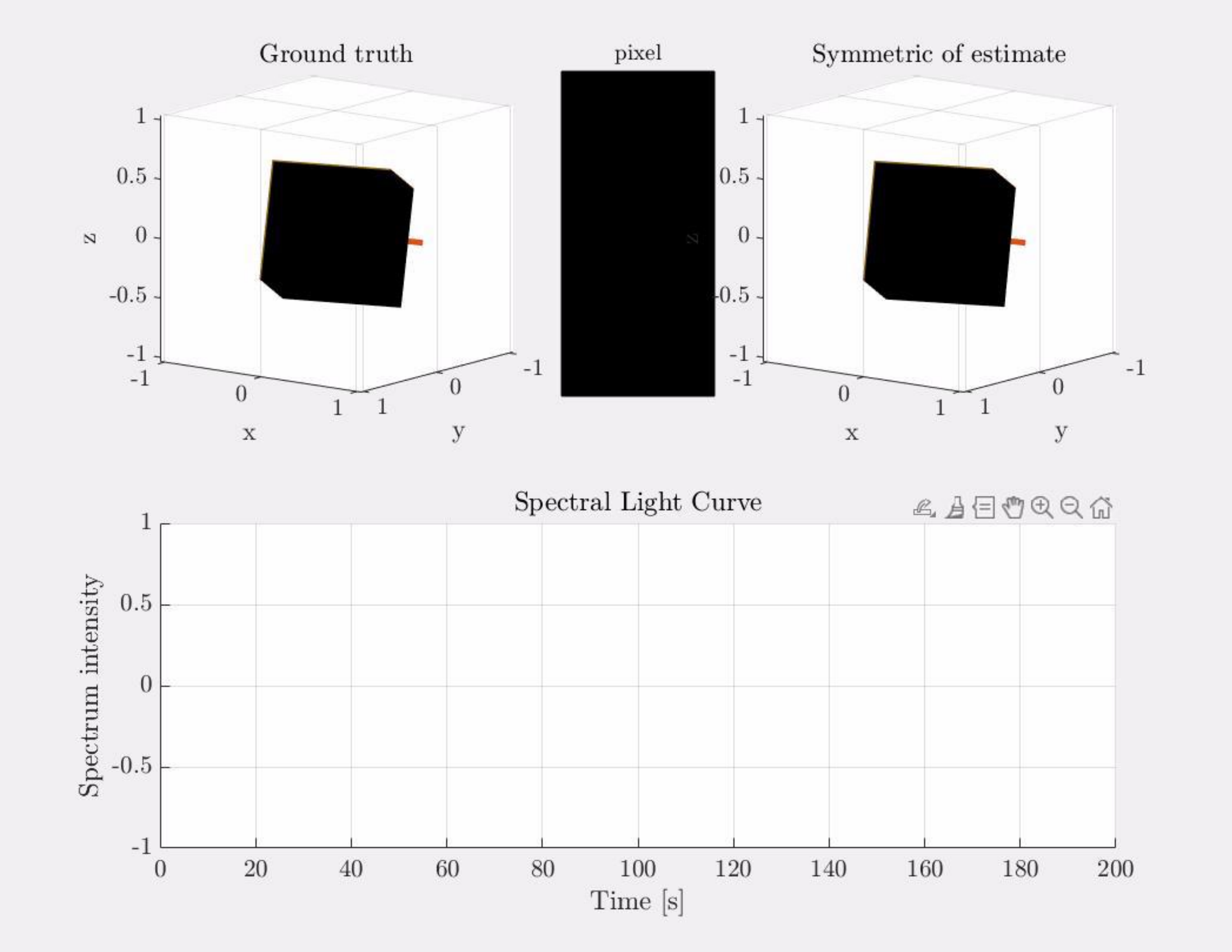

LS results – cube with symmetry

- The use of symmetry group improves the quality of the results. Starting only from the initial guess obtained with PDM+grid search (grey column) would lead to worse results:

Table 1: $log_{10}(L)$ when using elements of $\mathcal{R}(\mathbf{q}_0)$ as initial guess

method	interior point				DDP			
T_b	I	T_{BR}			I	T_{BR}		
T_h	I	$R_h(\pi)$	T_{Hsv}	T_{HM}	I	$R_h(\pi)$	T_{Hsv}	T_{HM}
$\hat{S}^{(1)}$	-3.59	$\mathbf{-11.89}$	-0.62	0.00	-4.82	-8.53	-0.64	0.05
$\hat{S}^{(2)}$	-1.81	$\mathbf{-11.67}$	-1.05	0.17	-4.19	-8.28	-5.95	-0.08
$\hat{S}^{(3)}$	-3.95	-2.13	0.28	0.04	-4.99	-3.98	0.27	0.59
$\hat{S}^{(4)}$	-1.34	-2.43	0.08	$\mathbf{-12.21}$	-2.56	-4.63	0.07	-8.55
$\hat{S}^{(5)}$	-11.54	-1.55	-1.55	-0.62	-8.65	-1.52	-1.54	-0.86
$\hat{S}^{(6)}$	-4.33	$\mathbf{-13.27}$	-0.69	-5.63	-6.03	-9.29	-0.74	-6.23

- DDP usually produces worse results for the loss function, but in this case only slightly (these are log values), but it's much faster:
  - interior-point: $\mu = 29s$
  - DDP: $\mu = 19s$
- A probable reason for DDP's inferior performance may be related to the current implementation's use of finite difference instead of analytical gradients used with interior point.

LS results – cube with symmetry

- Occasionally, the model will still converge to a symmetric case, but for fixed axis rotation, in the absence of noise the ground truth has the lowest cost

T_b	I		T_{BR}	
T_h	I	$R_h(\pi)$	T_{Hsv}	T_{HM}
$\hat{S}^{(1)}$	0.00°	180.00°	91.43°	114.38°
$\hat{S}^{(2)}$	0.00°	180.00°	111.12°	110.83°
$\hat{S}^{(3)}$	122.09°	126.39°	1.47°	179.52°
$\hat{S}^{(4)}$	0.00°	180.00°	125.67°	122.00°
$\hat{S}^{(5)}$	0.00°	180.00°	112.13°	113.19°
$\hat{S}^{(6)}$	0.00°	180.00°	76.93°	135.52°

RMS θ for test case 1A comparing estimated attitude to closest element of $\mathcal{R}$

The method should be seen as providing the user with a family of possible attitudes, depending on symmetries

More challenging dataset – Dragon capsule precessing

- A new dataset was generated where the ground truth object is more complex – a Dragon capsule, and it is precessing
- The old method to generate an initial guess was failing often, so a more robust approach was designed
- A combination of a grid search for the initial state followed by iteratively building up the attitude history one time step at a time
- No need for PDM or assumptions of fixed axis rotation to get the initial guess
- Promising results so far (next slide)
- Ideal for use with best-first search algorithm – next step

- For each q0 in grid, in order of how close resulting spectra is to first observation
  - qHist = {q0}
  - For n from 2 to N_T
    - Minimise J for lightcurve up to t_n using previous qHist as initial guess, and update qHist
    - cost = J(qHist)
    - If current cost is above smallest_cost, stop
  - smallest_cost = min(cost, smallest_cost)

More challenging dataset – Dragon capsule precessing

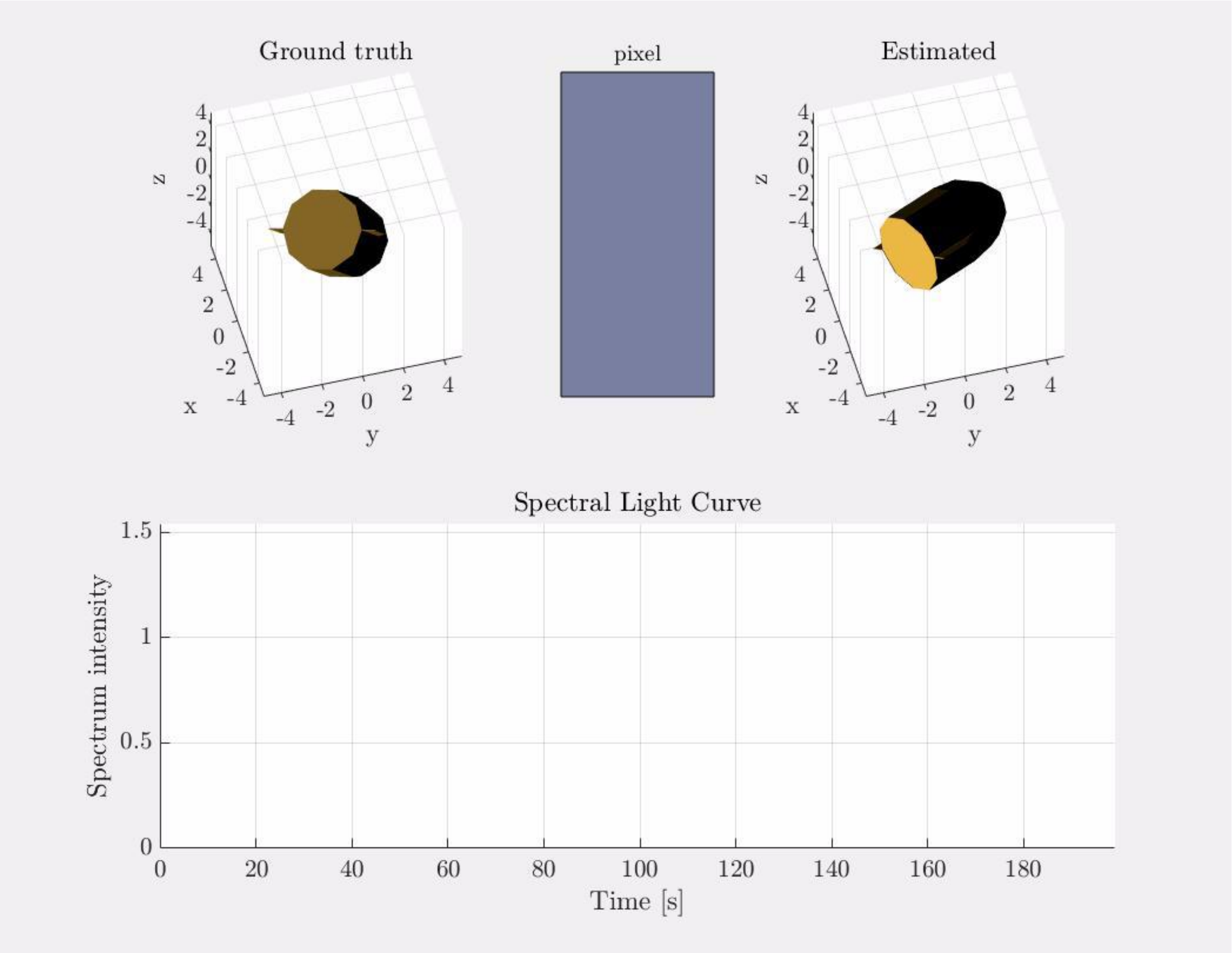

RMS θ for test case 2 comparing estimated attitude to closest element of $\mathcal{R}$

J	I	J_1	J_2
$\hat{S}^{(1)}$	$0.00°$	$0.03°$	$6.07°$
$\hat{S}^{(2)}$	$0.04°$	$0.50°$	$0.11°$
$\hat{S}^{(3)}$	$0.03°$	$0.04°$	$0.03°$
$\hat{S}^{(4)}$	$0.43°$	$0.19°$	$0.10°$
$\hat{S}^{(5)}$	$0.01°$	$0.20°$	$0.05°$

Machine learning - recap

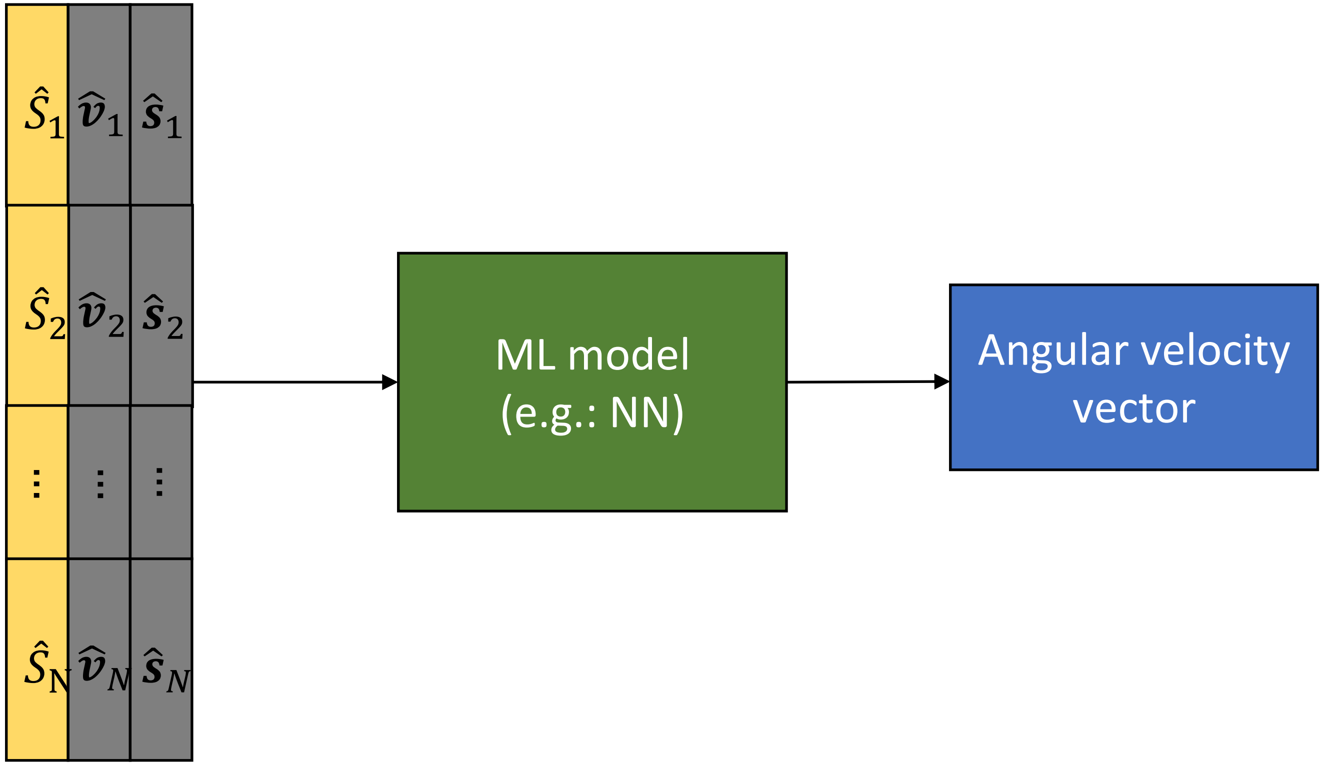

Training data:

- Fixed and non-fixed axis rotation
- Different object models
- Different orbits
- Different observation geometries
  - Orbit simulated, with constraints previously mentioned on elevation, illumination and night observation

Machine learning - recap

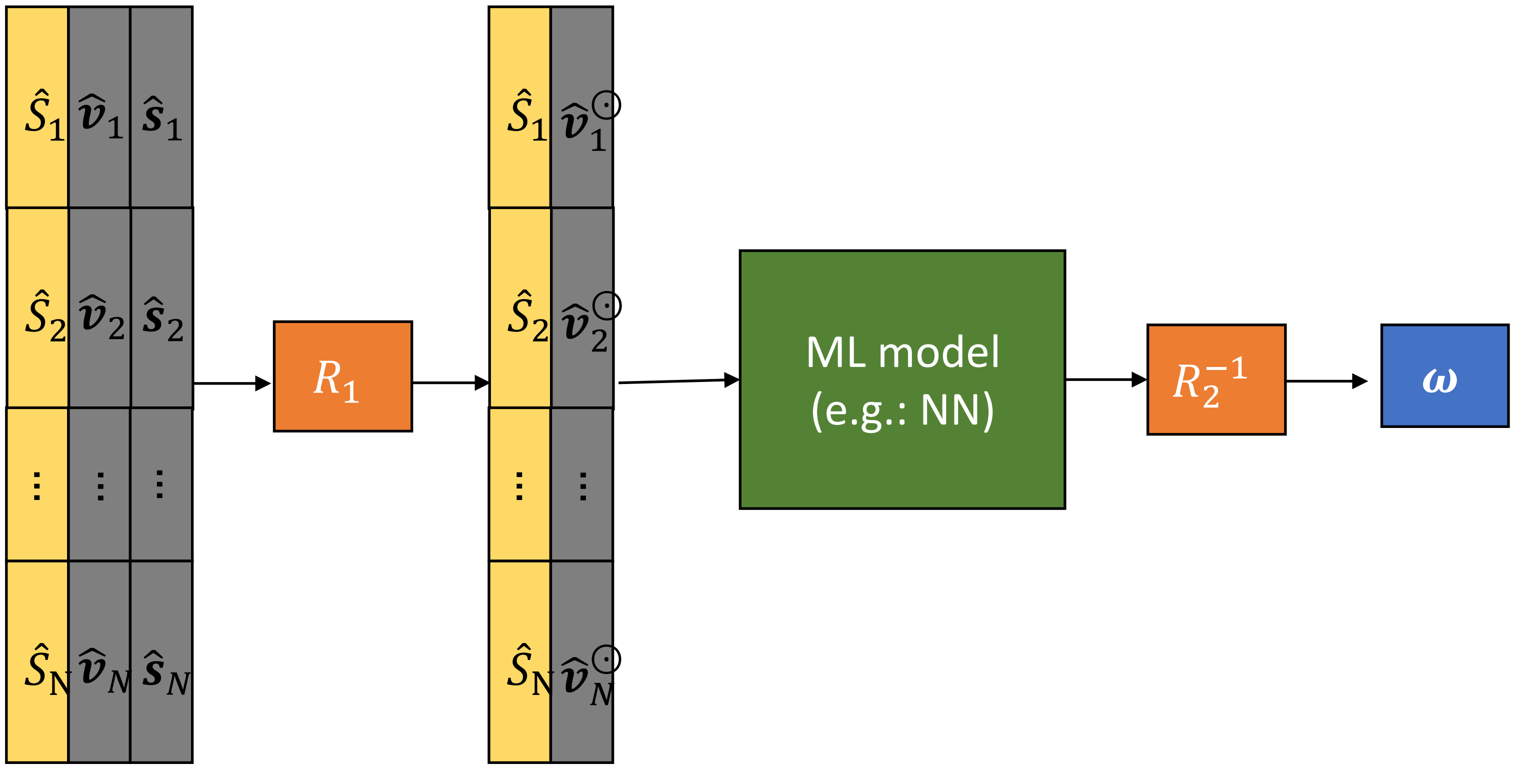

- Redundant data:
  - Rotating s and v vectors in input would correspond to the same rotation in the output
  - The sun direction varies very little
- Reducing this redundancy can allow significantly reducing the amount of input dimensions
- Choosing a frame where s is [1,0,0], and writing v and angular velocity in that frame

Machine learning - tests

- Different frames tested for both input and output

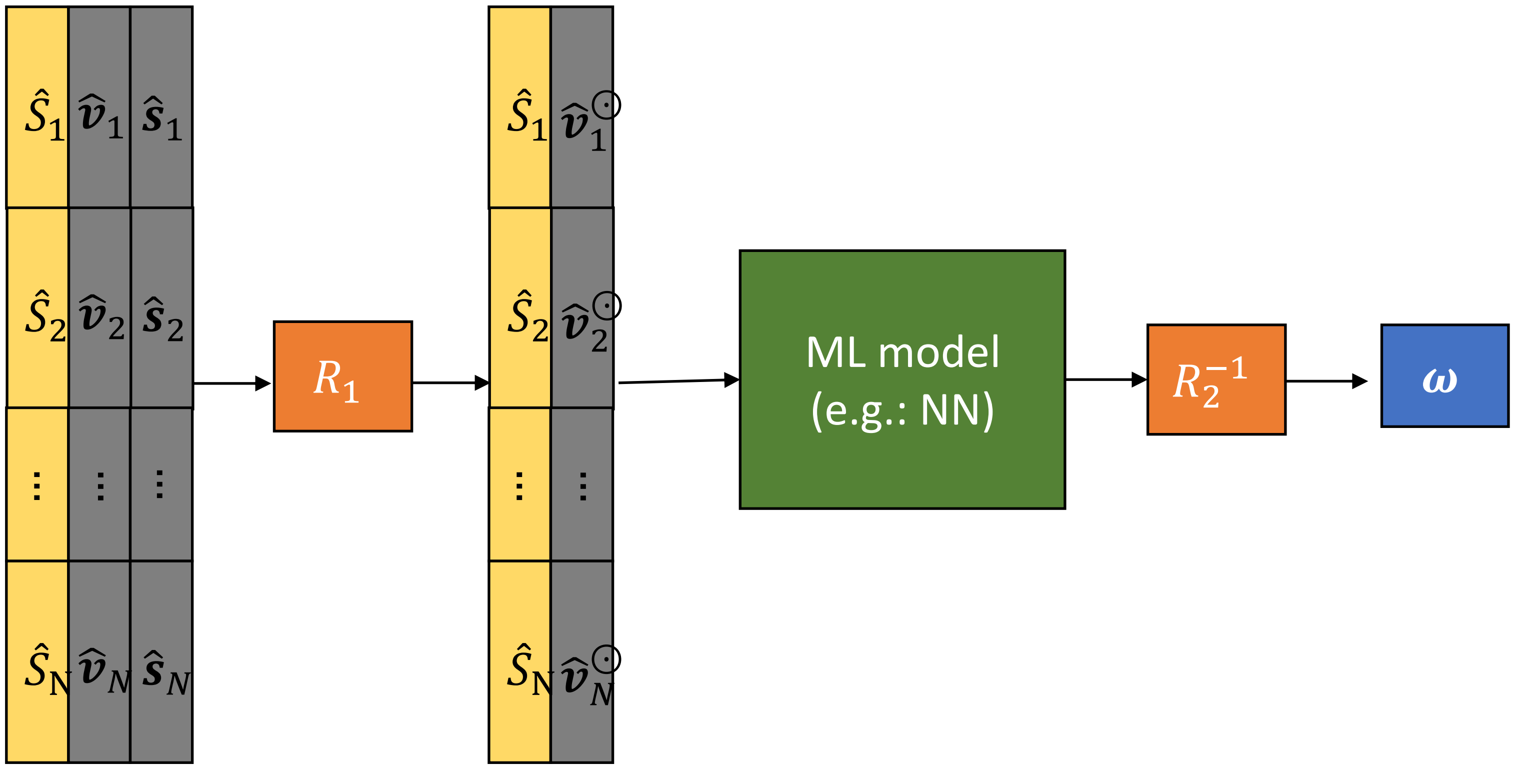

- Input data:
  - v and s in inertial frame
  - v only, in “Sun” frame
  - v only, in Sun-view frame
- Output data: midpoint angular velocity vector in
  - inertial frame
  - body frame
  - H frame
  - other
- Model:
  - Single layer
  - Two layers
  - Two layers with dropout

ML results – different input frames

- Input data:
  - v and s in inertial frame
  - v only, in “Sun” frame
  - v only, in Sun-view frame
- Output data: midpoint angular velocity vector in
  - inertial frame
  - body frame

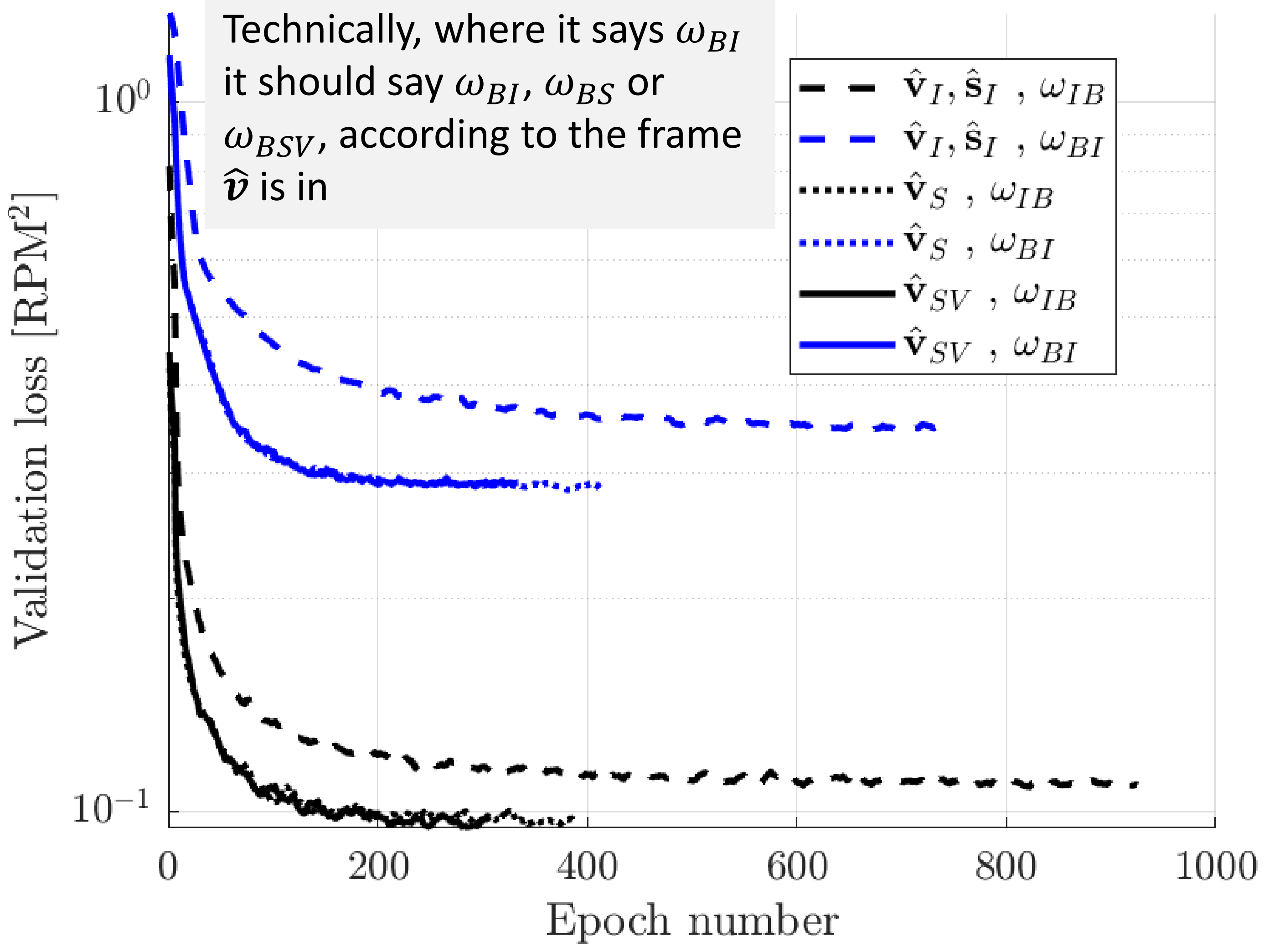

Technically, where it says ω_{BI} it should say ω_{BI}, ω_{BS} or ω_{BSV}, according to the frame $\hat{\boldsymbol{v}}$ is in

ML results – output frame

- Input data:
  - v only, in Sun-view frame
- Output data: midpoint angular velocity vector in
  - inertial frame
  - body frame
  - H frame
  - symmetry removal tests

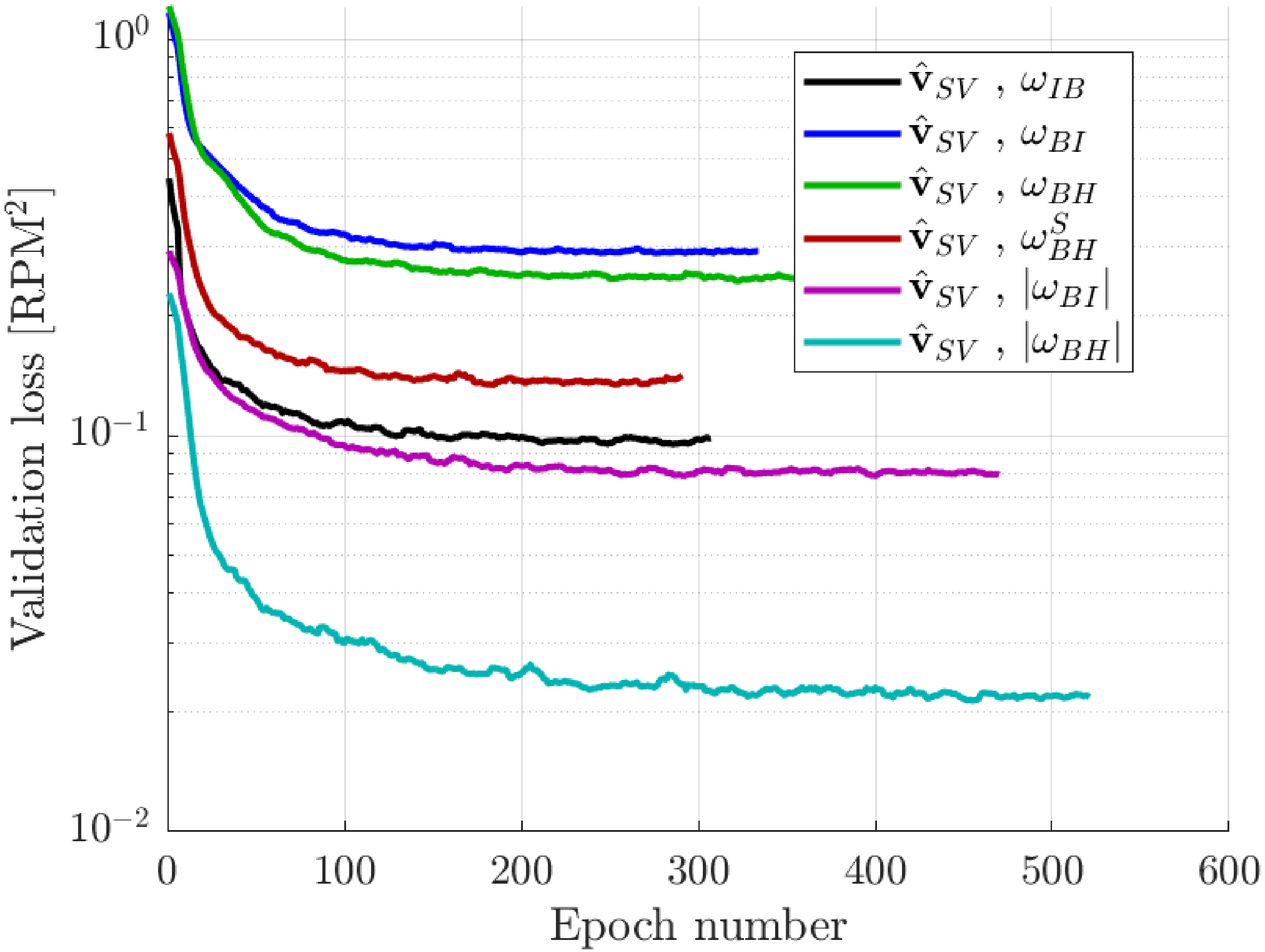

ML results – model architecture

- Input data:
  - v only, in Sun-view frame
- Output data: midpoint angular velocity vector in
  - inertial frame
  - symmetry removal tests
- Model:
  - Single layer (600)
  - Two layers (600, 50)
  - Two layers with dropout (600, 20%, 50)
  - (1000, 20%, 100, 20%)
  - (1000, 20%, 200, 20%, 50, 20%)

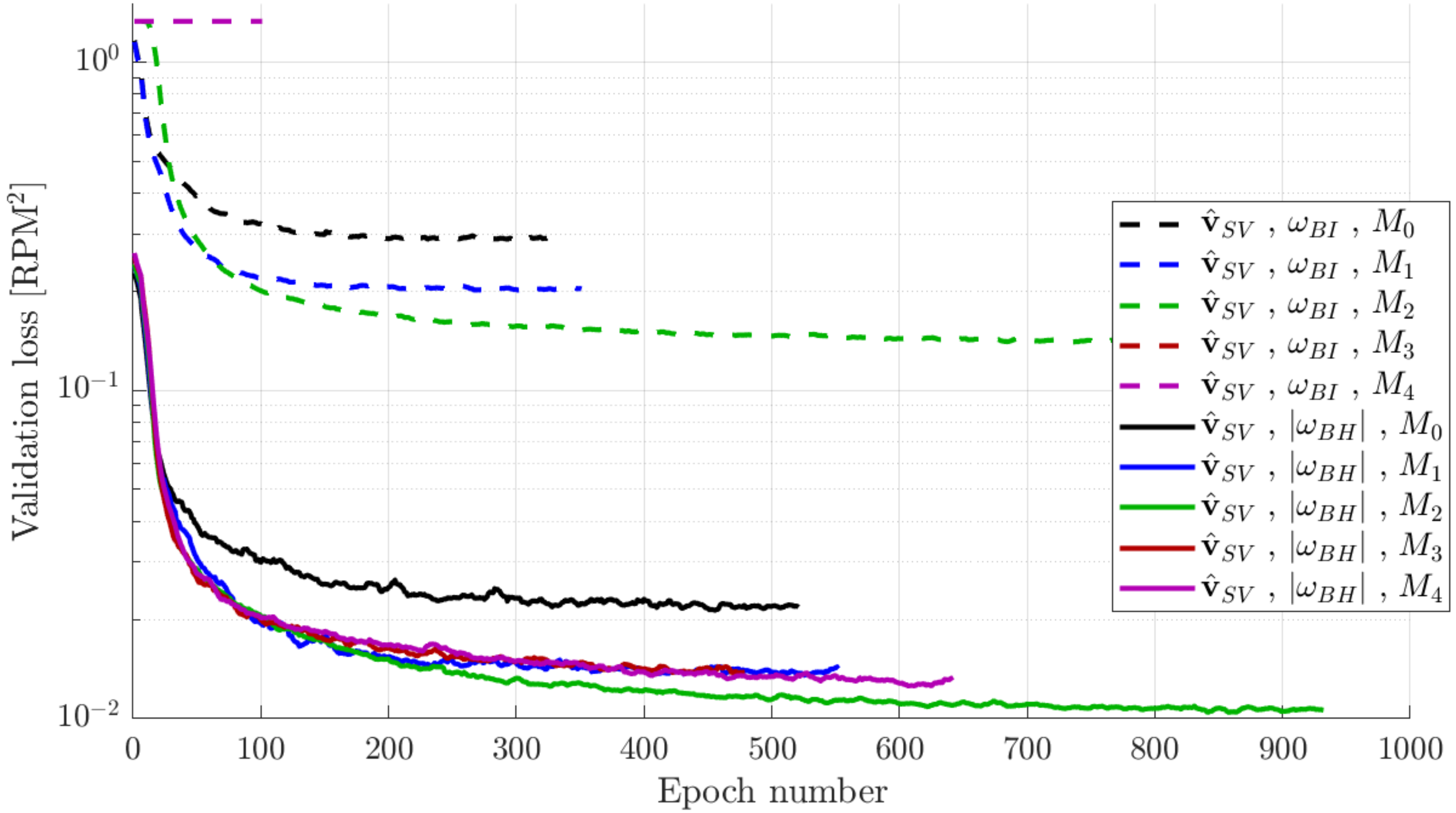

WP3 – Testing in relevant environment and prototyping

- Model Calibration
- Experimental validation
- Endmember analysis from lab data

Experimental setup

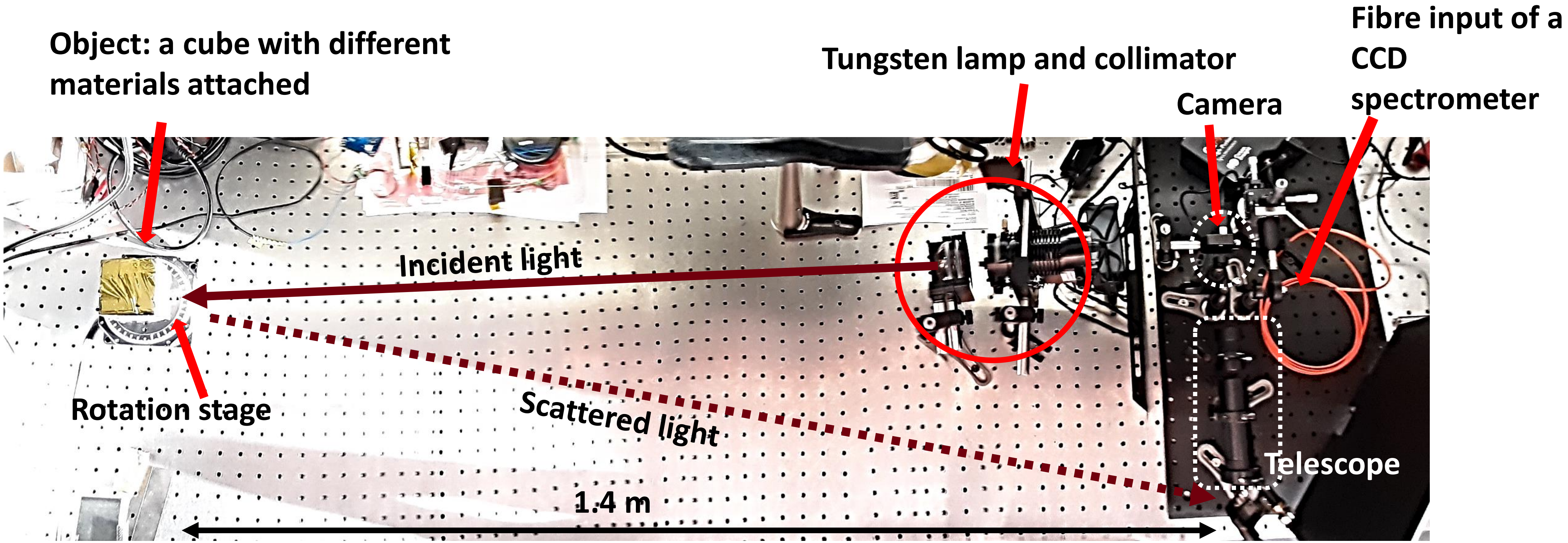

Experimental setup

Camera view of a cube

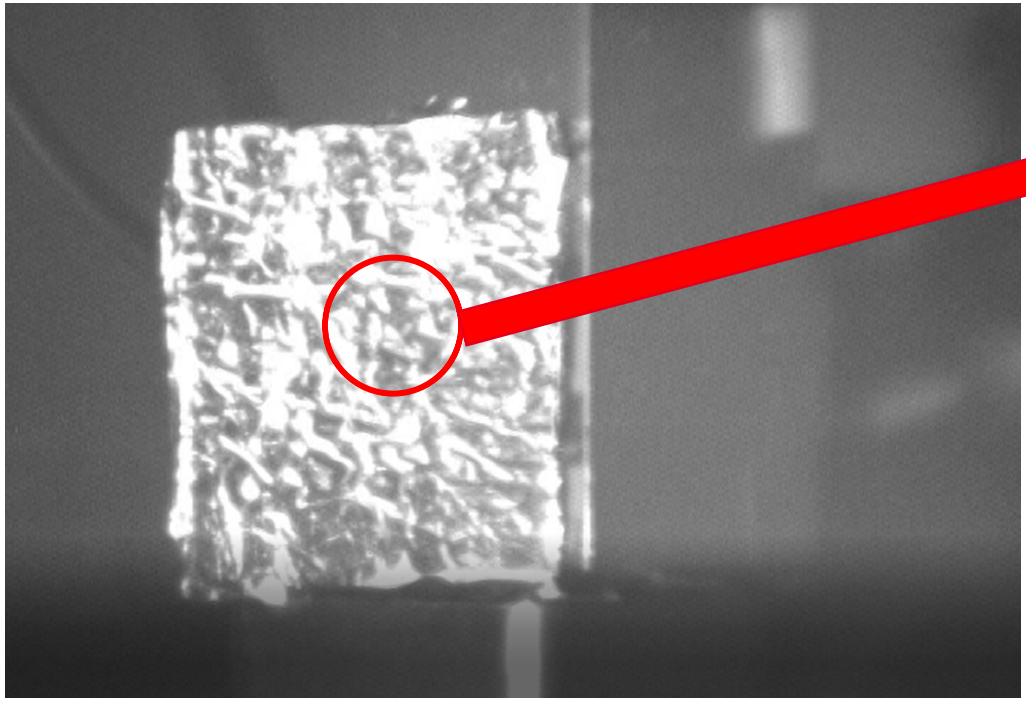

Signal from 1.5 cm diameter area is measured by spectrometer

Corresponds to 200um fibre input diameter of spectrometer

Experimental results

Rotating cube, 6°/s , materials: Al and gold foil

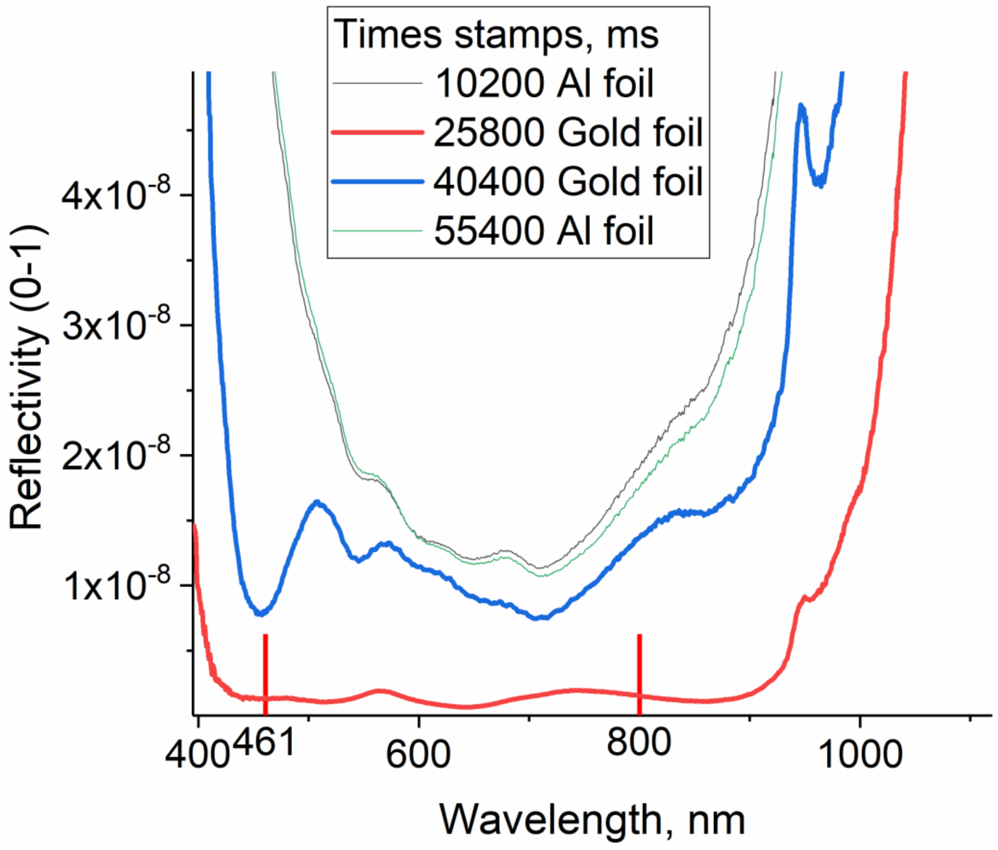

Some examples of R spectra at max signal

The spectra are shown for different time from the start of experiment (time stamps), which correspond to different rotation angle of the cube

Distinct features in R spectra at ~461 and 800 nm

Experimental results

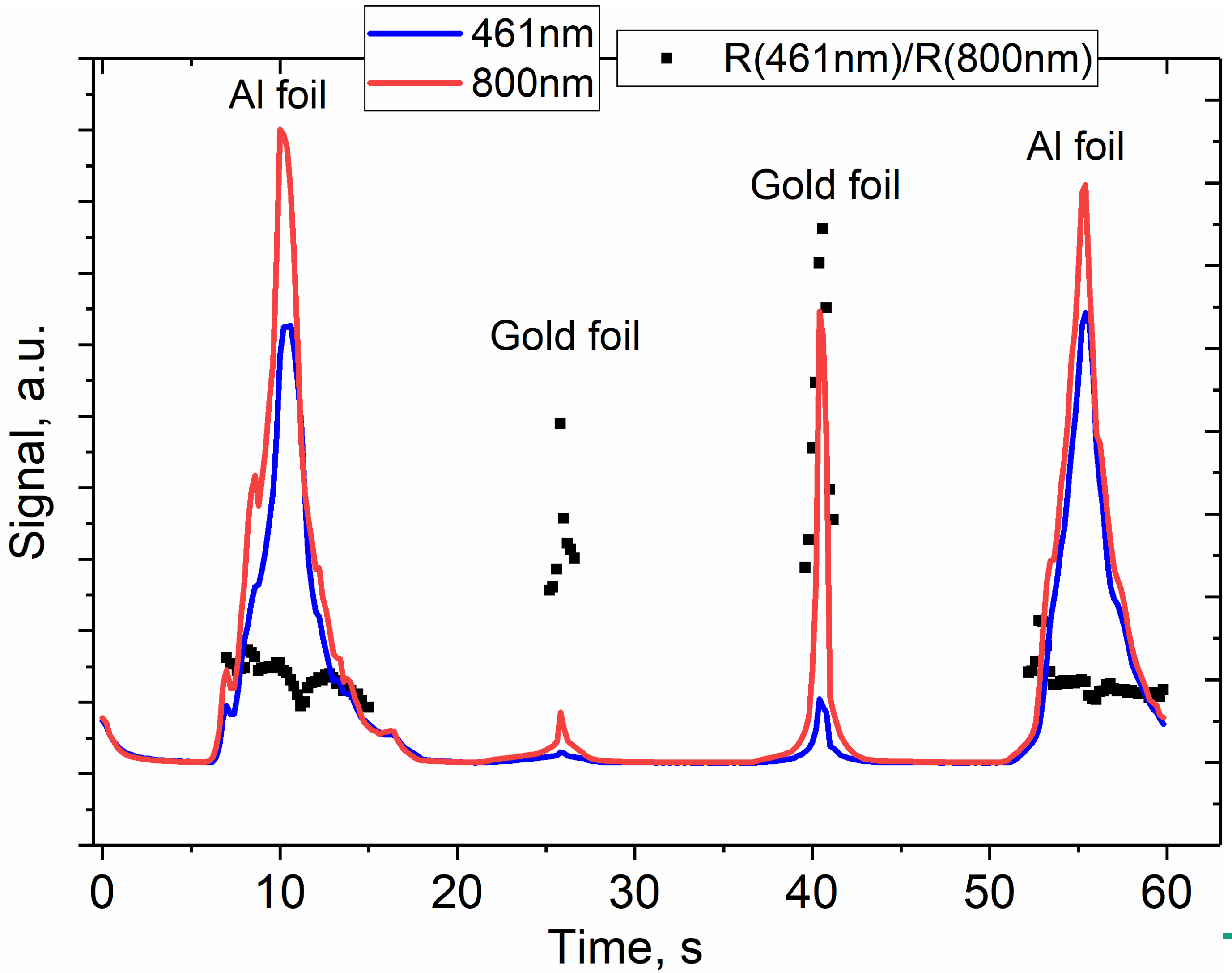

The ratio of reflectivity of Al and gold foil at the wavelengths of 461 and 800 nm (squares) as a function of rotation time

Solid lines – the actual signal at these two wavelengths
The ratio is shown only at the time stamps corresponding to max signal at these two wavelengths, otherwise the signal ratio noise ratio is too small

Some information about materials

Full R spectrum analysis for more complex cases (e.g. mixture of materials) - Endmemeber analysis above

Consistency of R measurements

setup with and without a diffuser in front of fibre input of monochromator

- ✓ Without diffuser, 20 ms/ spectrum, monochromator alignment for max signal
- ✓ With diffuser, 100 ms/spectrum, monochromator alignment for max signal
- ✓ Without diffuser, 100 ms/diffuser, same fibre alignment as above (i.e. the signal is not optimised for max)

Consistency of R measurements: setup with and without a diffuser in front of fibre input of monochromator

Gold-Al (crinkly) surface 1 -Al (crinkly) surface 2 -Al (smooth) on rotating cube

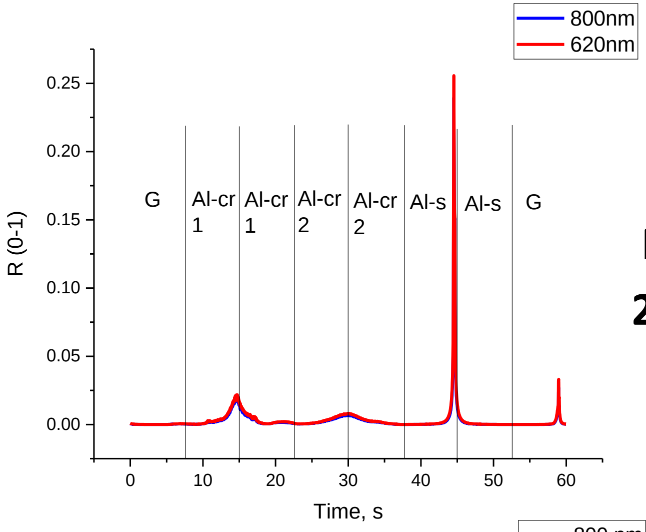

No diffuser

20 ms /spectrum

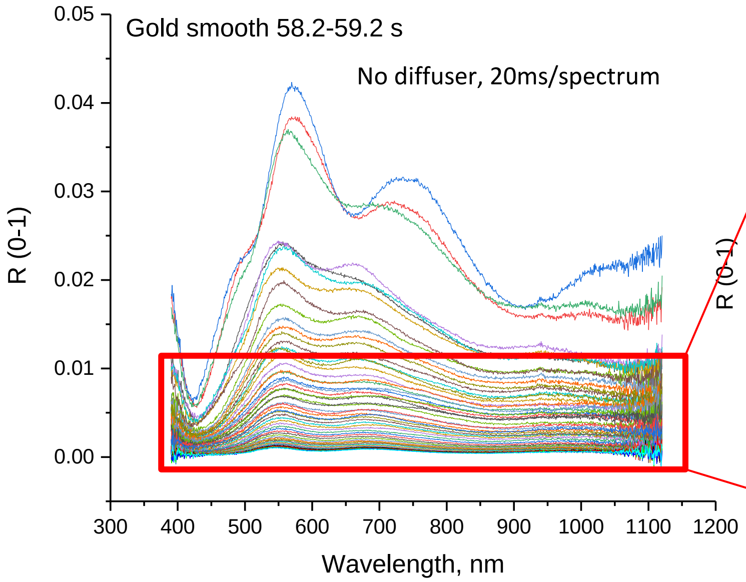

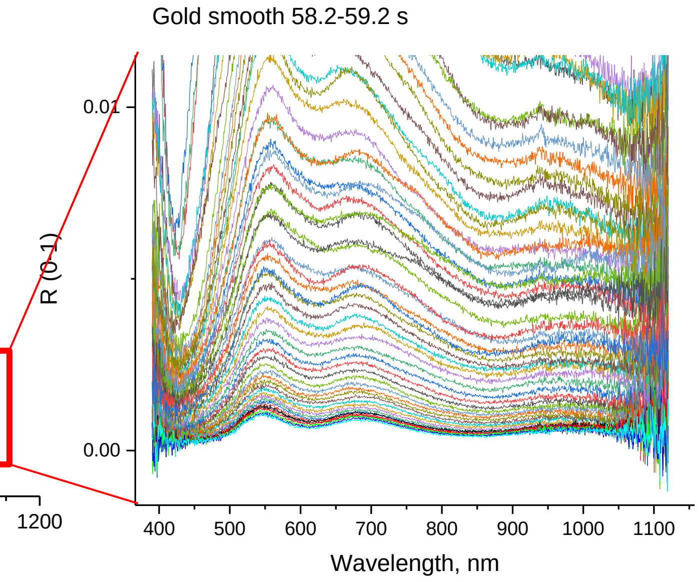

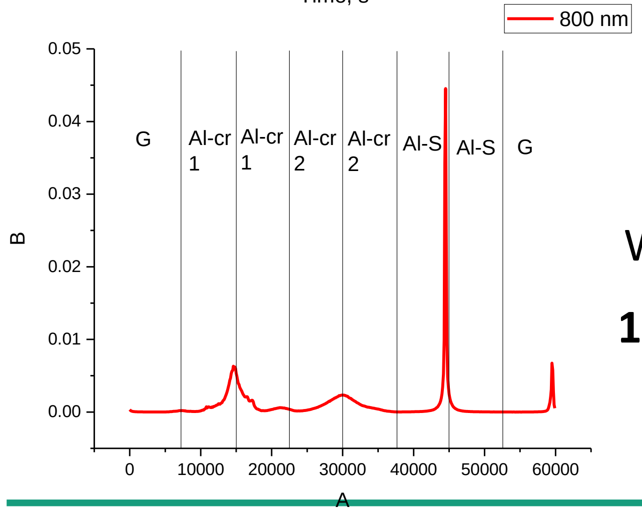

With diffuser

100 ms /spectrum

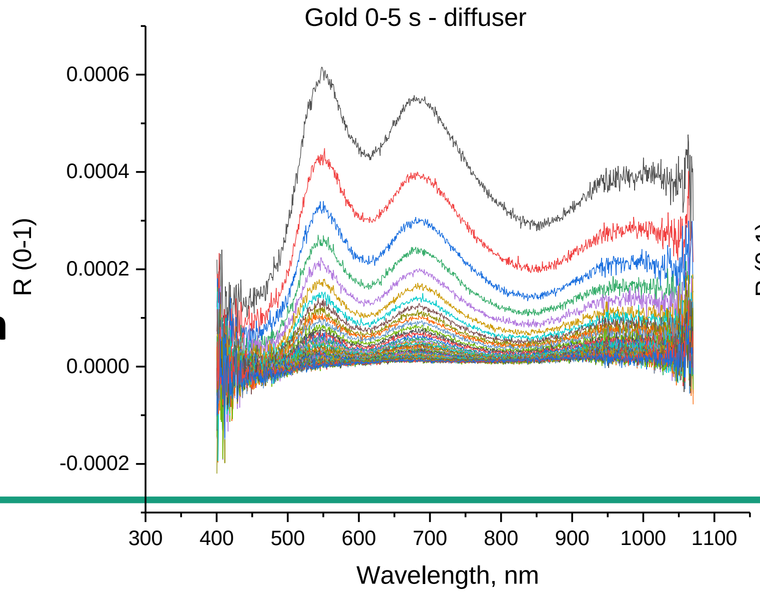

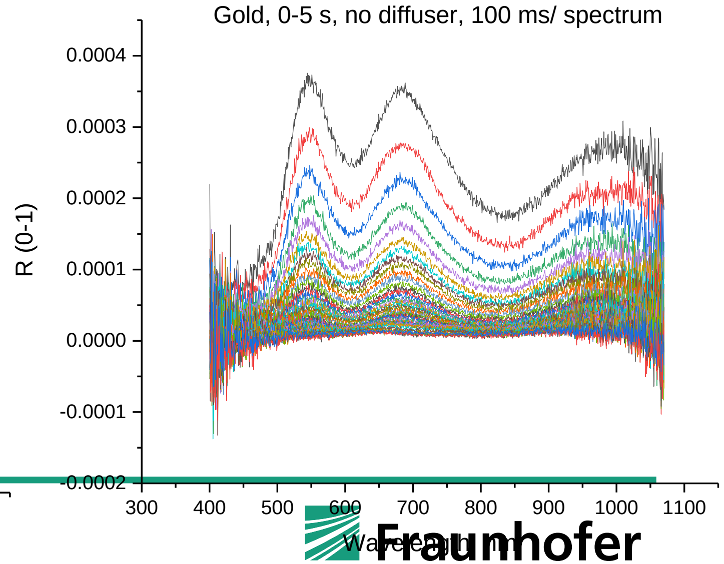

Consistency of R measurements: setup with and without a diffuser in front of fibre input of monochromator

Gold-Al (crinkly) surface 1 -Al (crinkly) surface 2 -Al (smooth) on rotating cube

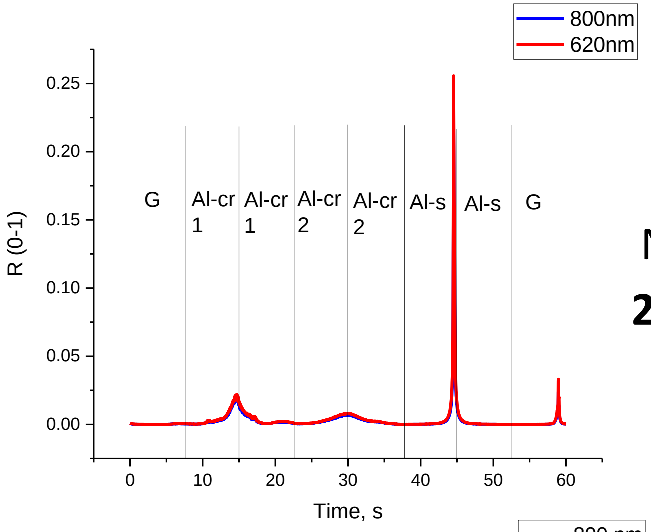

No diffuser

20 ms /spectrum

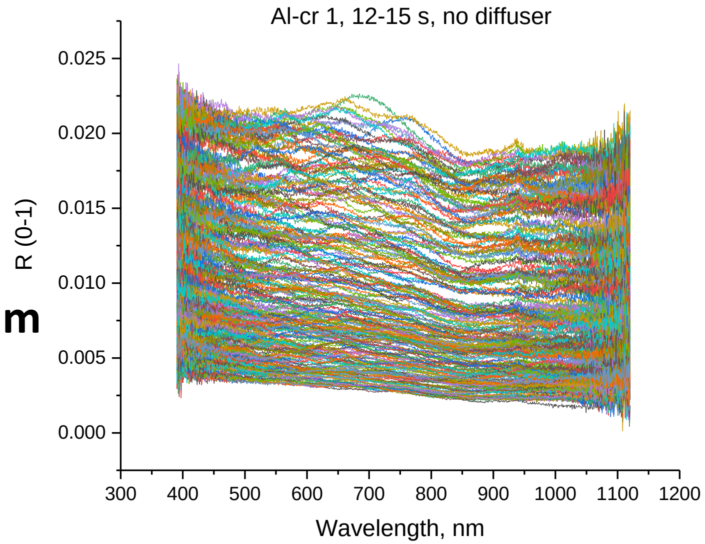

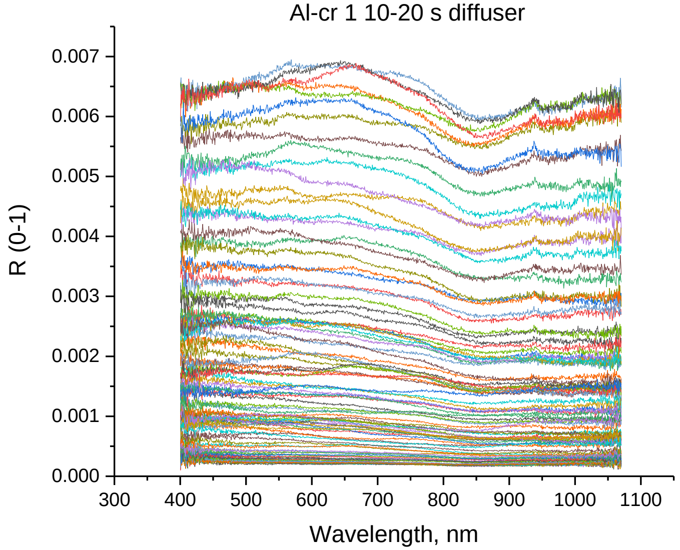

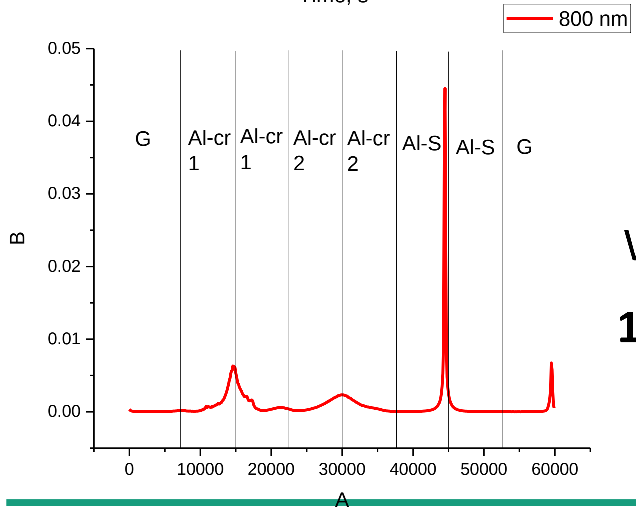

With diffuser

100 ms /spectrum

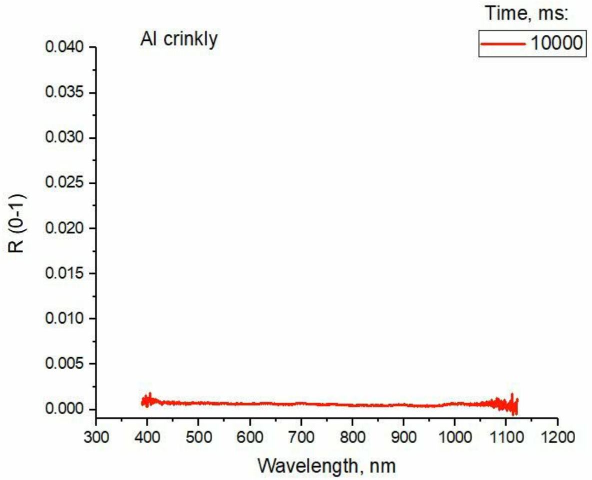

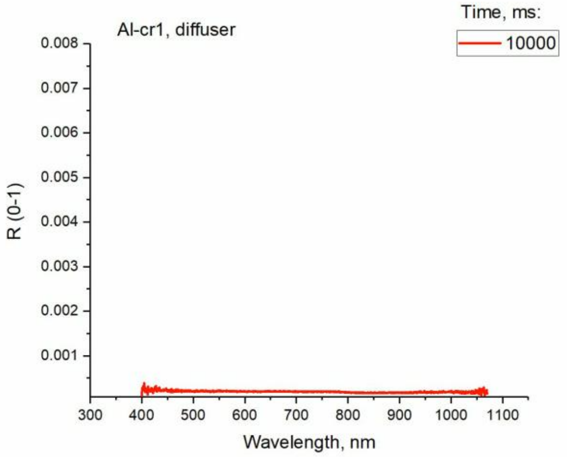

Consistency of R measurements: setup with and without a diffuser in front of fibre input of monochromator

Gold-Al (crinkly) surface 1 -Al (crinkly) surface 2 -Al (smooth) on rotating cube

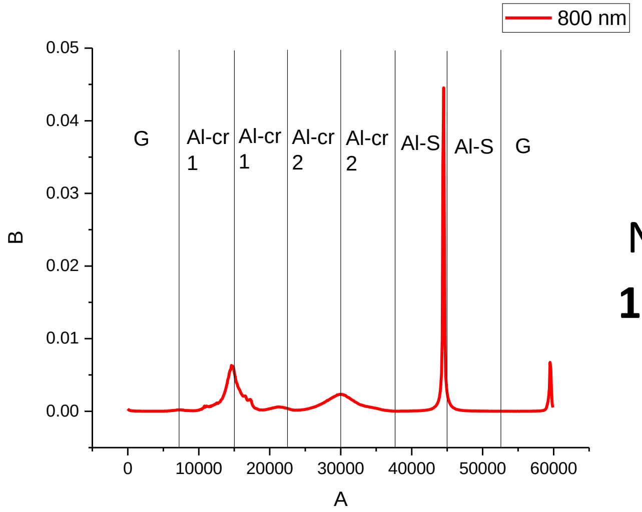

No diffuser

100 ms /spectrum

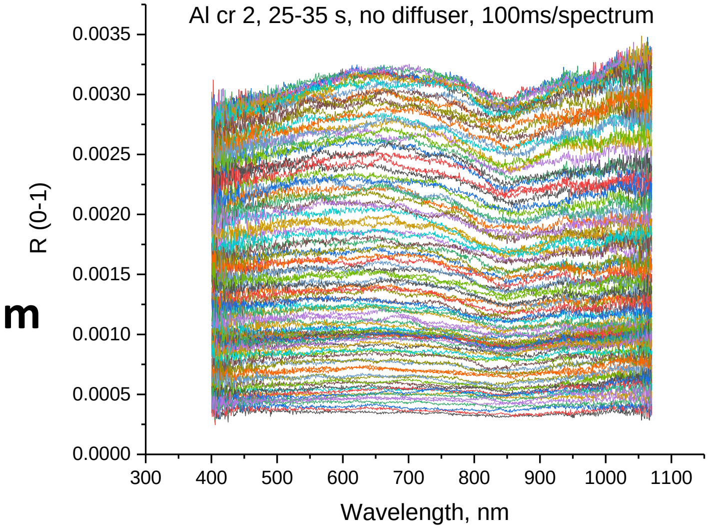

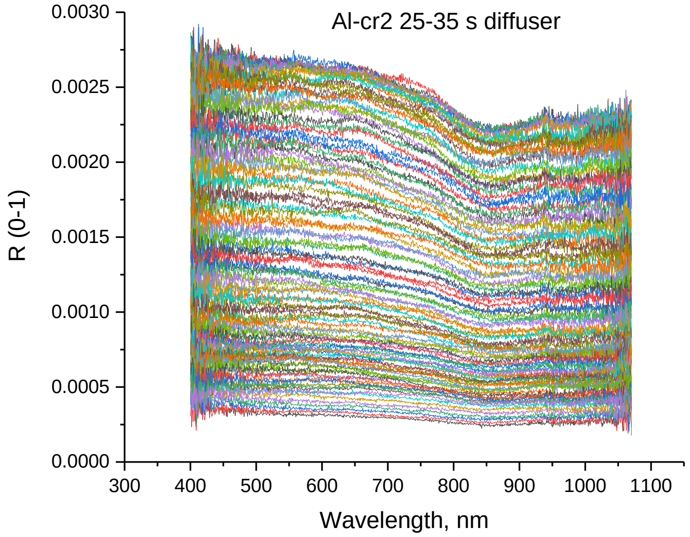

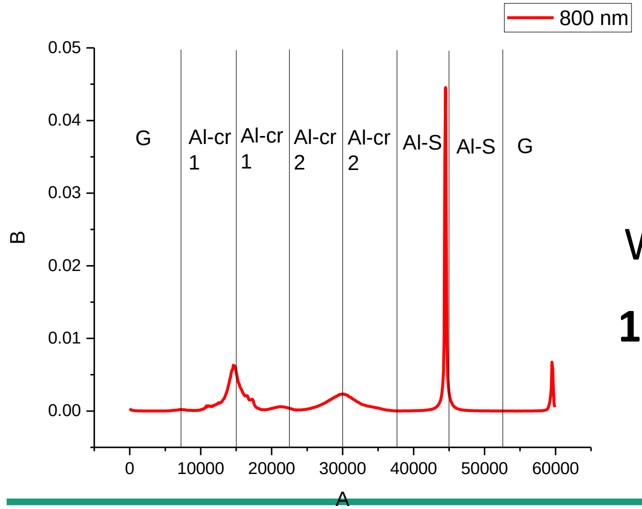

With diffuser

100 ms /spectrum

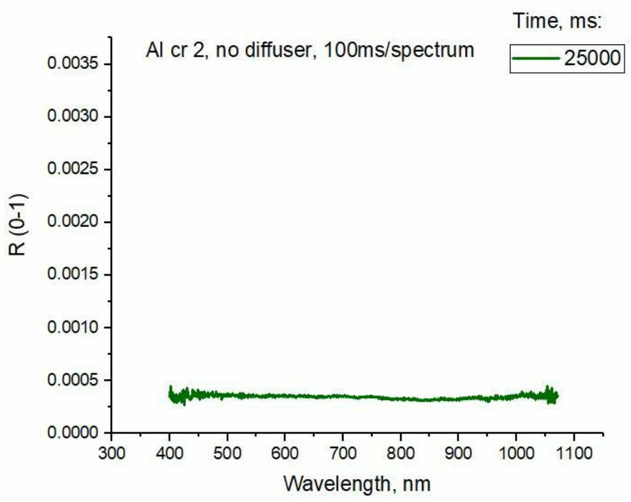

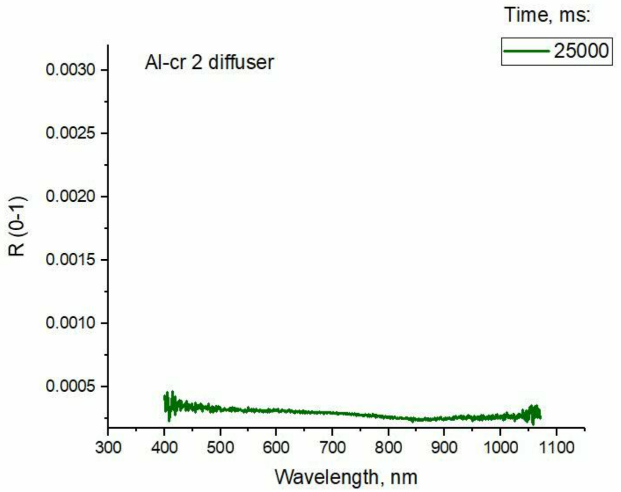

UK

Consistency of R measurements: setup with and without a diffuser in front of fibre input of monochromator

Gold-Al (crinkly) surface 1 -Al (crinkly) surface 2 -Al (smooth) on rotating cube

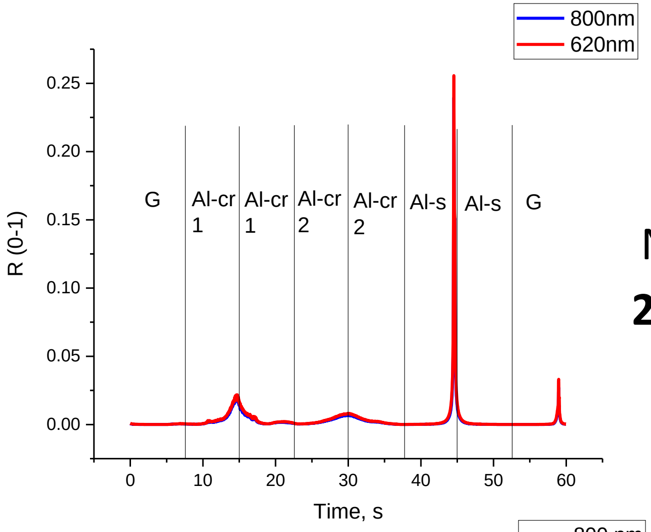

No diffuser

20 ms /spectrum

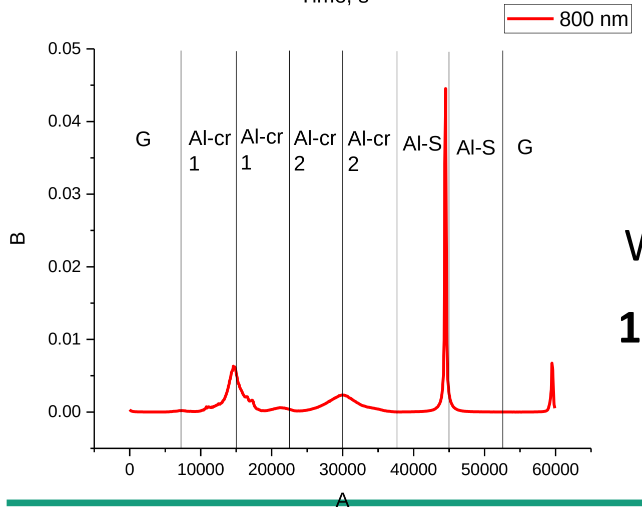

With diffuser

100 ms /spectrum

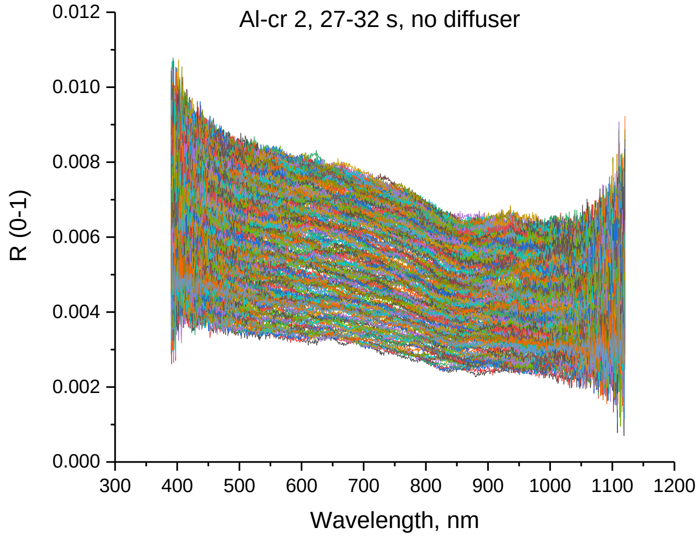

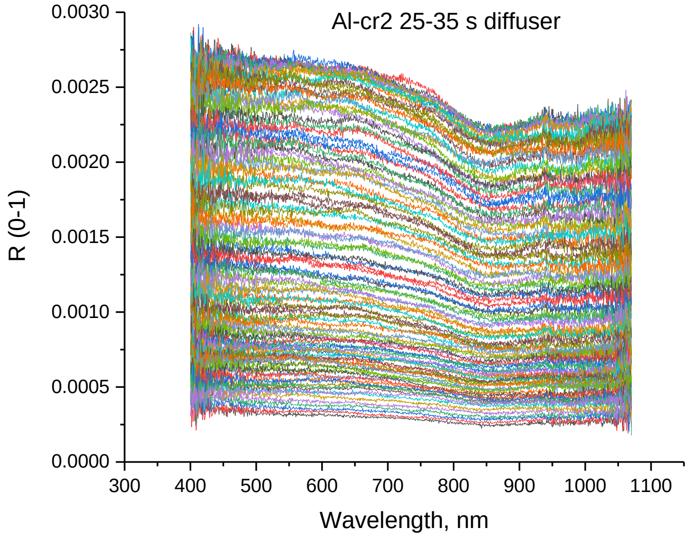

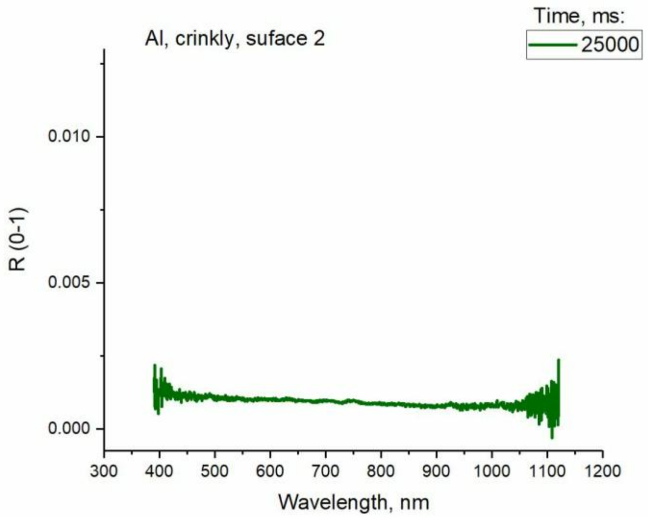

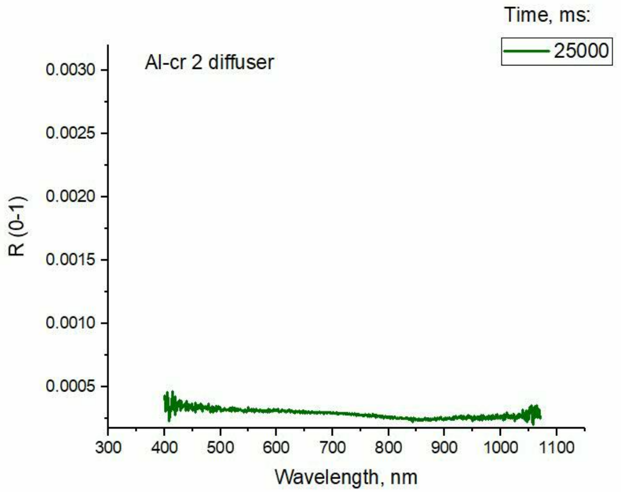

Consistency of R measurements: setup with and without a diffuser in front of fibre input of monochromator

Gold-Al (crinkly) surface 1 -Al (crinkly) surface 2 -Al (smooth) on rotating cube

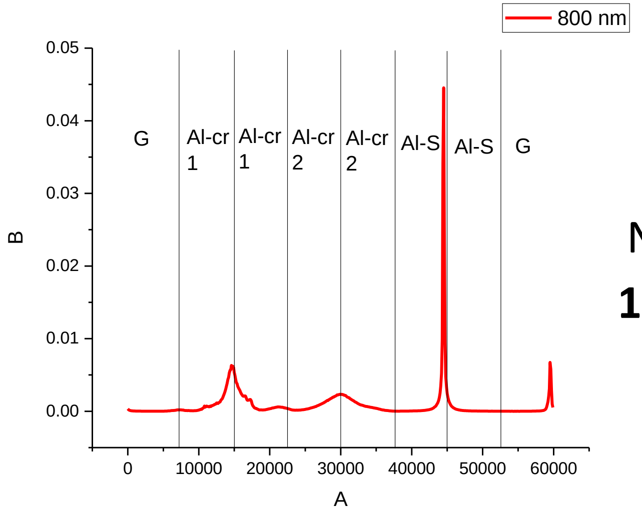

No diffuser

100 ms /spectrum

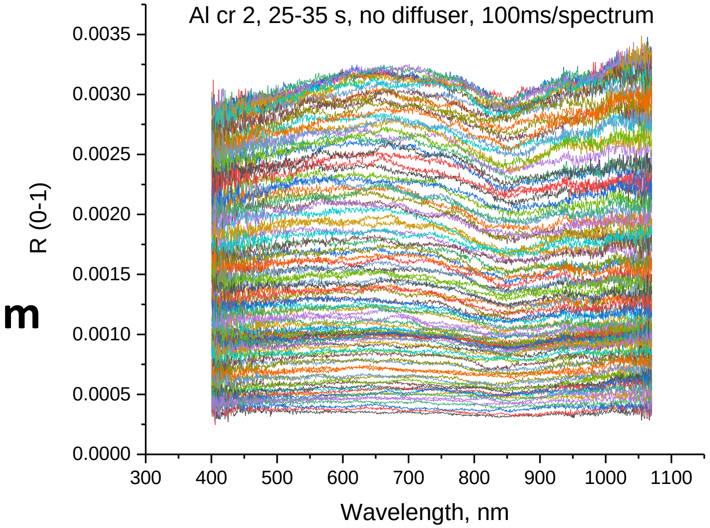

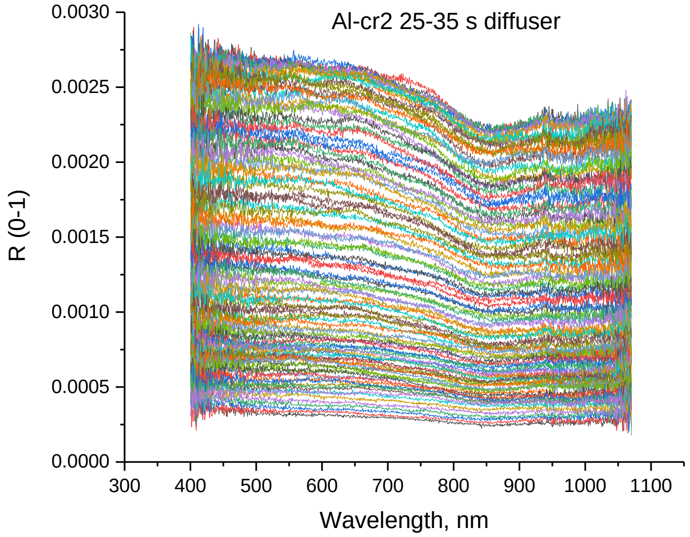

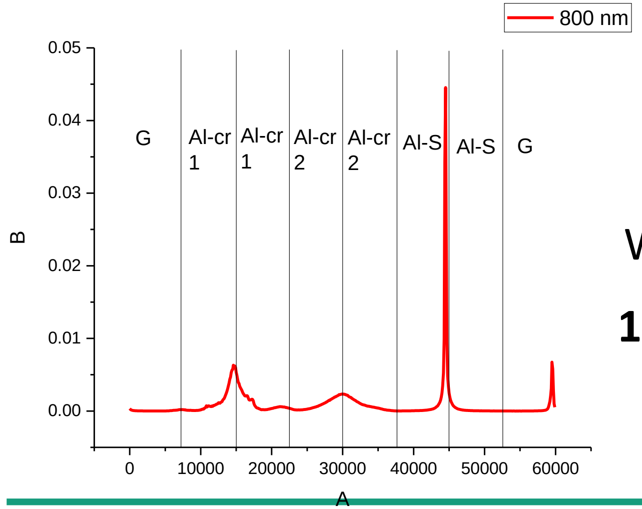

With diffuser

100 ms /spectrum

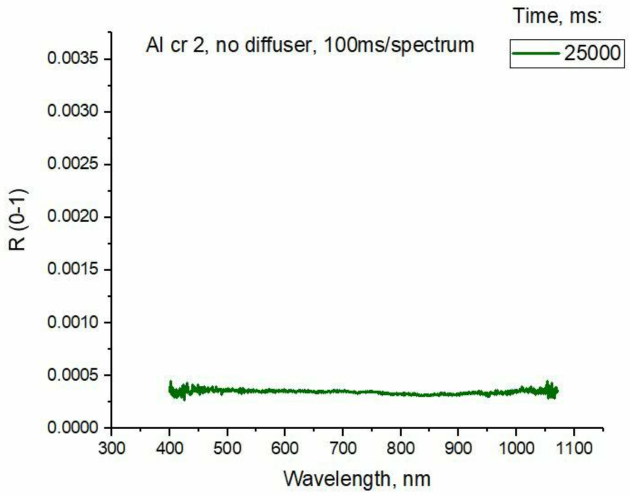

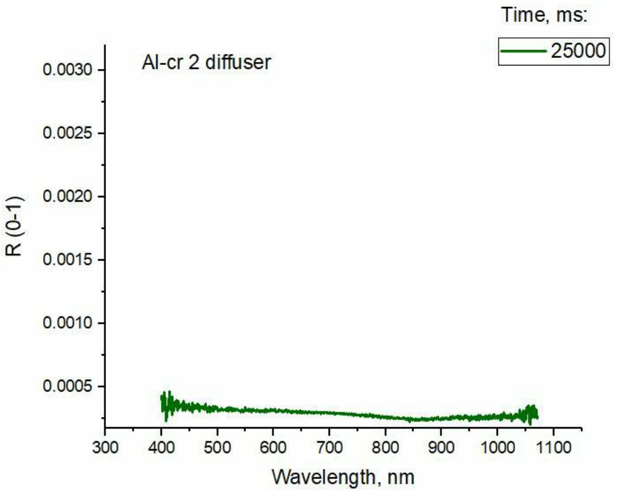

Consistency of R measurements: setup with and without a diffuser in front of fibre input of monochromator

Gold-Al (crinkly) surface 1 -Al (crinkly) surface 2 -Al (smooth) on rotating cube

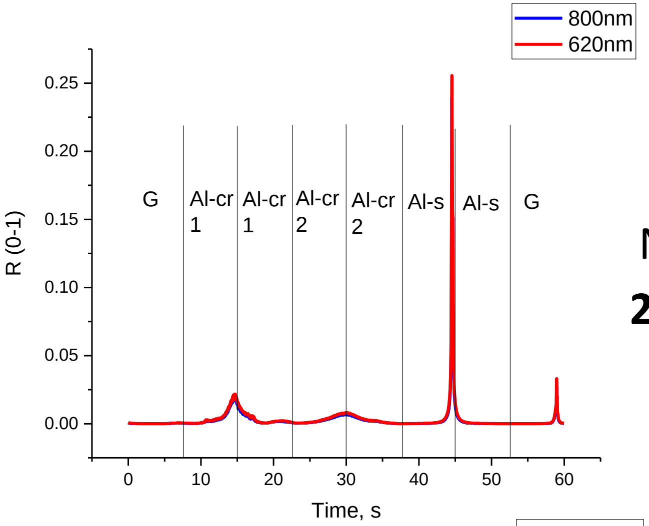

No diffuser

20 ms /spectrum

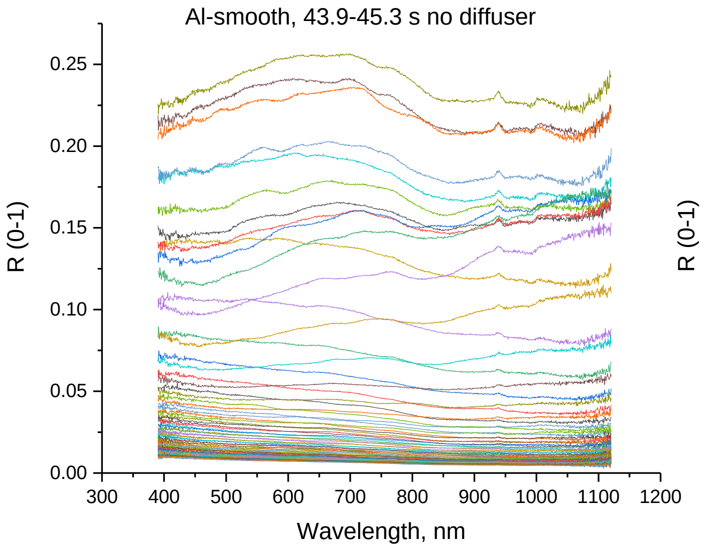

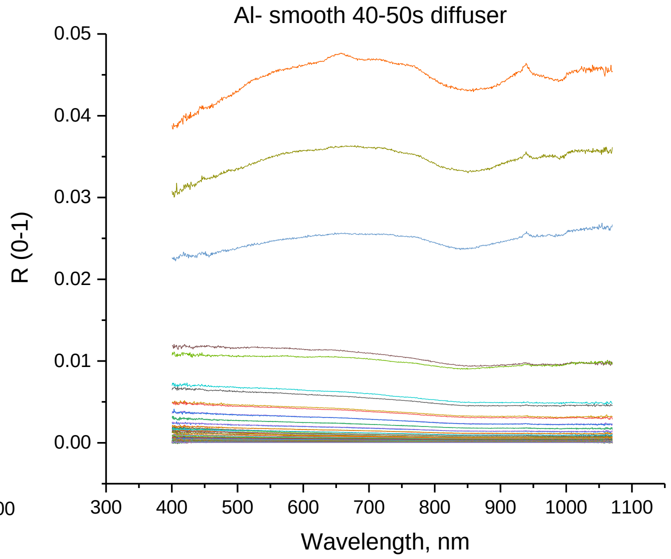

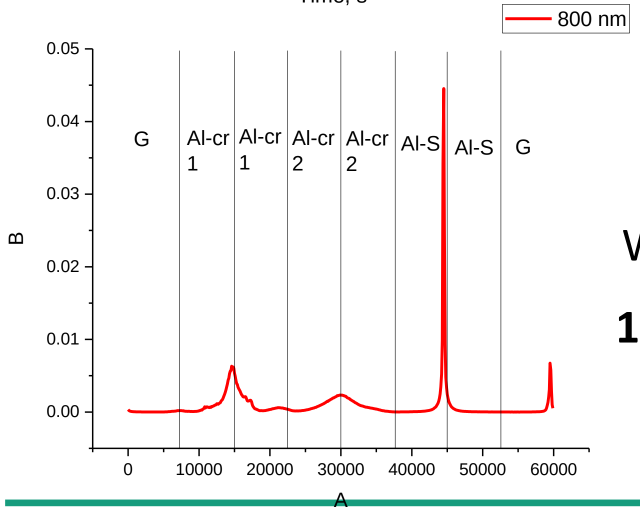

With diffuser

100 ms /spectrum

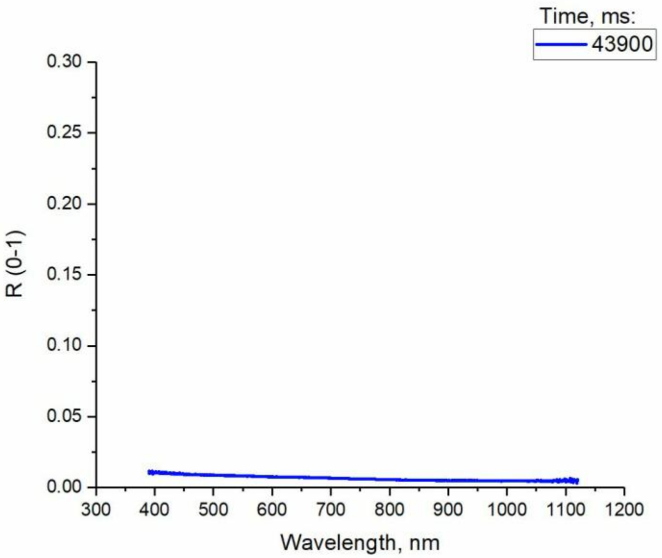

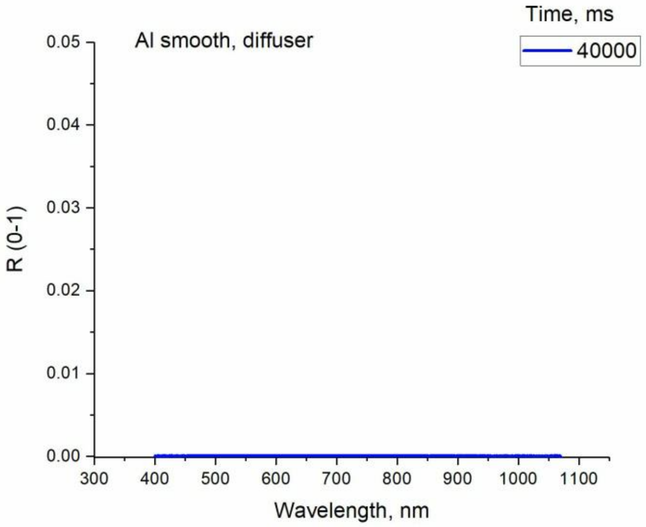

Consistency of R measurements: setup with and without a diffuser in front of fibre input of monochromator

Gold-Al (crinkly) surface 1 -Al (crinkly) surface 2 -Al (smooth) on rotating cube

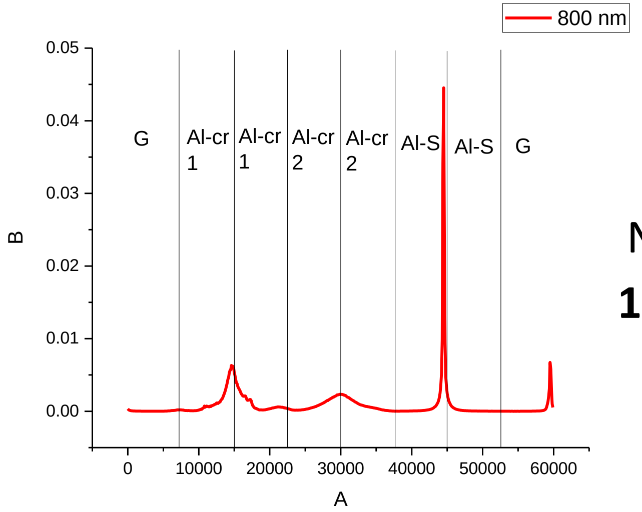

No diffuser

100 ms /spectrum

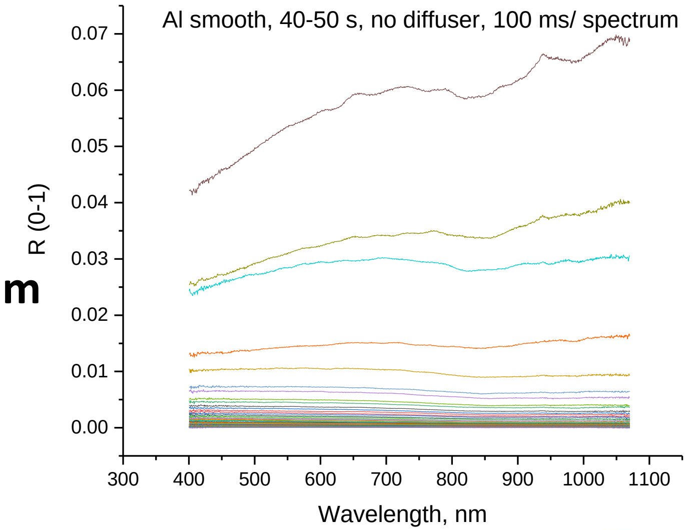

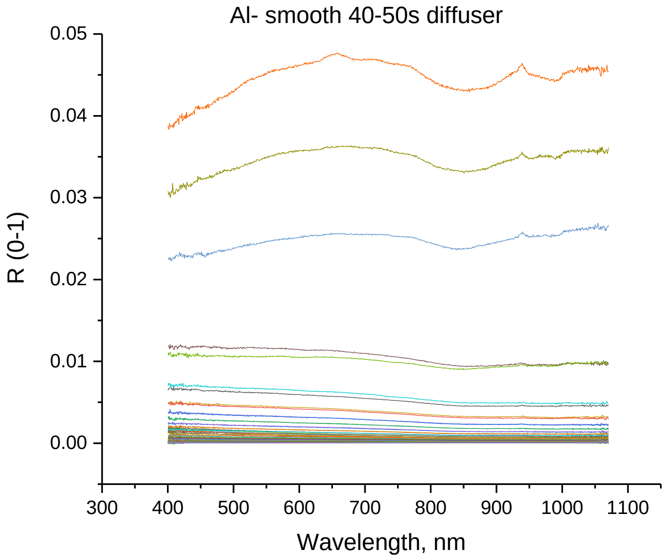

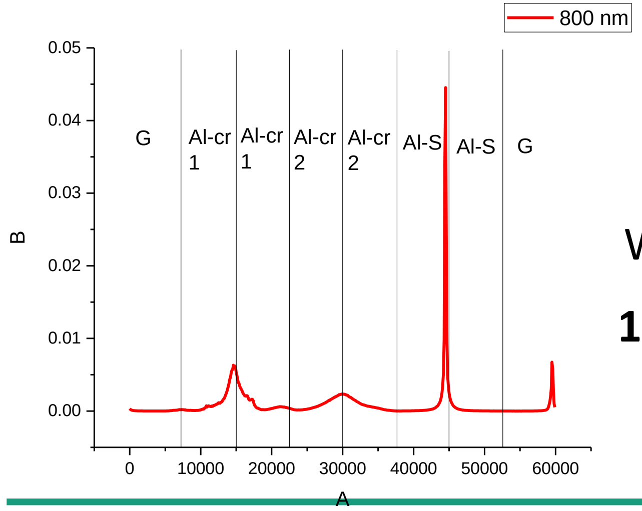

With diffuser

100 ms /spectrum

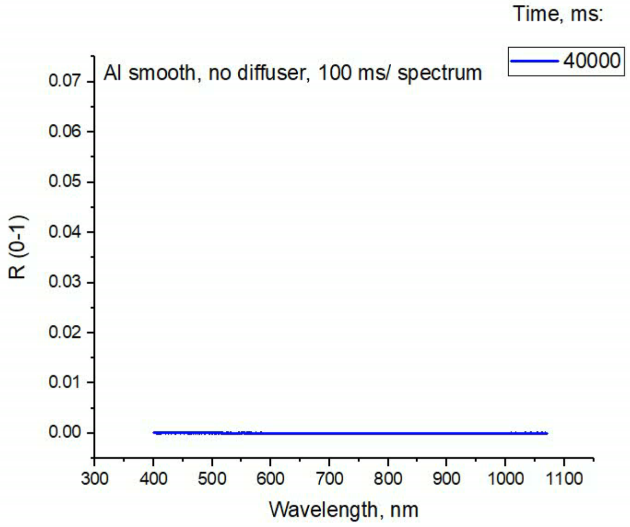

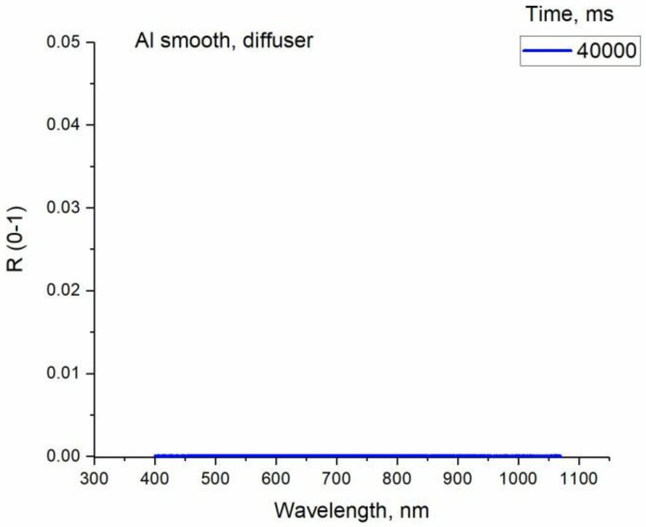

Consistency of R measurements: setup with and without a diffuser in front of fibre input of monochromator

Gold-Al (crinkly) surface 1 -Al (crinkly) surface 2 -Al (smooth) on rotating cube

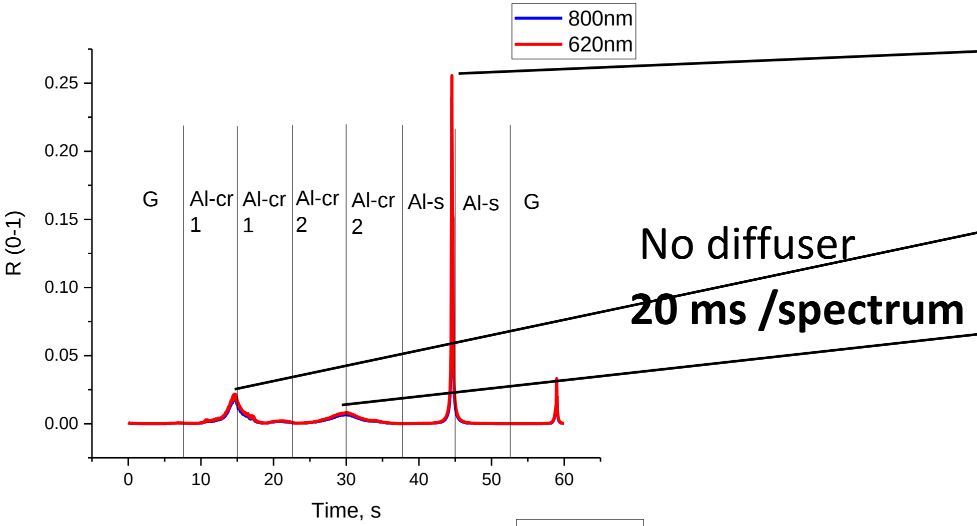

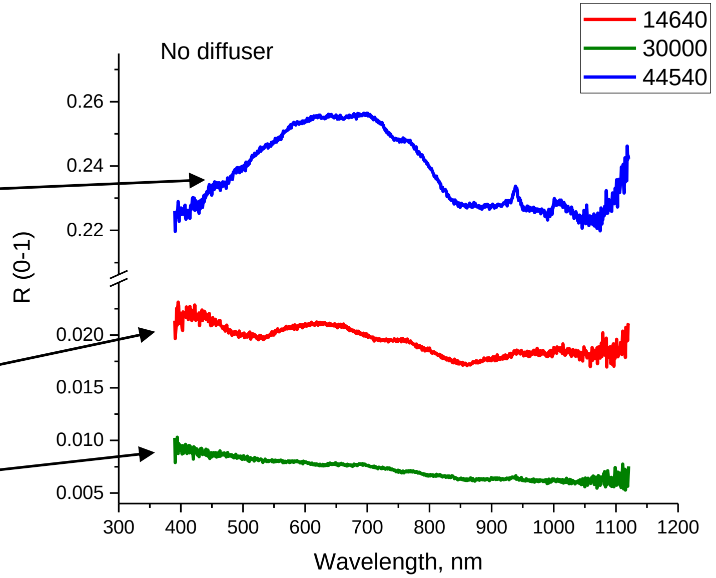

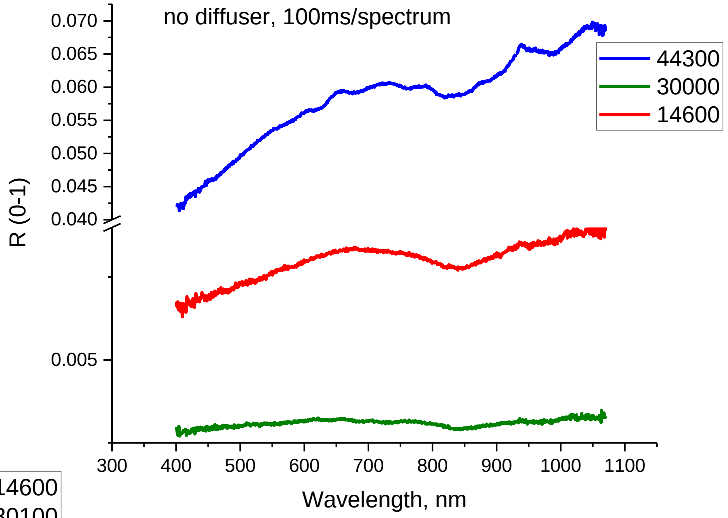

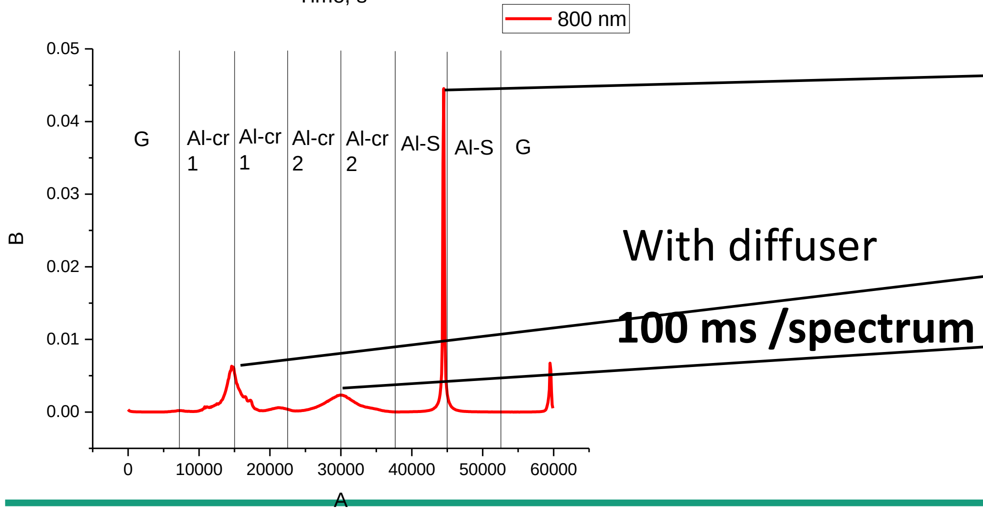

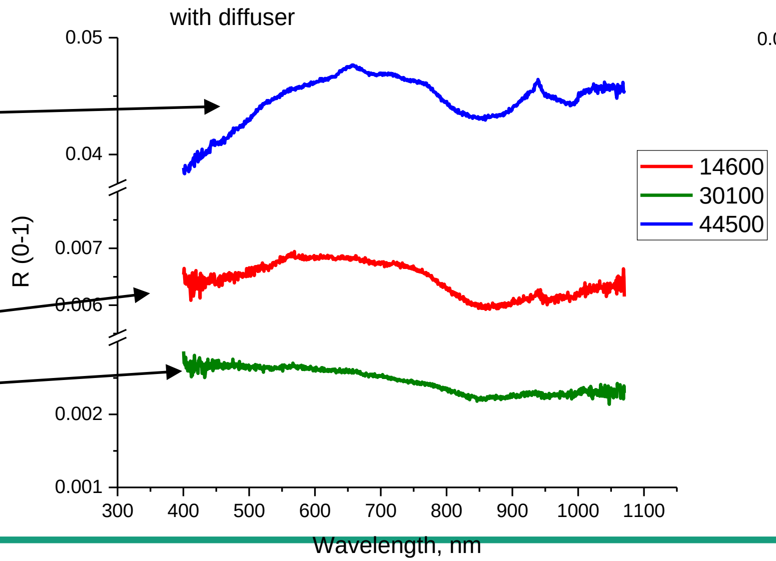

Fraunhofer UK

Consistency of R measurements

Conclusions:

Acquisition time of 100 ms: averaging of spectra collected over 0.6 degrees rotation (given experimental settings)

=1/10th of the rotation speed of the object

=> considered as an optimal regime for data collection

Consistency of R measurements and material identification

Aluminium-Steel-Brass-Gold on rotating cube, R@800nm

R spectra as is, no correlation with "library" spectrum (R=-0.82)

Same spectra after smoothing, normalisation and baseline subtraction

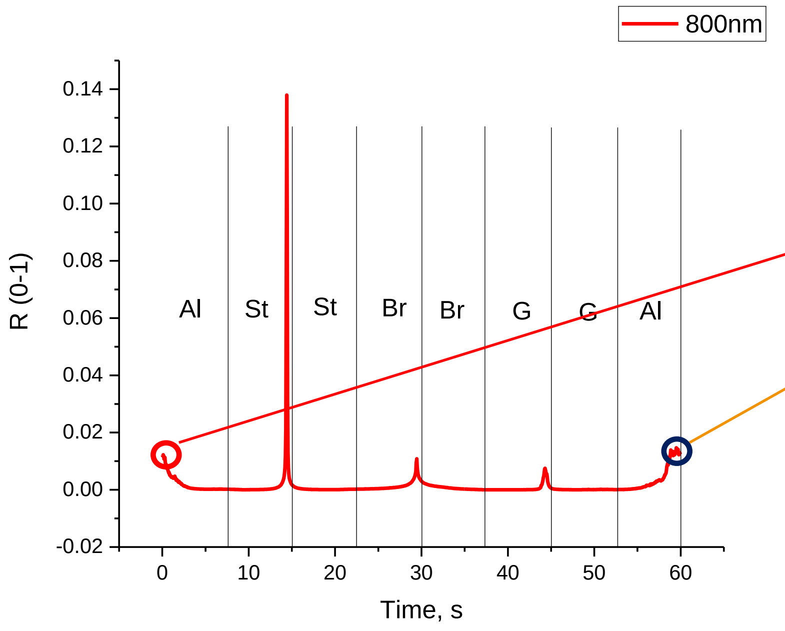

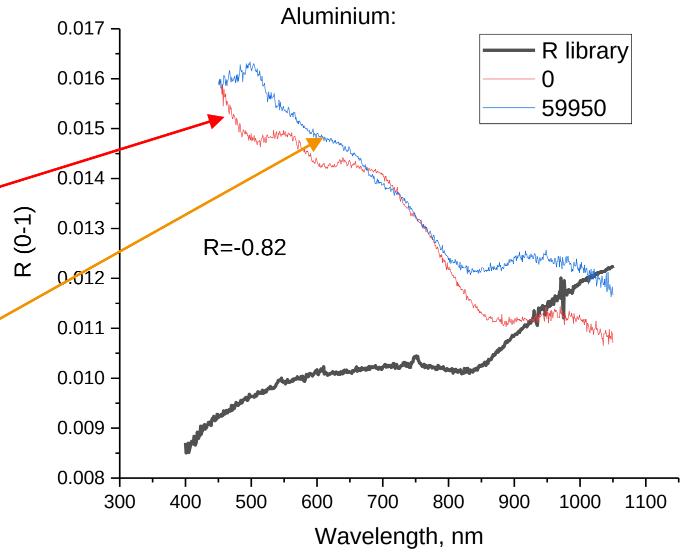

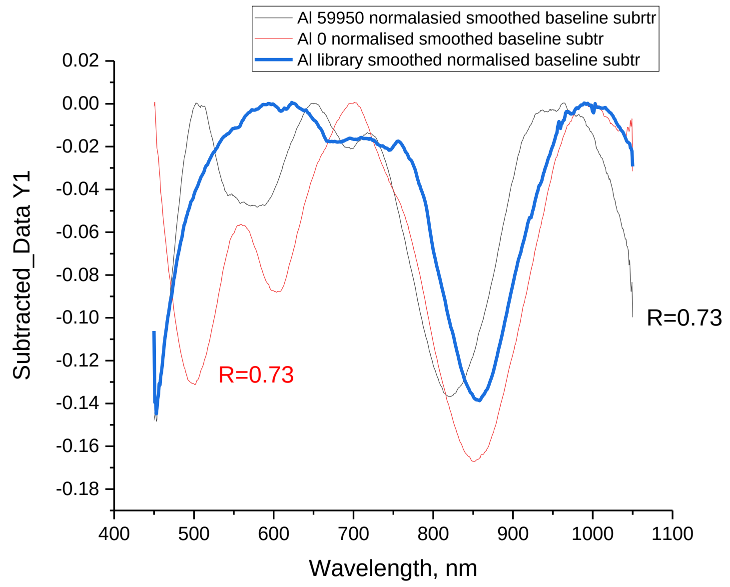

Reasonable correlation with "library" spectrum (R=0.73)

Fraunhofer UK

Consistency of R measurements and material identification

Black-Black-Aluminium-Black on rotating cube, R@860nm

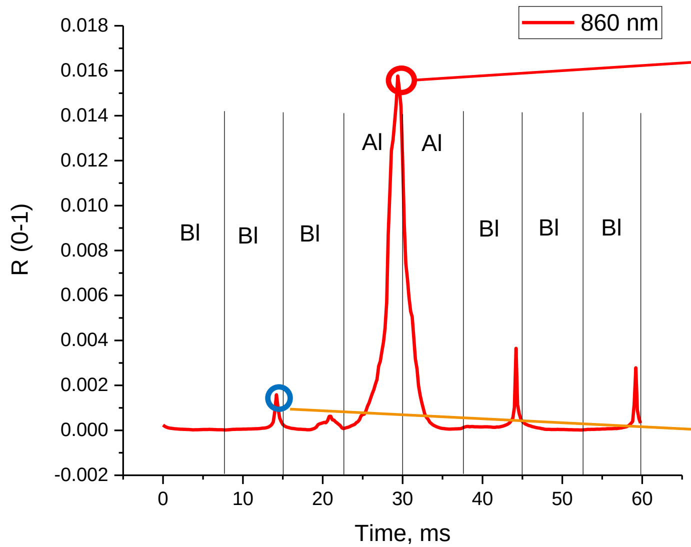

R spectra as is, no correlation with “library” spectrum (R=-0.78)

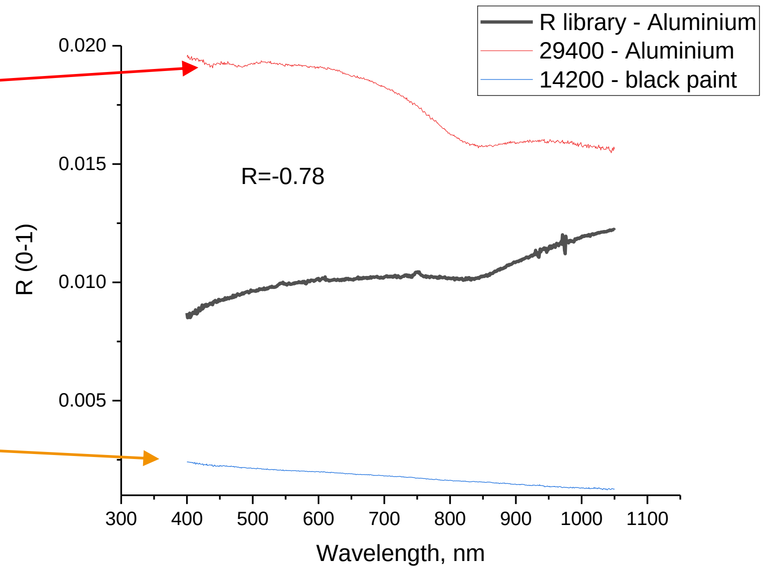

Same spectra after smoothing, normalisation and baseline subtraction

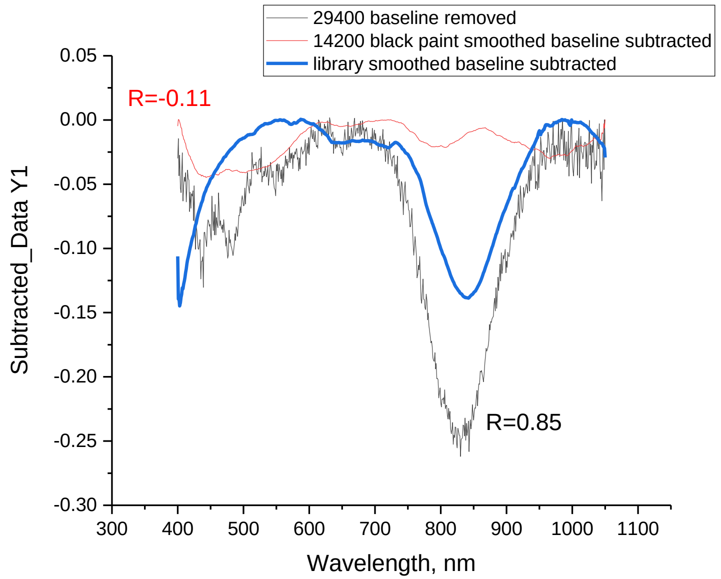

Reasonable correlation with “library” spectrum (Al) (R=0.85)
No correlation between black paint and Al “library” spectrum (R=-0.11)

Fraunhofer UK

Consistency of R measurements and material identification

Aluminium-Steel-Brass-Gold
on rotating cube, R@800nm

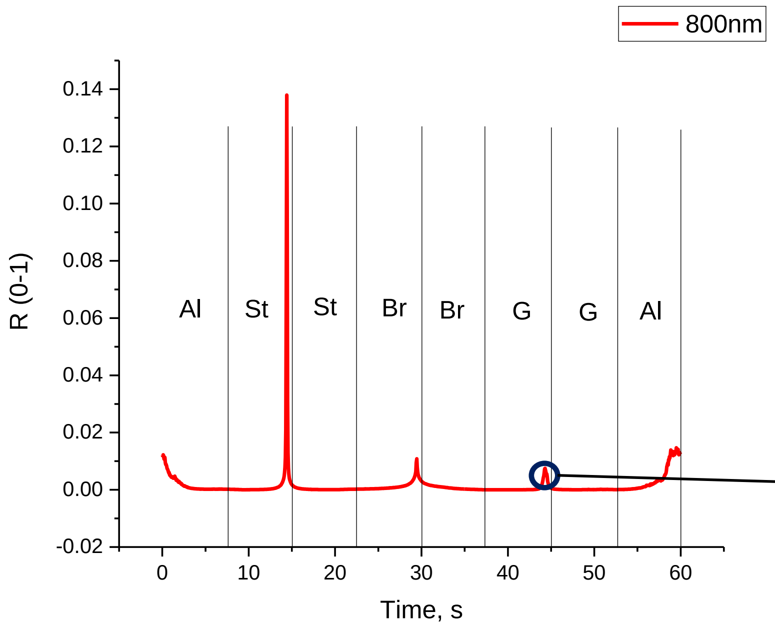

R spectra as is, poor correlation
with “library” spectrum (R=0.62)

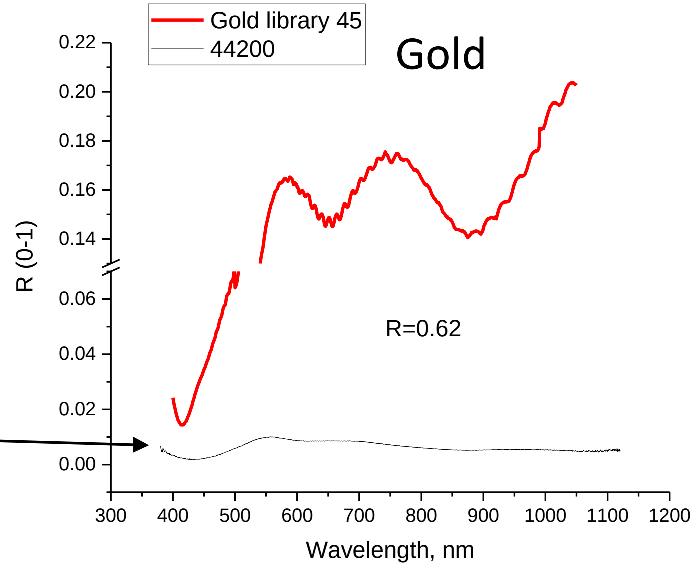

Same spectra after smoothing,
normalisation and baseline
subtraction

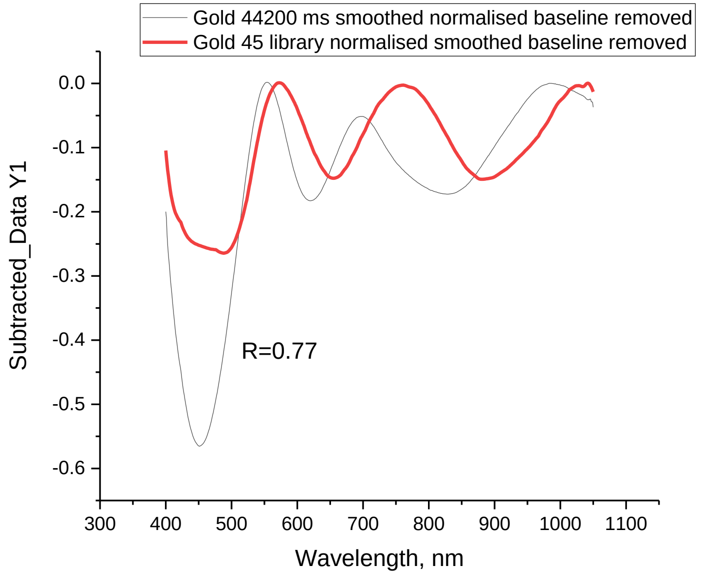

Reasonable correlation with
“library” spectrum (R=0.77)

Fraunhofer UK

Consistency of R measurements and material identification

- **Importance of baseline correction of the reflectivity spectra for accurate identification of materials**
- **To be applied in the algorithm at the later stages of development**
- **FhCAP is experienced in developing algorithms for automated baseline correction**

Reflectivity spectra of GaAs and GaAs based solar panel

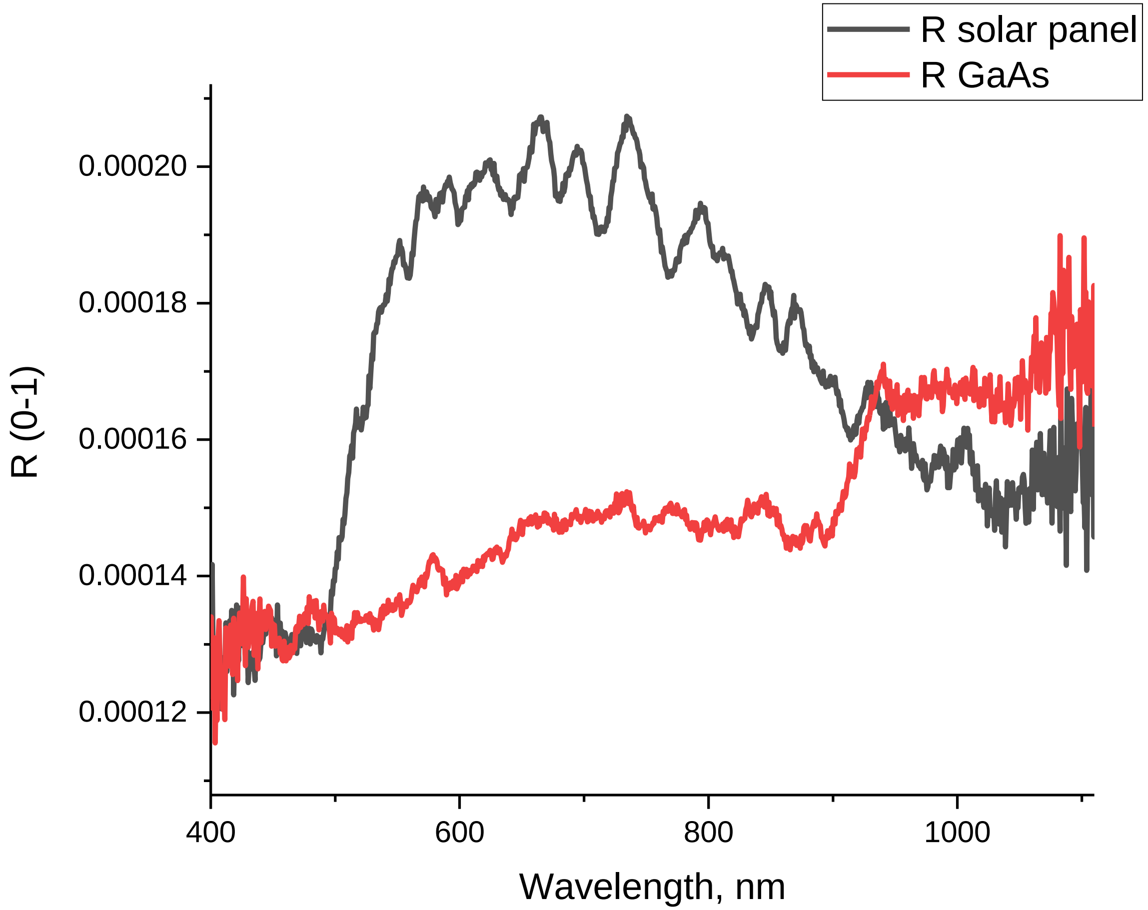

GaAs

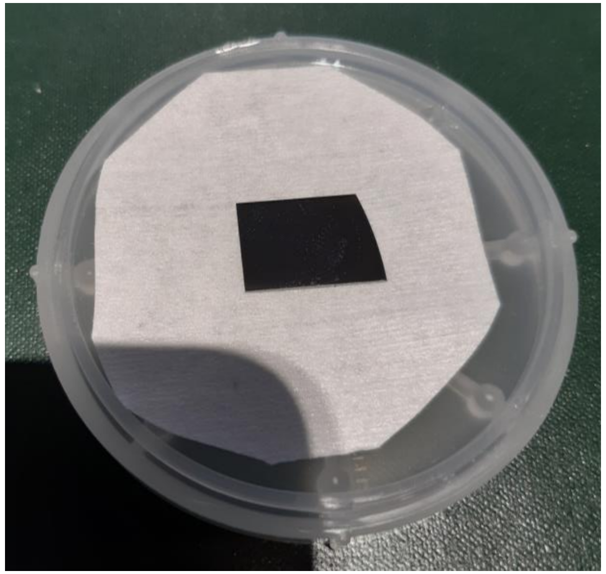

Solar panel chip

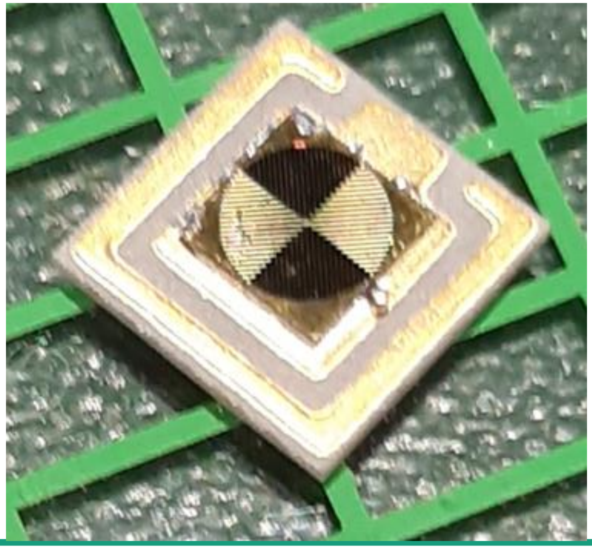

Distinct reflectivity feature in solar panel => prospects for identification

Fraunhofer UK

Testing the mixture of materials

Cube:
Side 1: Al
Side 2: 50/50 Gold + Al
Side 3: 50/50 Stell + Gold
Side 4: Gold

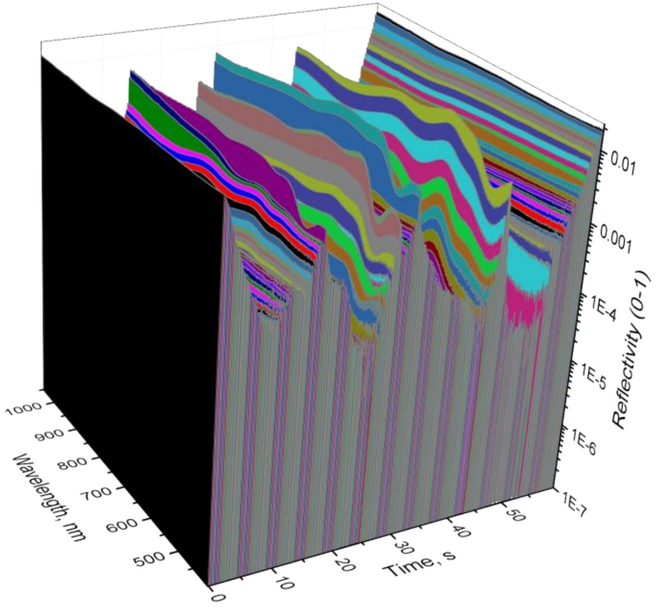

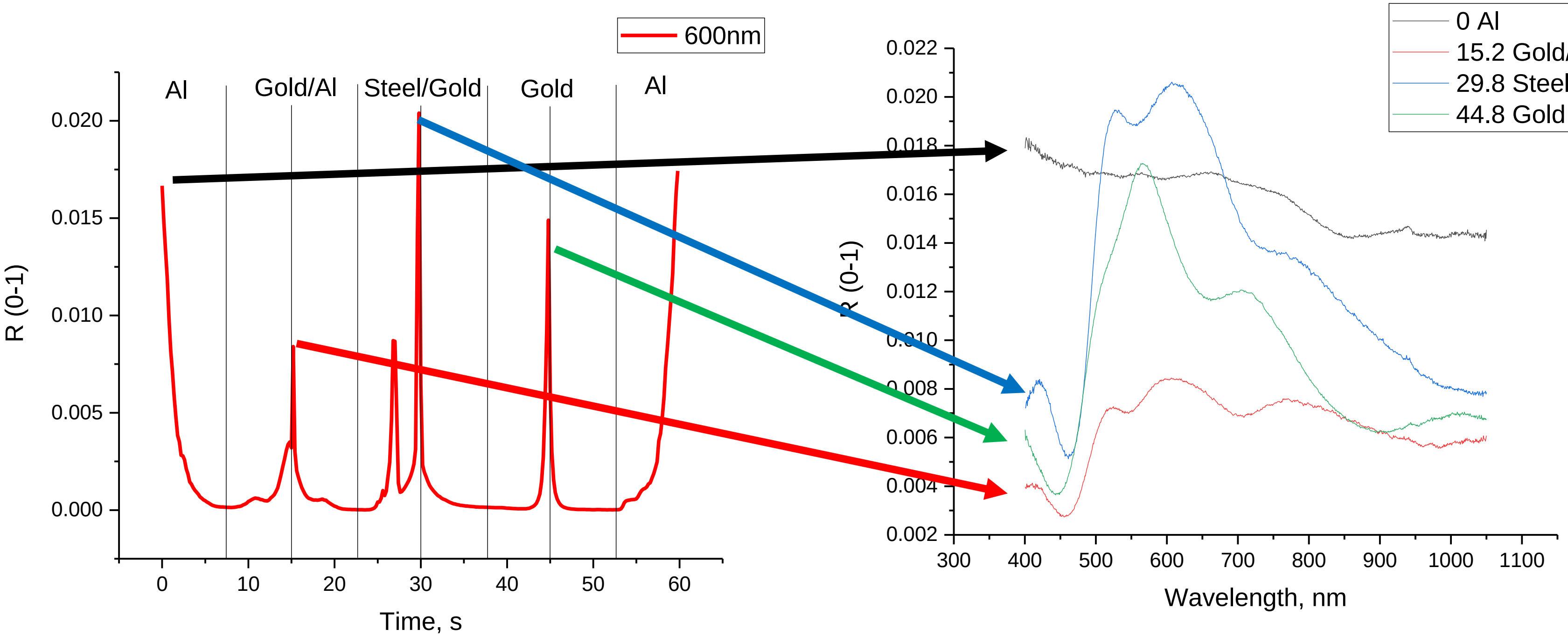

For mixture of materials:
Need "end-member" analysis
Baseline removal algorithm

Fraunhofer UK

Principle design of the ground sensor

Ground-based sensor

Telescope: Celestron EdgeHD 1400: F=3910mm, D=356mm

Sensor: Phase 1 CCD spectrometer and camera

Fibre core diameter 200 um

Objects <20 m size (@400km distance) will be fully projected onto the fibre core

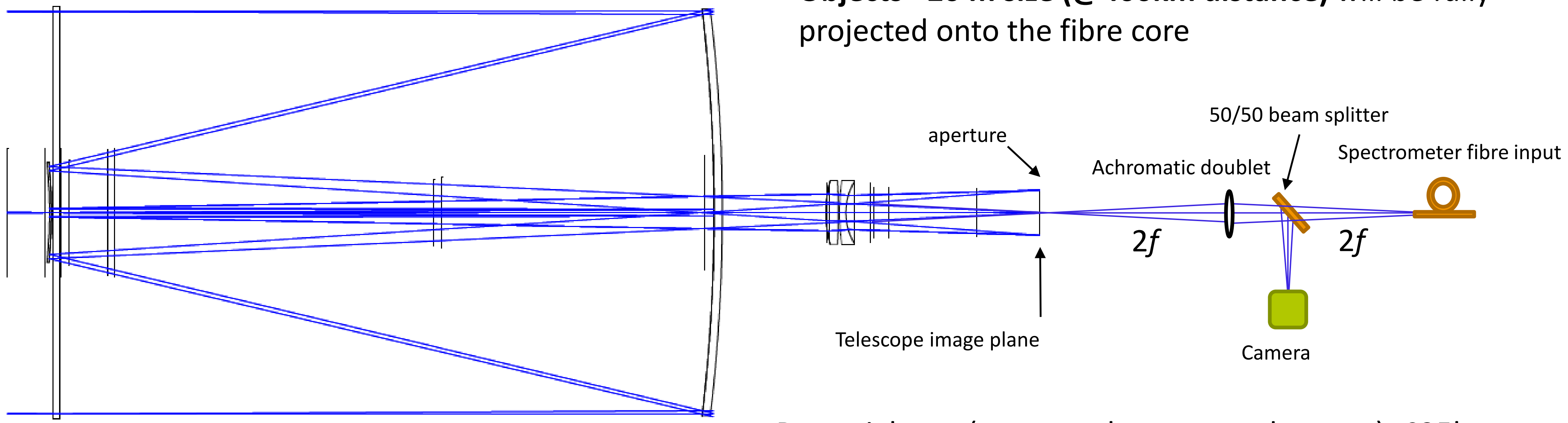

Potential cost (sensor, telescope, and mount): £35k

Phase 2: telescope and mount to be bought with FhCAP budget. Other options for telescope can be considered.

Sensor – Phase 1

Principle design of the ground- and space-based sensors

Space-based sensor

Space qualified telescope (designed in FhCAP, not part of this project): f=400 mm, D=80 mm. Size 100x100x160 mm

Sensor: no COTS space-qualified CCD spectrometers for 400-1100 nm spectral range

Similar space-qualified spectrometer:
Thoth technology Inc
1000-1700 nm
80x46x80 mm, 280g, -20 C - +40C
Cost $49.5k

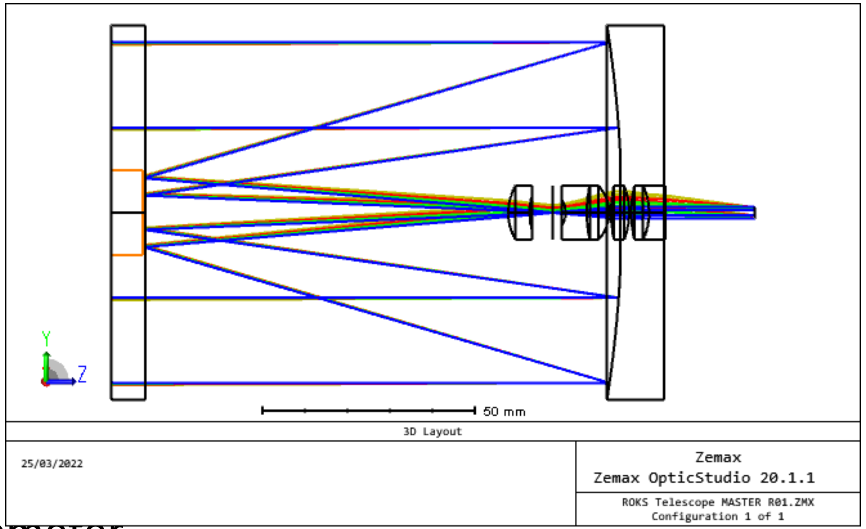

FhCAP: to design and build (Phase 2) space-qualified 400-1100 nm spectrometer
Teledyne – space-qualified CCD sensor
Horiba - space-qualified diffraction grating
Texas instruments - space-qualified electronics
Potential cost of components for spectrometer: £45k

Telescope experiments

Aligning the telescope

Pointing model:

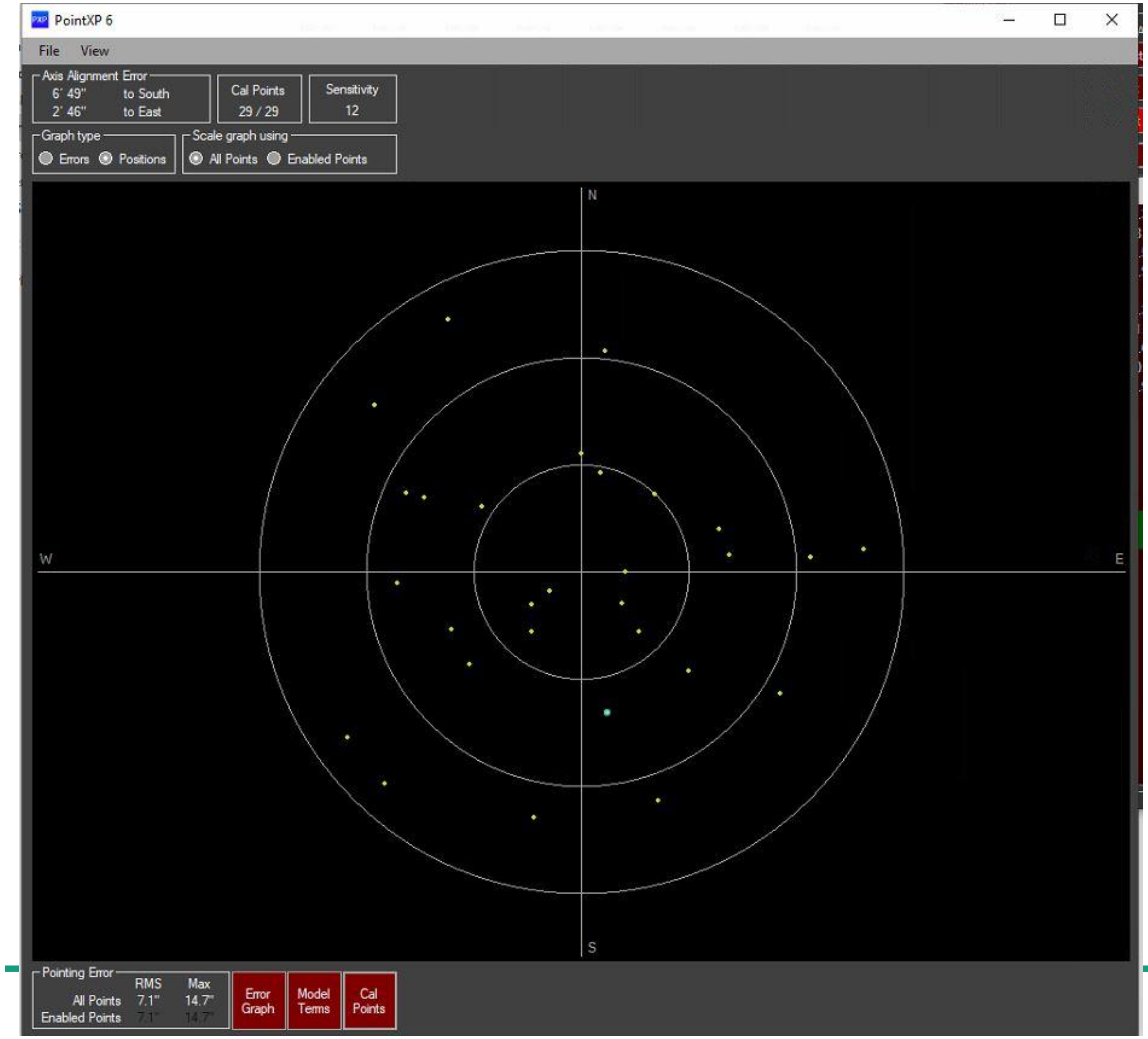

Error analysis, pointing accuracy +- 10 arc. sec

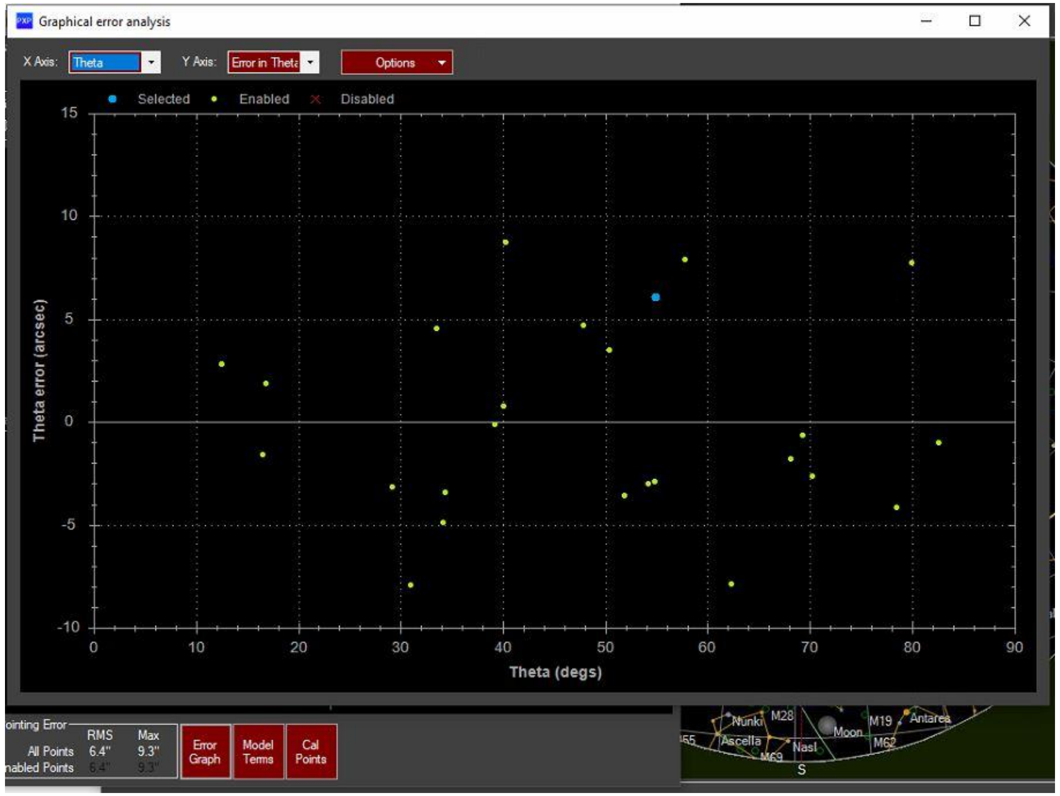

Fraunhofer UK

Telescope experiments

Satellite tracking, first attempt. 19/01/2023, ~17.28 Cosmos-1300

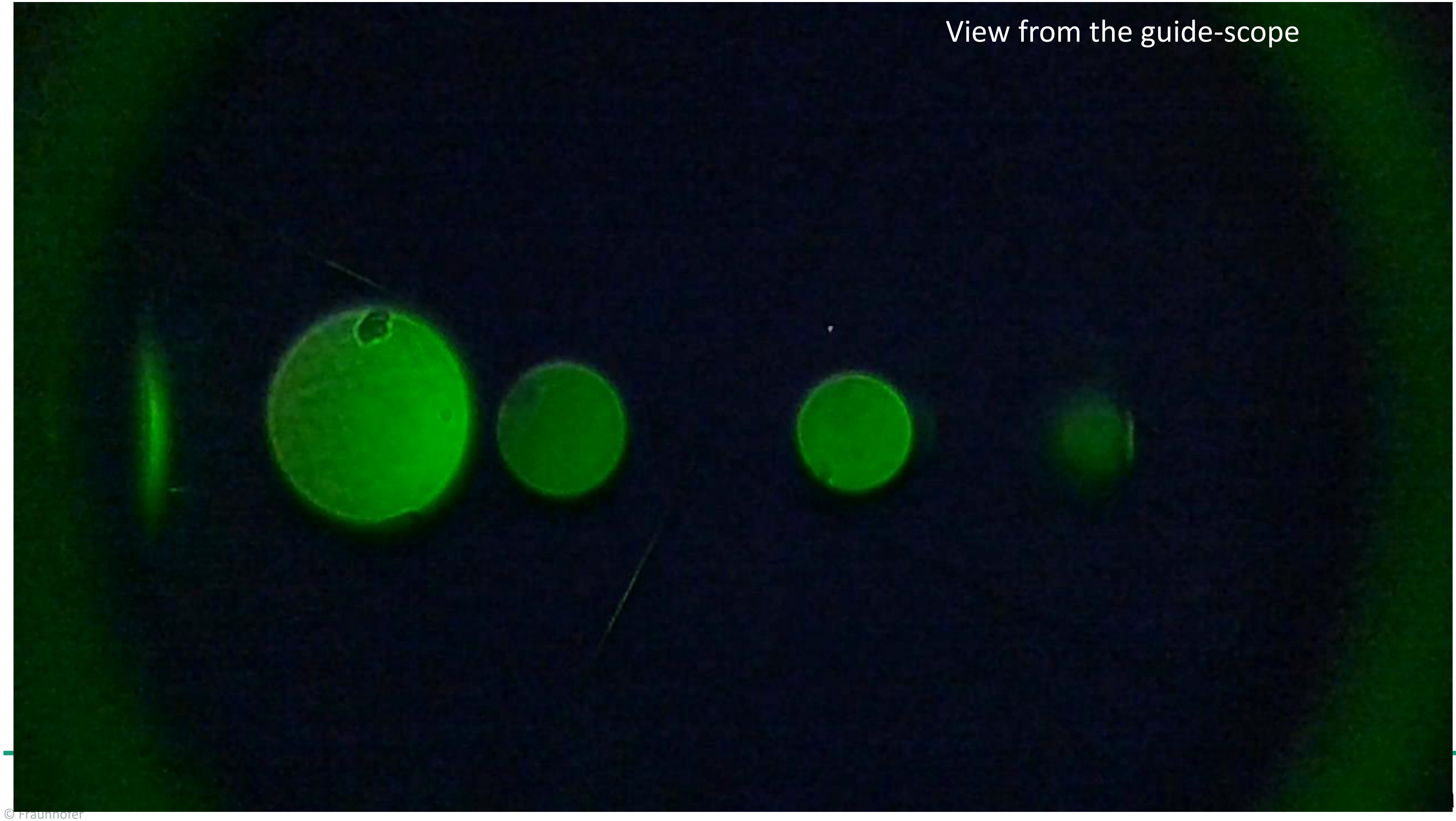

Telescope experiments

Satellite tracking, first attempt. 19/01/2023, ~17.28 Cosmos-1300

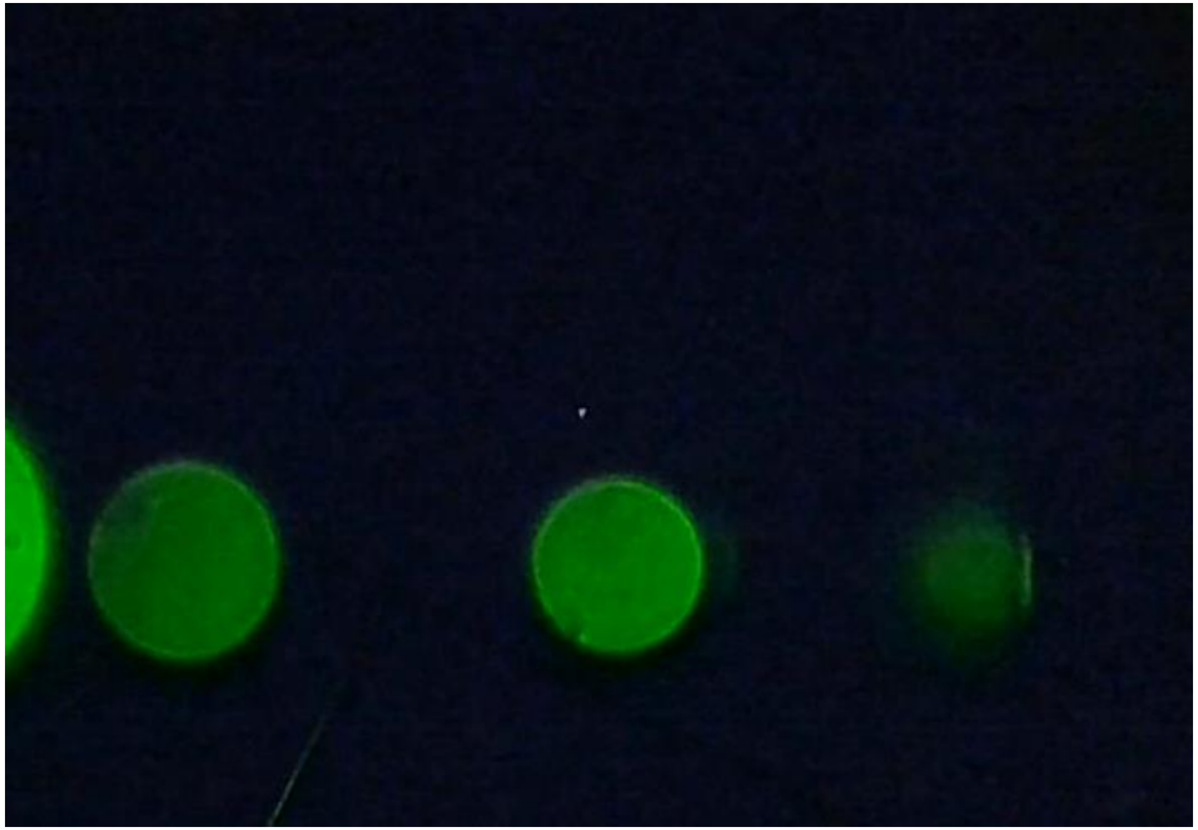

Problems: satellite is not at the centre of the camera

Reasons: 1) alignment needs improvement
2) PC clock accuracy
3) TLE data

Remedy: 1) “Dimension 4” software installed to synchronise PC clock with Internet Time Server (using Manchester server now)
2) Re-alignment with synchronised clock
3) Make sure TLE is up to date

Misalignment analysis

Arcturus: 11*26 arcsec
Or 149*350 um in the image plan

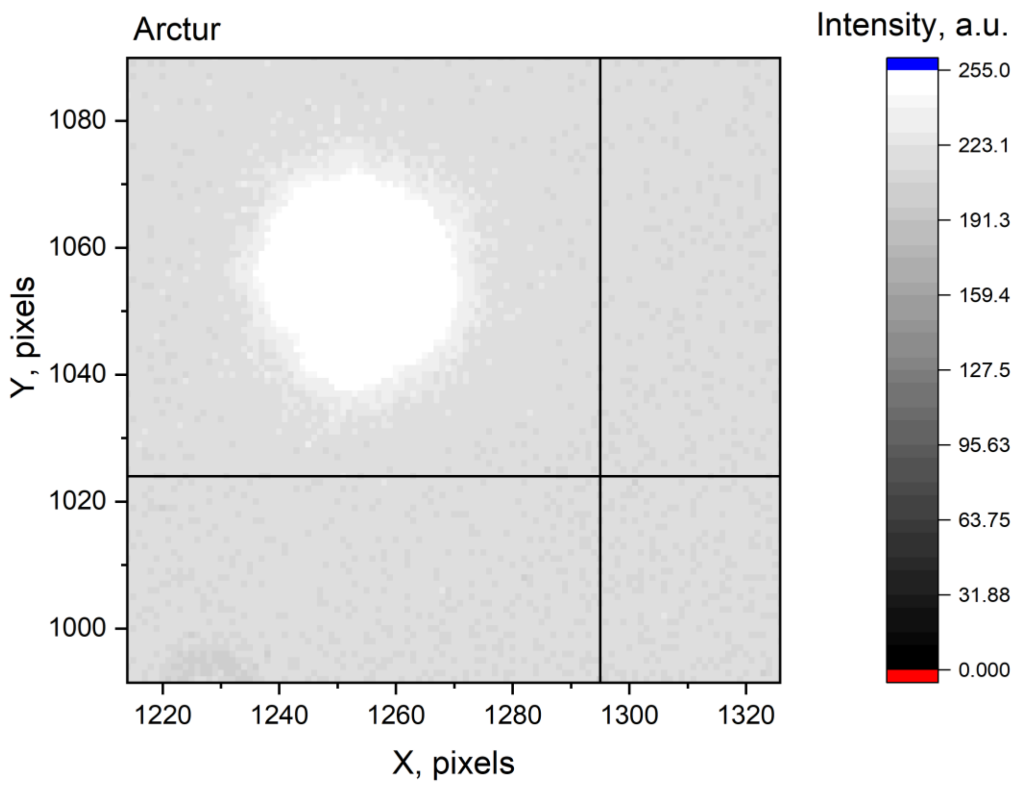

Vega: 11*21 arcsec
Or 153*288 um in the image plan

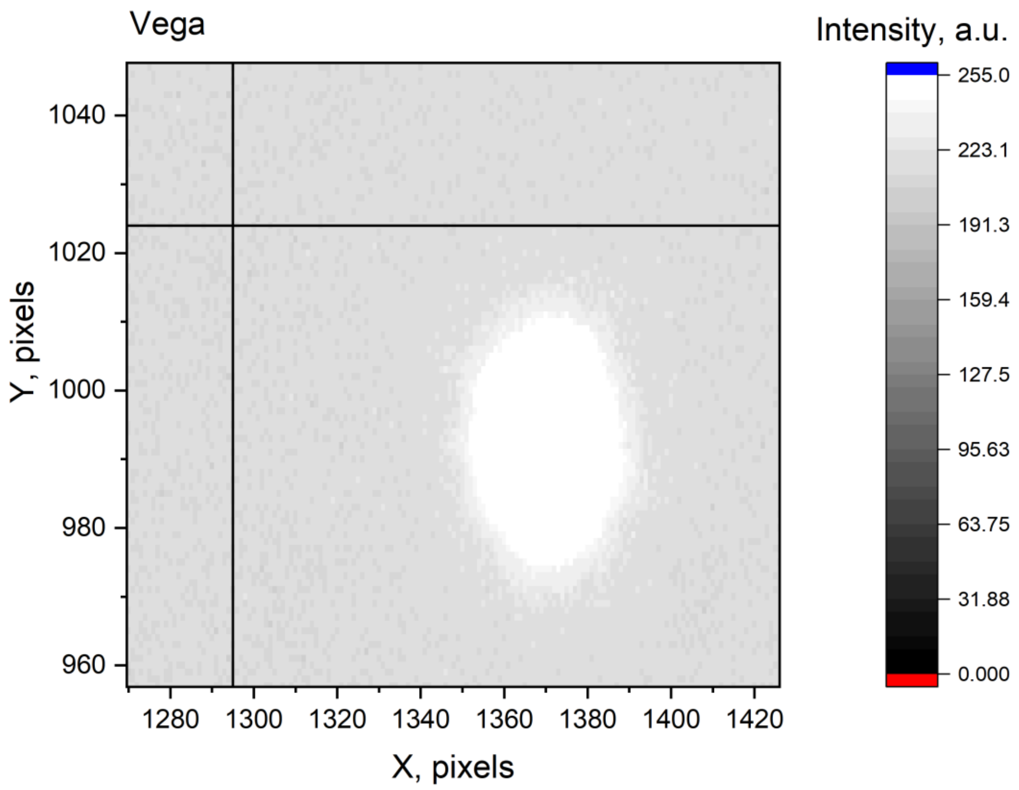

Replaced fibre to 400um diameter one, replaced focusing mirror to 30 mm for better light collection

Fraunhofer UK

Misalignment analysis

With new focusing lens and optical fibre, 40 arcsec misalignment can be accommodated

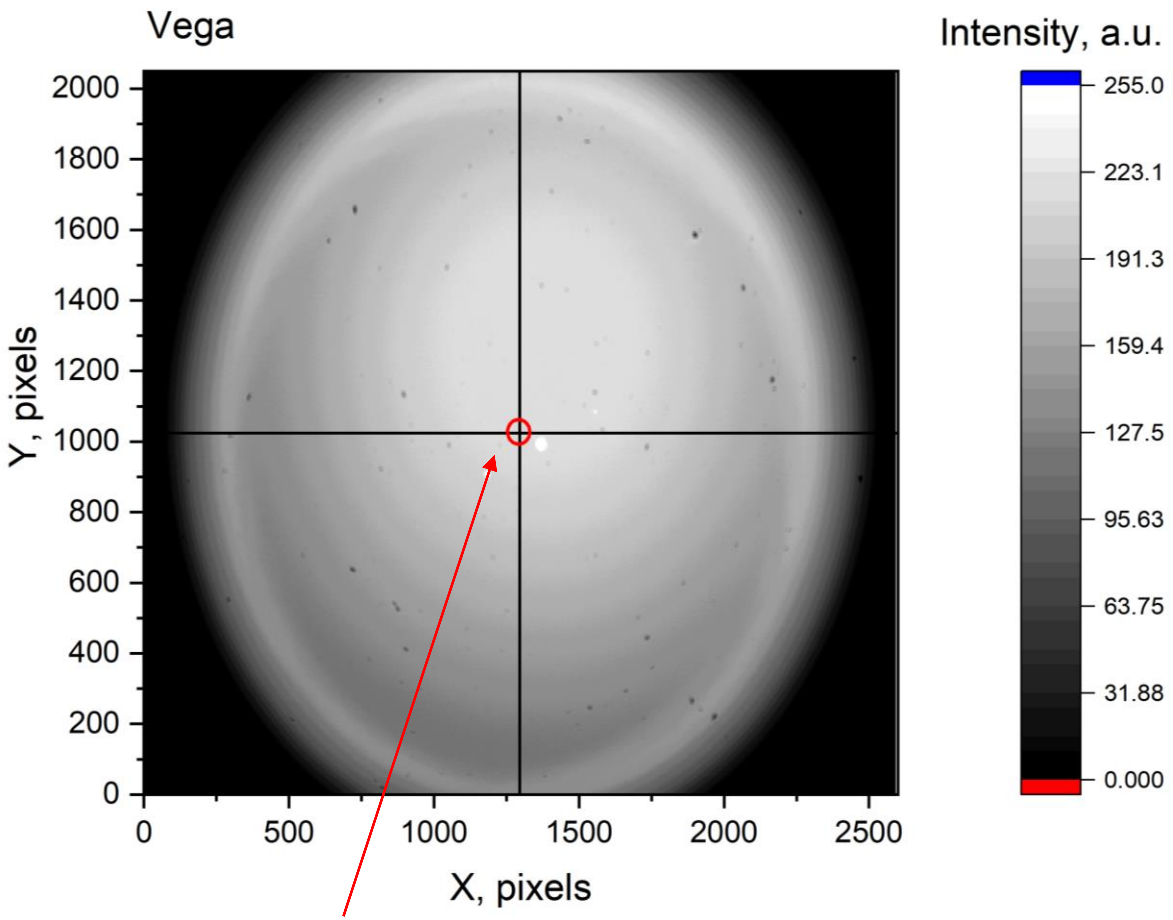

Projection of a 200um core fibre
into the camera

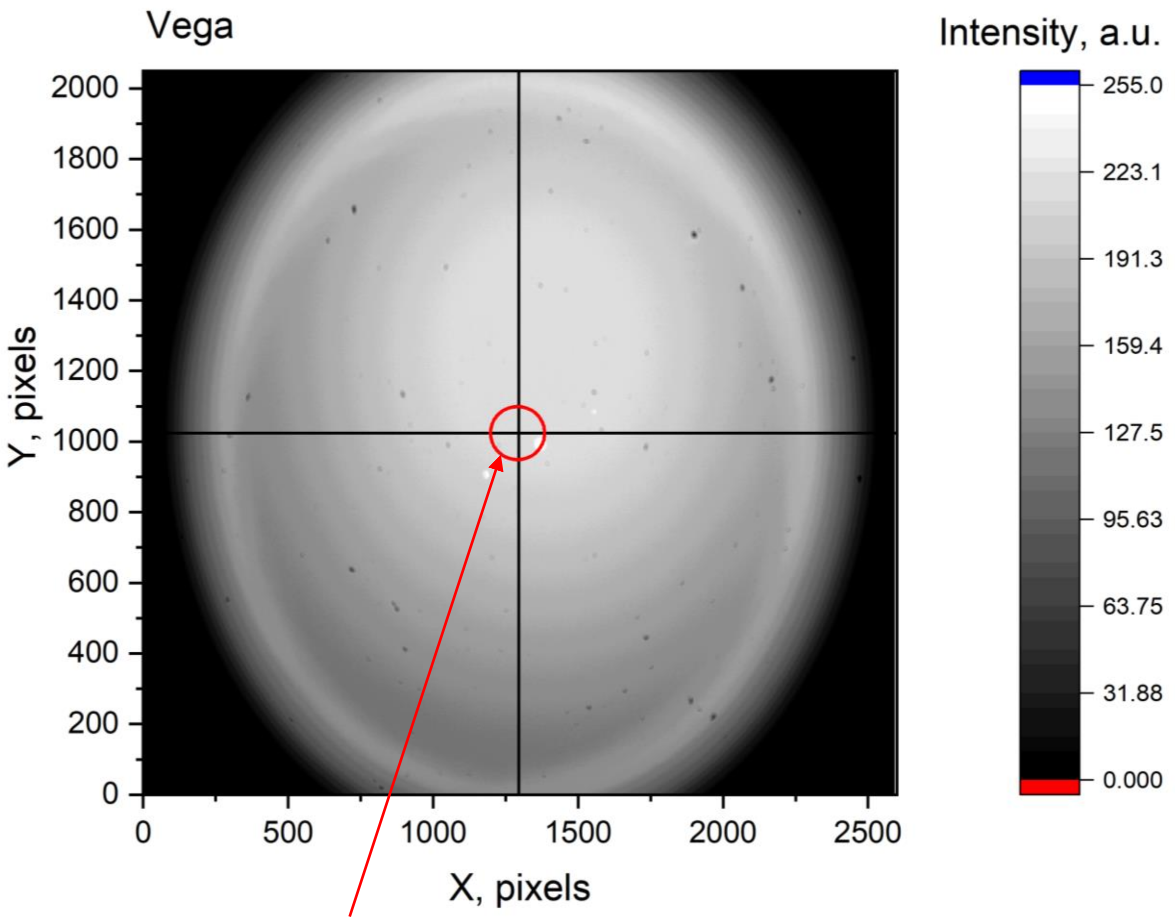

Projection of a 400um core fibre
into the camera with 2x tighter focusing

Telescope experiments

Checking the sensitivity of the sensor
Measurements of the spectra of planets and stars with various Magnitude

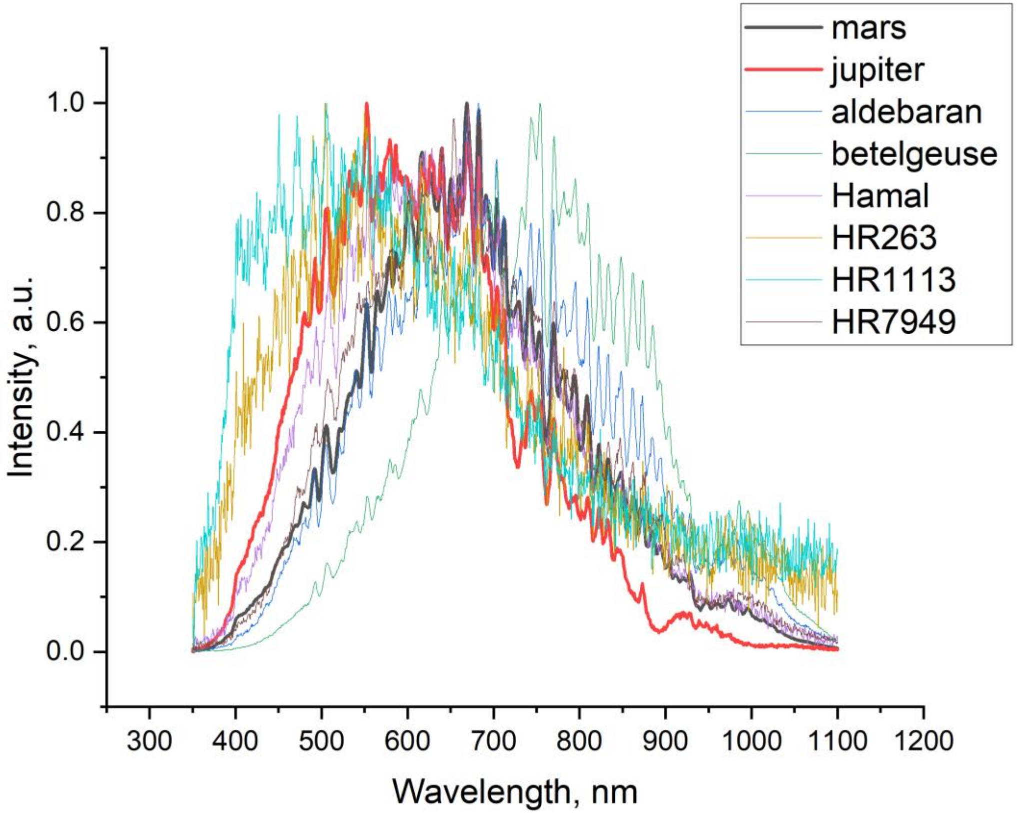

All spectra are corrected for spectral sensitivity of the system: telescope + sensor + atmosphere

Telescope experiments

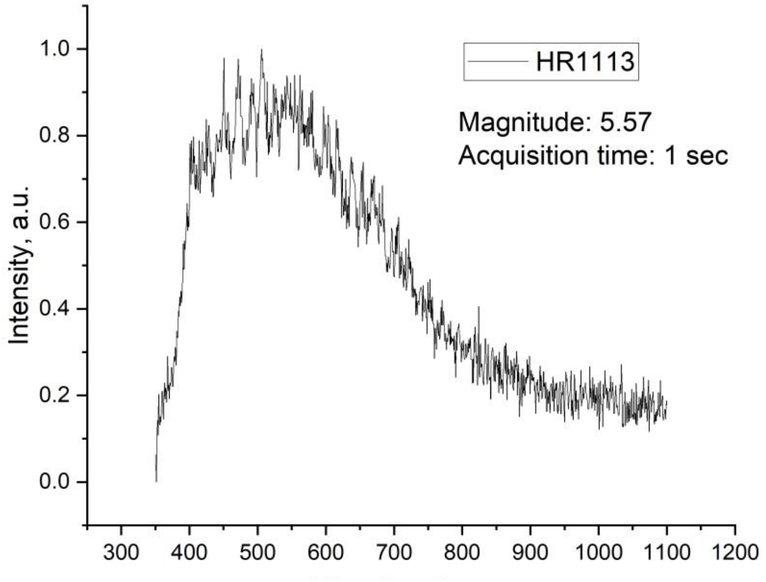

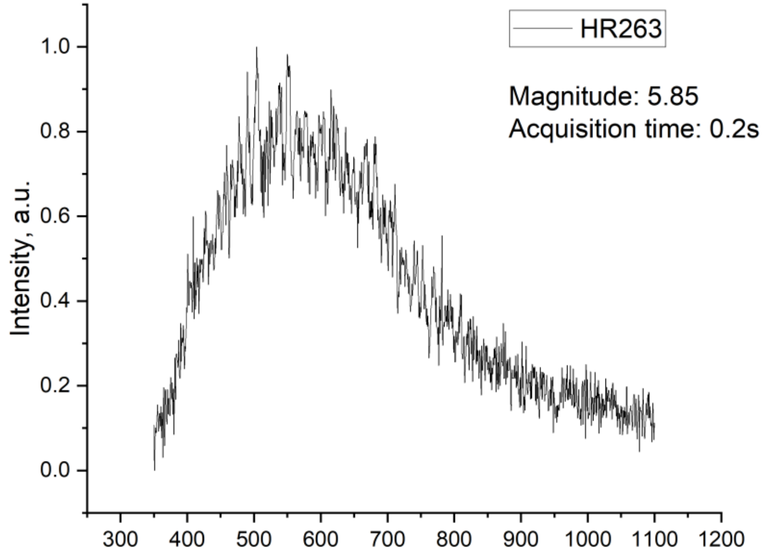

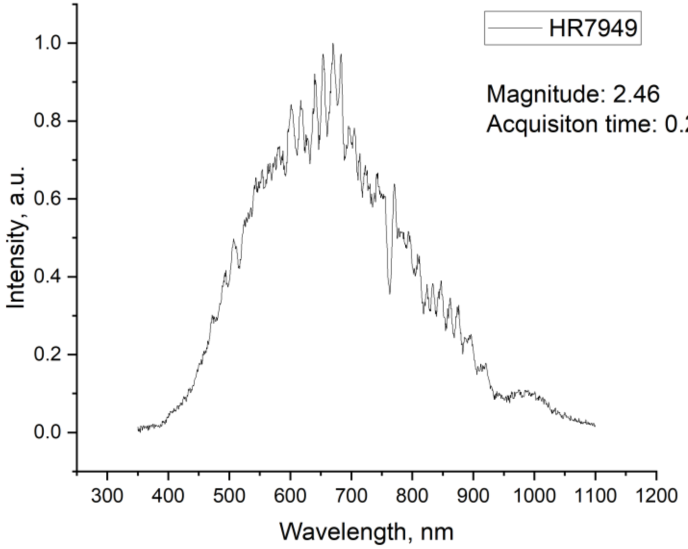

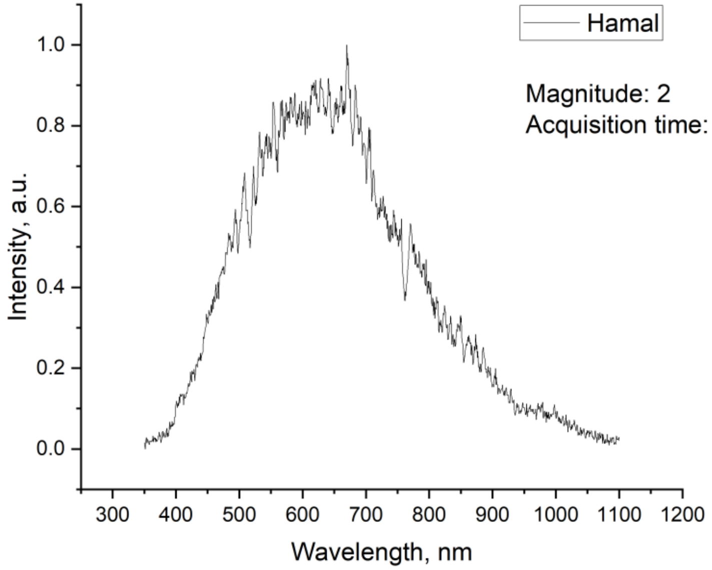

Fraunhofer
UK

Telescope experiments

Comparing with literature date

Sensor measurements

https://www.astrogeo.va.it/astronom/spettri/pianetien.htm

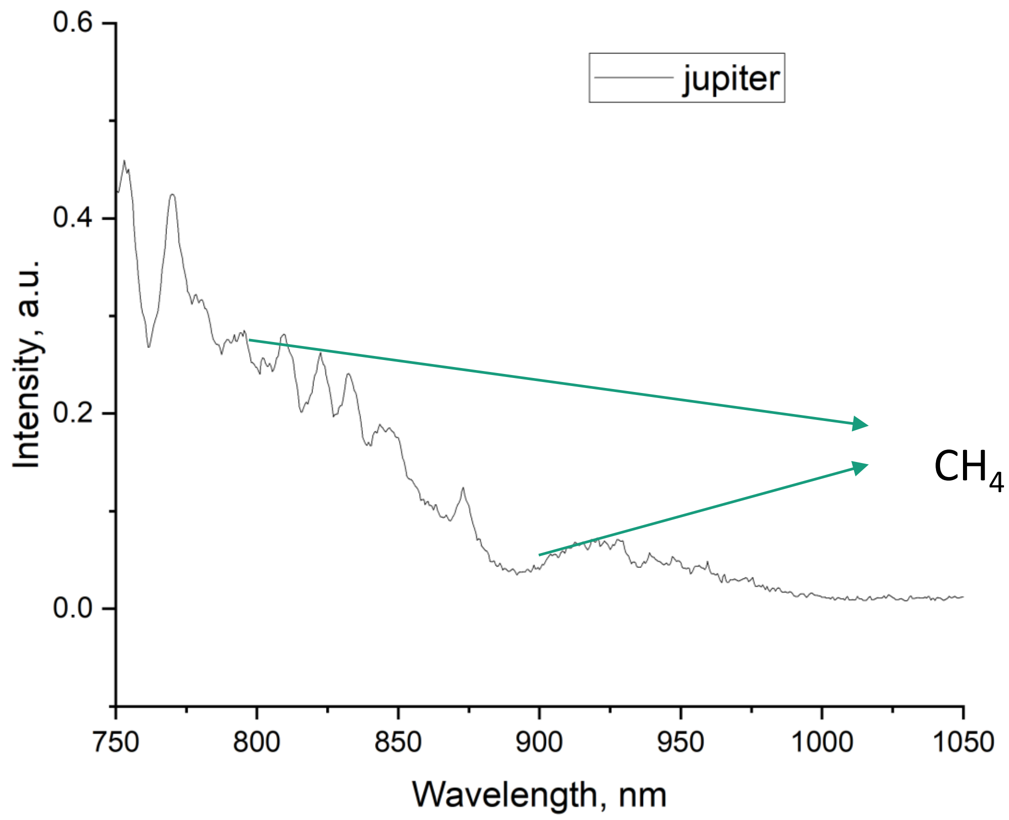

CH_4

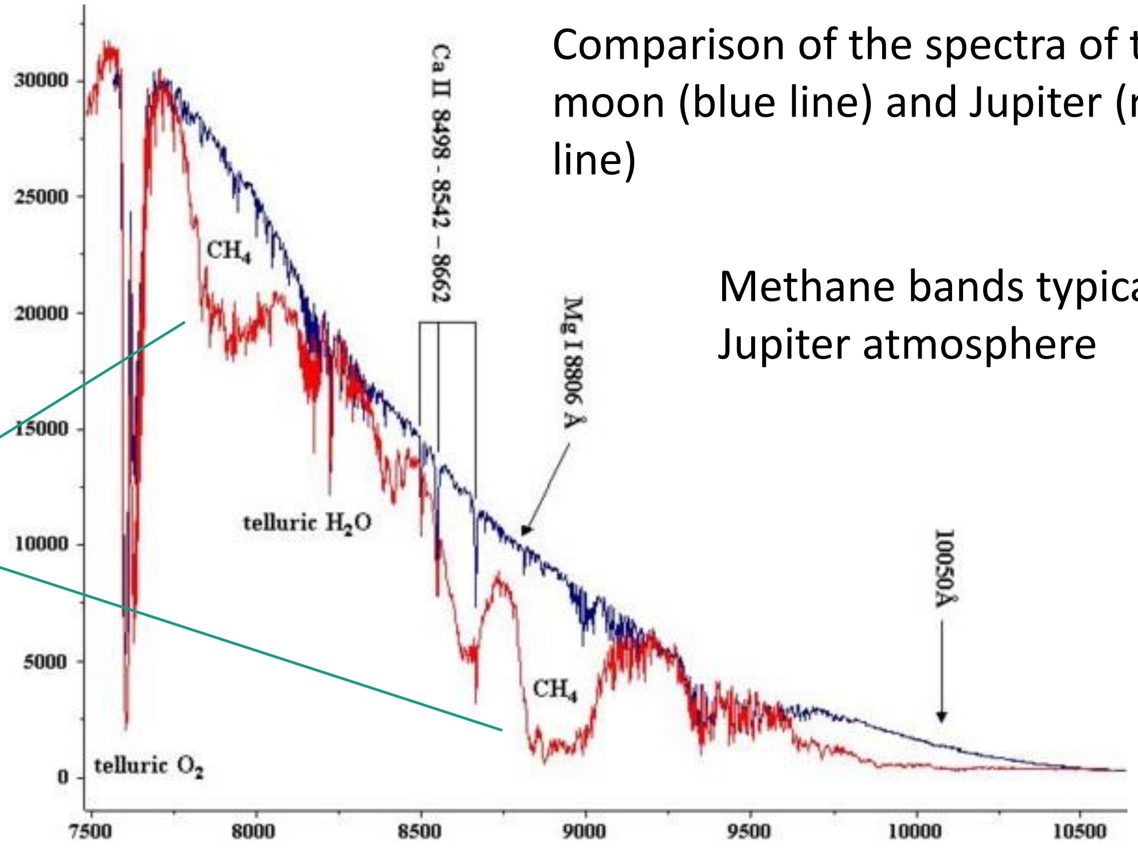

Comparison of the spectra of the moon (blue line) and Jupiter (red line)

Methane bands typical of Jupiter atmosphere

Fraunhofer UK

Telescope experiments

Conclusions: Sensor can detect objects with magnitude down to ~6 with acquisition time of ~0.2-1 s per spectrum
Correction for spectral sensitivity gives satisfactory agreement between the measured and reported spectra of space objects

Next step: realigning the telescope with synchronised PC clock
Measurements of satellites

Designing the telescope and spectrometer for space platform

Spectrometer design

Spectral resolution: 7 nm
Spectral range: 450-950 nm
Sensor size: 20.48 mm
Pixel size: 10 um
Required dispersion: 35 nm/mm
Grating: 300/mm
Entrance slit: 200 um

Calculated focal length of objective: 95.2 mm
Assuming F#=4, required objective diameter: 23.8 mm (close to standard 1” optics)

Designing the telescope and spectrometer for space platform

Spectrometer initial design

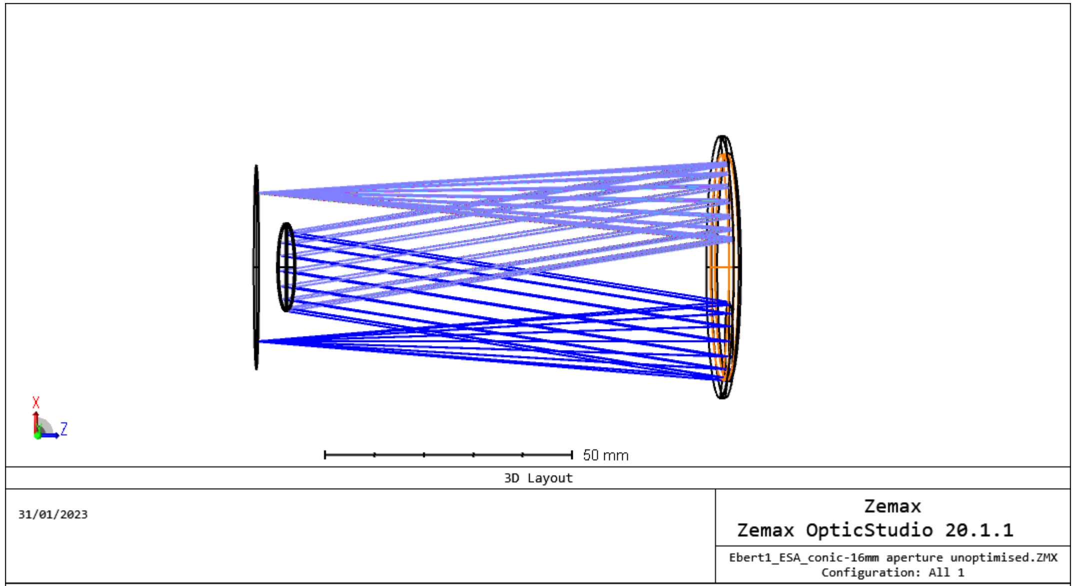

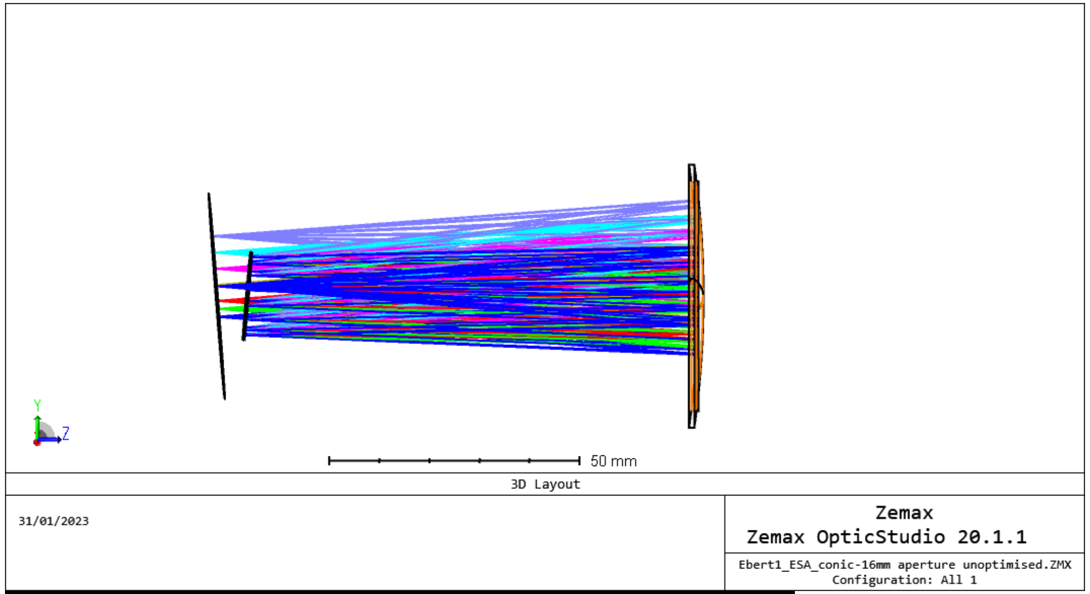

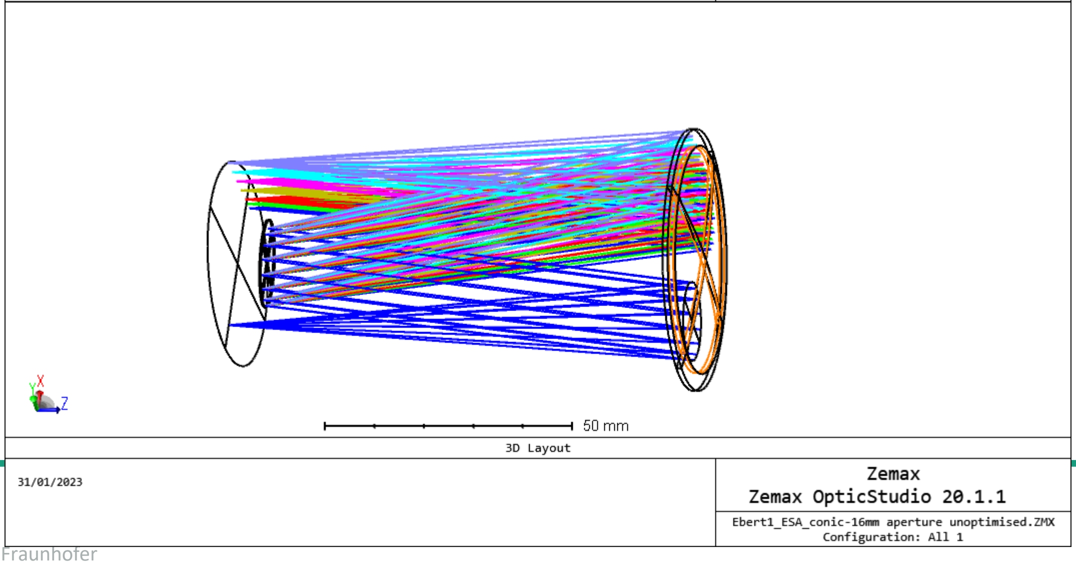

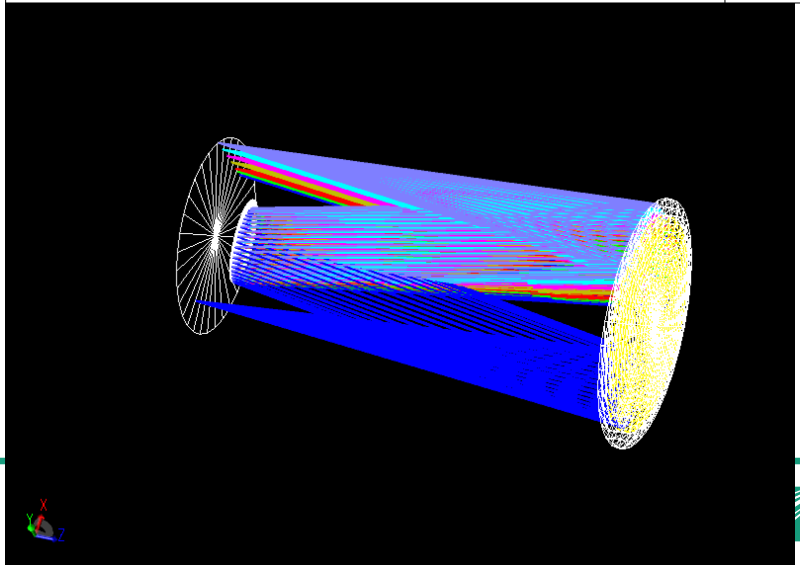

Designing the telescope and spectrometer for space platform

Spectrometer optical design optimisation

Slightly increased distance between the objective and diffraction grating: Input slit, the grating and the sensor are in the same plane now (simplifying design and assembly)

Objective – aspherical surface

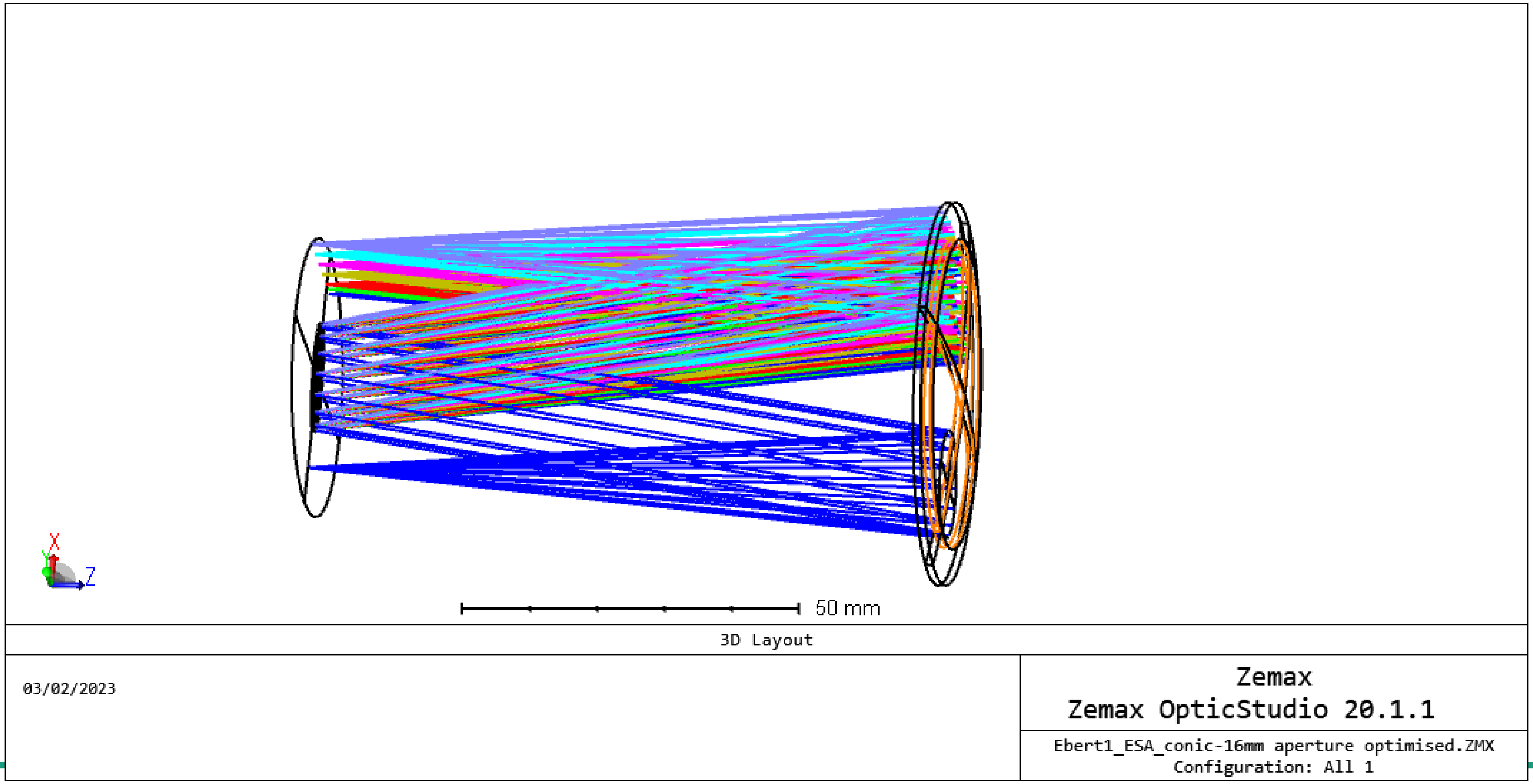

Designing the telescope and spectrometer for space platform

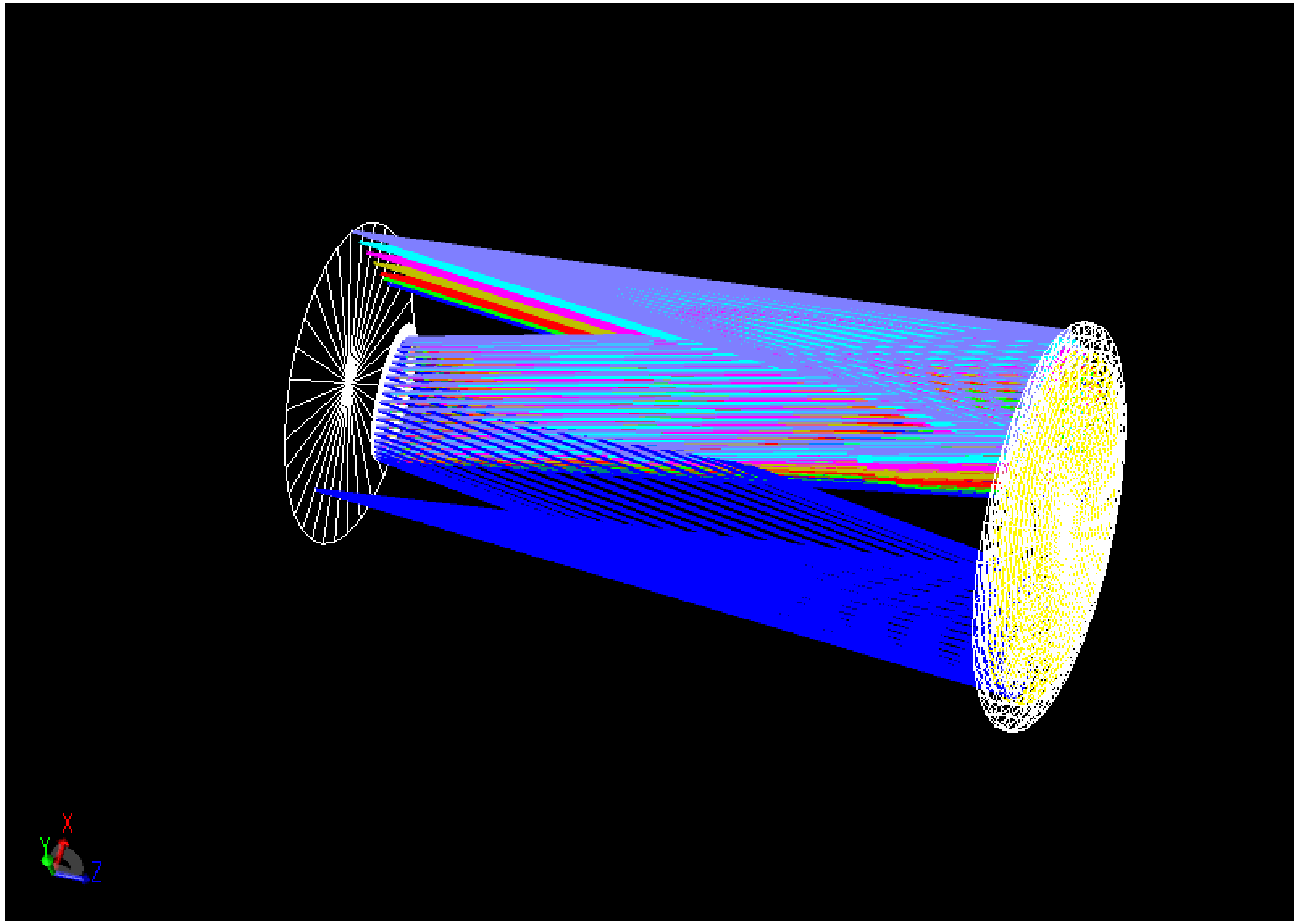

Designing the telescope and spectrometer for space platform. Spot diagrams

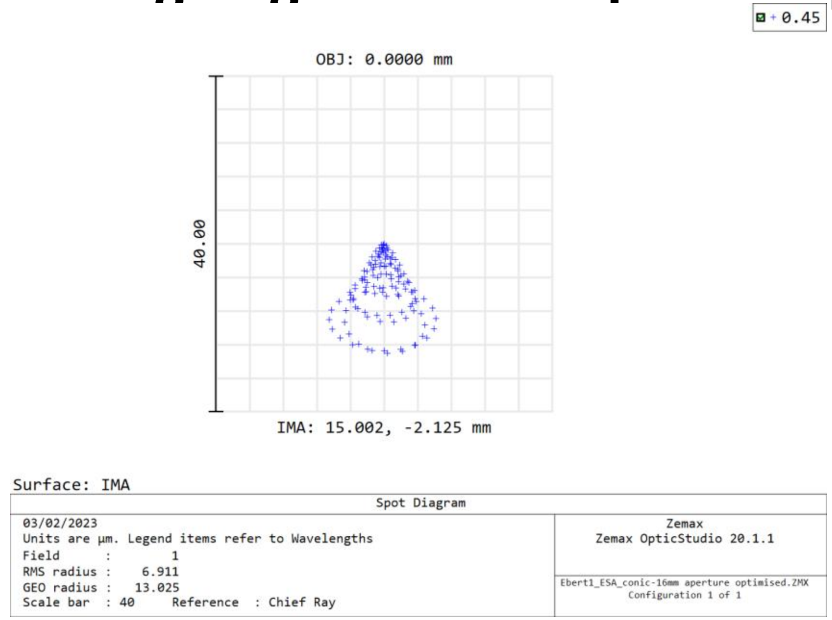

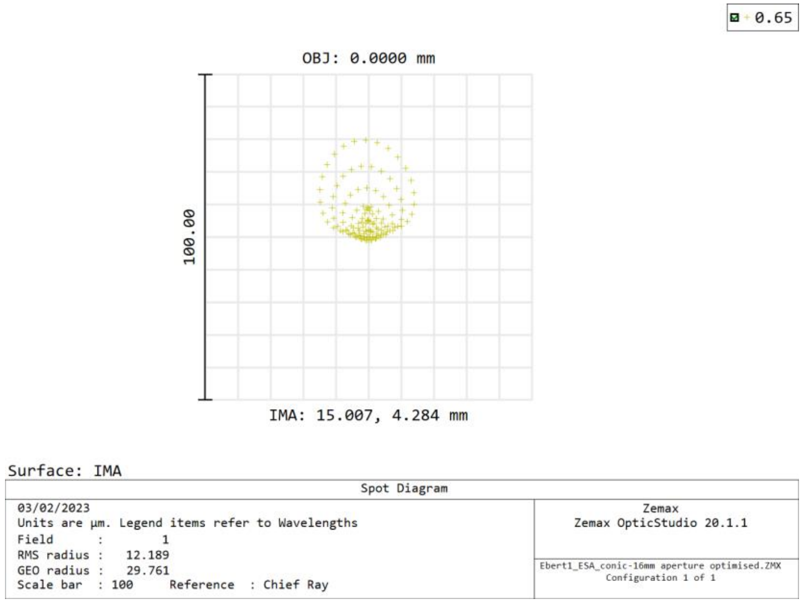

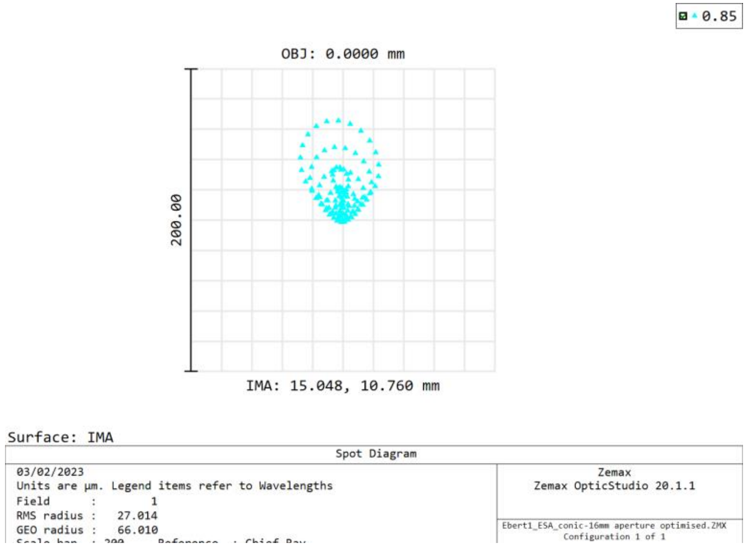

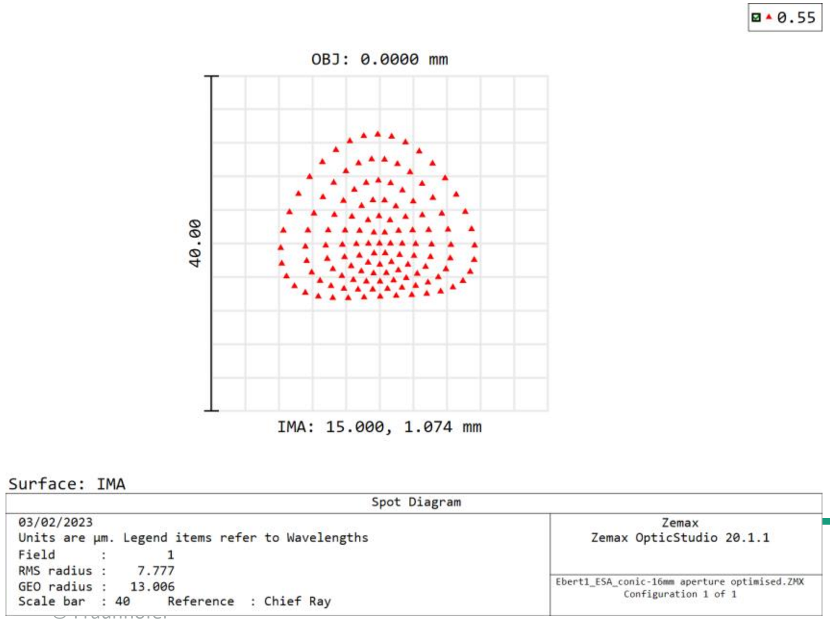

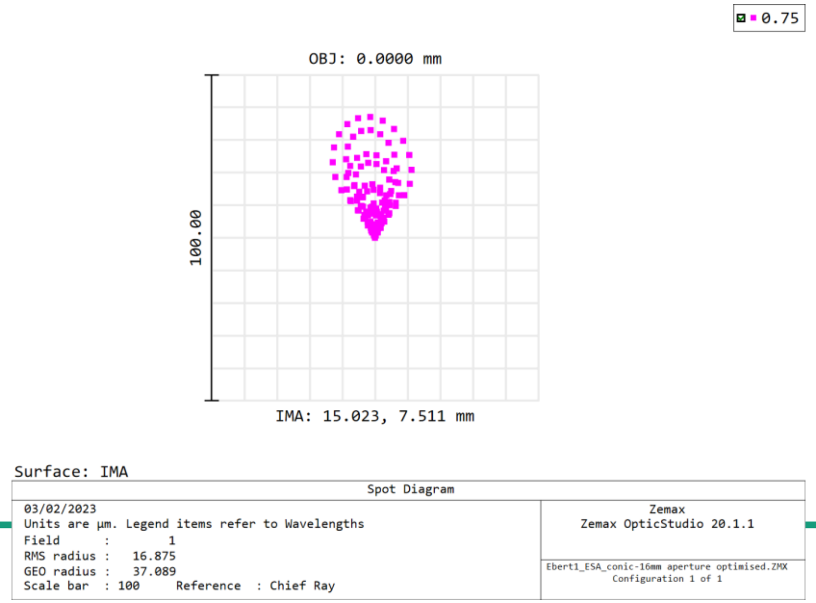

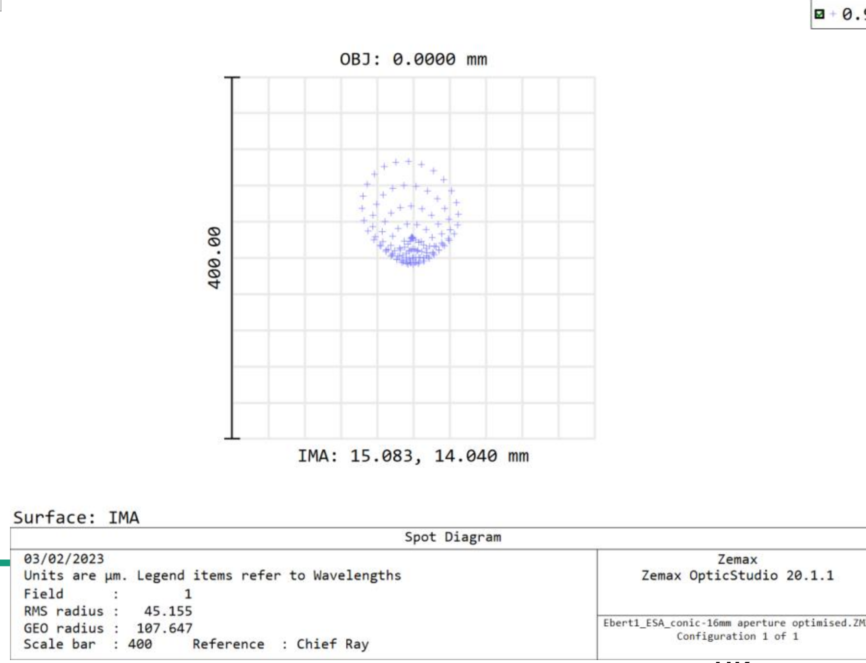

Designing the telescope and spectrometer for space platform

Conclusions

Optical design of the telescope and spectrometer for sensing in space is finished

Telescope: Cassegrain type, with aspherical achromats for light focusing into a 200um fibre
Fibre coupling efficiency >50%.
Mechanical sizes 400x150 mm

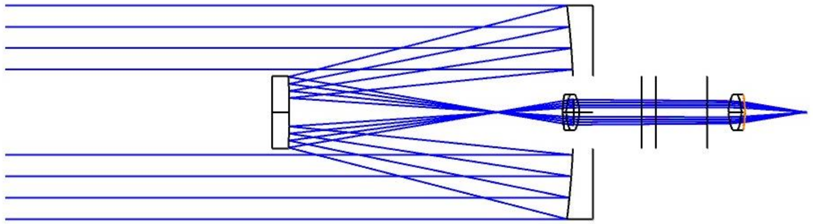

Spectrometer: Ebert scheme. With 200 um input slit. Sensor - Capella CIS120. 2048*2048 pixels
Mechanical sizes 100x50 mm

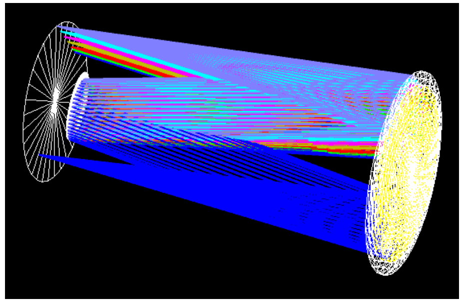

Zemax files with optical schemes will be attached to the report

Telescope experiments, using mount offset

Starlink 1272, 7/3/23, 20:20

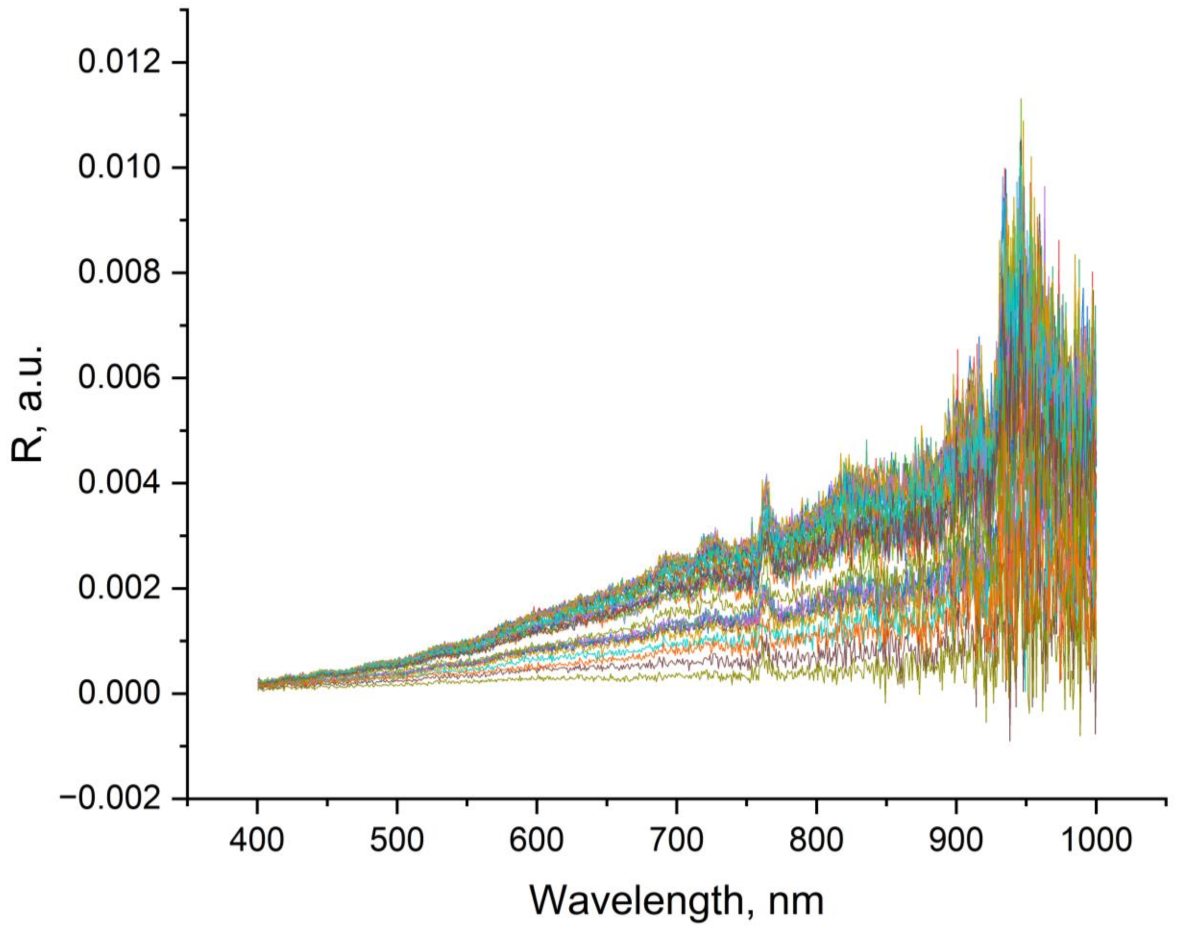

Starlink 1293, 7/3/23, 20:30

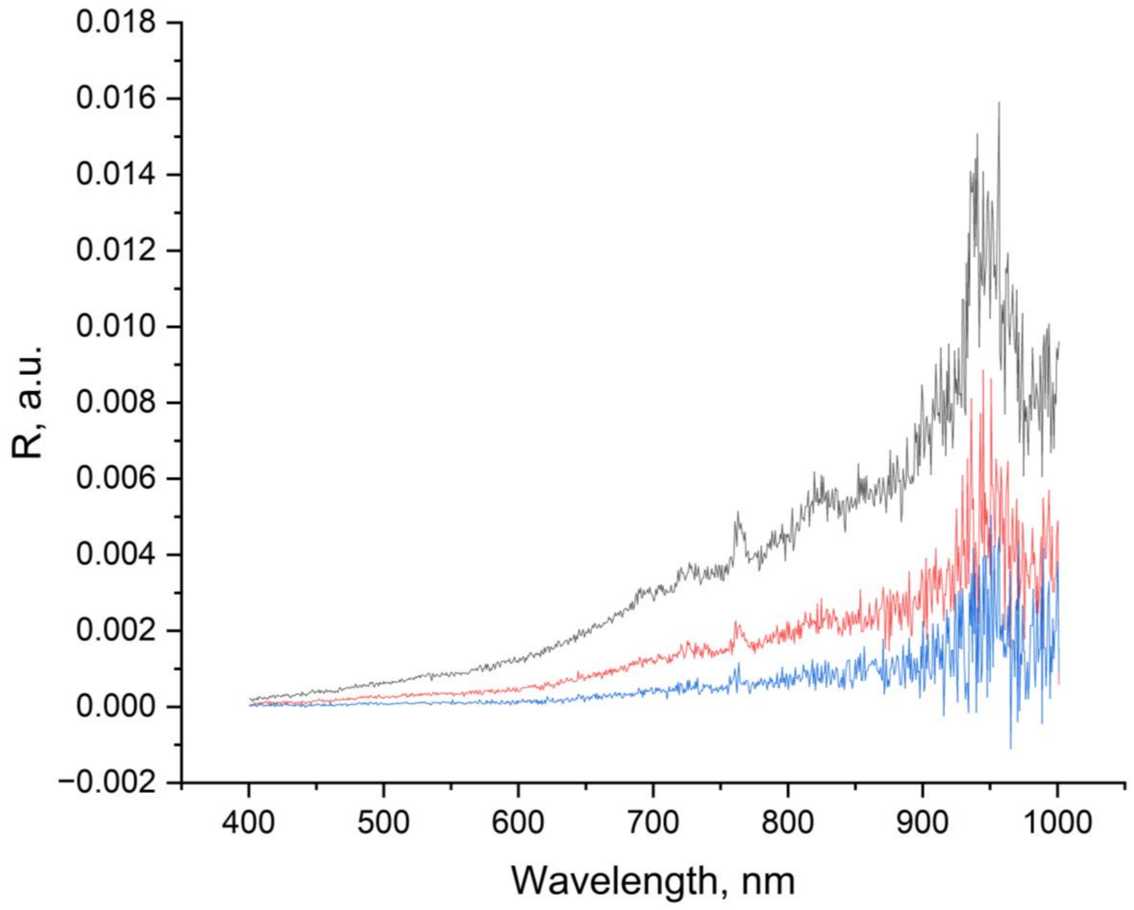

Telescope experiments, using mount offset

Starlink 1301, 7/3/23, 20:02

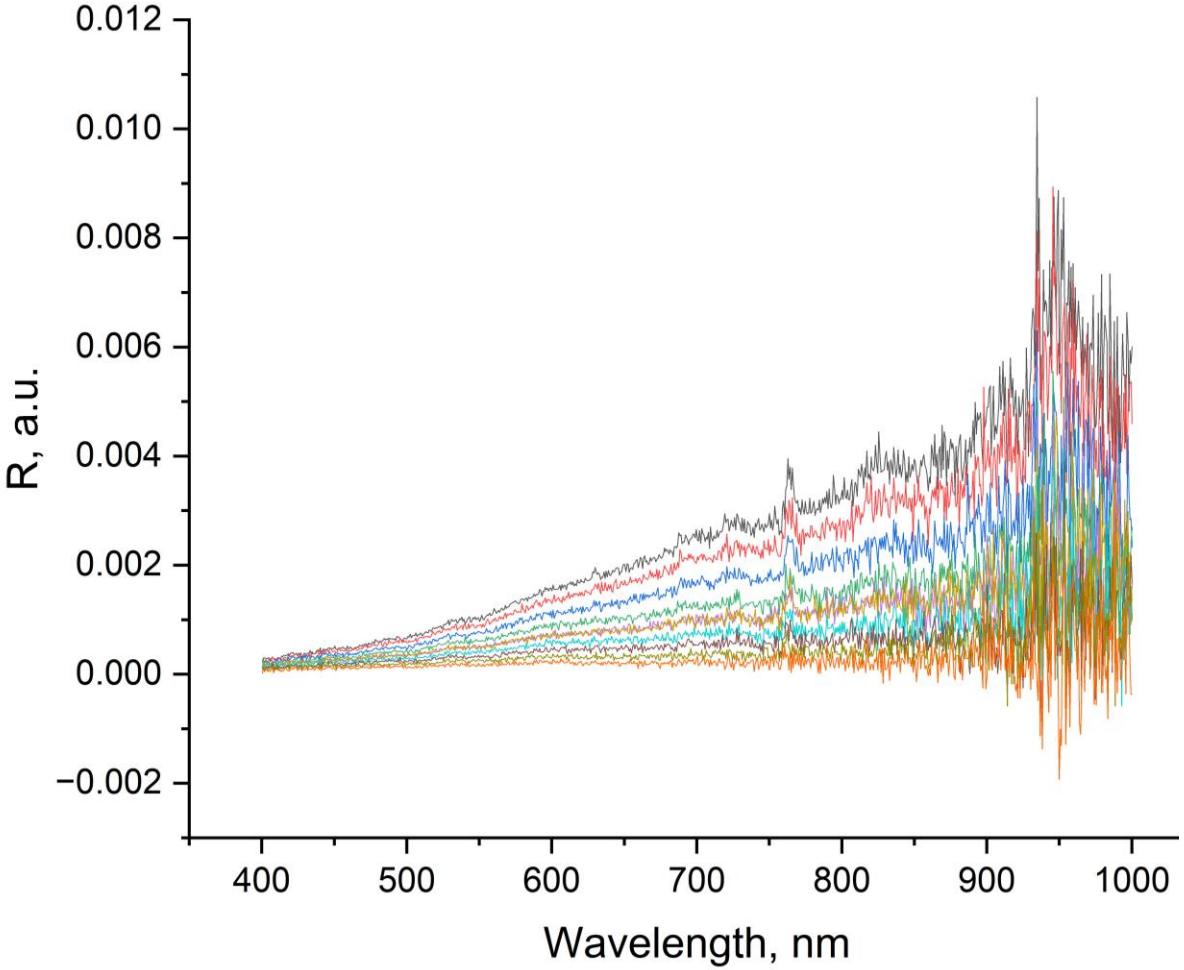

Landsat5, 7/3/23, 20:42

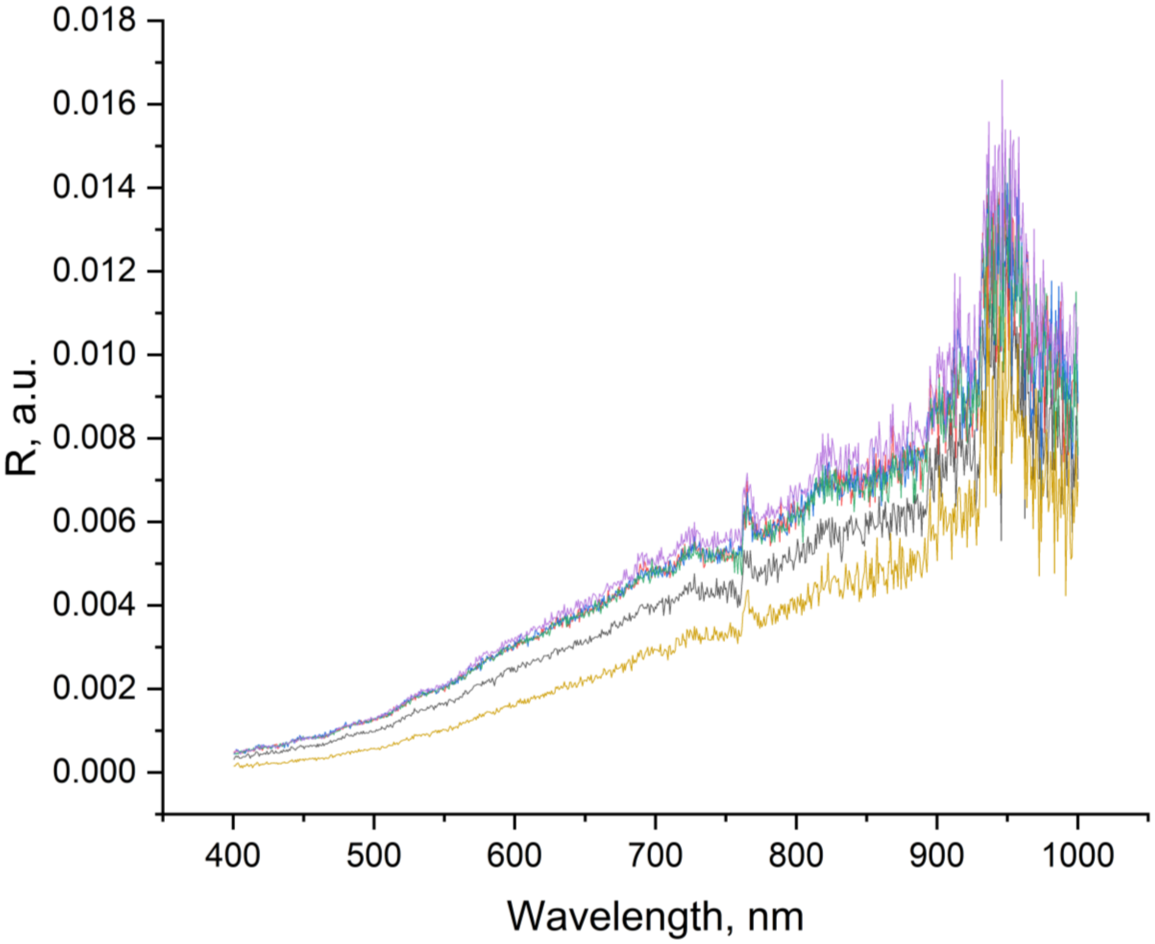

Fraunhofer UK

Ground sensor results and the modelling

Measured reflectivity of an object in space, R_m_o:

R_m_o= I_m_earth/I_m_illum_sun

R_m_o= (I_sun***T_atm***T_sys*R_m_o)/(I_sun***T_atm***T_sys)

Simulated reflectivity of an object in space, R_s_o:

R_s_o= I_s_earth/I_s_illum_sun

R_s_o= (I_sun***T_atm_MODTRAN***R_s_o)/(I_sun***T_atm_MODTRAN**)

Ideally: R_s_o=R_m_o and I_s_earth=I_m_earth

I_m_earth – intensity of light from the object **measured** by the telescope system on Earth

I_m_illum_sun – intensity of sunlight **measured** by the telescope system on Earth

T_atm – transmittance of the atmosphere

T_sys – transmittance of the telescope system

I_sun – intensity of sun, extra-terrestrial

I_s_earth – **simulated** intensity of light from the object on the telescope system on Earth

I_s_illum_sun – **simulated** intensity of sunlight on the telescope system on Earth

T_atm_MODTRAN –transmittance model of the atmosphere used in simulation

Ground sensor results and the modelling

Experiment – measurements through real atmosphere
Simulation – using MODTRAN model
Potential discrepancy

Possible solution:

Setting I_s_earth=I_m_earth

⇩

R_s_o = R_m_o*k*Tsys where k=T_atm/T_atm_MODTRAN

Measuring k*Tsys at cleat sky conditions:

k*Tsys=I_m_clear_sky/(I_sun*T_atm_MODTRAN)

I_sun – using 2000 ASTM Standard Extraterrestrial Spectrum Reference E-490-00
T_atm_MODTRAN – data available

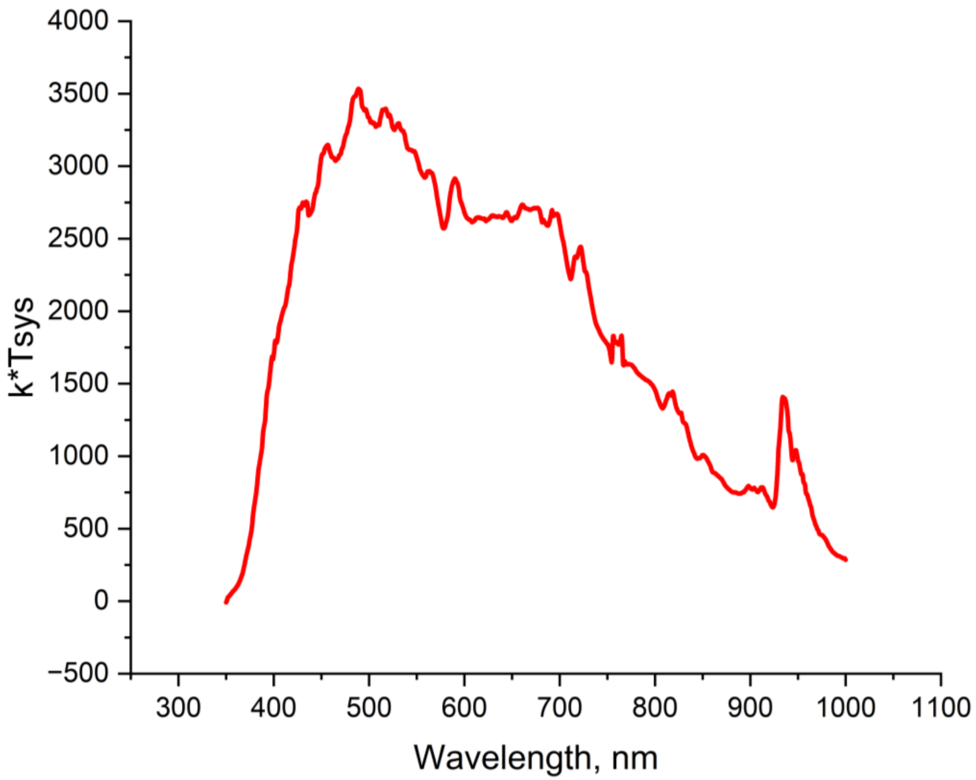

Straight From Sensor/ Simulation

- Data taken directly from the sensor or simulation differ significantly. There are clearly differences between what was captured with real atmospheric conditions and what was simulated based on MODTRAN

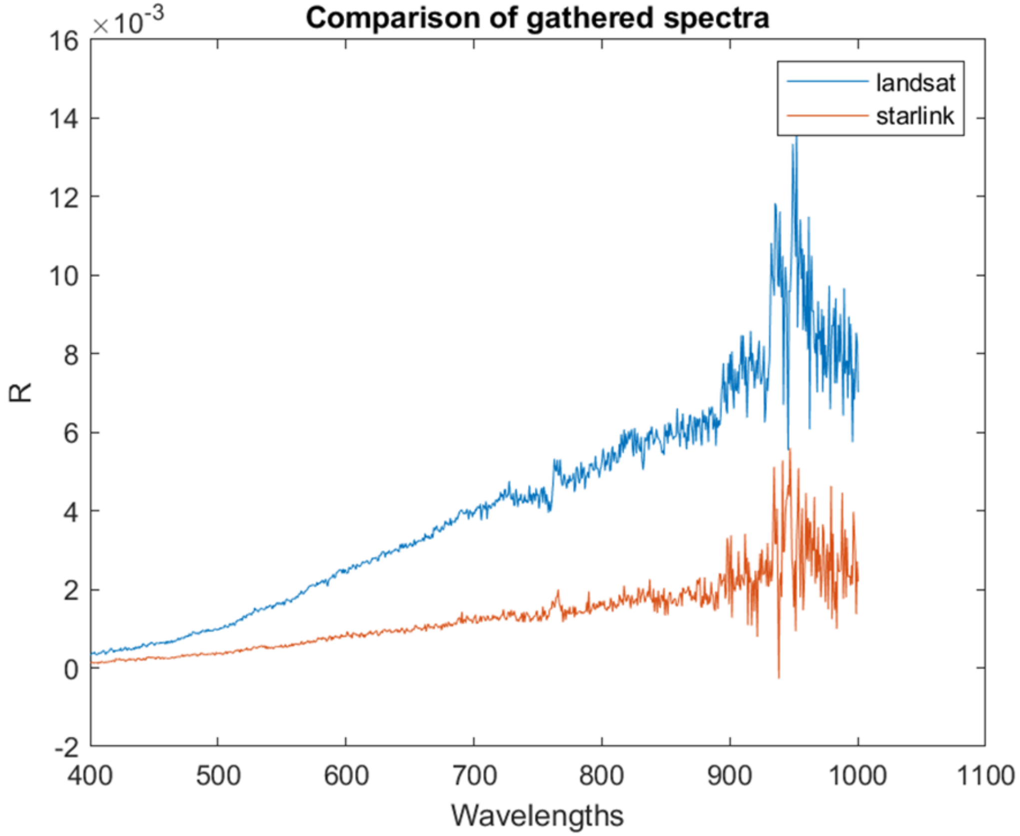

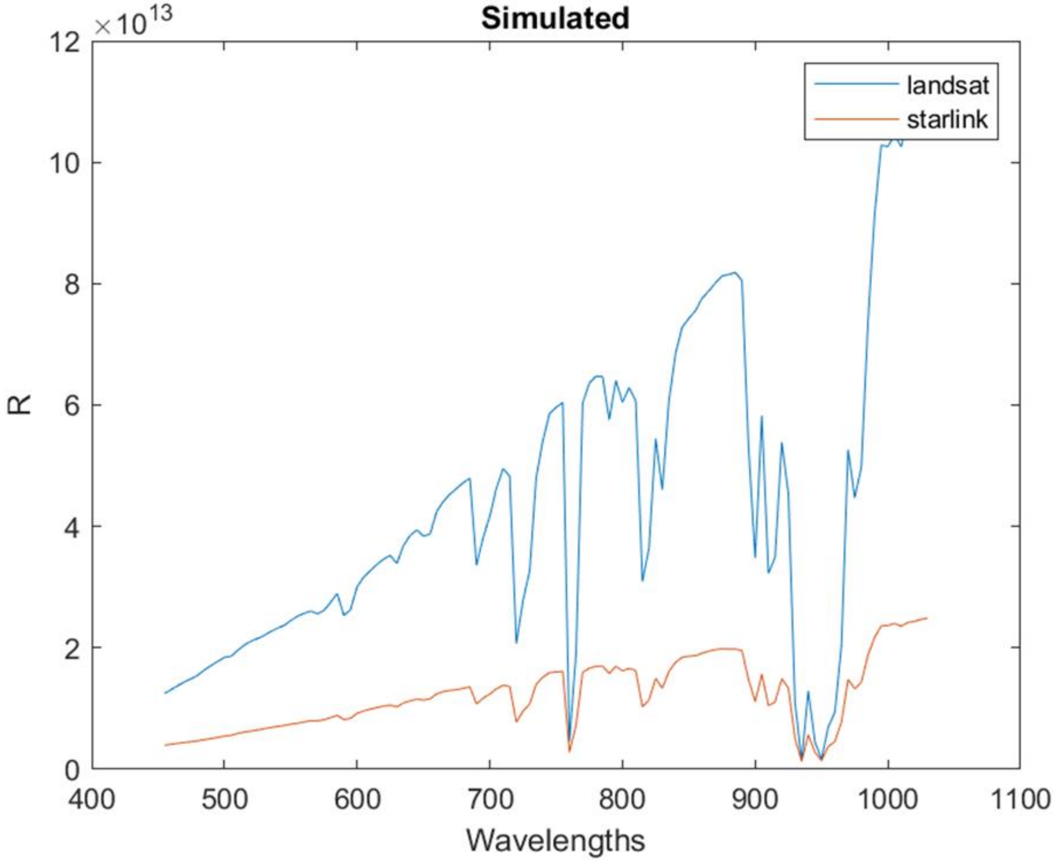

After Atmospheric Correction

- After correction we have more similar spectra. This does, however, require a different atmospheric correct function be used for the real data than the simulation
- This is not the same, but we also have solar panels in 1 but not the other.

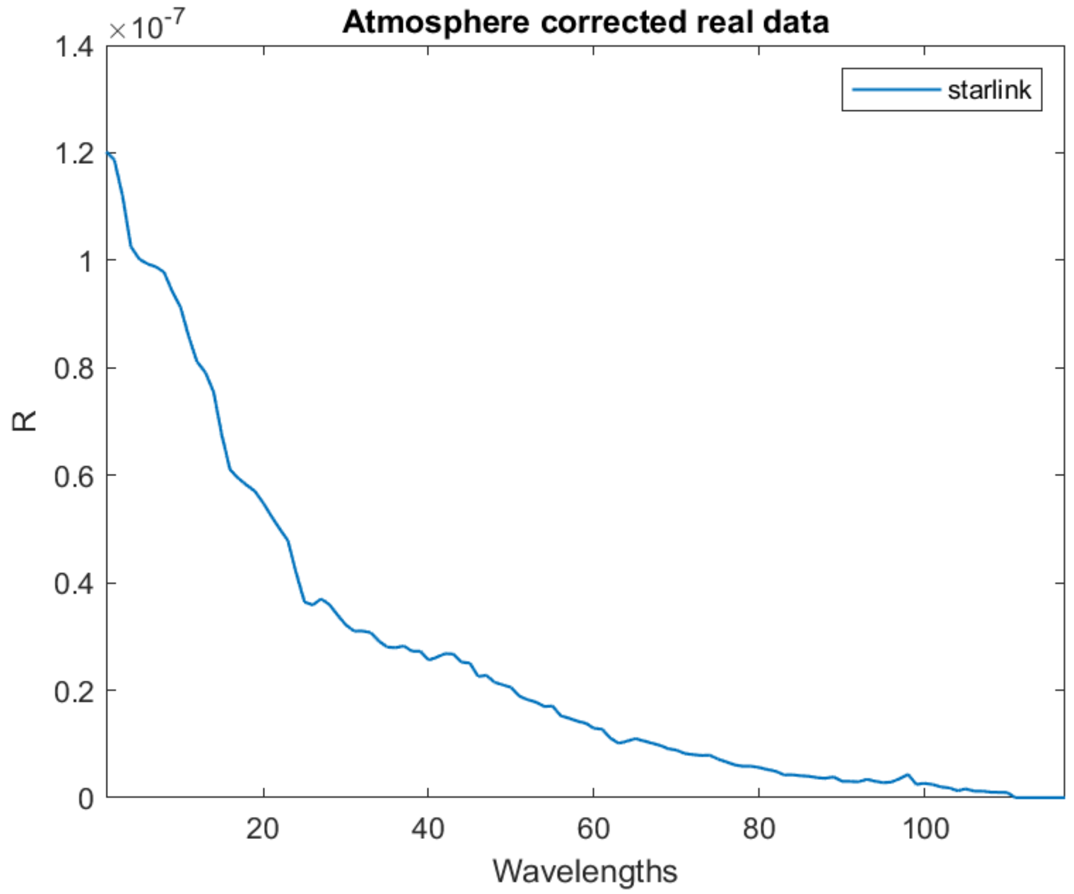

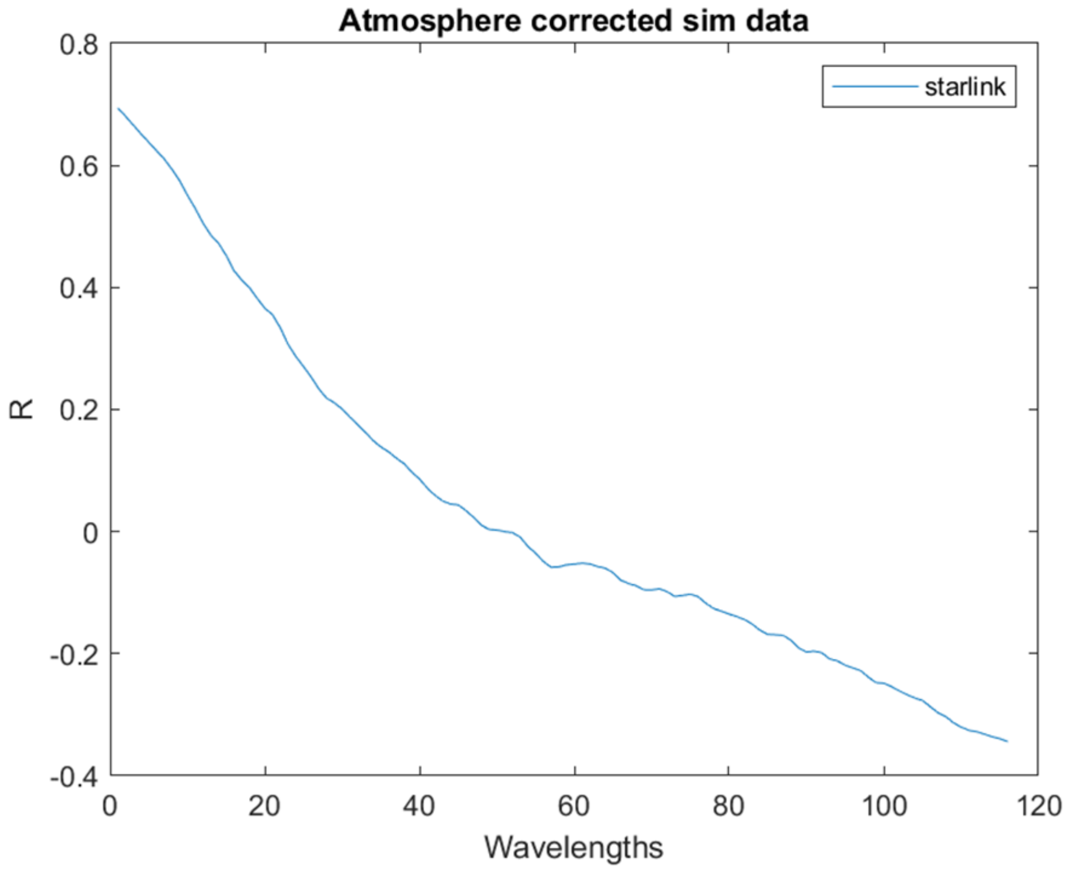

After All Pre-Processing

- After all pre-processing spectra appears ready for unmixing

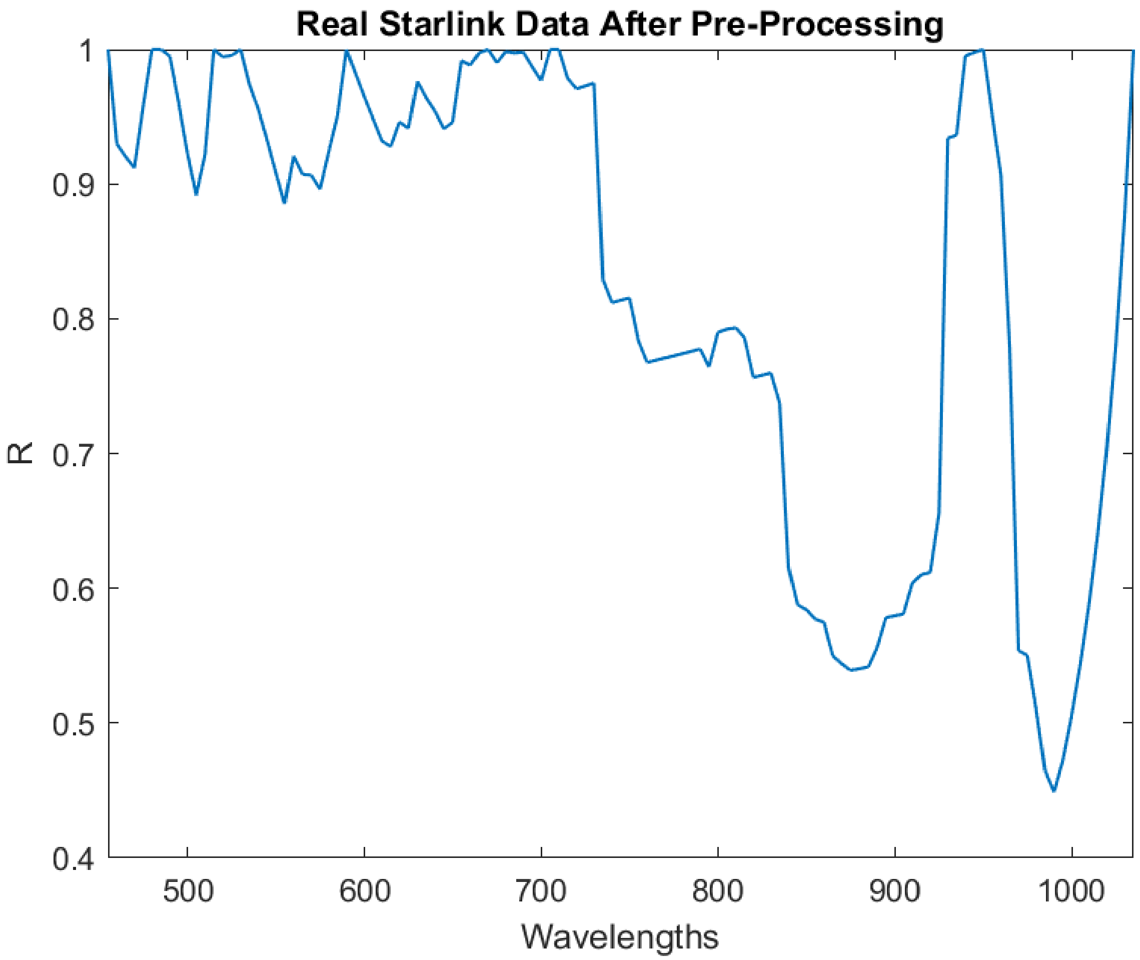

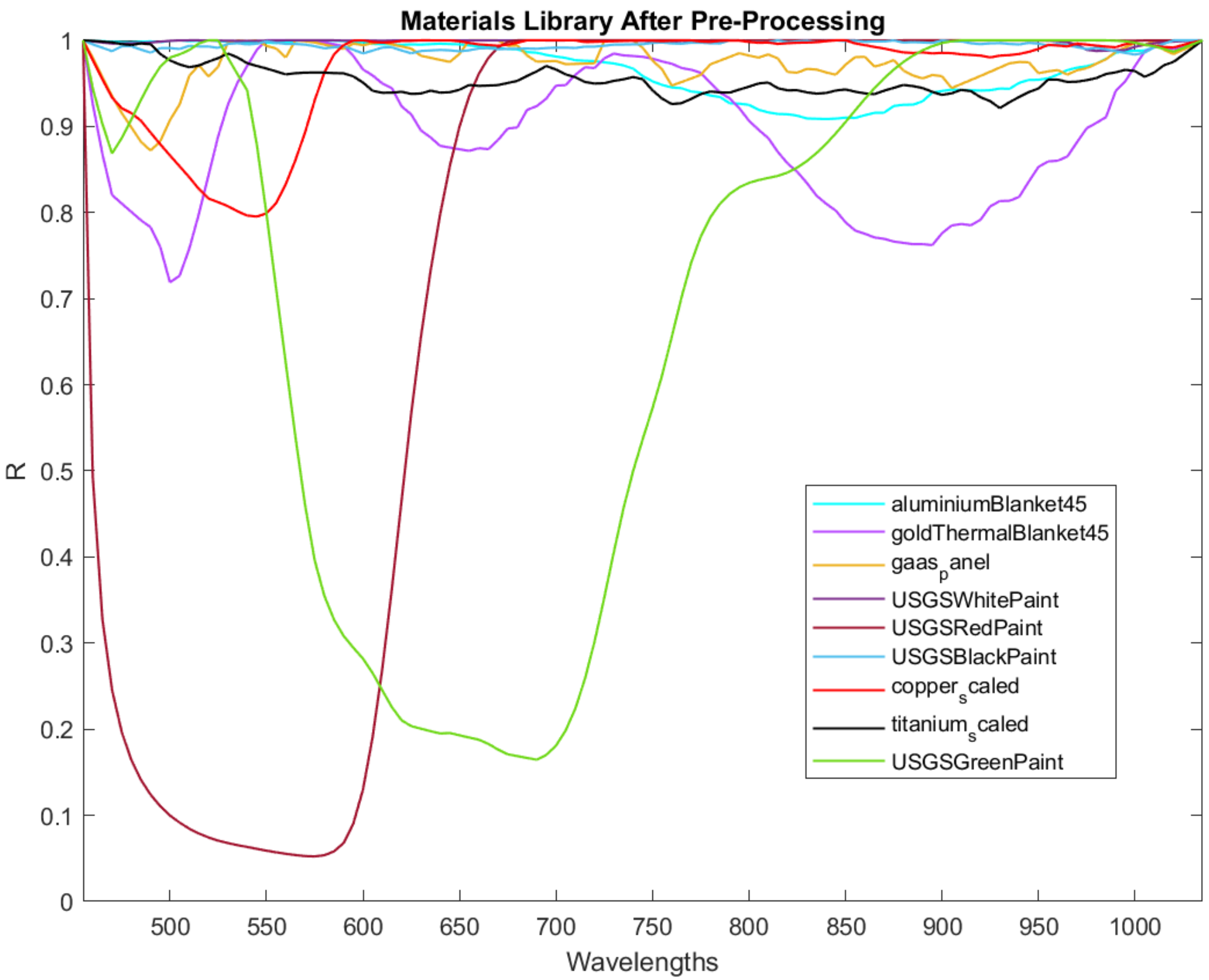

Unmixing of Starlink Satellites

AEROSPACE CENTRE of EXCELLENCE

- Unmixing of Starlink satellites show aluminum and gold blanket, but no solar panel – materials seen are consistent over time and satellites

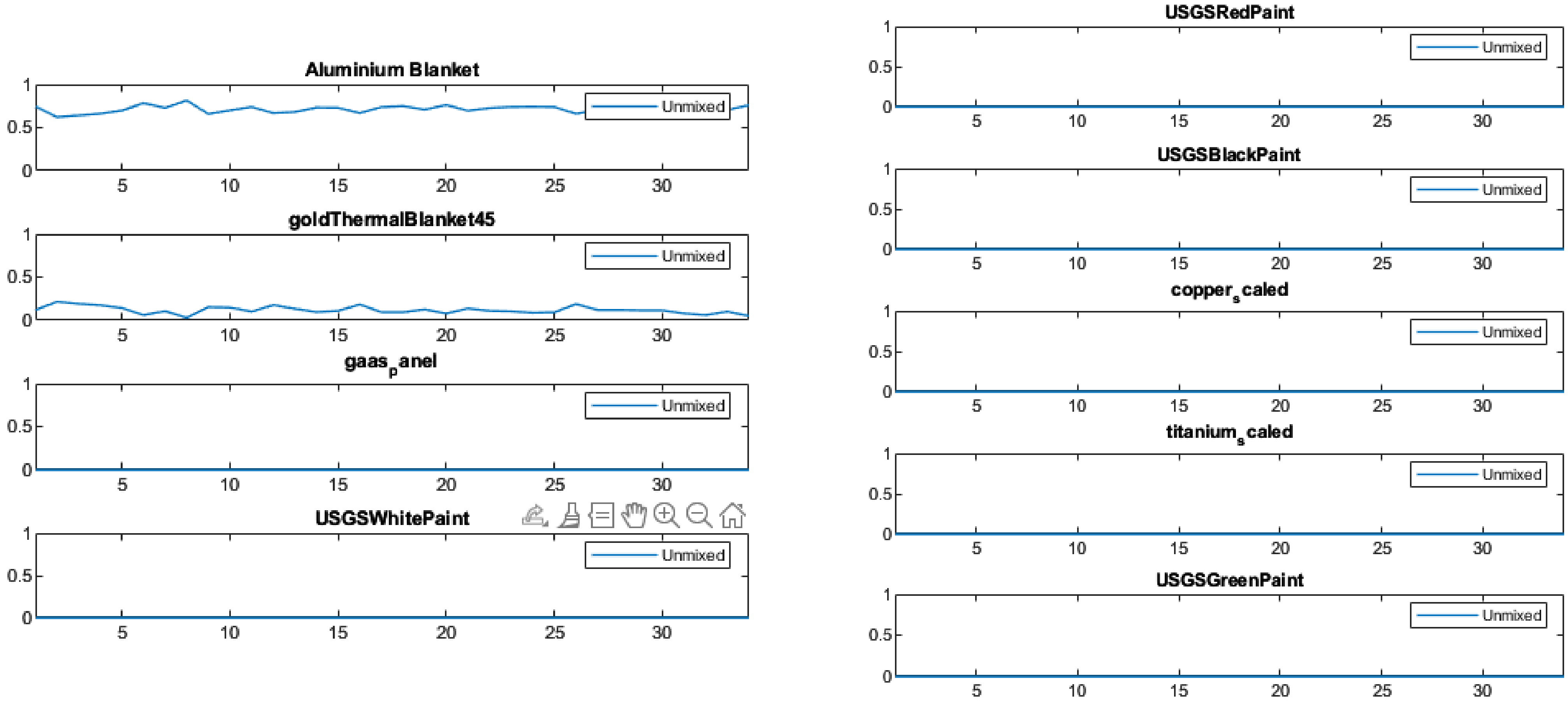

Figure: Unmixing of Starlink 1272 Satellite with 34 time series measurement

Unmixing of LandSat Satellites

- Unmixing of Landsat satellite also shows aluminum and gold blanket, but no solar panel – materials seen are again consistent over time though only 1 satellite was measured

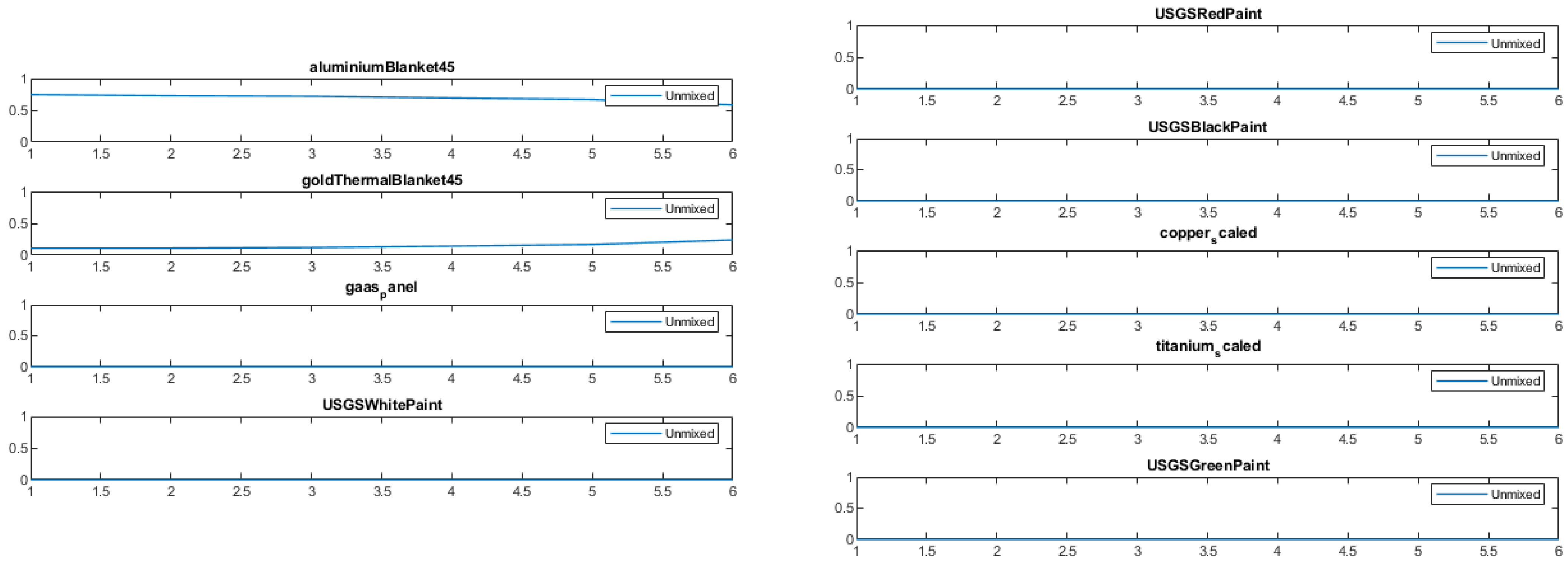

Figure: Unmixing of Landsat5 Satellite with 6 time series measurement

Unmixing of ISS

- Unmixing of ISS show a slightly wider variety of materials – and a variation in material detection around time 60

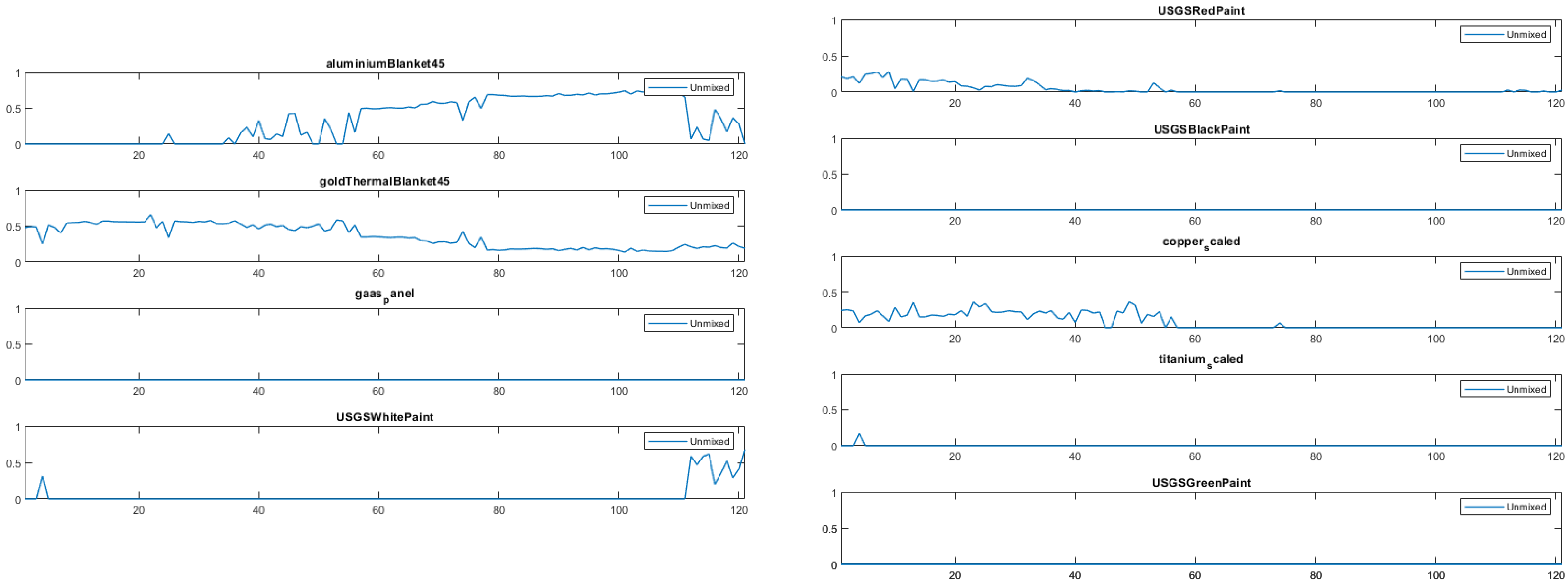

Figure: Unmixing of ISS with 120 time series measurement

Material Abundance and Prediction

- Previous demonstrated unmixing of real data, however, lack of solar panels made us unsure of reliability of results

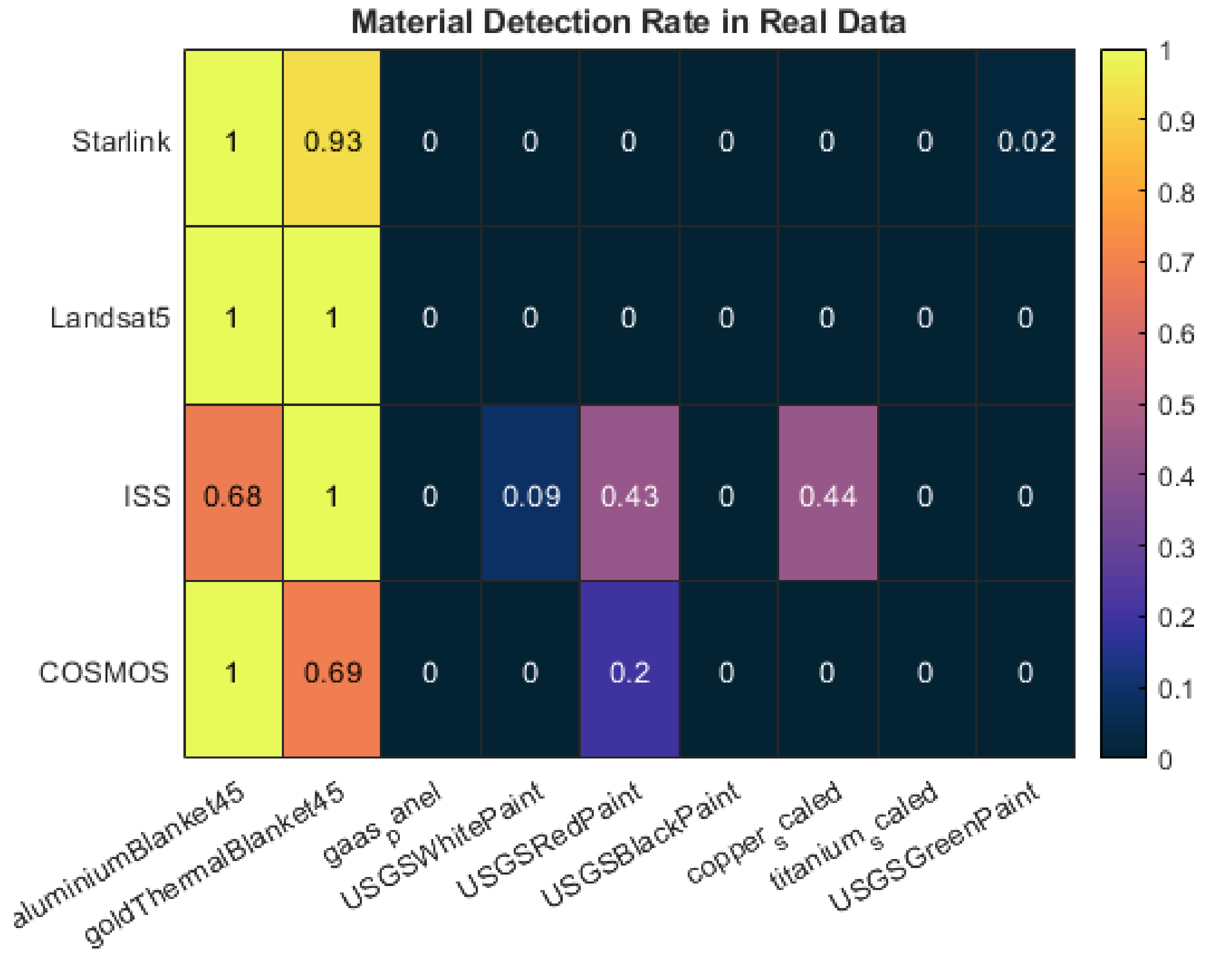

Further Exploration of Real Data Unmixing

- New solar panel imaged in our lab to explore spectra of panel components

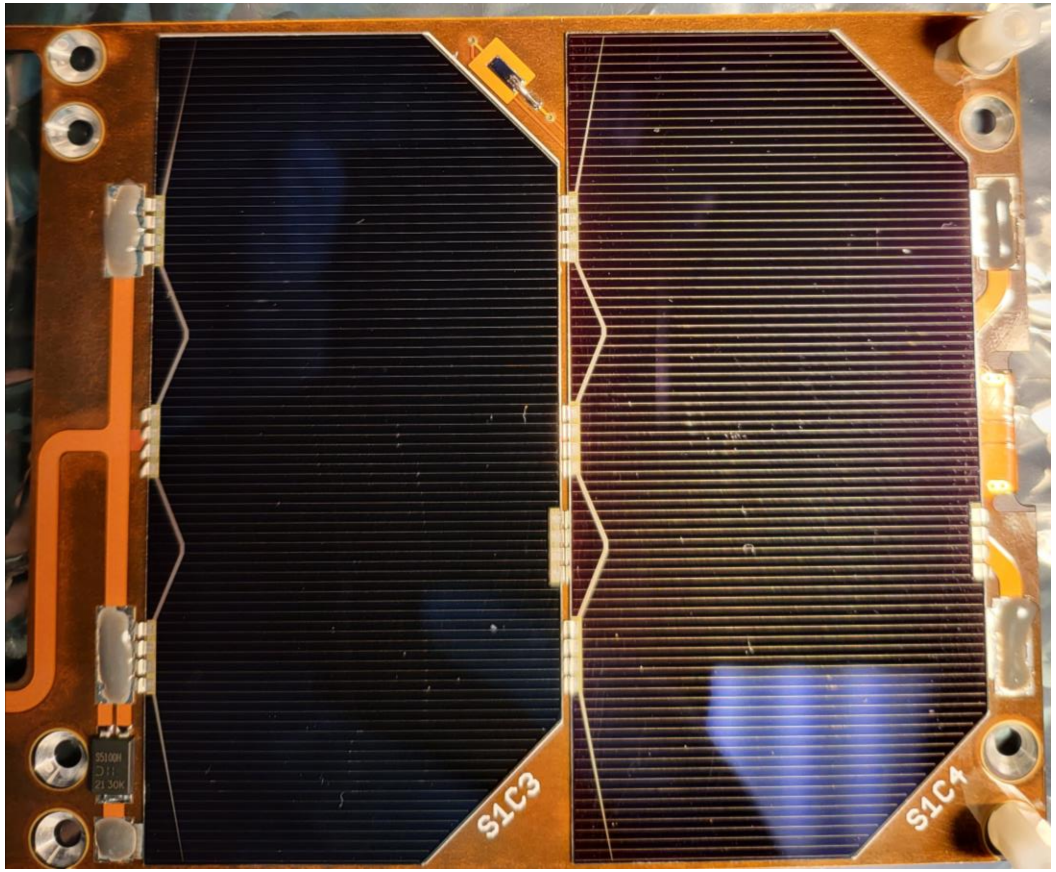

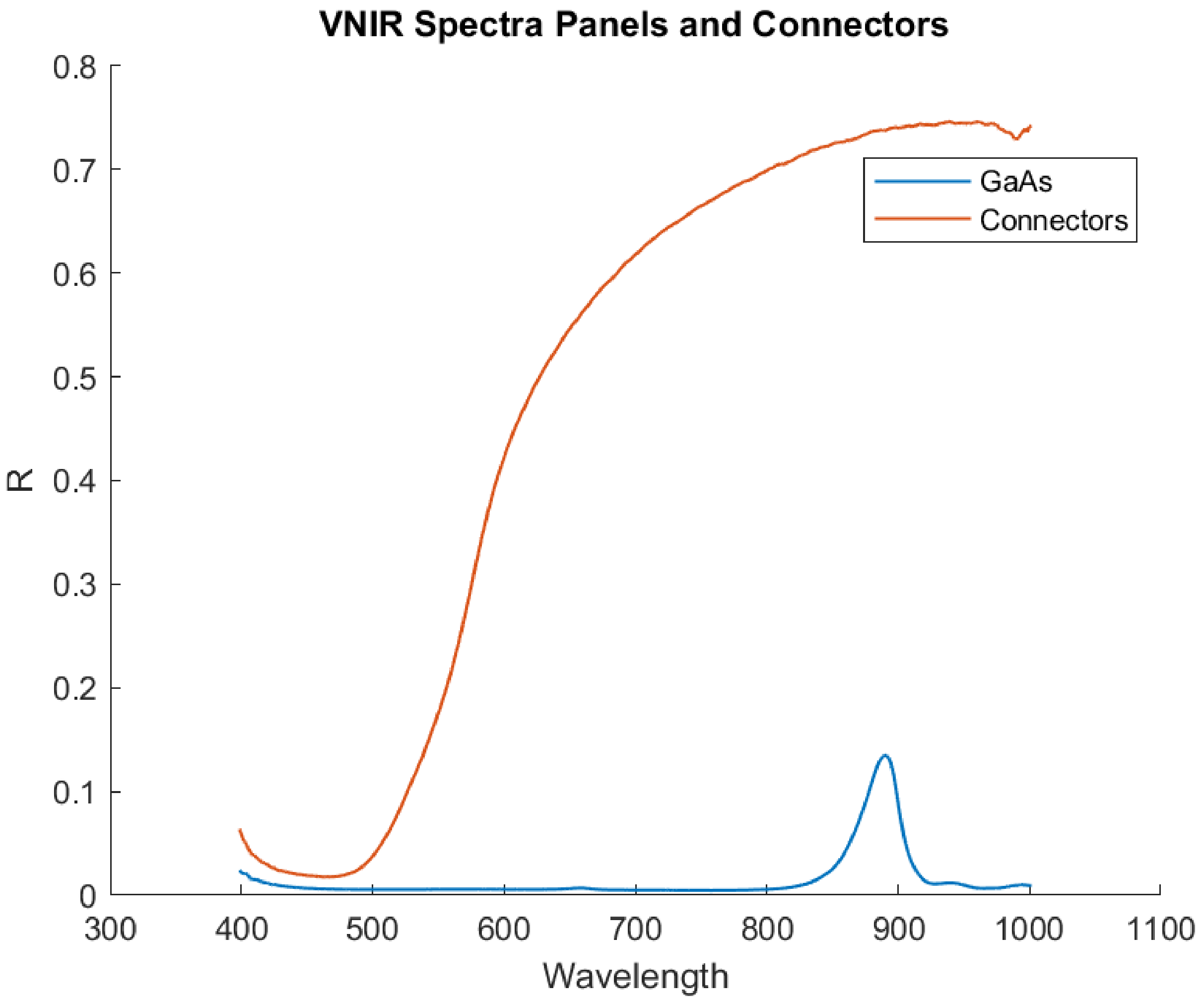

Further Exploration of Real Data Unmixing

- We were unable to find much of these in the real data, perhaps suggesting the connector material and panel is different than what we observed here

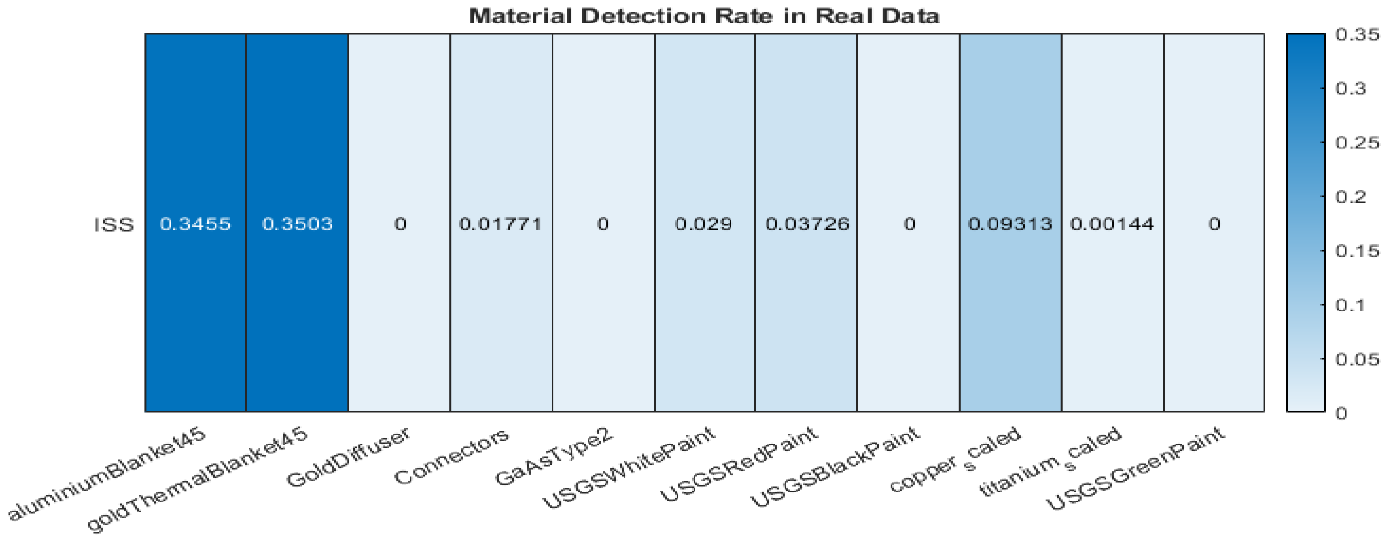

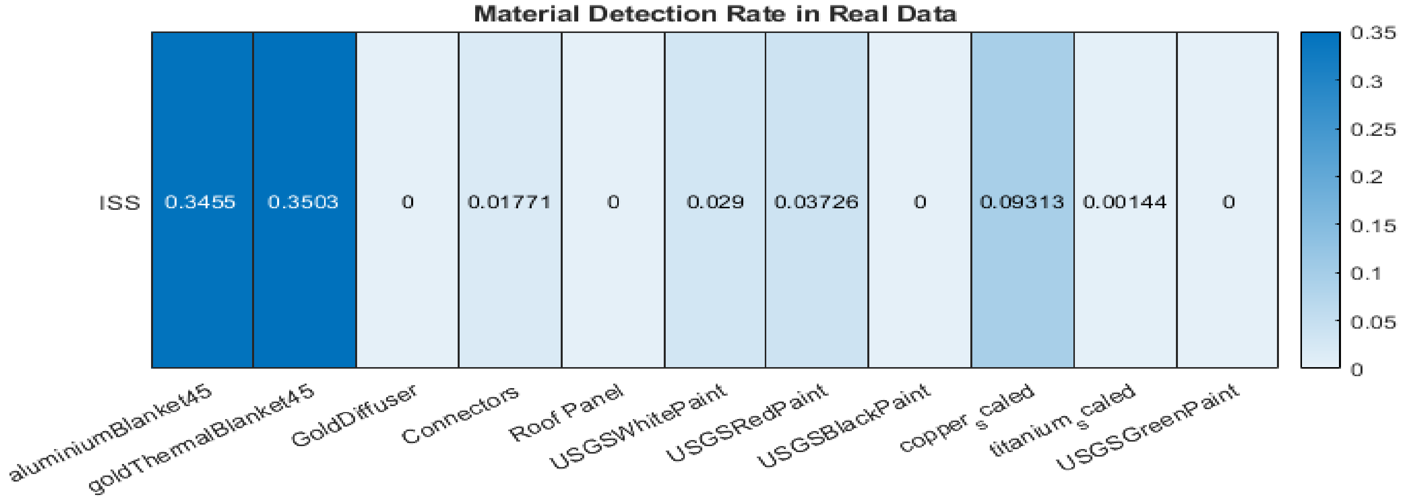

Further Exploration of Real Data Unmixing

- The unmixing algorithms estimates the abundance of each material present
- We can compute this synthetic mix and compare to the received signal to assess how accurate the results appear to be
- It is clear that for the solar panel on earth, where we know we have the right materials in the library, performance is good
- For the ISS where we are not sure of this, performance is worse
- This is supported by the good results for the simulation
- The logical conclusion is that there are materials or spectral differences not accounted for in our existing library

ISS

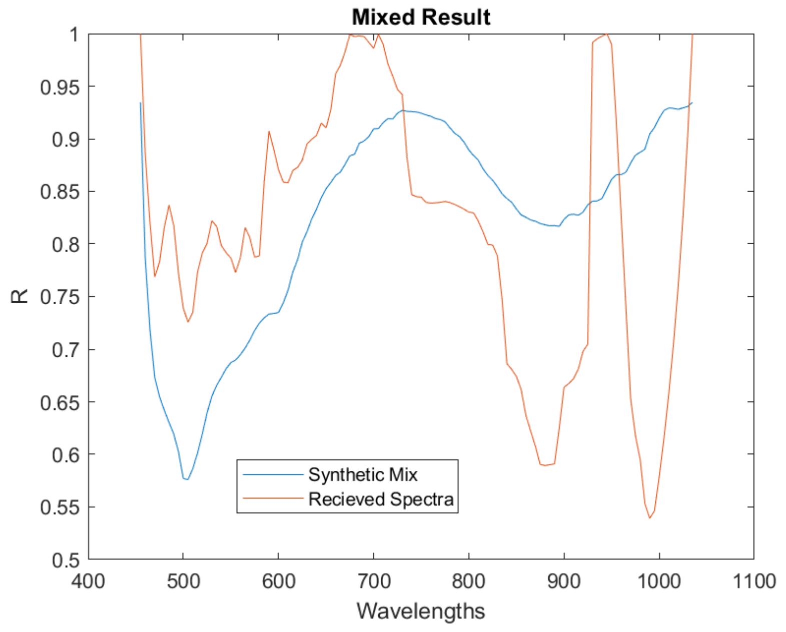

Solar Panel Imaged on Roof

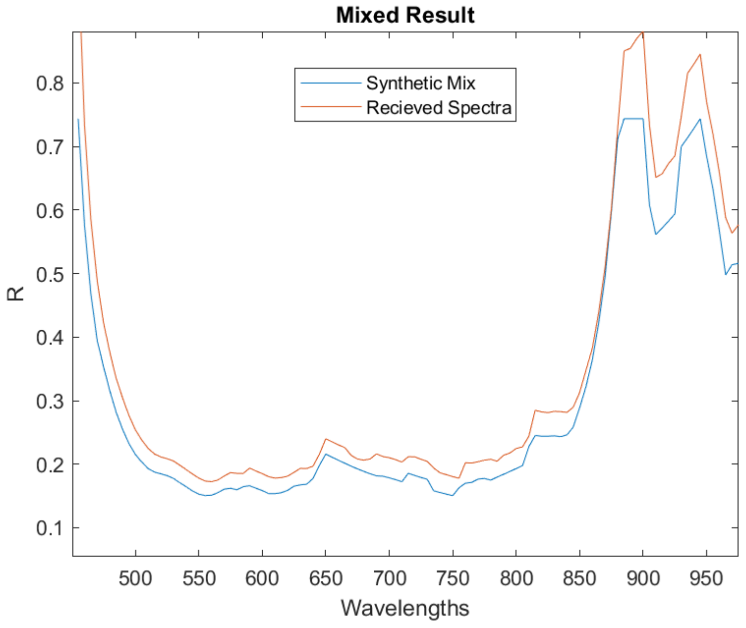

Further Exploration of Real Data Unmixing

- Performance appears better for other satellites
- Again this suggests it depends on how accurately our library represents the spectra of materials that are present

Very different gold foil

COSMOS

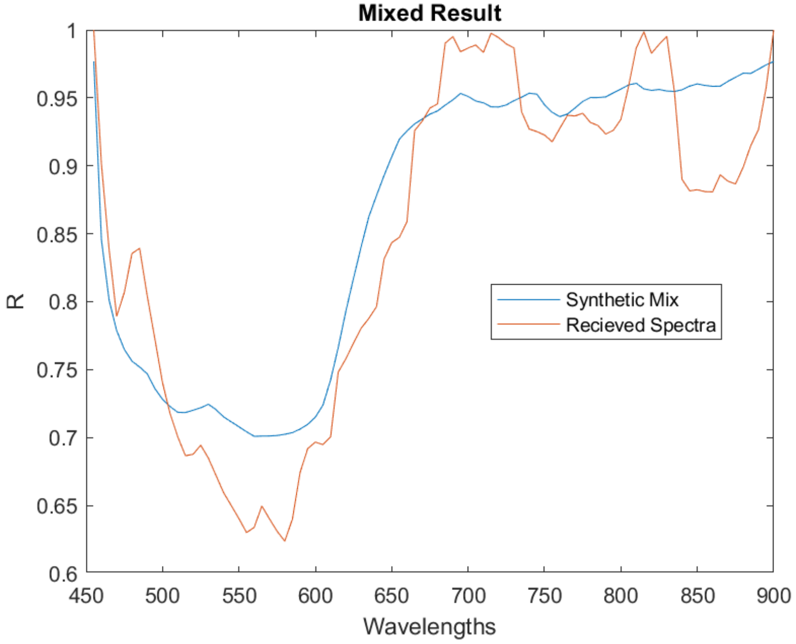

COSMOS (with matt gold blankets)

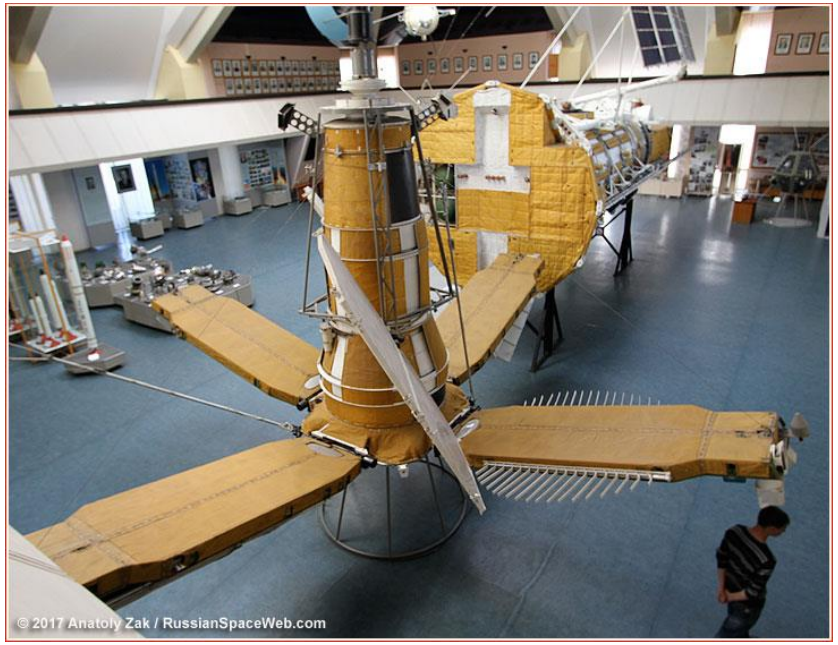

Material Detection Rate in Real Data

	aluminiumBlanket45	goldThermalBlanket45	GoldDiffuser	Connectors	GaAsType2	USGSWhitePaint	USGSRedPaint	USGSBlackPaint	copper_scaled	titanium_scaled	USGSGreenPaint
COSMOS	0.0004288	0	0	0	0.003091	0	0.2697	0	0.01722	0.6582	0.01739

Next Steps

1. Create an object classification system.
   - Improve current model to include material degradation and other effects
   - Create a database of objects and associated material distribution on their surfaces. Note that accuracy of shape is not essential but rough material abundance per surface is important.
   - Generation of a database of spectral time series for different attitude motions for each object.
   - Training a deep-classifier to associate spectral time series to object type
2. Extend the work on attitude motion
   - Exploit the analogy with image classification
   - Extend the database of time-varying spectral responses
   - Train a deep-learning model to return quaternions from time series
   - Develop a measurement model to associate pointing direction to spectral responses
   - Association of materials to pseudo-surfaces (unknown shape)
   - Association of directions to pseudo-surfaces
3. Validation
   - Acquisition of observational data of known objects
   - Spectral unmixing
   - Application of algorithms and validation of assumptions

University of Strathclyde Glasgow